SYNCHRONIZATION OF EARTH STATIONS

SYNCHRONIZATION OF EARTH STATIONS TO A COMMUNICATIONS SWITCHING SATELLITE

by

Charles Ruskin Carter, B.A.Sc., M.A.Sc.

A Thesis

Submitted to the Faculty of Graduate Studies

in Partial Fulfilment of the Requirements

for the Degree

Doctor of Philosophy

McMaster University

August, 1974

DOCTOR OF PHILOSOPHY (1974) McMaster University
(Electrical Engineering) Hamilton, Ontario

TITLE : Synchronization of Earth Stations to a Communications Switching Satellite.

AUTHOR : Charles Ruskin Carter, B.A.Sc. (U.B.C., 1962)
M.A.Sc. (U.B.C., 1966)

SUPERVISOR : Dr. S. S. Haykin

NUMBER OF PAGES : xix, 277.

ABSTRACT

The problem of synchronizing earth stations to the switching sequence of the SDMA/SS-TDMA communications satellite system described by COMSAT Laboratories is examined in detail. System synchronization is discussed and two techniques for locking the time bases of all earth stations to the sync window of the satellite are described.

It is established that synchronization for an individual earth station can be separated into three distinct modes of operation called the coarse search mode, the fine search mode and the tracking mode. Three different methods for achieving coarse search synchronization are described.

In the fine search mode, the synchronization loop is analysed assuming that the pertinent earth station transmits sync bursts which are modulated by the sync window. Results of this analysis show that a receiver configuration employing an integrator provides a set of error detection characteristics which relate an error voltage measured in the earth station to the timing error measured at the satellite. It is shown that the average timing error is reduced to zero with successive transmissions of sync bursts around the loop.

The timing error due to constant velocity satellite motion can be eliminated by employing a tracking network. The tracking network uses an integrator to adjust the earth station time base clock.

A laboratory model, which closely approximates the actual physical

model used in the theory, has been designed and constructed. The coarse search, fine search and tracking modes of operation are all included in this experimental study, and a provision which simulates satellite motion is described. Details of experiments, which confirm the theoretical predictions, are provided.

The major contributions of the thesis are summarized below.

(1) A technique for providing synchronization for all earth stations operating in the system, employing three control stations, is described.

(2) A new technique for achieving coarse search synchronization using coded search signals has been developed.

(3) Three new implementations of the sync burst have been described.

(4) The behaviour of the synchronization loop has been analysed in detail and a concept using error detection characteristics has been explored.

(5) A tracking network can be employed to eliminate timing errors caused by constant velocity satellite motion.

(6) A laboratory model has been designed and constructed.

(7) A special coherent receiver for demodulating bursts of PSK signals has been developed.

(8) Results of experiments using the laboratory model are demonstrated to agree closely with theoretical predictions.

ACKNOWLEDGEMENTS

It is with pleasure that the author acknowledges the contributions and suggestions of his supervisor, Dr. S. S. Haykin, in the preparation of this thesis. Special thanks are due to Dr. R. de Buda who provided a number of useful comments and to Dr. T. J. Kennett for serving on the supervisory committee.

The author is grateful for financial support from the National Research Council of Canada.

Finally, the author would like to thank Mr. C. D. Hawkes for proof-reading the thesis and Miss D. Tudin for assisting in the typing.

TABLE OF CONTENTS

LIST OF ILLUSTRATIONS

LIST OF TABLES

LIST OF PRINCIPAL SYMBOLS

$E\{\cdot\}$	= expectation of $\{\cdot\}$
f_O	= center frequency of the VCO
L	= number of sync bursts integrated in the receiver
m	= dimensionless loop constant
$m(t)$	= sync window modulation characteristic
N_O	= single-sided noise spectral density
$q(t)$	= receiver input gate of L pulses
r	= number of transmissions of sync bursts (iterations)
$s(t)$	= envelope of the PSK sync burst
S	= sensitivity of the VCO in Hz per volt
SNR_D	= downlink signal-to-noise ratio
SNR_U	= uplink signal-to-noise ratio
$t_E(\cdot)$	= timing error after $(\cdot)$ iterations
t_{capt}	= capture range of the synchronizer
$t_M(1)$	= path length time delay change in one round trip time
t_N	= timing error due to noise
T_D	= space delay between the ground station and the satellite
T_G	= duration of the timing adjustment gate
T_I	= integrator time constant

T_O = interpulse spacing of sync bursts with $v_E = 0$

T_P = sync burst duration

T_Q = duration of each input gate.

T_W = sync window duration

v_E = error voltage on the control terminal of the VCO

v_N = integrated noise voltage

v_S = integrated signal voltage

$x_1(t)$ = in-phase component of the complex uplink noise

$x_2(t)$ = in-phase component of the complex downlink noise

ASK = amplitude shift keying

FDMA = frequency division multiple access

FSK = frequency shift keying

PSK = phase shift keying

SDMA = space division multiple access

SDMA/SS-FDMA

= space division multiple access/ spacecraft switched-frequency division multiple access

SDMA/SS-TDMA

= space division multiple access/spacecraft switched-time division multiple access

TDMA = time division multiple access

CHAPTER 1

Introduction

Communications satellites have continuously evolved since the launch of Telstar in 1962 resulting in increased complexity and improved efficiency. April 6, 1974 marked the ninth anniversary of the launch of Early Bird (later named INTELSAT I), the first commercial communications satellite. In that short nine-year span, advances in spacecraft technology have resulted in satellites such as INTELSAT IV with 25 times the traffic-carrying capacity of Early Bird and five times the projected lifetime [1]. The capacity differences between these satellites tends to overshadow other advances that have equal or greater impact on network efficiency and flexibility. These techniques are applied to the earth segment rather than the space segment and take the form of efficient modulation techniques, complex multiple access methods and advanced signal processing networks.

The growth of communications systems using satellites is illustrated in Fig. 1-1 which shows the increase in the total number of circuits of the INTELSAT system [2]. The traffic is increasing at approximately 15 to 25 percent per year compounded; and this rate is expected to continue for the next 10 to 20 years. Thus, there exists a need for high capacity communications satellite systems.

The high capacity can be achieved through the use of spot beam zone technology. The spot beam zones are produced on earth by highly-directive antennas on-board the satellite, which is in a stationary

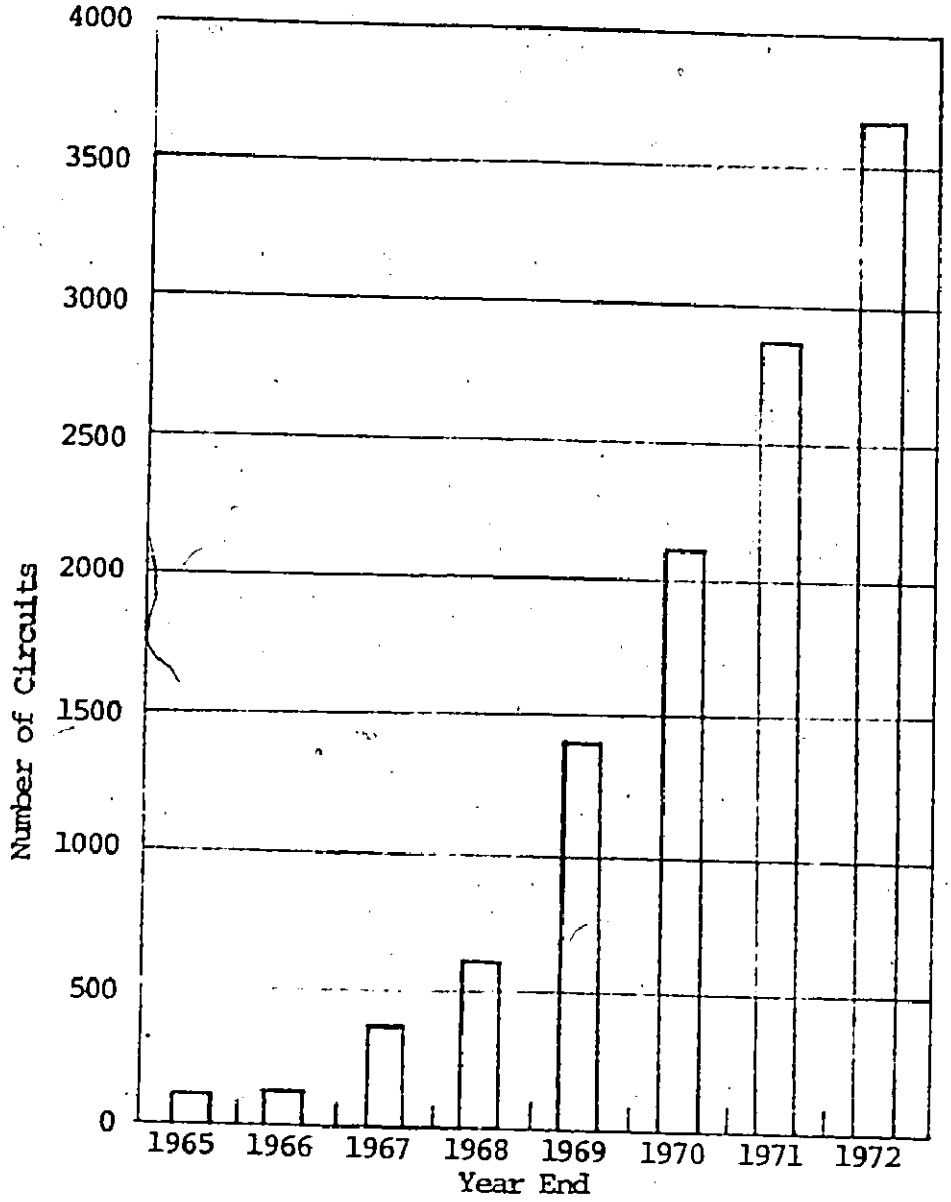

Fig. 1-1 System growth in total number of circuits.

orbit. Earth station transmissions from one spot beam zone can be interconnected to other spot beam zones through circuitry in the satellite. The objective of this thesis is to examine one particular aspect of a new system which employs spot beam zone technology, namely the problem of synchronization.

1.1 SURVEY OF SPOT BEAM ZONE TECHNOLOGY

As the lower bands of the microwave spectrum become more crowded, it is necessary to consider the use of millimeter wavelengths in the design of the next generation of communications satellites [3 - 10]. The shorter wavelengths reduce the size of microwave antennas and thus provide the feasibility of employing highly-directive antennas producing multiple spot beam zones, as shown in Fig. 1-2, creating a system called space division multiple access (SDMA). Use of spot beam antennas for both receiving and transmitting channels increases the effective isotropic radiated power and provides a frequency reuse feature which is not possible if only global-coverage antennas are used [3].

The system comprises one satellite serving a number of different spot beam zones and a number of earth stations located in each of the spot beam zones. Each repeater uses the same two passbands each of bandwidth B, with one for the uplink and the other for the downlink, as shown in Fig. 1-3. Hence, instead of requiring a total bandwidth of 2 N B for N transponders which would be the case if frequency reuse were not possible this communication system utilizes a bandwidth of 2 B for an N-fold saving.

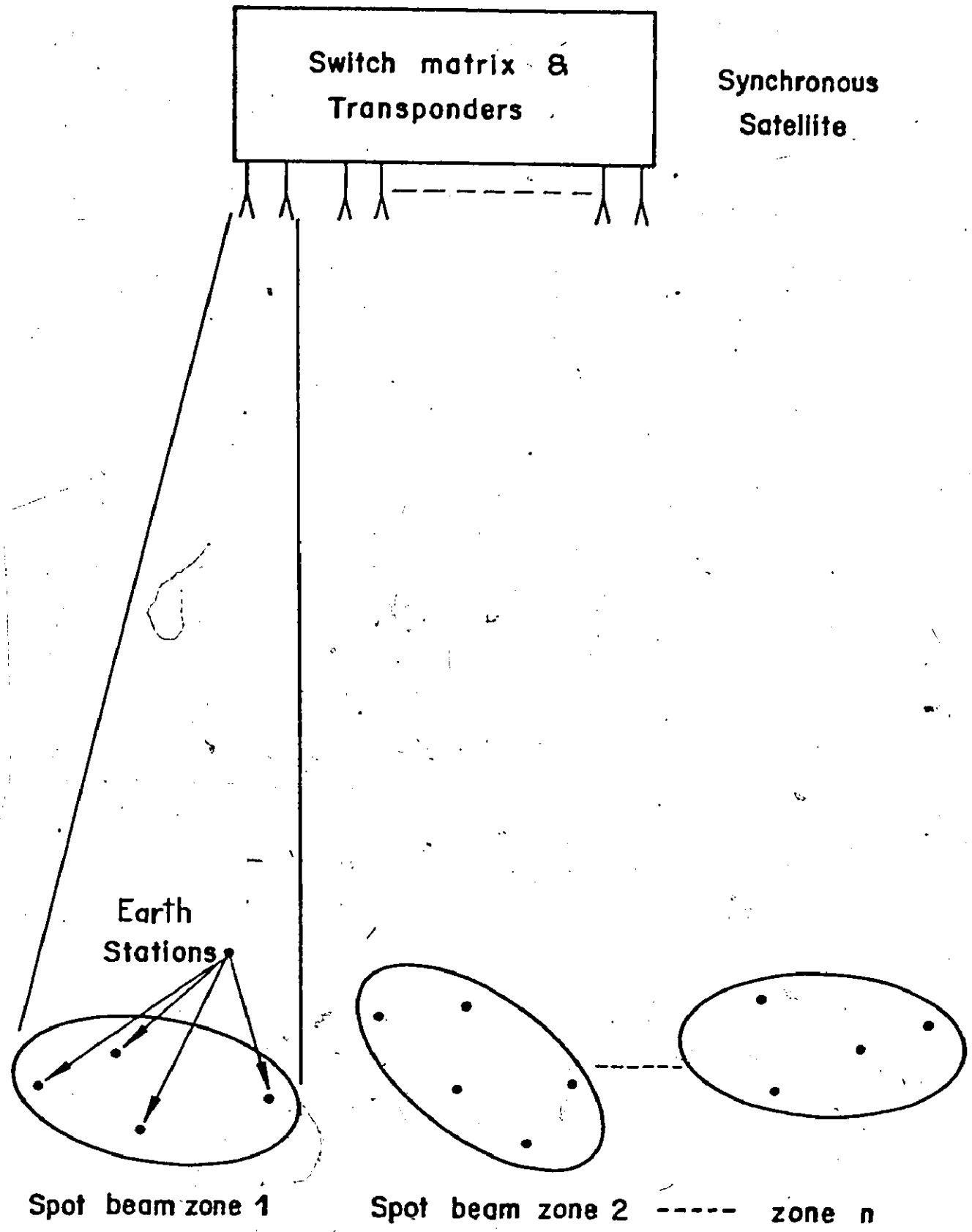

Fig. 1-2 Space division multiple access (SDMA) satellite communications system.

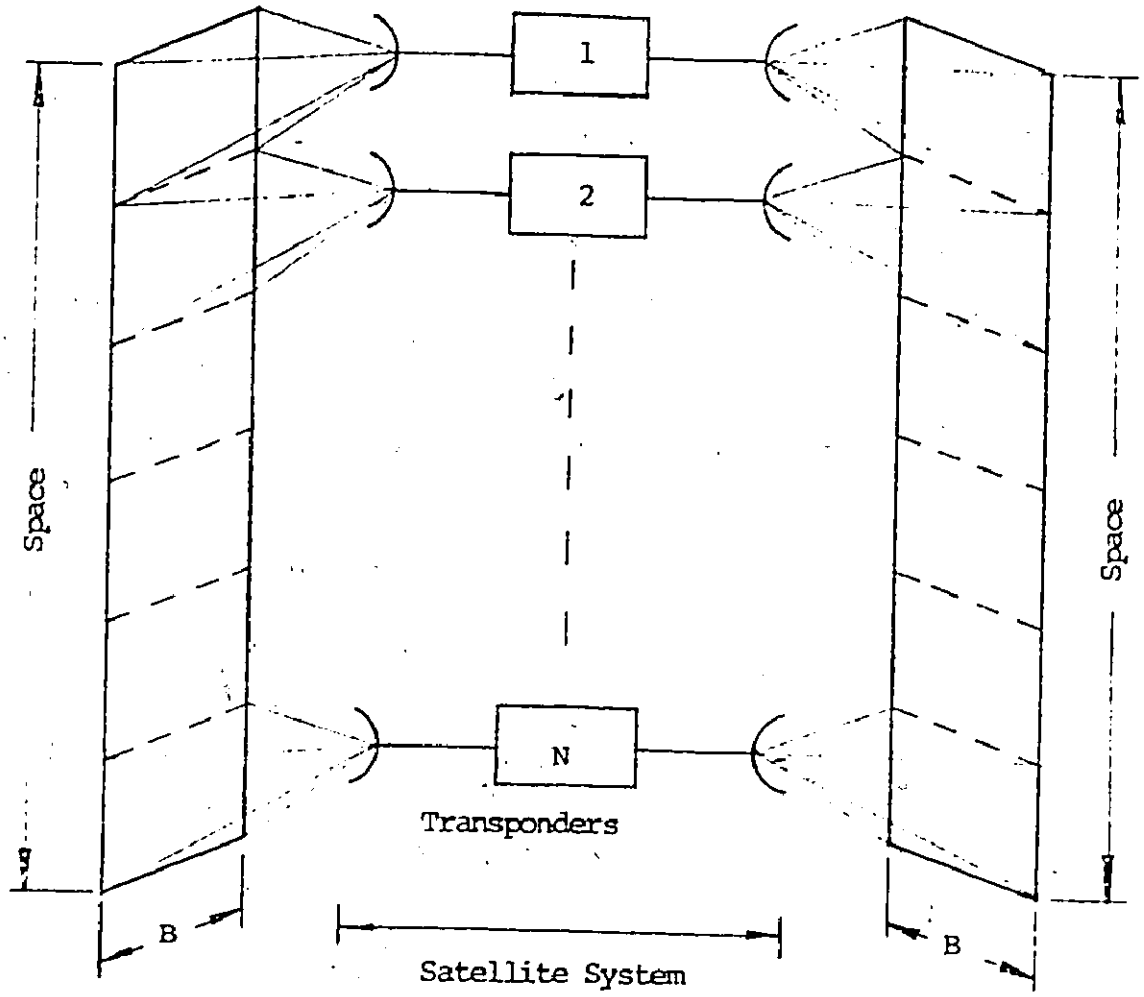

Fig. 1-3 Frequency spectrum reuse by employing multiple spot beam zone satellite antennas.

without requiring more power than one global beam of 1/N times the capacity [3].

To realize the benefits of spectrum reuse, SDMA must be combined with time division multiple access (TDMA) or frequency division multiple access (FDMA) [4], [9]. Multiple access by time division is accomplished by having each earth station transmit in time slots selected to eliminate signal overlap at the satellite input and this is usually achieved by the division of time into frames of length 125 μs. Multiple access by frequency division is a technique whereby each earth station transmits continuously in an assigned and distinct frequency band. If TDMA is used with SDMA, the satellite must carry high-speed electronic switching networks that can rapidly rearrange the connections among receiving and transmitting beams, and the system is then called space division multiple access/spacecraft switched-time division multiple access (SDMA/SS-TDMA). If FDMA is used with SDMA, filters, frequency converters and switches must be used to separate the received signals from each beam and recombine them in different arrangements for each transmitting beam [11], [12], and the resulting system is referred to as space division multiple access/spacecraft switched-frequency division multiple access (SDMA/SS-FDMA).

The SDMA/SS-TDMA system has advantages in that 1) the interconnectivity of all spot beam zones is provided at the satellite by a low weight, high-speed diode switching matrix, 2) only one carrier is amplified by each output travelling wave tube (TWT) amplifier in the satellite thus eliminating multiple-carrier intermodulation problems, and

3) a low power (5 to 10 W) output TWT amplifier can be used [1], [4], [9]. The main disadvantage of this system is that synchronization to the satellite switching sequence is required for all earth stations.

The only advantage of the SDMA/SS-FDMA system is that synchronization is not required. The disadvantages include 1) increased complexity and weight due to a network of filters, frequency converters and switches on-board the satellite, 2) decreased capacity due to the multiple-carrier intermodulation problems of the output TWT amplifier, and 3) requirement for a high power (20 to 50 W) output TWT amplifier to give linear amplification [4], [9]. Thus, for these reasons, the main effort in SDMA systems has focussed on the SDMA/SS-TDMA technique since increased complexity in the earth station can provide the necessary synchronization, and reduced complexity in the satellite increases its reliability.

As a consequence of the lower weight SDMA/SS-TDMA system, a more economical rocket launch is possible. Fig. 1-4 compares the beginning-of-life satellite weight versus the number of usable channels for SDMA/SS-TDMA and SDMA/SS-FDMA*. The former can be launched using an Atlas-Centaur rocket which costs about $14 million whereas the latter requires a Titan Centaur rocket which costs about $29 million per launch [13]. Thus, the SDMA/SS-TDMA system has a sizable economic advantage. For these reasons, no further discussion of the SDMA/SS-FDMA system is presented here.

---

*Private communication from W. G. Schmidt.

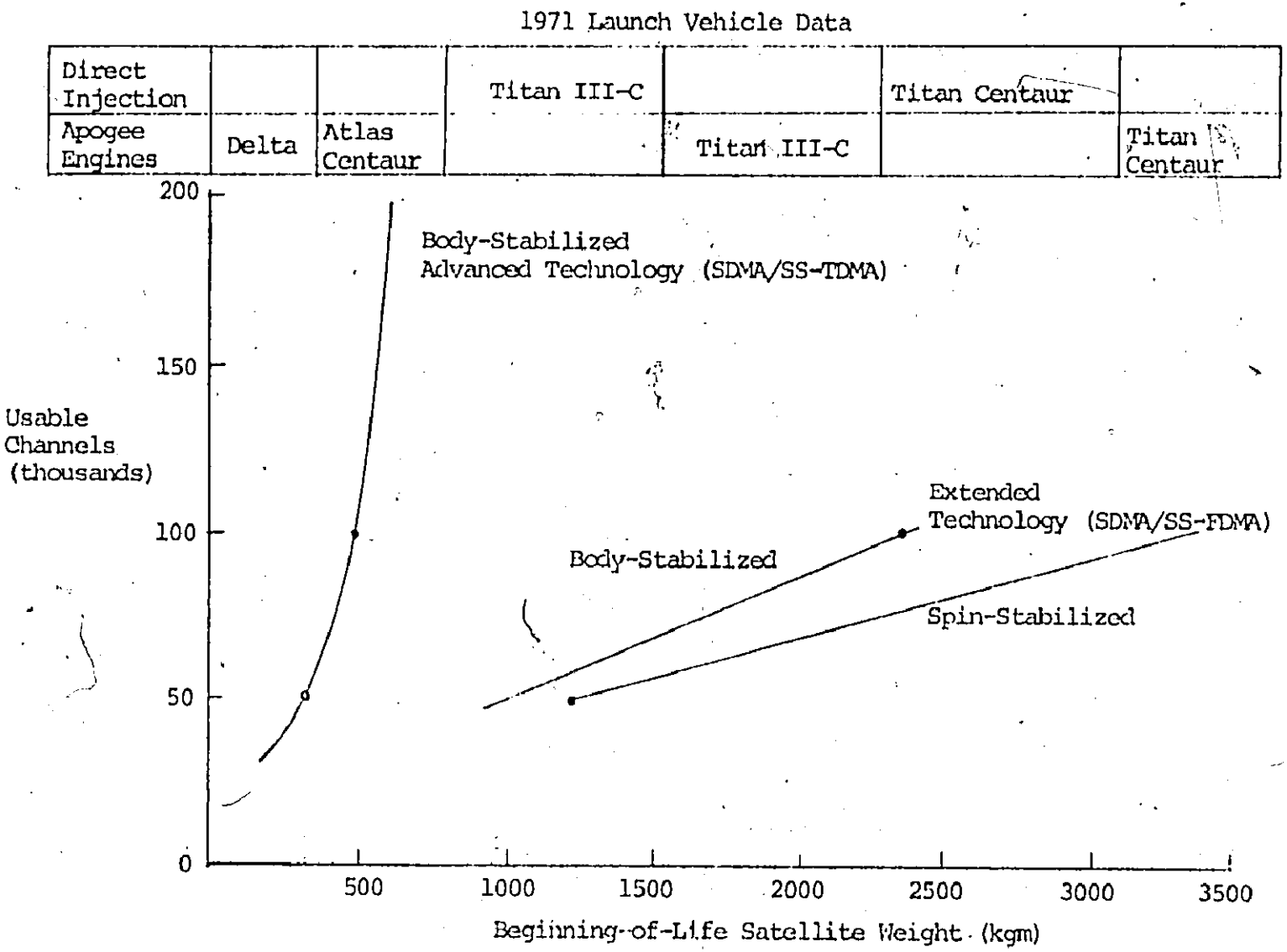

Fig. 1-4 Comparison of the launch weight of satellites using SDMA/SS-TDMA with those using SDMA/SS-FDMA.

Three different types of spot beam zone communications satellite systems are now briefly described. The first, developed by the Communications Satellite Corporation (COMSAT) Laboratories, is an SDMA/SS-TDMA system which requires all earth stations to transmit synchronization signals. Second, another SDMA/SS-TDMA system, developed by Kokusai Denshin Denwa (KDD) Laboratories in Japan, is described which provides an alternative to the COMSAT Laboratories system. Third, a spot beam zone system called the Communications Technology Satellite (CTS), which does not use a switch on-board the satellite (SDMA/TDMA), is described since a variation of the method used for synchronization in this system can be adapted to provide synchronization in the COMSAT Laboratories system. This adaptation is described in the thesis.

1.2 THE COMSAT SYSTEM

In the SDMA/SS-TDMA system studied by COMSAT, the satellite consists of a number of transponders all interconnected by a network called the SATSWITCH [6], [8], [14]. The SATSWITCH, shown in Fig. 1-5, is a digitally controlled microwave switching matrix which provides interconnections for the different spot beam zones and is controlled through a telemetry link by an earth station control center which programs and updates an on-board memory depending on user requirements. In order that earth stations transmissions reach the satellite at the proper time to be switched by the SATSWITCH, it is necessary to synchronize all earth stations to the satellite switching sequence and track the satellite

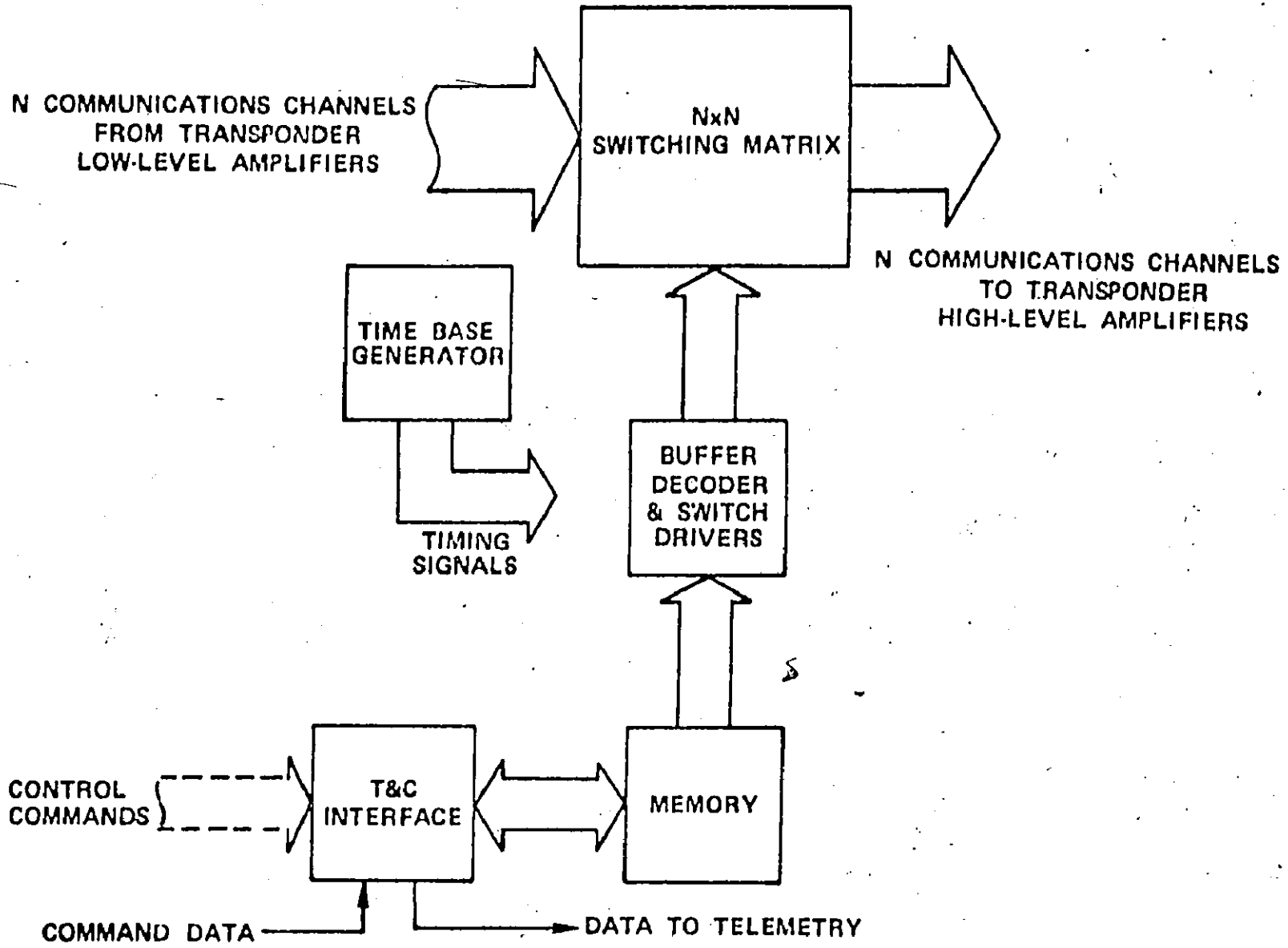

Fig. 1-5 Block diagram of the SATSWITCH

on-board clock, due to the varying range to the satellite and the clock instabilities.

Two different requirements exist for synchronization in a satellite system which employs SDMA/SS-TDMA [15], [16]. First, all stations in the system must be linked by a common reference which is controlled by the switching sequence of the satellite. This synchronization for the SDMA is necessary because it is the key to maintaining a proper time relation between the data burst trains of the uplinks and the switching operations which distribute these transmissions among the downlinks of each zone. The second form of synchronization required is for the TDMA of stations in each spot beam zone.

The switching sequence to the SATSWITCH is illustrated in Fig. 1-6 [14]. The first portion of the switching sequence, called the sync window, is a short duration connection in the SATSWITCH where each receiver which serves a spot beam zone is connected to the transmitter that serves the same spot beam zone [16]. Any signals arriving at the satellite in the interval are looped back toward the spot beam zone of their origin. Every spot beam zone has its own sync window and all sync windows occur simultaneously.

The portion of the frames between the sync windows is divided into data windows. A data window is the interval in a frame allotted to a data connection between one particular uplink spot beam zone and a particular downlink spot beam zone. For example, in Fig. 1-6, the first data window is used to transmit data from stations in spot beam zone no. 1 to stations in spot beam zone no. 2. Similarily, the second

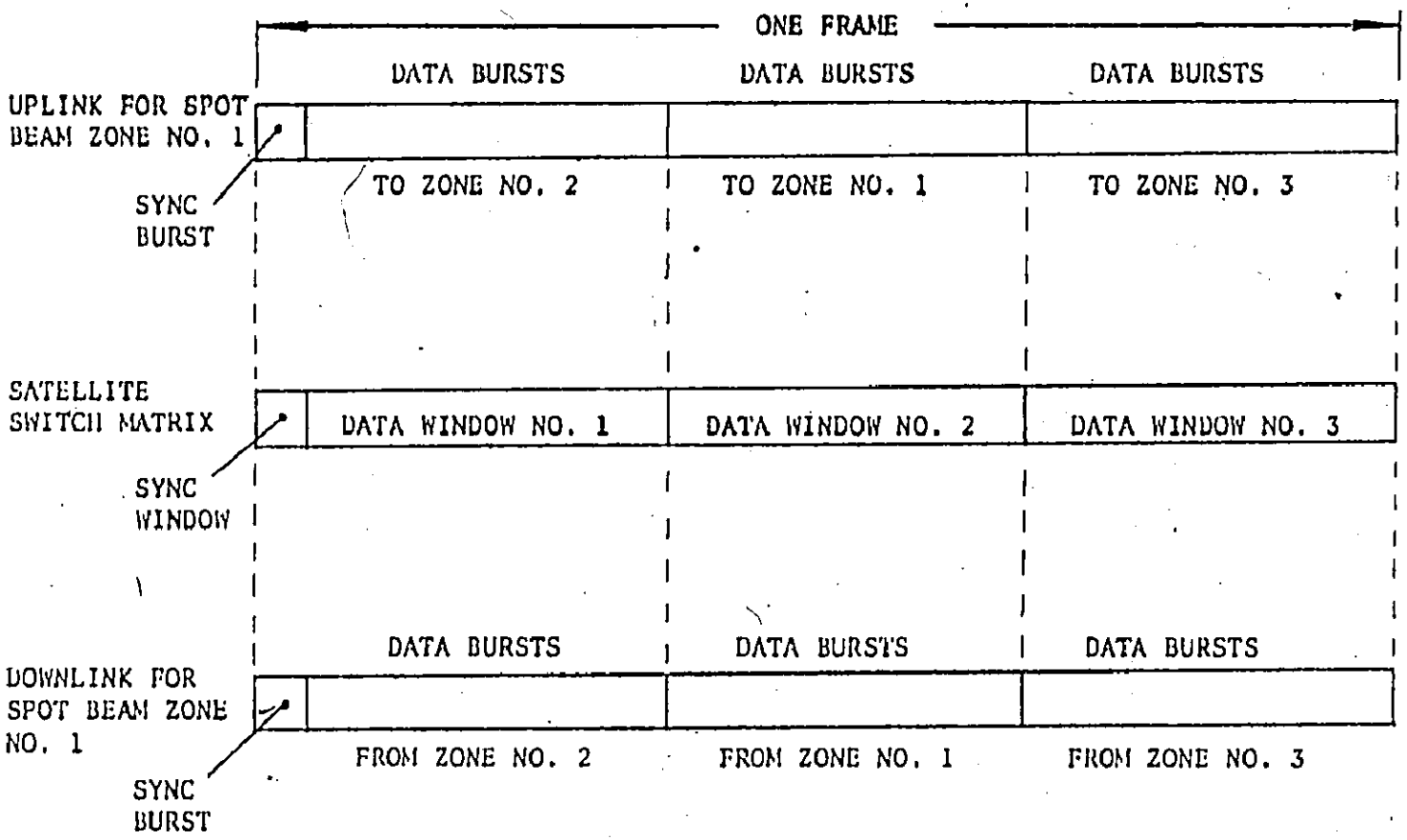

Fig. 1-6 Typical switching sequence at the satellite.

data window is used to transmit data from stations in spot beam zone no. 1 to other stations in spot beam zone no. 1. The necessity for precise synchronization now becomes obvious because data bursts must fall in the proper slots in the data windows, otherwise messages overlap and large numbers of errors can occur.

There has been some variation in the numerical values of the operating parameters of the satellite. For example, frame lengths of 125 μs, 250 μs and 750 μs have all been suggested as well as sync window durations ranging from 969 ns to 6 μs. Similarly, symbol rates from 200 MBd to 400 MBd have been mentioned. In Table 1-1, some typical satellite parameters are listed [5 - 9], [14], [16], [17].

1.3 THE KDD SYSTEM

Another technique for providing a high capacity SDMA/SS-TDMA communications satellite system is based on the use of the regenerative repeater, as suggested by Nosaka and Muratani of KDD Laboratories of Japan [18]. In the proposed satellite system, an earth station transmits a double differential encoded PSK (DDPSK) signal in burst mode and the satellite transponder regenerates this signal to an ordinary differential encoded PSK (DPSK) signal without the requirements of carrier and bit timing recovery.

The use of differential encoding eliminates the problems of carrier recovery at the satellite and back at the earth stations. To maintain the same bit error rate as conventional PSK, the signal power must be increased which can easily be accomplished in the uplink by simply

TABLE 1-1

Typical Parameter Values for the COMSAT System

Parameter	Value
Number of spot beam zones	8 to 14
Total number of stations	256 maximum
Stations per spot beam	10 to 20
Satellite bandwidth	200 to 400 MHz
Carrier freq. (uplink/downlink)	6/4 GHz, 14/11GHz, 30/20 GHz
Carriers per repeater	1
Spot beam zone beamwidths	1 to 4 degrees
Polarizations	2
Earth station G/T	40.7 dB
Voice channels per repeater	12,500
Maximum range rate variation	18 ns per round trip time
Frame length	125 μs to 750 μs
Number of data windows per frame	62 to 124
Sync window duration	969 ns to 6 μs
Timing stability of the satellite clock	0.3 parts in 10^{-8} per 0.3 s 1 part in 10^{-7} per day 1 part in 10^{-5} lifetime
Guard time	50 ns
Matrix switching time	20 to 50 ns

transmitting more power from the earth station.

The system, shown in Fig. I-7, comprises one receiver for each spot beam zone, a switching matrix operated by a control unit with telemetry and a transmitter for each spot beam zone. The DDPSK signal is detected in the receiver and fed through a hard limiter to the switching matrix operated by a control unit. The control unit is programmed using a telemetry link by an earth station to meet the varying traffic distributions.

A sync burst signal is supplied to each PSK modulator serving the spot beam zone, along with the demodulated data, and all PSK modulators are fed from a single high power oscillator controlled by a crystal oscillator. This configuration removes the output TWT amplifiers which are needed for each spot beam zone in the system proposed by COMSAT Laboratories thus reducing the weight of the satellite transponder and the power requirements.

Synchronization of earth station transmissions to the switching sequence of the satellite is achieved by generating the sync burst on-board the satellite which is then sent to all spot beam zones. The sync burst consists of demodulator synchronization bits (for bit timing recovery at the earth station) and a unique word. Earth station synchronization is achieved by comparing earth station transmissions with the transmitted sync burst from the satellite. Thus, the data signals can be transmitted to reach the satellite at the proper time so as to be rerouted to the appropriate spot beam zone by the switch matrix.

Essentially, this system provides approximately the same fade

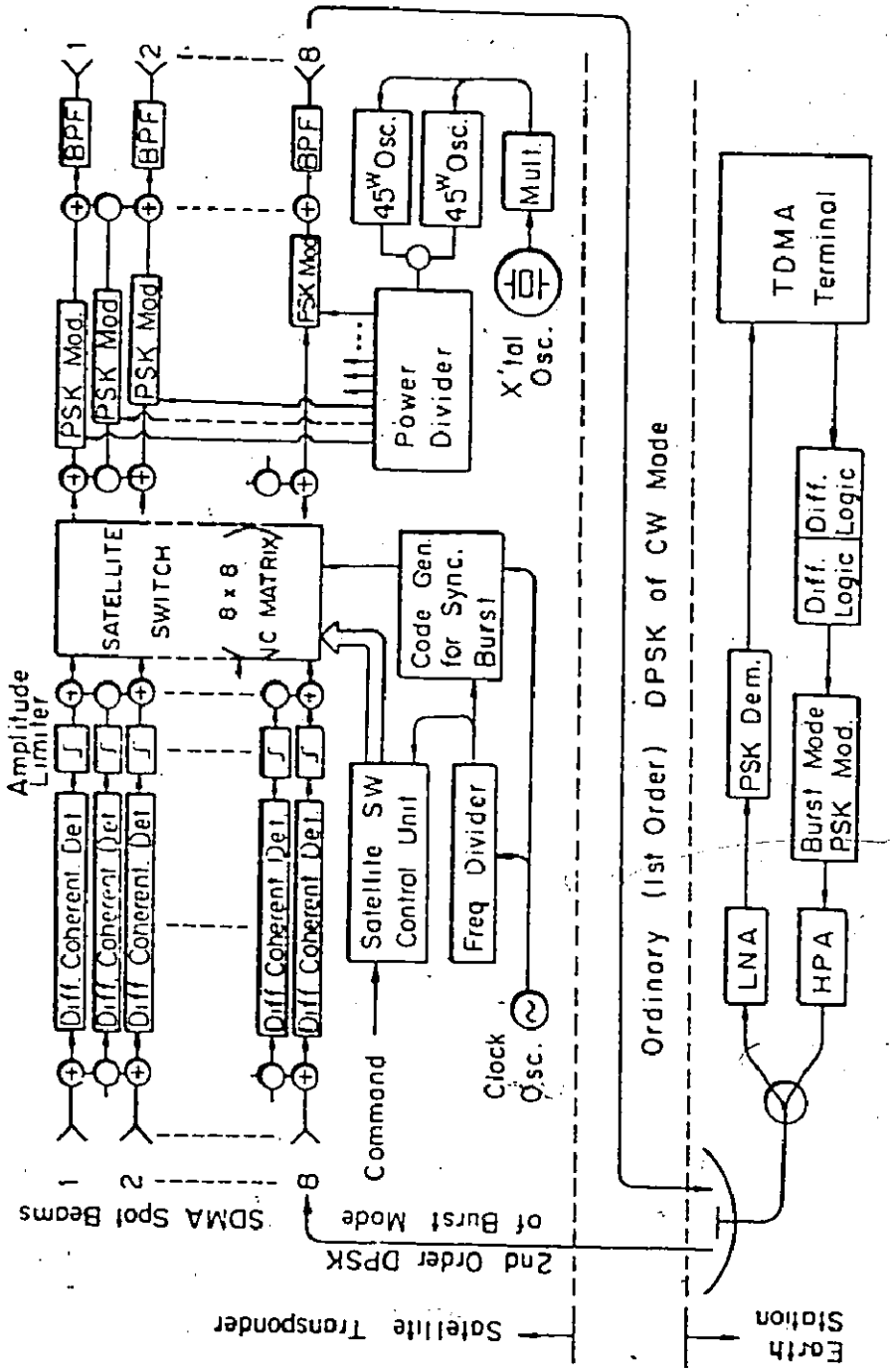

Fig. 1-7 Regenerative repeater with DDPSK.

margin as the COMSAT system but there is a large decrease in the weight since no TWT amplifiers are required. A summary of the system parameters is presented in Table 1-2. The main disadvantage of the system is the greatly increased satellite complexity due to the demodulators, and the difficulties of providing reliable high power, high speed PSK modulators. Such complexity is very undesirable on-board satellites since failures cannot be repaired.

TABLE 1-2

Typical Parameters for the KDD System

Parameter	Value
Number of spot beam zones	8
Satellite bandwidth	200 MHz
Carrier frequency	14 GHz uplink 11 GHz downlink
Spot beam zone beamwidths	1.4 degrees
Earth station G/T	40.0 dB
Voice channels per repeater	5000

1.4 THE CTS SYSTEM

The CTS project is a joint program between Canada and the United States to explore the application to satellite communication systems of developments in advanced technology [19-21]. A block diagram of the satellite to be launched in late 1975 is shown in Fig. 1-8A. The transponder has four 85-MHz passbands, two for transmitting in the 11.7 to 12.2 GHz band and two for receiving in the 14.0 to 14.3 GHz band, as shown in Fig. 1-8B. The satellite has two spot beam antennas having nominal 3 dB beamwidths of 2.5 degrees steerable on earth station command to point to any position within the earth's hemisphere visible from the satellite.

Signals received in the lower receive channel by the appropriate antenna are translated to the lower transmit channel and transmitted through the other antenna. The upper transmit/receive channel carries signals in the opposite direction. Hence, single hop communications is possible only between spot beam zones and not within a spot beam zone.

A synchronization scheme which is to be tested on the CTS system is the Processing Oriented Multiple Access (POMA) system which was developed by Canadian General Electric [22 - 26]. In this system, a control earth station broadcasts, over the satellite, start-of-frame synchronization bursts. Measurements of the position of the satellite are obtained at the control station by using three ranging stations. The transmitters of the ranging stations are synchronized to the control station by employing two-hop delay lock loops with error control being performed at the control station. The control station measures the loca-

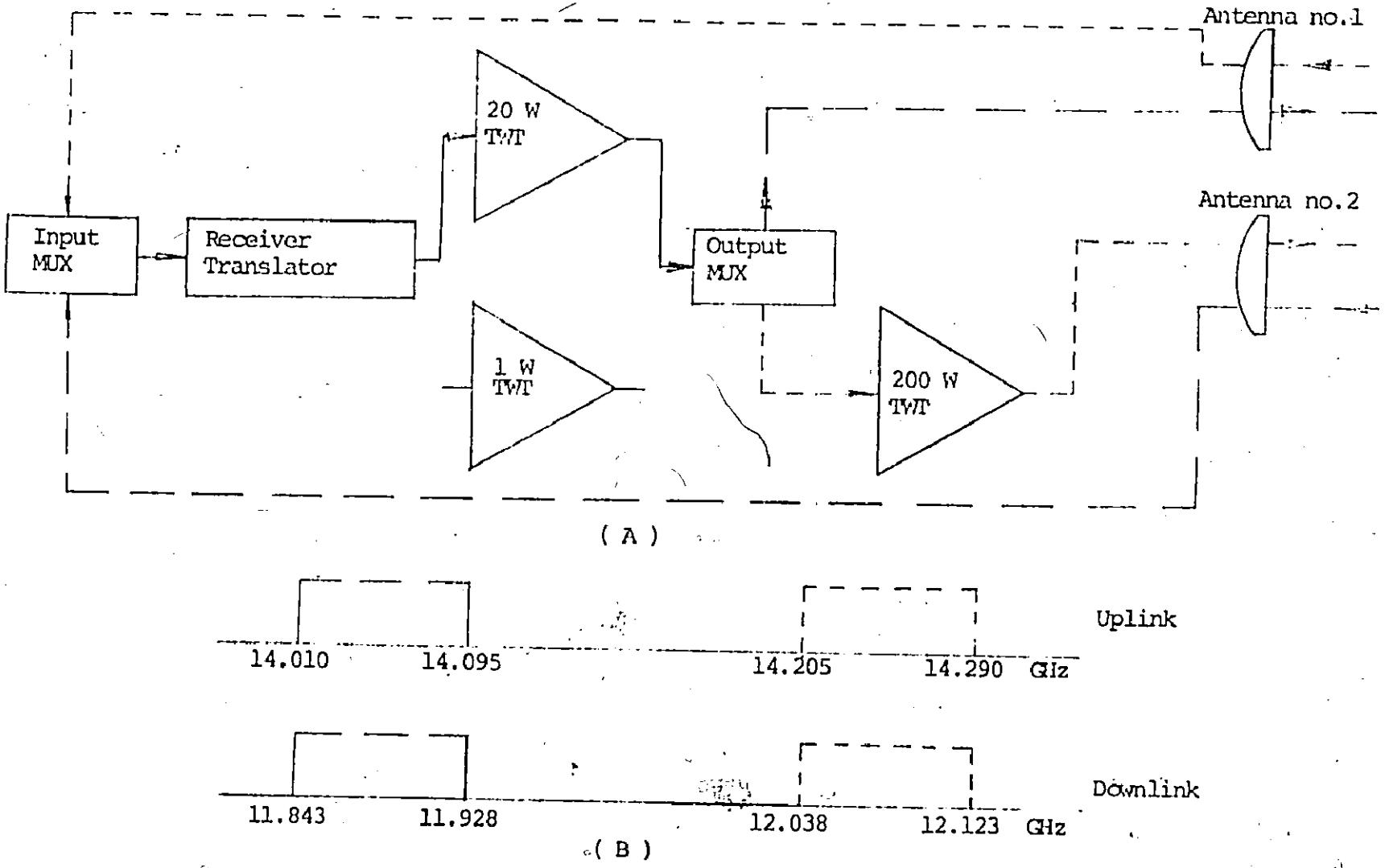

Fig. 1-8 (A) Block diagram of the CTS transponder, (B) frequency bands.

tion of the transmission from each ranging station with respect to a reference time, and sends suitably encoded instructions to change the timing of the ranging station transmitters until lock is achieved. These instructions contain the combined effective space delays in digital format. Any associated station can receive and interpret these four space delays and interpolate from them its own space delay. Thus, without ever transmitting any synchronization signals, any number of associated stations can achieve synchronization.

1.5 SCOPE OF THE THESIS

The problem of synchronizing earth stations to the switching sequence of the SDMA/SS-TDMA communication satellite system described by COMSAT Laboratories is examined in detail. System synchronization is discussed in Chapter 2 where two techniques for locking the time bases of all earth stations to the sync window of the satellite are described. It is shown that the synchronization signals from only three earth stations can provide all other stations with proper synchronization. Also, it is established that synchronization for an individual earth station can be separated into three distinct modes of operation called the coarse search mode, the fine search mode and the tracking mode.

In Chapter 3, three different methods for achieving coarse search synchronization are described. The first employs short duration signals called sync bursts, the second relies on PN-sequences and a correlation technique, and the third uses a new technique implemented through coded search signals.

The fine search mode is examined in Chapter 4. The synchronization loop is analysed assuming that the pertinent earth station transmits sync bursts which are modulated by the sync window. Results of this analysis show that a receiver configuration employing an integrator provides a set of error detection characteristics which relate an error voltage measured in the earth station to the timing error measured at the satellite. It is shown that the average timing error is reduced to zero with successive transmissions of sync bursts around the loop.

In Chapter 5, it is shown that the timing error due to constant velocity satellite motion can be eliminated by employing a tracking network. The tracking network uses an integrator which provides a small offset dc voltage.

A laboratory model, which closely approximates the physical model used in the theory, has been designed and constructed and is described in Chapter 6. The coarse search, fine search and tracking modes of operation are all included in this experimental study, and a provision which simulates satellite motion is described. A special coherent receiver has been built which uses a phase adjusting network and is specifically intended for pulsed signals of known frequency.

Chapter 7 provides the details of experiments which confirm the theoretical predictions of Chapters 3, 4 and 5.

Chapter 8 presents conclusions and suggestions for future work.

CHAPTER 2

System Synchronization

Possibly the most important factor in a SDMA/SS-TDMA system is the realization of an accurate and efficient method of synchronization for the total system. The switching satellite requires that each earth station synchronize its transmissions to the satellite switching sequence to communicate with other stations in the same spot beam zone or with stations in other spot beam zones. This requirement can be satisfied by using one of two possible satellite configurations.

2.1 SYSTEM WITH INDIVIDUALLY SYNCHRONIZED STATIONS

One method of achieving system synchronization is to require each station in the entire system to transmit its own synchronization signals thus obtaining synchronization independently of all other stations [15], [16], [17]. These signals are used to measure the timing relationship between the earth station time base and the satellite sync window. Synchronization signals, with certain characteristics as described in Chapter 3, are transmitted by the earth station and, after a one-way trip space delay, reach the satellite. The sync window returns the signals back to the spot beam zone of their origin by providing a rectangular amplitude modulation once per frame which can be used as a reference. Thus, the sync window modulated signals return to the earth station one round trip time after initial transmission. The earth station then performs the appropriate adjustment to its time base, again

transmits synchronization signals and the procedure is repeated.

In this system, several problems can arise which are described as follows:

(a) All synchronization signals emanating from a given spot beam zone must reach the satellite when sync windows occur. These signals may pass through the sync window at the same time, and thus, the sync window operates effectively in an FDMA mode. The inherent problems of FDMA, such as the non-linearity of the output TWT amplifier, may cause intermodulation if there are a large number of synchronization signals.

(b) Since each earth station in the system requires its own unique synchronization signals, there is a practical limit to the number of stations in the system due to the bandwidth restriction of the satellite.

(c) Each earth station estimates the timing relationship between its time base and the sync window independently of all other stations. Consequently, as the number of stations in the system increases, the guard time between data bursts will increase.

(d) There is always the possibility of an earth station losing synchronization and transmitting synchronization signals in data windows thus producing interference. More seriously, when synchronization is lost, data bursts are transmitted in the wrong data slots. This situation can remain undetected for one round trip time due to the propagation delay of synchronization signals, and the probability of this occurring increases with the number of stations.

(e) It is shown in Chapter 3 that whenever an earth station initially attempts to achieve synchronization, interference is generated which occurs in data windows. Consequently, in this system, every station generates interference when synchronizing.

2.2 SYSTEM USING THREE CONTROL STATIONS

System synchronization may be achieved by employing three different earth stations designated as control stations. Each such station is located preferably, but not necessarily in different spot beam zones. Each control station is initially required to lock to the sync window independently of the other control station; however, once this is accomplished, two of the control stations may be locked to the synchronization signals of the third control station.

The main advantages of the method using three control stations over the first method are that the five problems listed in Section 2.1 do not occur. However, there is increased complexity in the synchronization equipment of the earth stations and, a modified sync window connection (as described below) on-board the satellite, is required. Nevertheless, it is shown that the modified sync window provides a useful communications link between all spot beam zones which can be used not only for synchronization signals, but for other stationkeeping messages.

To achieve synchronization with a switching satellite system using three control stations, it is required that for the duration of the sync window, all satellite transmitters be connected to all satellite receivers. This produces total connectivity throughout the system for the sync window duration in that the synchronization signals from any one spot beam zone are transmitted to all spot beam zones. This new connection will be referred to as the modified sync window to distinguish it from the sync window connection used in the first method in which the transmitter of each transponder is connected to its own receiver for the sync window duration.

2.2.1 Spacecraft Switching Subsystem and the Modified Sync Window

The feasibility of the modified sync window connection can be examined by considering the spacecraft switching subsystem which consists of a microwave switching matrix (MSM) and a distribution control unit (DCU) as shown in Fig. 2-1A. The uplink beams and the downlink beams are interconnected in a programmable frame through the MSM under control of the DCU. Traffic flow data required to allocate capacity are stored in a small memory in the DCU and used to directly control the operation of the MSM.

The switching format may, for example, be organized into a 750 μs frame length which is divided into 125 6-μs segments [6]. This requires 125 words of 64 bits each, divided into 16 four-bit bytes. Thus, time within the frame may be allocated for traffic in 6 μs blocks. The first 6 μs interval in each frame is reserved for system synchronization in which the MSM is directed by the DCU to connect the transmitter of each transponder to its own receiver. This connection, called the sync window, allows earth stations to sequence lock their time bases to the switching sequence of the satellite by transmitting synchronization signals. These synchronization signals, arriving at the satellite after a one-way trip time delay, are modulated by the sync window and returned to the earth station after a further one-way trip time delay.

The MSM consists of a 16 by 16 array of PIN-diode switches implemented in a stripline structure [6]. Switch driver circuits, controlled through the DCU, are built into the array. Each of the 16 four-bit bytes from the DCU is applied to 1-of-16 buffer decoders, as

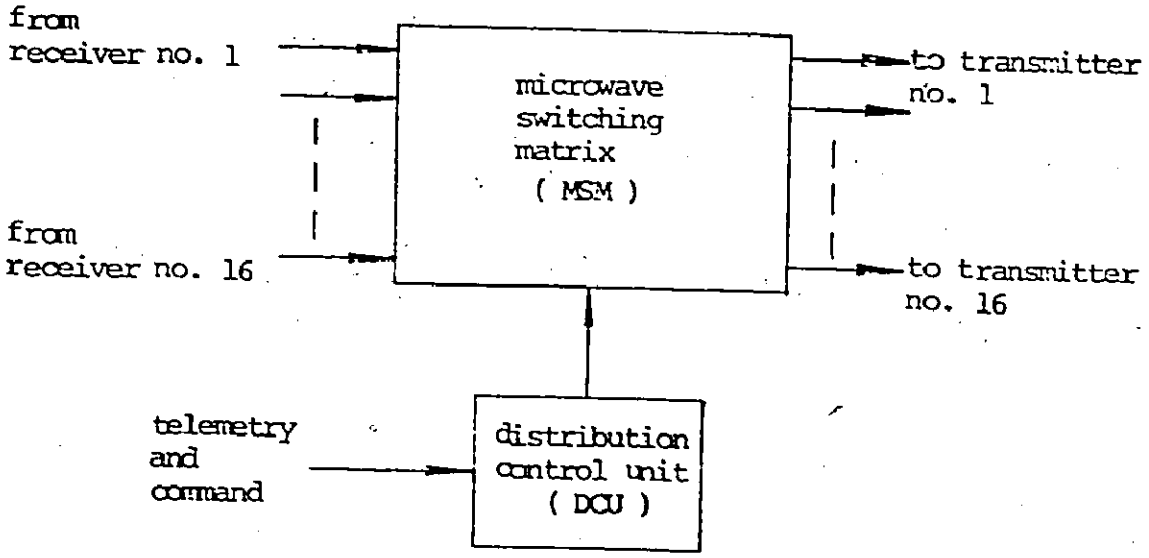

(A)

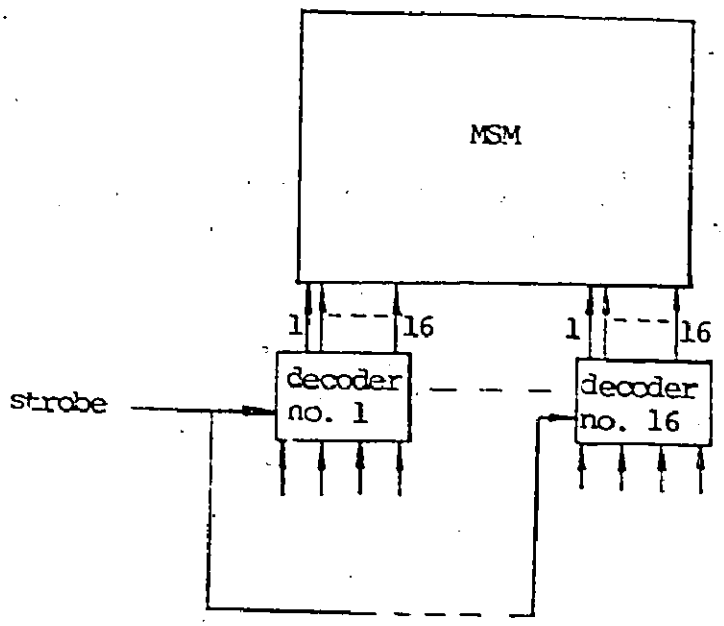

(B)

Fig. 2-1 Spacecraft switching subsystem. (A) Block diagram, (B) strobe for the modified sync window.

shown in Fig. 2-1B. Each buffer decoder is associated with a MSM array row and, consequently, one PIN-diode switch per row can be operated at a time.

It appears that the only change required to implement the modified sync window connection is that all PIN-diode switches in the MSM be closed simultaneously for the sync window duration. This causes all receivers to be connected to all transmitters, which interconnects all spot beam zones, and any synchronization signals reaching the satellite in this duration are sent to all earth stations in the system. The modified sync window could probably be achieved by simply applying a strobe to all the buffer decoders for the duration of the sync window, as illustrated in Fig. 2-1B.

By connecting all receivers to all transmitters, the uplink signal-to-noise ratio for any one spot beam zone is decreased by the number of receivers. However, it is the downlink signal-to-noise ratio which usually limits performance and this is unaffected by the modified sync window connection. Thus, the detection of synchronization signals at the earth station remains essentially unchanged by the modification.

2.2.2 Ranging and Synchronization

In the satellite system using three control stations, an earth station can achieve precise synchronization if two conditions are satisfied [23-26]:

(a) The range from the earth station to the satellite must be available.

(b) A reference signal passing through the modified sync window is required.

By advancing the time base of the earth station by twice the range time delay relative to the reference signal, the earth station transmitter is locked to the modified sync window of the satellite. Data transmissions can then take place, but the need for every earth station transmitting synchronization signals is eliminated.

The coordinates of the switching satellite can be calculated by determining the range to the satellite from each of three control stations of known position (not all colinear). The range measurements and separation distances between earth stations can be specified in terms of propagation delays which are more useful to the other earth stations wishing to achieve synchronization.

Consider Fig. 2-2 where the coordinate system has been located to define a plane specified by the three control stations at A, B and C. The coordinates of the satellite at S are (x,y,z) and the coordinates of an additional earth station at D are (x',y',z'). The distances l_1, l_2 and l_3 remain fixed since these are the spacings between stations at A, B and C (preferrably in different spot beam zones to increase distances and improve accuracy). Consequently, the coordinate values of x_1, z_1 and z_2 once determined remain fixed. These are given by solving the following three equations:

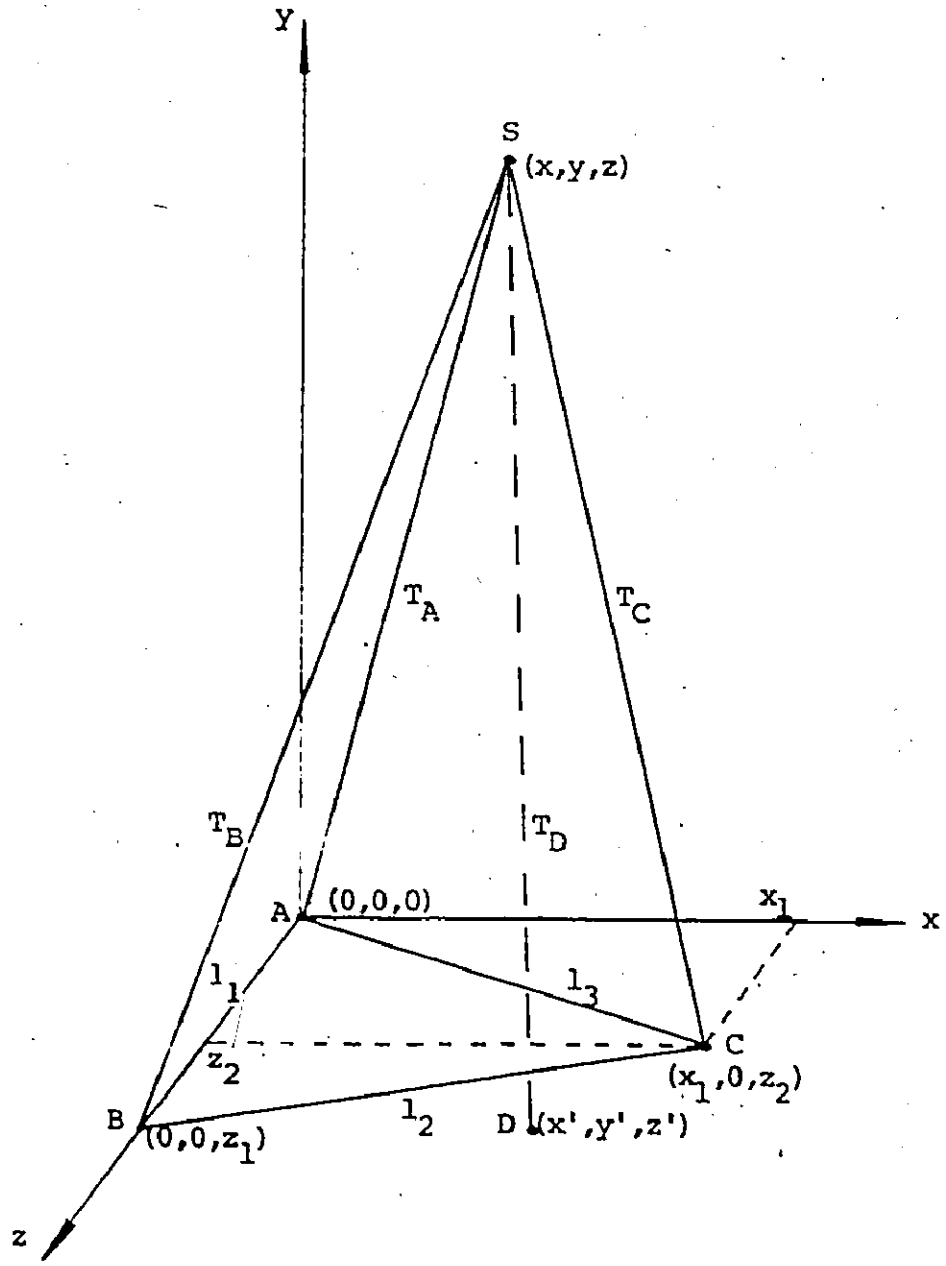

Fig. 2-2 Coordinate system showing the three control stations at A, B and C, earth station at D and satellite at S.

$$l_1 = z_1$$
$$l_2^2 = x_1^2 + (z_1 - z_2)^2 \qquad (2\text{-}1)$$
$$l_3^2 = x_1^2 + z_2^2$$

Thus,

$$z_1 = l_1$$
$$z_2 = \frac{1}{2}[l_1 + \frac{l_3^2 - l_2^2}{l_1}] \qquad (2\text{-}2)$$
$$x_1 = \{l_3^2 - \frac{1}{4}[l_1 + \frac{l_3^2 - l_2^2}{l_1}]^2\}^{\frac{1}{2}}$$

Expressed in terms of propagation delays, these coordinates then become

$$T_1 = z_1/c$$
$$T_2 = z_2/c \qquad (2\text{-}3)$$
$$T_3 = x_1/c$$

where c = velocity of propagation.

Now, it is possible to determine the coordinates (x,y,z) transformed to propagation delays (T_X,T_Y,T_Z) in terms of T_1, T_2 and T_3 and

the one-way propagation delays T_A, T_B and T_C. The equations are given by

$$\begin{aligned} T_A^2 &= T_X^2 + T_Y^2 + T_Z^2 \\ T_B^2 &= T_X^2 + T_Y^2 + (T_Z - T_1)^2 \\ T_C^2 &= (T_X - T_3)^2 + T_Y^2 + (T_Z - T_2)^2 \end{aligned} \tag{2-4}$$

The solutions for T_X, T_Y and T_Z can be obtained by solving (2-4), but the notation is simplified by solving for T_Z first, T_X second and T_Y last; thus,

$$\begin{aligned} T_Z &= \frac{1}{2}[T_1 + \frac{T_A^2 - T_B^2}{T_1}] = a_1 \\ T_X &= \frac{1}{2}[T_3 + \frac{T_A^2 - T_C^2 - T_2(2a_1 - T_2)}{T_3}] = a_2 \\ T_Y &= \{T_A^2 - (a_1^2 + a_2^2)\}^{\frac{1}{2}} \end{aligned} \tag{2-5}$$

The coordinates for station D are also fixed in relation to stations at A, B and C and can be represented by propagation delays as shown by

$$\begin{aligned} T_{X'} &= x'/c \\ T_{Y'} &= y'/c \\ T_{Z'} &= z'/c \end{aligned} \tag{2-6}$$

Hence, the propagation delay T_D can be calculated from

$$T_D = \{(T_X - T_{X'})^2 + (T_Y - T_{Y'})^2 + (T_Z - T_{Z'})^2\}^{\frac{1}{2}} \quad (2\text{-}7)$$

After each of the three control stations has independently locked to the modified sync window; the one-way propagation delays can be accurately measured. The value of T_A is determined by the station at A, the value of T_B is obtained by the station at B and the value of T_C is measured by the station at C. These values can easily be encoded with the transmission of appropriate synchronization signals.

When an earth station requires synchronization, the three signals giving values of T_A, T_B and T_C must be received. The value of T_D is deduced and the time base is locked to one of the three signals. A correction for satellite motion may also be applied. Finally, the transmitter timing is advanced by T_D relative to the reference and the station can then transmit data bursts. Since the modified sync window can be used to communicate with all stations in the system, a useful stationkeeping link is also provided.

2.3 THE BASIC SYNCHRONIZATION LOOP

The two methods which have been described in this chapter for achieving system synchronization in the COMSAT system have one basic feature in common. Both require that an earth station be able to lock to the sync window of the switching satellite. The problem to be resolved

is how to design the basic synchronization loop consisting of the transmitter of the earth station, the sync window of the satellite and the receiver of that same earth station connected together in a feedback control fashion. The various features of this basic synchronization loop are treated in detail in subsequent chapters. In so far as the operation of this loop is concerned, there will be no distinction made between the two methods described in Sections 2.1 and 2.2.

The synchronization procedure is separated into three separate modes called the coarse search mode, the fine search mode and the tracking mode. The coarse search mode provides an initial estimate of the timing relation between the earth station time base and the sync window, as described in Chapter 3. The fine search mode serves to reduce the initial timing error in a convergent series of steps, as shown in Chapter 4, and the tracking mode provides a means of eliminating timing errors caused by constant velocity motion, as depicted in Chapter 5.

It is noted here, however, without going into further details, that more complicated loops are coming into use. In particular, the CTS [19 - 23] will use a modified form of the three-control station system, synchronizing with a different loop arrangement. This arrangement can work with a transparent satellite because the signals of the loop can always pass through data windows so that this scheme does not require a special sync window.

CHAPTER 3

Coarse Search Mode

Initially, an earth station does not have synchronization. This means that the timing relationship between the earth station time base and the occurrence of sync windows at the satellite is not known at the earth station. This is illustrated by the model, shown in Fig. 3-1, where the space delay from the earth station to the satellite is unknown and the times at which the sync windows occur are also unknown. The first operation which must be performed is to obtain an estimate of the time at which a sync burst must be transmitted in order to reach the satellite at the correct time so as to pass through the sync window and, thus, be returned to the earth station. Three different methods which can be implemented are:

(a) sync burst method,

(b) PN-sequence method,

(c) coded search signal method.

The first two are described briefly and a detailed study of the third is presented.

3.1 SYNC BURST METHOD

Coarse search synchronization can be achieved by using sync bursts as originally suggested by Rapuano and Shimasaki [15], [16] who proposed the FSK sync burst and the coded-PSK sync burst. A sync burst

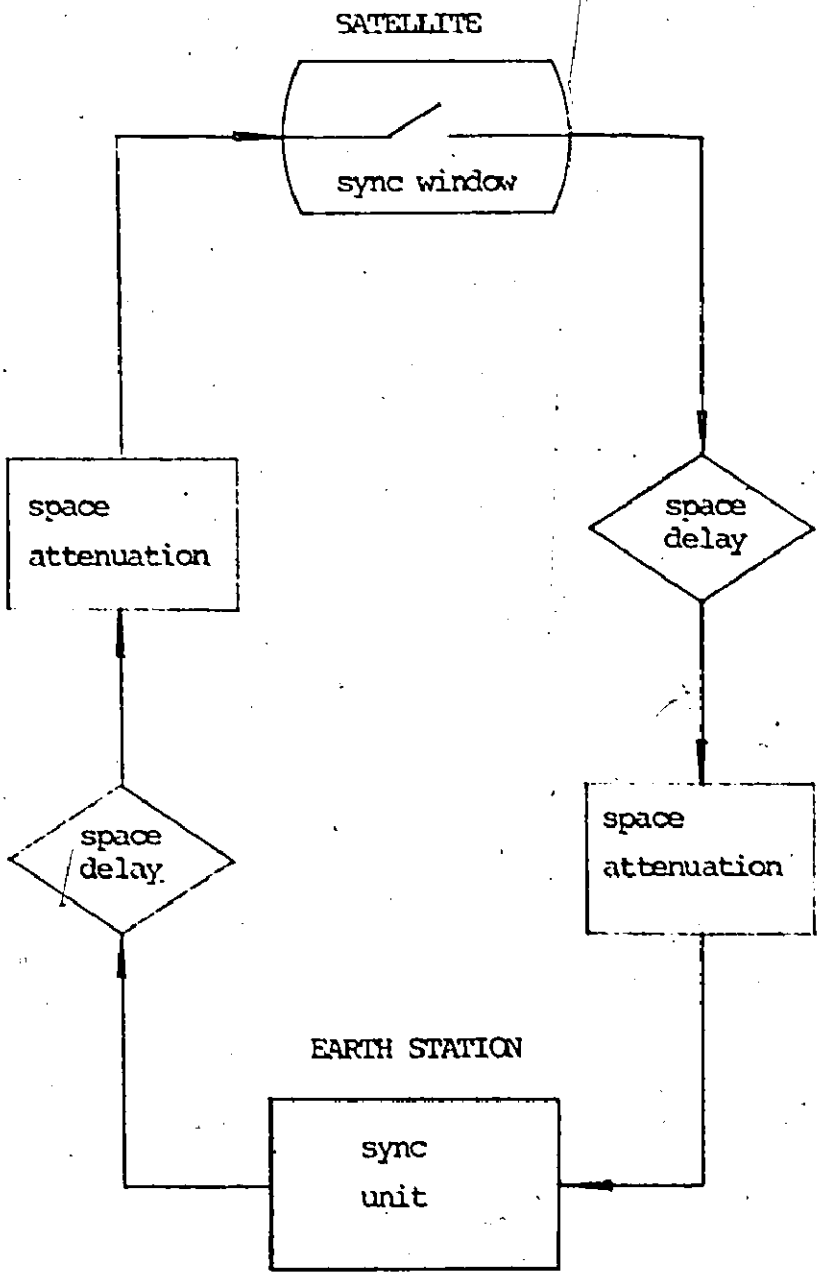

Fig. 3-1 Simplified synchronization loop model.

is a short duration signal which is longer than the sync window and, except for one case, has a built-in timing reference. Six possible candidates, including the two mentioned above, are shown in Fig. 3-2 [27]. The first is the ASK sync burst which is simply a pulse of carrier. It is the burst with no built-in reference mentioned above and it would be desirable to use one of the other sync bursts commencing with the fine search mode, as described in Chapter 4. Second is the coded-ASK sync burst which contains a code word and a metric. Third is the PSK sync burst consisting of two pulses of the same carrier but with different phase shifts, namely 0 degrees and 180 degrees. Fourth is the coded-PSK sync burst comprising a preamble, code word and metric. Fifth is the FSK sync burst which consists of two pulses of different carriers side-by-side. Sixth is the coded-FSK sync burst which also contains a code word and a metric. The list, summarized in Table 3-1, is similar to that presented in reference [17] although the ASK sync burst was not included there. Also, the coded-FSK sync burst was independently derived here. Spectrum requirements are described in Appendix A.

Briefly, any earth station in the system achieves synchronization by transmitting a train of one of these types of sync bursts having a unique feature identified with that station such as frequency for the ASK, PSK and FSK sync bursts or code words for the coded-ASK, coded-PSK and coded-FSK sync bursts. If by chance the train of sync bursts arrives at the satellite when a sync window occurs, the bursts are modulated by the window, as shown in Fig. 3-3, and returned to the earth station after one round trip time of approximately 270 ms. Except for this case which has a probability of less than $(2T_p + T_W)/T_F$, where T_p is the sync burst

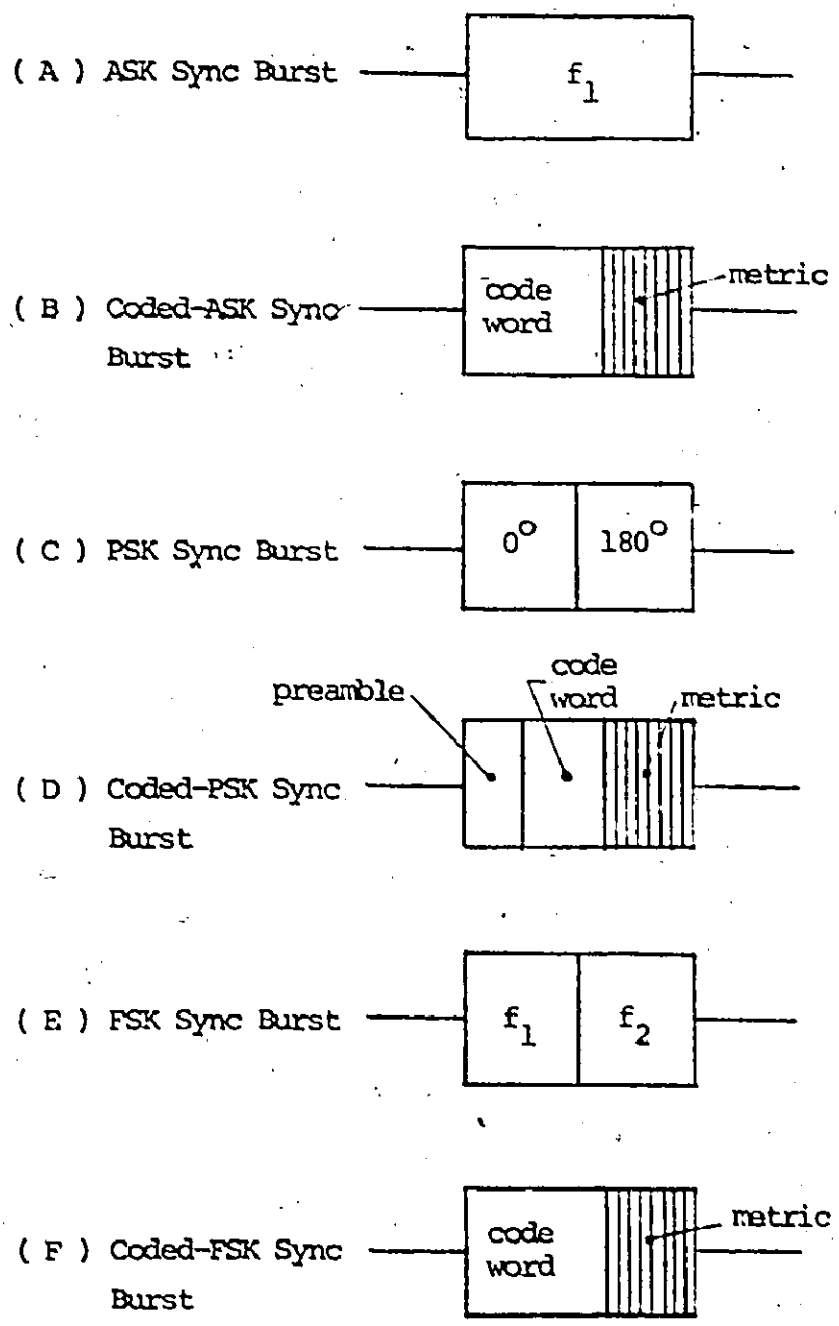

Fig. 3-2 Different types of sync bursts.

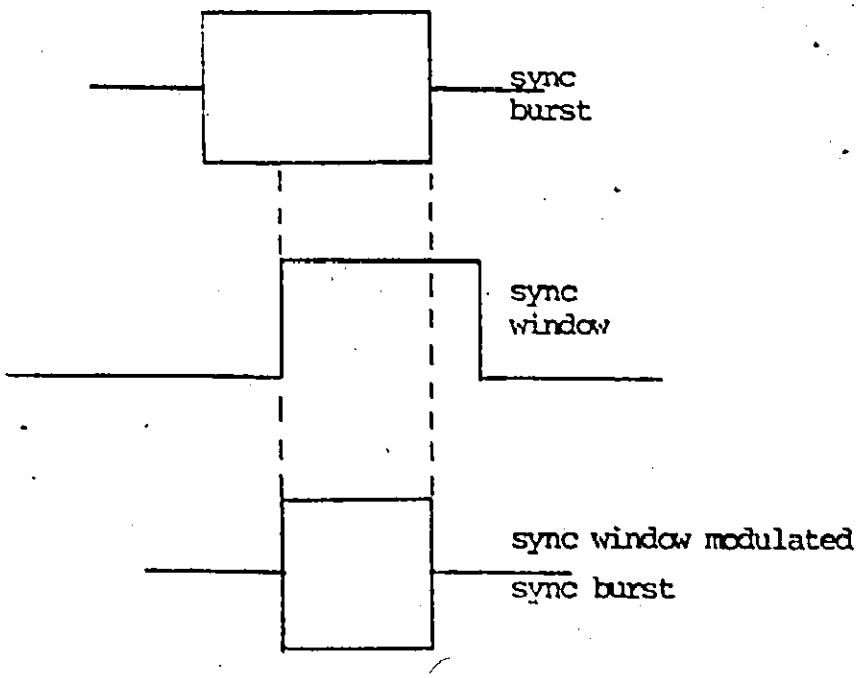

Fig. 3-3 Sync window modulation of sync bursts.

TABLE 3-1

Different Types of Sync Bursts

Keying	Sync Burst	Reference
ASK	ASK sync burst	[27]
	coded-ASK sync burst	[17]
PSK	PSK sync burst	[17], [28], [29]
	coded-PSK sync burst	[16], [17]
FSK	FSK sync burst	[16], [17]
	coded-FSK sync burst	[17], [27], [28]

duration, T_W the sync window duration and T_F the frame length, no sync bursts are received at the earth station. For $T_P = 2\ T_W$ and $T_F = 125\ T_W$ [29], this probability is only 0.04. Thus, after a delay of one round trip time, the earth station increments a system clock by a small amount equal to approximately the sync window duration for the ASK, PSK and FSK sync bursts and a fifth of this amount for the coded-ASK, coded-PSK and coded-FSK sync bursts [16] and repeats the procedure until the sync bursts pass through the sync window. In the worst case, incrementing is required for the total duration of the frame length.

The time required to achieve synchronization using the sync burst method can be estimated from the acquisition time given by [30]

$$T_{ACQ} = M(2T_D + T_{GP}) \qquad (3\text{-}1)$$

where M is the smallest integer satisfying the relation $M > T_B/T_{IN}$ and

T_B = the time difference at the satellite between the arrival of the first sync burst and the occurrence of the next subsequent sync window,

T_{IN} = increment time,

$2T_D$ = round trip propagation time,

T_{GP} = earth station processing time.

Figure 3-4 shows T_{ACQ} versus T_B. It is seen that coarse search synchronization with the ASK, PSK and FSK sync bursts is much faster than with the coded-ASK, coded-PSK and coded-FSK sync bursts. Also, higher ratios of frame length to sync window duration require proportionately more time.

An estimate of the bandwidths required for these different sync bursts can be obtained by considering the bit rates used in their construction. Table 3-2 shows typical values assuming a 125 μs frame length and a 1 μs sync window duration. The bit rates for the 750 μs frame length, 6 μs sync window are one-sixth of these values. The ASK sync burst provides the narrowest bandwidth while the coded-ASK, coded-PSK and coded-FSK sync bursts require the largest bandwidth. It is also possible to amplitude modulate the PSK and FSK sync bursts to modify their spectral shapes. This will be described in more detail in Chapter 4.

There are several advantages to using the narrowband sync bursts in that less transmission power is required for the same signal-to-noise ratio at the output of the earth station receiver. The lower power

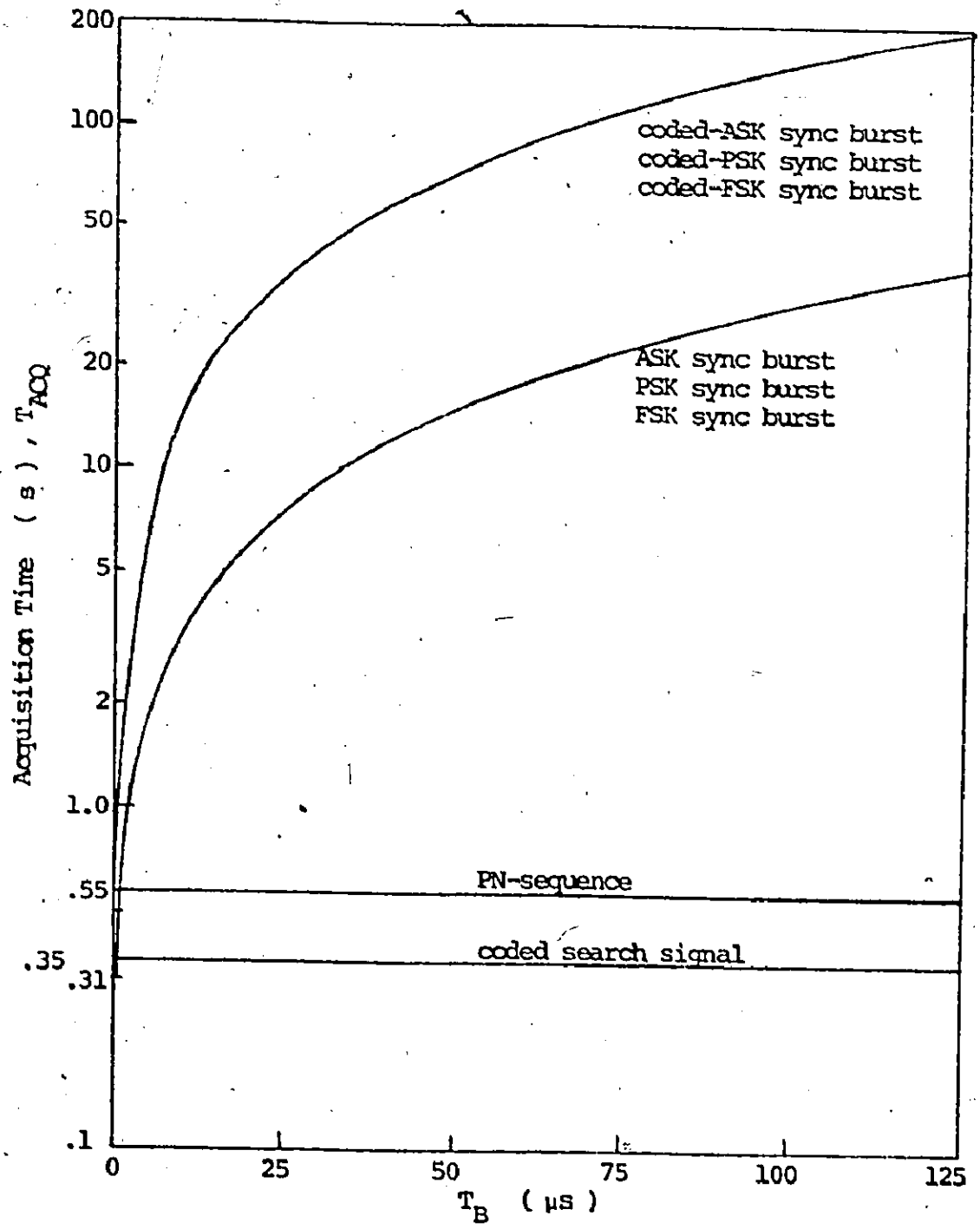

Fig. 3-4 Comparison of acquisition times for various methods of coarse search synchronization.

TABLE 3-2

Sync Burst Parameters for the 125 μs Frame Duration

Sync burst	Sync Acquisition Time	Bit Rate	Average Interference Duration	
			25 pulse train	continuous train
ASK	310 ms to 40 s	1 Mb/s	3.1 ms	320 ms
PSK	310 ms to 40 s	2 Mb/s	3.1 ms	320 ms
PSK	310 ms to 40 s	4 Mb/s	3.1 ms	320 ms
coded-ASK*	310 ms to 200 s	32 Mb/s	7.8 ms	800 ms
coded-PSK*	310 ms to 200 s	32 Mb/s	7.8 ms	800 ms
coded-PSK*	310 ms to 200 s	32 Mb/s	7.8 ms	800 ms

* The bit rate of these sync bursts is determined mainly by the metric comprising pulses of 31 ns duration.

signals will be in a more linear portion of the satellite output TWT amplifier curve during the sync window and, thus, cause less interference for other sync bursts in the sync window due to non-linear amplification. Also, the lower power levels cause less interference when sync bursts fall in data windows.

There is a problem of interference due to sync bursts falling in data windows during the search. On the average, synchronization using the ASK, PSK and FSK sync bursts will require about 20 s and the coded-ASK, coded-PSK and coded-FSK will require about 100 s. Hence, these bursts will be falling in data windows during these intervals causing interference. The average interference duration can be determined by the relation

$$T_{IF} = \frac{\frac{1}{2} N_P T_P T_F}{T_{IN}} \qquad (3\text{-}2)$$

where N_P is the number of pulses in each transmitted train.

Assuming 25 pulses per train, $T_P = 2\ T_W$, $T_F = 125\ \mu s$ and $T_{IN} = T_W$, the value of T_{IF} is 3.1 ms for the ASK, PSK and FSK sync bursts. For the coded-ASK, coded-PSK and coded-FSK sync bursts, assume $T_P = T_W$, $T_F = 125\ \mu s$ and $T_{IN} = 0.2\ T_W$. A 25 pulse train of these sync bursts produces a value for T_{IF} of 7.8 ms. The average interference duration for a continuous train of sync bursts is given by $T_{ACQ} T_P / T_W$ which is approximately two orders of magnitude higher than the values for the sequence of 25 pulse trains. Values for the average interference duration are summarized in Table 3-2.

Clearly, the ASK, PSK and FSK sync bursts are superior to the coded-ASK, coded-PSK and coded-FSK sync bursts because of simplicity, reduced acquisition time, smaller bandwidth requirement, lower transmission power and reduced interference.

A problem which arises with this method of synchronization is the possibility of an earth station locking to its own data window instead of the sync window [17]. The first train of sync bursts received at the earth station may have either passed through the sync window or a data window. If no data window is assigned for communications amongst earth stations in a given spot beam zone, then no problem occurs. However where such a data window does occur, the probability of initially locking to the data window is $T_{DATA}/(T_{DATA} + T_W)$ where T_{DATA} is the length of time provided for the data window. Since data windows are usually much longer than the sync window, this outcome appears to be quite likely. Thus, if the earth station determines that lock to the data window has been obtained, then the search must once again begin.

3.2 PN-SEQUENCE METHOD

Coarse search synchronization can be accomplished in approximately 550 ms (see Fig. 3-4) by continuously transmitting a PN-sequence of duration less than the sync window with the frame period being an integer multiple of one PN-sequence period [31]. When this signal reaches the satellite, the sync window modulates one PN-sequence and transmits this signal back to the earth station where a delay-lock-loop is used to synchronize to the sync window modulated PN-sequence. After lock has been achieved, the successive transmitted PN-sequences can be assigned

different burst phase numbers by modulating each PN-sequence with its assigned number coded in binary form. After one round trip time, the earth station can thus identify the PN-sequence which passes through the sync window by decoding the binary number.

There are an integral number of PN-sequences in a frame length, thus the burst phase number identifies the timing relation between the earth station time base and the sync window. This aspect of the method is similar to the coded search signal method which is described in detail in the next section.

The bandwidth of the transmitted signal can be estimated by noting that the burst phase numbers require at least 7 bits which must be contained in one sync window duration for a ratio of frame length to sync window duration of 125. Thus, for the 1 μs sync window, the bit rate is 7 Mb/s. Since the signal is transmitted continuously, the average interference duration is 550 ms.

3.3 CODED SEARCH SIGNAL METHOD

Coarse search synchronization can be achieved in approximately one round trip time, independent of the frame length, by using a coded search signal of duration at least equal to the frame length [28], [29], [30], [32]. The coded search signal provides a sufficiently good estimate of the relationship between the sync window and the earth station time base so that a train of sync bursts can then be transmitted at the proper time in order to pass through the sync window.

The required relationship may be found on an absolute time basis by considering the following three parameters:

(a) The transmission time delay between the earth station and the satellite T_D.

(b) The time difference between the arrival of the leading edge of a transmitted signal (from an earth station) at the satellite and the occurrence of the first subsequent sync window T_S.

(c) The frame length of the satellite switching sequence T_F.

Typically, the value of T_D is of the order of 135 ms with a small variation due to the motion of the satellite. The value of T_S may fall anywhere between zero and T_F. The value of T_F is determined by a stable oscillator on-board the satellite and, as a result, its expected value $\hat{T}_F$ would normally be known to within 1 part in 10^5 over the lifetime of the satellite [8].

It will be shown here that values for T_D, T_S and T_F can all be deduced at the earth station by transmitting a suitably encoded signal called the coded search signal, illustrated in Fig. 3-5. This signal consists of two parts the first being a carrier of duration $T_C \geq 2\hat{T}_F$ (but not necessarily a multiple of $\hat{T}_F$) and the second a sync sentence structure of duration $\hat{T}_F$ or a multiple thereof. The carrier is used to accurately measure the value of T_F and the sync sentence provides an estimate of T_S. The value of T_D is obtained by calculation; however, earth station synchronization can be achieved by determining T_S and T_F but not necessarily T_D since only the relative timing relationship between the earth station time base and the sync window is required.

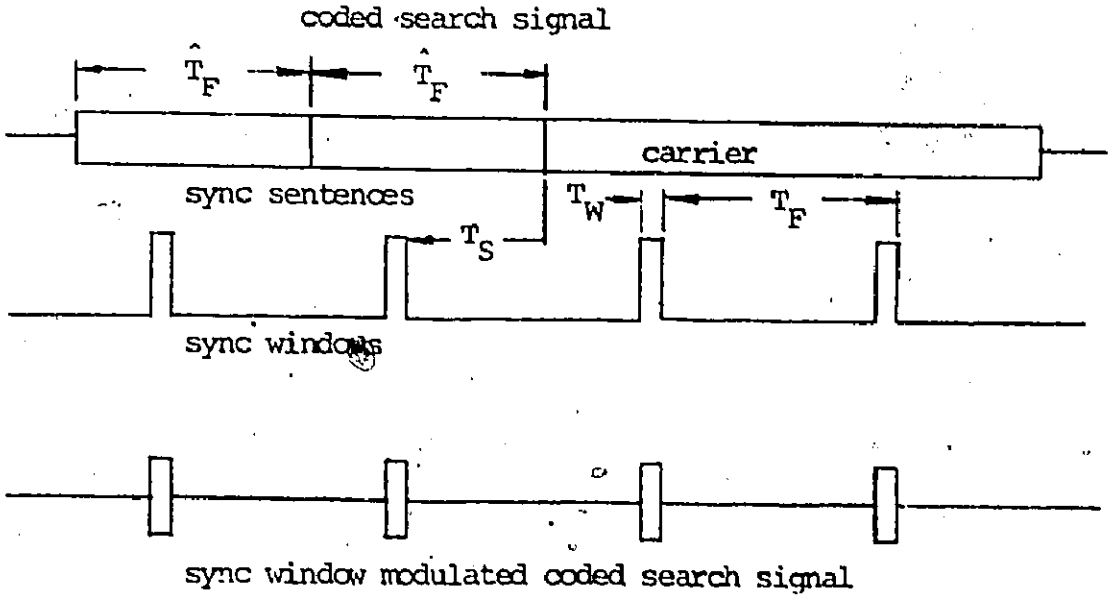

Fig. 3-5 Coded search signal and sync window modulation.

3.3.1 Single Frame Sync Sentence

(a) Timing Relationships

Assume the leading edge of the coded search signal (carrier portion) is transmitted at time T_1. At time $T_1 + T_D$, the leading edge reaches the satellite and, after a period between zero and T_F, a sync window of duration T_W occurs, as shown in Fig. 3-5, modulating the carrier portion of the coded search signal, i.e., passing a pulse of length T_W from the receiver to the transmitter (The sync window duration is controlled by the stable oscillator on-board the satellite; thus, the ratio T_F/T_W is always a known constant). Depending on the length of the carrier portion of the coded search signal, a train of pulses of carrier is produced with interpulse spacing T_F and the total number of pulses, J, is bounded by

$$2 \leq J < \frac{T_C}{T_F} + 1 \qquad (3\text{-}3)$$

At time $T_2 \geq T_1 + 2T_D$, the first pulse of carrier reaches the earth station and at times $T_3(N) = T_2 + NT_F$, where N is an integer, successive pulses of carrier are received so that T_F can be calculated from the relation

$$T_F = \frac{1}{N}(T_3(N) - T_2) \qquad (3\text{-}4)$$

Carrier lock for decoding pulses of the sync sentence can be obtained from these pulses.

The leading edge of the sync sentence, transmitted at time $T_4 = T_1 + T_C$, reaches the satellite at time $T_4 + T_D$, and at a time T_S later, the sync window modulates the sync sentence portion of the coded search signal producing a pulse. At time $T_5 = T_4 + 2T_D + T_S$, this pulse reaches the earth station where the time difference between T_4 and T_5 is given by

$$T_R = T_5 - T_4 = 2T_D + T_S \qquad (3\text{-}5A)$$

or

$$T_D = \frac{1}{2}(T_R - T_S) \qquad (3\text{-}5B)$$

The value of T_S can be measured by employing a suitable type of sync sentence as will be shown below and consequantly, the value of T_D can be calculated.

Finally, there remains only the problem of predicting the time at which the first pulse of a train of sync bursts with interpulse spacing T_F, should be transmitted in order to pass through the sync window. This predicted time, T, which would be calculated at the earth station by time T_6, say, can be related to either the transmission time T_4 or to the time at which one of the sync window modulated carrier pulses is received, $T_3(N)$. Specifically, the value of T is given by

$$T = T_4 + T_S + P\,T_F \quad ; P = \text{integer} \qquad (3\text{-}6A)$$

or

$$T = T_3(N) - 2T_D + Q\,T_F \quad ; Q = \text{integer} \qquad (3\text{-}6B)$$

The values P and Q are selected prior to transmission of the coded search signal to ensure that the condition $T > T_6$ is satisfied.

The error in the value of T must be small compared to the sync window duration, otherwise, little or none of the sync burst signal would be passed by the sync window. The main source of error in determining T arises from the value of T_F since any error in T_F is multiplied by either P or Q. In practice, typical values for P and Q are of the order of 2500. Consequently, for accurate values of the prediction time T, the error in the product terms $P\,T_F$ or $Q\,T_F$ must be small compared to a sync window duration. This can be achieved by using a sufficiently long carrier portion of the coded search signal so that the time difference in (3-4) is large. For example, an error of $\pm$ 20 ns in the measurement of T_F over a 50 ms duration of carrier results in an error in T of approximately $\pm$ 120 ns. This error would cause no difficulty if the PSK or FSK sync burst were used for the fine search mode since these sync bursts are similar and the FSK sync burst has a pull-in range of $\pm$ 800ns [16].

Since (3-6A) is independent of T_D, coarse search synchronization can be achieved by measuring T_S and T_F without having to determine T_D. By using this type of coded search signal, synchronization can be acquired theoretically in one round trip time (which is typically 270 ms) plus the coded search signal length and a small processing delay for an estimated total of approximately 350 ms, independent of the frame length (see Fig. 3-4).

The average interference duration of the coded search signal is essentially the length of the carrier portion which may be of the order of 50 ms. However, this method is the only method which does not rely on a priori knowledge of the frame length. Neither the sync burst method nor the PN-sequence method will provide coarse search synchronization unless an accurate value for T_F is available at the earth station. Of course, T_F can be obtained in a separate measurement by transmitting carrier as described in this section.

(b) Fast Synchronization

If the value of T_F is accurately known at the earth station, then the carrier portion used to measure T_F may be greatly reduced in length or possibly eliminated entirely. Furthermore, the problem of determining the value for T using either (3-6A) or (3-6B) can also be simplified.

Assume that, at the earth station, there is a high-stability oscillator driving a binary counter, a decoder having a reset feature, and that the interpulse spacing of the output pulses is T_F. When the leading edge of the sync sentence is transmitted at T_4, the counter is reset. Upon reaching the satellite the sync window modulates the coded search signal and transmits a pulse of the sync sentence back to the earth station. The value of T_S can be measured by employing a suitable encoded type of type sentence as described below.

Finally, it is possible to determine the time at which a train of sync bursts should be transmitted to pass through the sync window. This predicted time can be related to the transmission time T_4 by

(3-6A). But the values of $T' = T_4 + PT_F$, for different P, are just the times at which pulses are appearing out of the decoder fed by the earth station oscillator and binary counter. Thus, if the counter is fed to one side of a comparator, and T_S is loaded into the other side of the comparator, the comparator equality output pulse can be used to reset the counter, and pulses from the decoder will thence mark the times at which sync bursts should be transmitted so as to pass through the sync window. Hence, coarse search synchronization is achieved in one round-trip time of approximately 270 ms, independent of the frame length.

(c) Measurement of T_S

The value of T_S can be measured by employing either a coded sync sentence structure or an FM sync sentence, as shown in Fig. 3-6. The coded sync sentences can be further divided into the null/code-word type and the signal/code-word type as described below.

(i) Null/Code-Word Sync Sentence

The null/code-word sync sentence contains a set of code words separated by nulls. The nulls are used to provide a marker to indicate the beginning of a code word. Two types of code word which can be used are the PSK code word where bits of information are encoded as zero degrees and 180 degrees, and the FSK code word where the bits are encoded using two different frequencies. Carrier lock for the PSK code words is provided by the sync window modulated carrier portion of the coded search signal as mentioned above. The code words are numbers in binary form

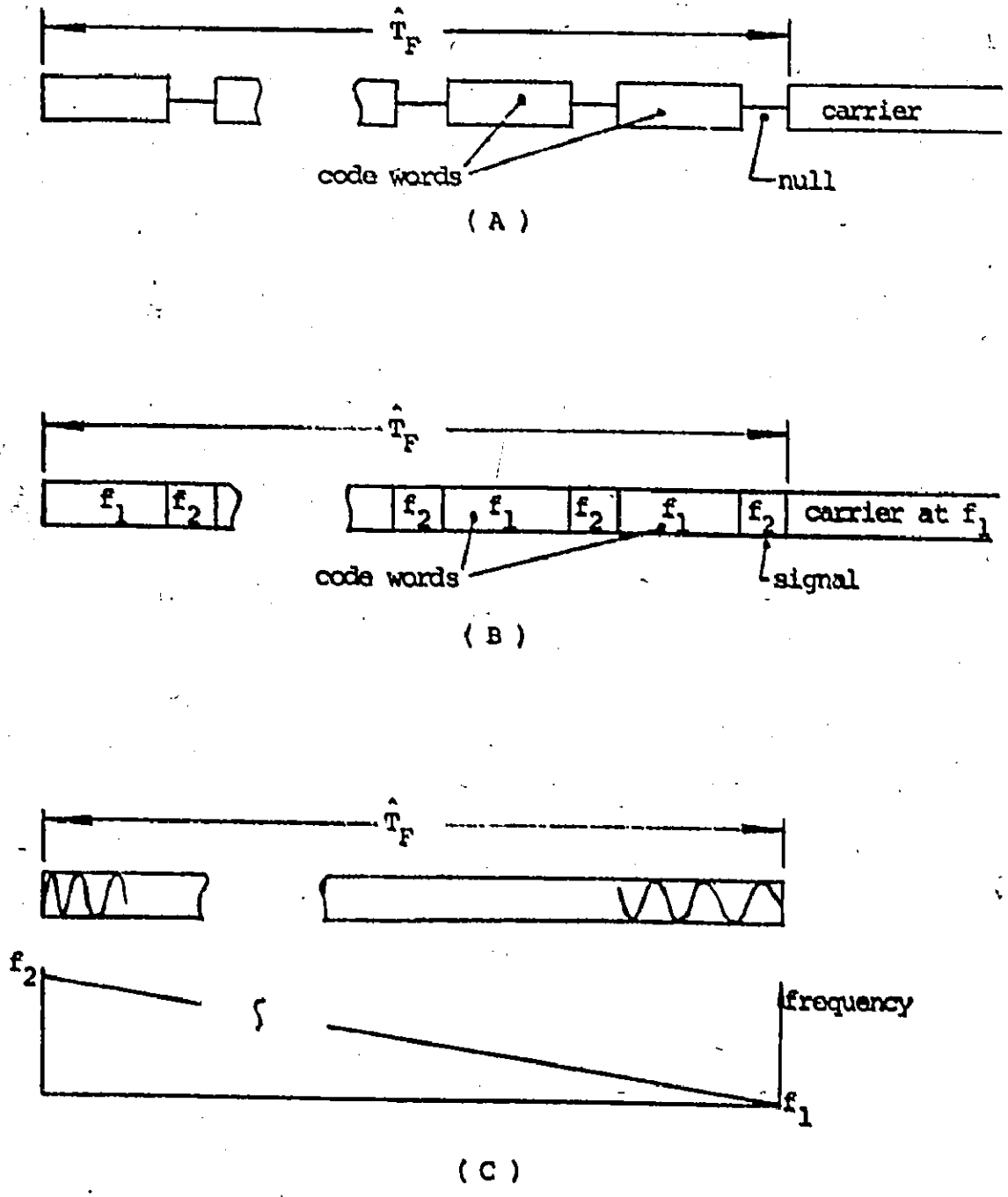

Fig. 3-6 Different types of sync sentences. (A) Null/code-word type, (B) signal/code-word type, (C) FM type.

starting at zero and increasing in consecutive order to an integer value K which is the smallest integer satisfying the following condition.

$$K \geq \frac{2\hat{T}_F}{T_W} - 1 \qquad (3\text{-}7)$$

Having determined K from this relation, the duration T_X which defines the length of one code word plus one null can be determined by using

$$T_X = \frac{\hat{T}_F}{K + 1} \qquad (3\text{-}8)$$

The number of bits required for the code word is N_B where N_B is the smallest integer satisfying the relation $2^{N_B} - 1 \geq K$. Thus, the duration of one bit, T_{BIT}, can be determined by

$$T_{BIT} = \frac{T_X - T_{NULL}}{N_B} \qquad (3\text{-}9)$$

where T_{NULL} is the duration of the null.

The sync window produces a pulse of the coded sync sentence of length T_W and returns the signal to the earth station, as shown in Fig. 3-7. Since the null marks the beginning of a code word, it is possible

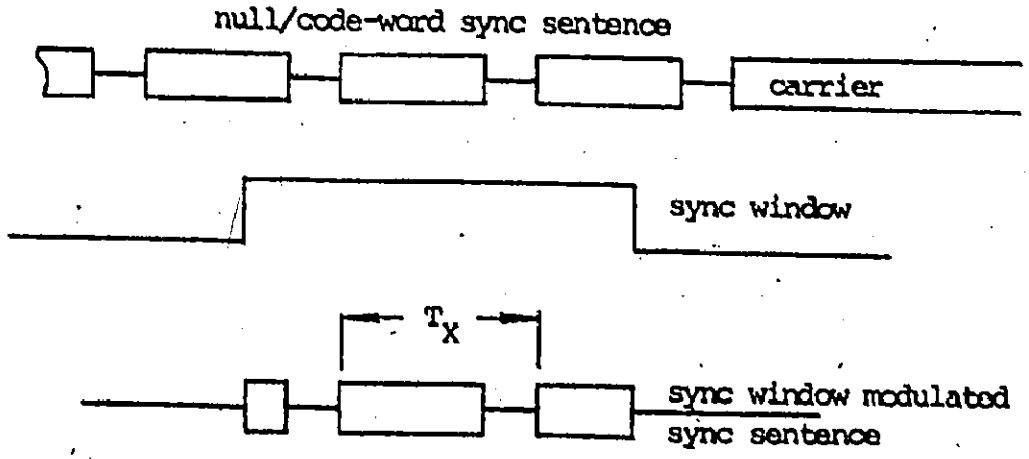

Fig. 3-7 Sync window modulated null/code-word sync sentence.

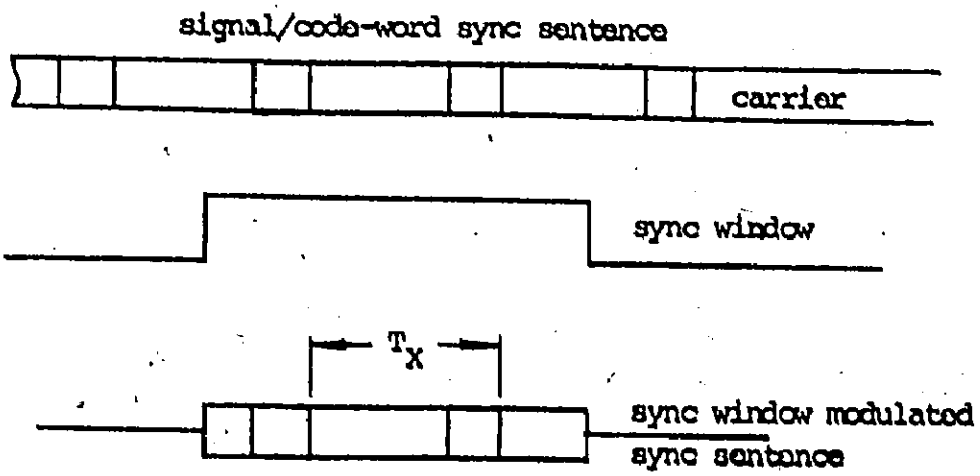

Fig. 3-8 Sync window modulated signal/code-word sync sentence.

to identify, at the earth station, the portion of the sync sentence modulated by the sync window by decoding the code word immediately following the null. The received signal always contains at least one full-length null and code word since the combination of the null and the code word has a time period less than or equal to half the duration of the sync window time period. The decoded value of T_S can be in error by an amount extending from zero up to $\frac{1}{2} T_W$ since the position of the null can fall anywhere in the first half of the sync window period. However, by a simple video detection of the received pulse of the coded sync sentence, an estimate of this error is possible since the location of the null can be measured with respect to the edge of the sync window modulation and the necessary correction can be applied. Thus, the coded sync sentence can be used to measure the value of T_S.

Assuming the fast synchronization technique and a 125 μs frame length, the average interference duration generated by the coded search signal using this sync sentence is approximately 1.4 ms due mainly to the carrier portion which provides carrier lock pulses [29]. The bit rate, estimated from (3-8), is of the order of 25 Mb/s.

(ii) Signal/Code-Word Sync Sentence

The signal/code-word sync sentence comprises a set of code words separated by pulses of signal at a different frequency, as shown in Fig. 3-8. The advantage of this method is that the beginning of a code word is determined by detection of a signal as compared to detection of no signal as in the null/code-word sync sentence. The addition of this

signal increases the total bit rate to approximately 35 Mb/s. Two types of code word which can be used are the ASK code word where the bits are encoded as signal or null, and the PSK code word which is identical to that used in the null/code-word sync sentence. Aside from these minor differences, the signal/code-word sync sentence is the same as the null/code-word sync sentence.

(iii) FM Sync Sentence

The FM sync sentence is simply a linearly frequency-modulated carrier which sweeps from frequency f_1 to frequency f_2 in one frame duration $\hat{T}_F$, as shown in Fig. 3-9. The value of T_S is related to the instantaneous frequency f_X by

$$T_S = \hat{T}_F \frac{f_X - f_1}{f_2 - f_1} \tag{3-10}$$

The sync window modulates a pulse of duration T_W of the FM sync sentence which is received at the earth station. A simple method of measuring the value of T_S is to count the number of zero-crossings contained in the pulse. This is given by $N_Z = 2\, T_W\, f_X$ and consequently the value of T_S is

$$T_S = \hat{T}_F \frac{\frac{N_Z}{2T_W} - f_1}{f_2 - f_1} \tag{3-11}$$

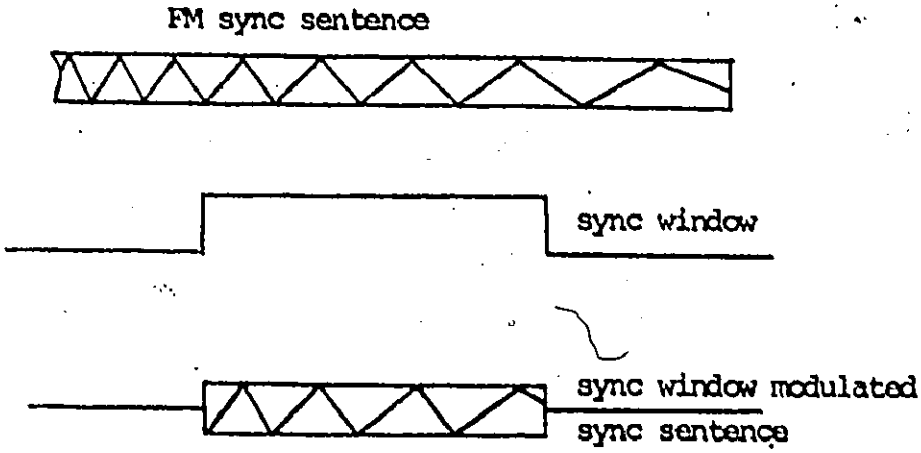

Fig. 3-9 Sync window modulated FM sync sentence.

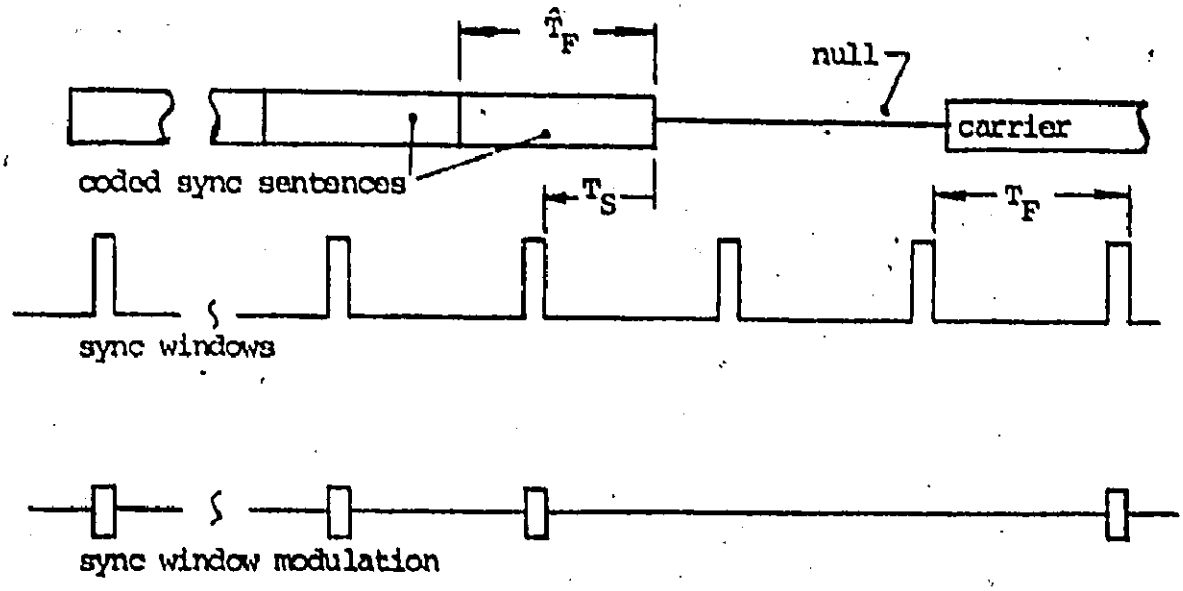

Fig. 3-10 Sync window modulation of the multi-frame coded search signal.

Since N_Z is an integer, the smallest change in T_S which can be detected, ΔT_S, occurs when N_Z changes by unity. Thus, the bandwidth requirement for this signal can be calculated and is given by

$$B_{FM} = f_2 - f_1 = \frac{\hat{T}_F}{2\Delta T_S T_W} \qquad (3\text{-}12)$$

The estimate of T_S provided by the FM sync sentence must be within approximately 1 μs in order that sync bursts pass through the sync window when the fine search mode commences. Assuming this value for ΔT_S and $T_F = 125\ T_W$, the bandwidth requirement is 62.5 MHz. Thus, a serious drawback of this method is the large bandwidth of the signal.

Assuming fast synchronization and a 125 μs frame length, the average interference duration for the coded search signal using the FM sync sentence is only 125 μs since no carrier portion is required.

3.3.2 Multi-frame Sync Sentence

(a) Timing Relationships

Another technique for achieving synchronization using a coded search signal is based on transmitting carrier followed by a multi-frame sync sentence, as shown in Fig. 3-10. The carrier is used to measure the value of T_F, as described in Section 3.3.1(a) and the multi-frame sync sentence provides an estimate of T_S.

The relationships in equations (3-5A) and (3-5B) apply here noting that the value of T_4 is now the transmission time of the leading edge of the multi-frame sync sentence and the value of T_5 is the arrival

time at the earth station of the first pulse of the multi-frame sync sentence. Similarily, the relationships in (3-6A) and (3-6B) can be used to estimate the time at which the first pulse of a train of sync bursts must be transmitted in order to pass through the sync window. The fast synchronization technique can also be applied. There remains only the problem of measuring T_S which is described next.

(b) Measurement of T_S

The value of T_S can be determined by transmitting either a multi-frame coded sync sentence or a multi-frame FM sync sentence, as shown in Fig. 3-11. In both cases, there is a null duration of several times the value of $\hat{T}_F$ between the carrier portion of the coded search signal and the multi-frame sync sentence. Thus, the signal arriving at the earth station consists of pulses of carrier followed by a null duration and finally pulses of the multi-frame sync sentence. The null duration is used in the receiver to indicate that pulses of the multi-frame sync sentence are about to arrive which can then be decoded to yield the value of T_S.

(i) Coded Sync Sentence

The multi-frame coded sync sentence, shown in Fig. 3-12, is a contiguous sequence of blocks of signal each of length $\hat{T}_F$ where the bit rate is halved with each succeeding block starting with Block no. 1. Either a PSK or an FSK structure can be employed as illustrated. The number of bits in the first frame length is given by K' where K' is the smallest integer satisfying the condition

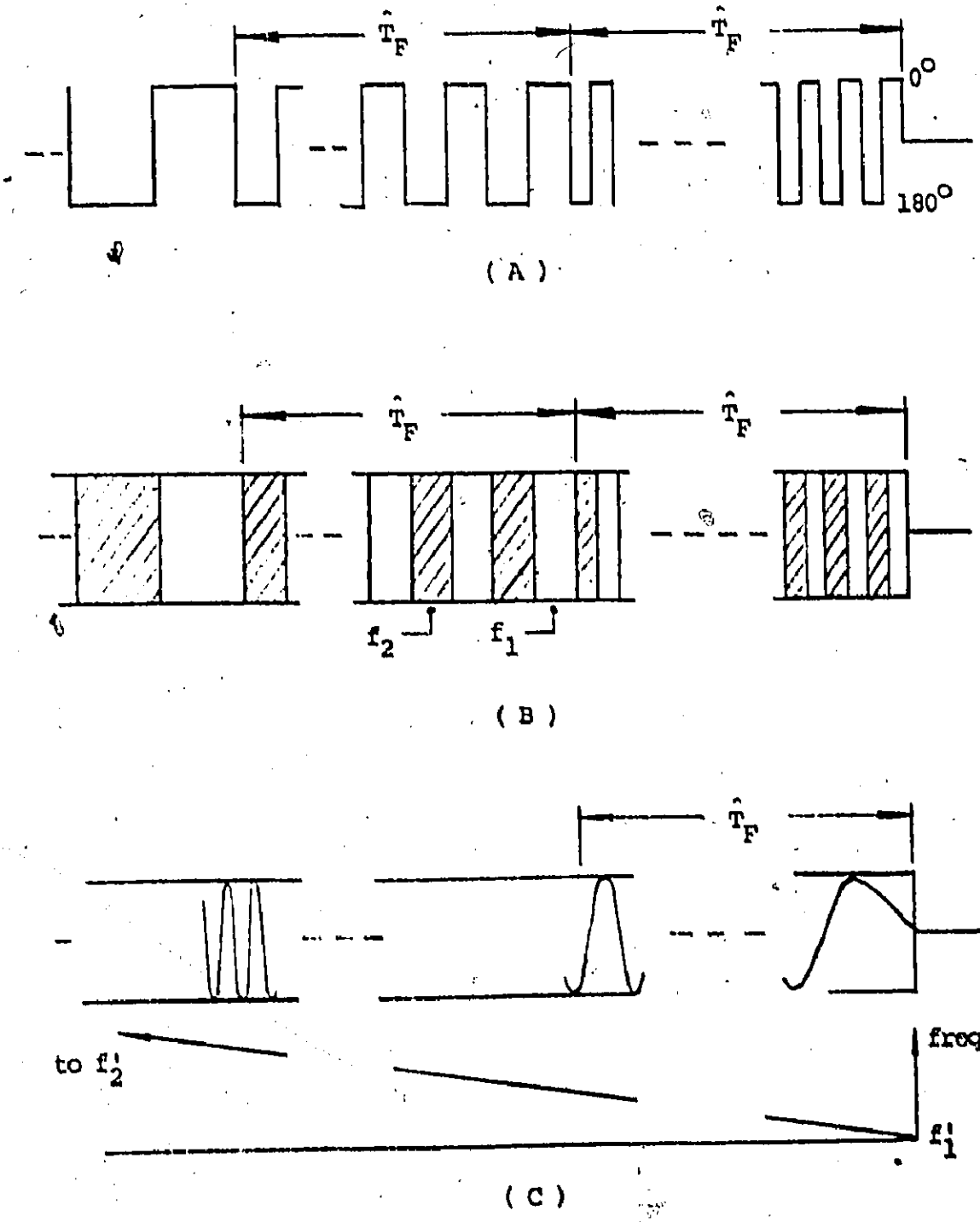

Fig. 3-11 Different types of multi-frame coded sync sentences.
(A) PSK multi-frame type, (B) FSK multi-frame type,
(C) FM multi-frame type.

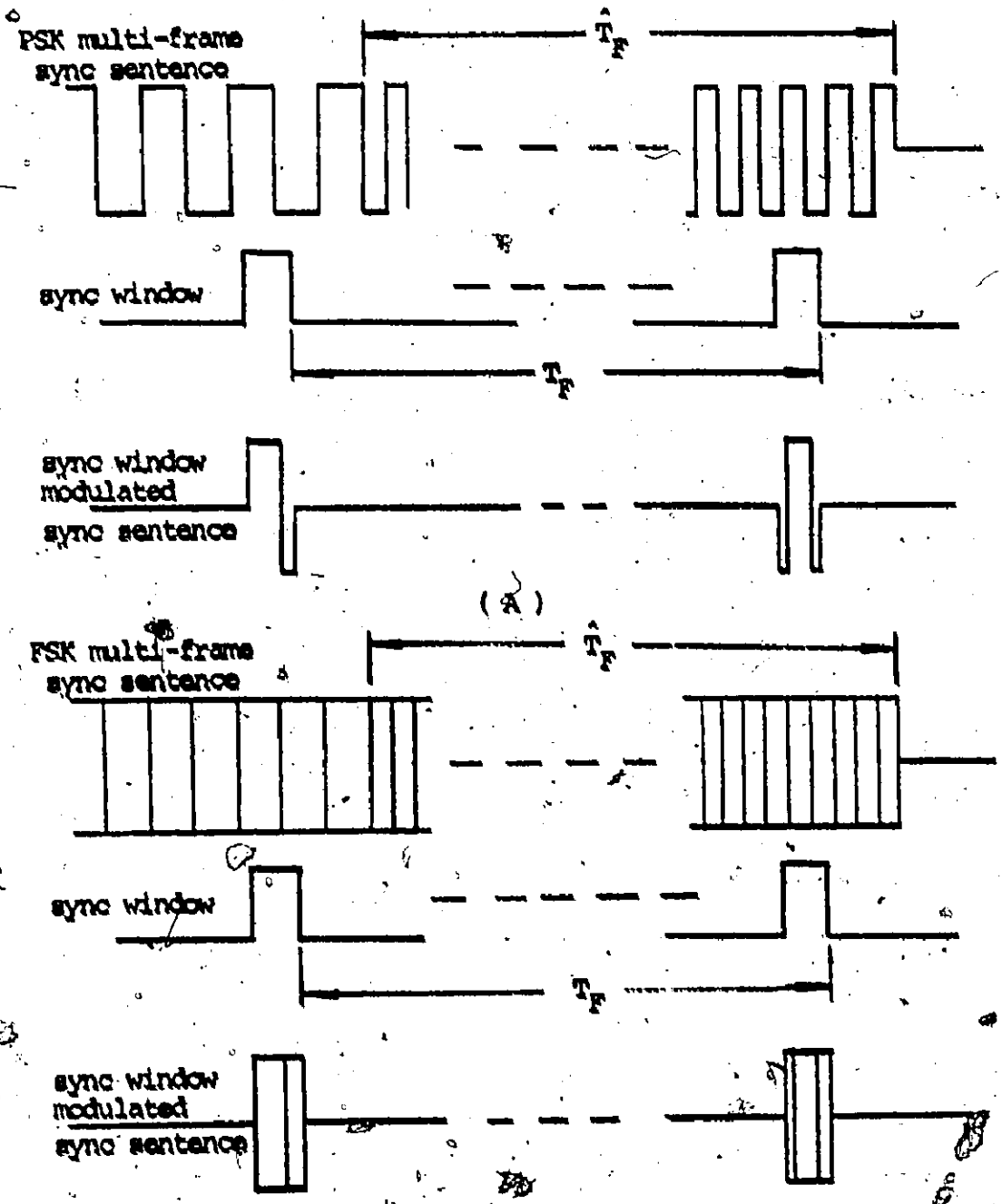

Fig. 3-12 Sync window modulation of multi-frame coded sync sentences.

$$K' \geq \frac{2\hat{T}_F}{T_W} \tag{3-13}$$

Hence, the length of one bit is

$$T_X' = \frac{\hat{T}_F}{K'} \tag{3-14}$$

The number of sentences required can be determined by calculating the smallest integer N' satisfying the relation

$$2^{N'} \geq K' \tag{3-15}$$

or

$$N' \geq \log_2 K' \tag{3-16}$$

When the sync window modulates the multi-frame coded sync sentence, a set of pulses is produced. Each pulse contains information as to the value of T_S and by decoding the complete set of pulses, the value of T_S can be deduced by the earth station.

The PSK multi-frame coded sync sentence can be decoded by simply noting the polarity of the bits, as shown in Fig. 3-12A. Carrier lock is provided by the pulses of carrier used for measuring T_F. The decoded number, in binary form, is T_S.

The FSK multi-frame coded sync sentence, illustrated in Fig. 3-12B, does not require carrier lock since decoding is possible using

envelope detectors. Hence, the signal can be decoded at the earth station to yield the value of T_S.

The value of T_S obtained by this method may be in error by an amount from zero up to $\frac{1}{2} T_W$. However, it is possible to compare the transition contained in the first pulse of the sync window modulated sync sentence with the edge of the modulation using video detection and provide the necessary correction.

It is assumed that the difference between the value of $\hat{T}_F$ and T_F is negligible over the duration of the multi-frame sync sentence. From Table 1-1, the variation in the oscillator frequency on-board the satellite is within 1 part in 10^5 over the lifetime of the satellite. Thus, the error produced for a multi-frame sync sentence of 1 ms duration is only 10 ns which is negligible.

Although the multi-frame coded sync sentence described above uses binary coding, other types of coding may also be useful. In particular, Rademacher functions [43] can be used to provide a signal having a gray code structure after sync window modulation, as shown in Fig. 3-13. If an error in the detection of one bit occurs due to a transition falling in the sync window modulated pulses, the error in the decoded message is minimized.

Assuming fast synchronization and a 125 μs frame length, the average interference duration for the coded search signals using the PSK multi-frame sync sentence and the FSK multi-frame sync sentence is approximately 2.25 ms [29] and 1 ms, respectively. The bit rate in the former case is 2 Mb/s and in the latter case 4 Mb/s.

Frame no. 1	0 0 0 0 0 0 0 0 1 1 1 1 1 1 1 1
Frame no. 2	0 0 0 0 1 1 1 1 1 1 1 1 0 0 0 0
Frame no. 3	0 0 1 1 1 1 0 0 0 0 1 1 1 1 0 0
Frame no. 4	0 1 1 0 0 1 1 0 0 1 1 0 0 1 1 0

Fig. 3-13 Multi-frame sync sentence with Rademacher function format. Vertical columns form a Gray code which minimizes the error caused by a transition in the sync window.

(ii) FM Sync Sentence

The multi-frame FM sync sentence is a linearly frequency-modulated carrier which sweeps from frequency f_1' to frequency f_2' in a duration of N_{FM} frame durations of $\hat{T}_F$, as shown in Fig. 3-14. The value of T_S is related to the instantaneous frequency of the first received pulse f_X' by

$$T_S = N_{FM} \hat{T}_F \frac{f_X' - f_1'}{f_2' - f_1'} \qquad (3\text{-}17)$$

The sync window modulates the signal producing a set of pulses each containing information on the value of T_S. The number of zero-crossings contained in this set is given by

$$N_S' = 2 T_W \left(N_{FM} f_X' + \frac{N_{FM} - 1}{2} (f_2' - f_1')\right) \qquad (3\text{-}18)$$

where $\hat{T}_F$ is assumed equal to T_F over the duration of the FM sync sentence. Hence, the value of f_X' can be calculated and substituted into (3-17) to give the value for T_S.

The bandwidth requirement of this signal can be determined by relating the smallest detectable change in T_S to a change in N_S' of unity. Thus,

$$B_{FM}' = f_2' - f_1' = \frac{\hat{T}_F}{2 \Delta T_S N_{FM} T_W} \qquad (3\text{-}19)$$

Comparing with (3-12), it is seen that the bandwidth of the multi-frame FM sync sentence is only $1/N_{FM}$ times the value for the single frame FM sync sentence.

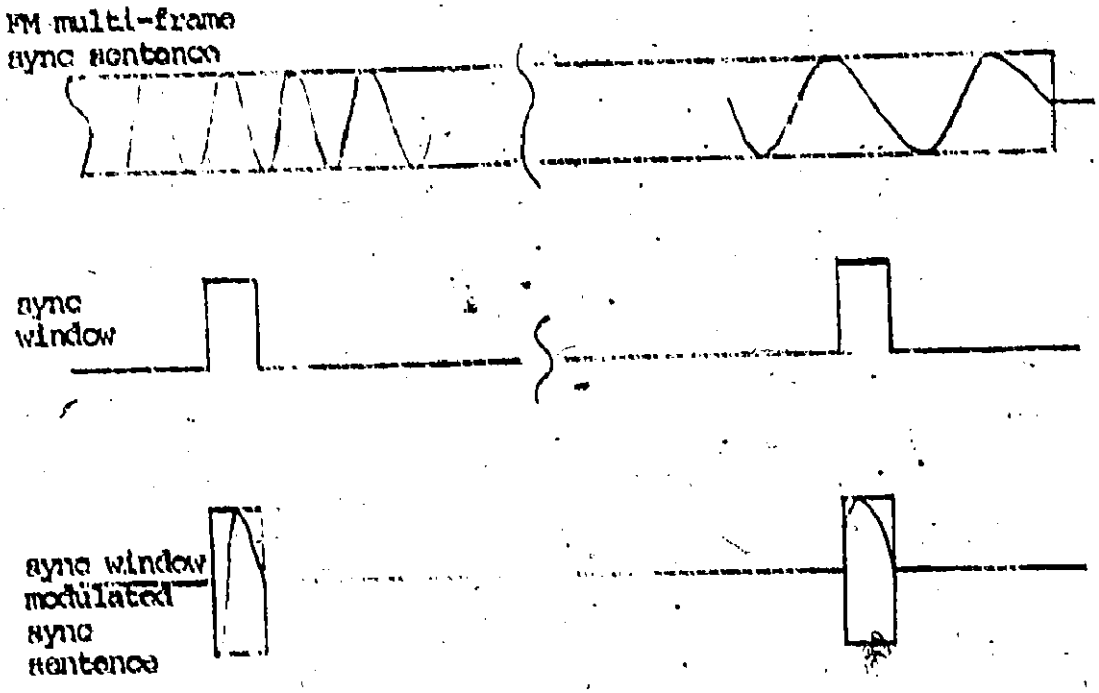

Fig. 3-14 Sync window modulation of the FM multi-frame sync sentence.

The interference duration for the multi-frame FM sync sentance is N_{FM} times the frame length. Thus, for T_F = 125 μs and N_{FM} = 10, the interference duration is 1.25 ms. The bandwidth requirement in this case is 6.25 MHz.

3.3.3 Integrated Synchronization System

An integrated synchronization system which combines the coded search signal and the sync burst signal is shown in block diagrammatic form in Fig. 3-15. Initially, the system is in the state shown with the switches in the 'A' position and the synchronization procedure starts by activating the sync request circuit. The coded search signal is transmitted and the clock time at which the leading edge of the coded sync sentence is sent, T_q, is recorded. When the coded search signal modulated by the sync window is received at the earth station after a propagation time of at least 2 T_D, the values of T_S and T_F are determined by search signal decoder.

Switches no. 1 and no. 2 are now connected to the 'B' position. The predicted time at which the sync bursts should be transmitted so as to pass through the sync window is determined in the timing predictor circuit which applies a set of, say 20, triggers at an interpulse spacing of T_F to the trigger driver. After the last of these triggers, switch no. 3 is connected to the 'B' position. This completes the coarse search mode and initiates the fine search mode. If in the course of operation the system falls out of synchronization, by any amount, the

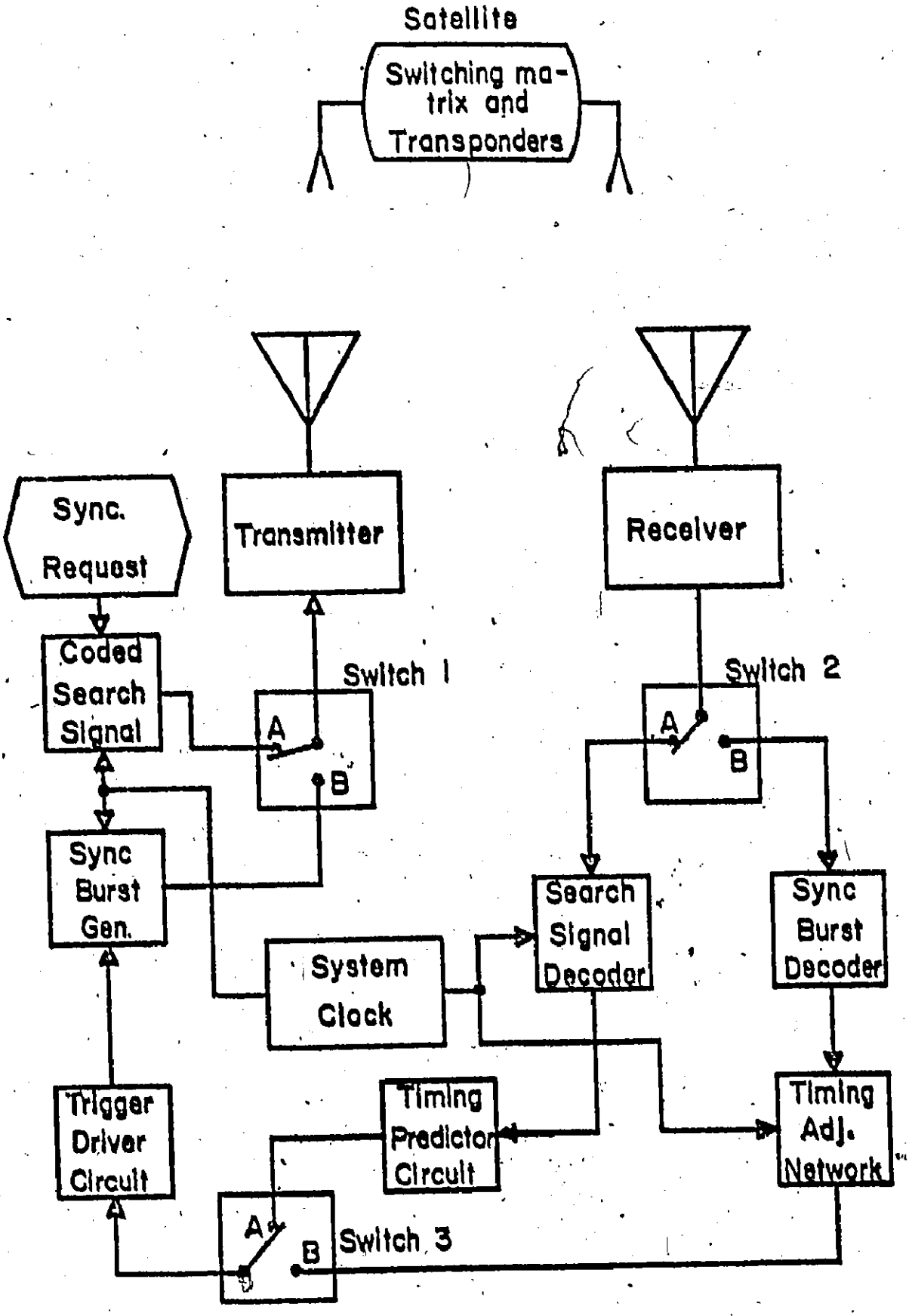

Fig. 3-19 Integrated synchronization system.

search method is re-activated and synchronization is restored in the estimated 350 ms.

3.3.4 Comparison of Coded Search Signals

A brief comparison of the different types of coded search signal is presented in Table 3-3. It is assumed that fast synchronization is used for each. Of all coded search signals, the type using the PSK multi-frame sync sentence appears to offer the best combination of fast acquisition, low bandwidth requirement and short average interference duration.

3.4 COMPARISON OF COARSE SEARCH MODE METHODS

The three different methods of coarse search synchronization are now compared in Table 3-4 assuming fast synchronization for the coded search signal method [27]. If fast synchronization is not possible due to the value of T_F being unknown, the coded search signal method still gives synchronization whereas the other two methods do not. Clearly, coded search signals offer the best combination of short synchronization acquisition time, low bit rate and small interference duration.

TABLE 3-3

Coded Search Signals with Different Sync Sentences

Sync Sentence	Sync Acquisition Time	Bit Rate or Bandwidth	Aver. Int. Duration
<u>Single Frame</u>			
Null/Code-Word	270 ms	25 Mb/s	1.4 ms
Signal/Code-Word	270 ms	35 Mb/s	1.4 ms
PM	270 ms	62.5 MHz	125 μs
<u>Multi-Frame</u>			
PSK	270 ms	2 Mb/s	2.25 ms
PSK	270 ms	4 Mb/s	1 ms
PM	270 ms	6.25 MHz	1.25 ms

TABLE 3-4 Comparison of the Methods of Coarse Search Synchronization

Method	Sync Acquisition Time	Bit Rate or Bandwidth	Average Interference Duration
Sync Burst			
ASK	310 ms to 40 s	1 Mb/s	3.1 ms to 320 ms
PSK	310 ms to 40 s	2 Mb/s	3.1 ms to 320 ms
PSK	310 ms to 40 s	4 Mb/s	3.1 ms to 320 ms
coded-ASK	310 ms to 200 s	32 Mb/s	7.8 ms to 800 ms
coded-PSK	310 ms to 200s	32 Mb/s	7.8 ms to 800 ms
coded-PSK	310 ms to 200 s	32 Mb/s	7.8 ms to 800 ms
PN-sequence	550 ms	7 Mb/s	550 ms
Coded Search Signals			
Single Frame			
Null/code-word	270 ms	25 Mb/s	1.4 ms
Signal/code-word	270 ms	35 Mb/s	1.4 ms
FM	270 ms	62.5 MHz	125 µs
Multi-frame			
PSK	270 ms	2 Mb/s	2.25 ms
PSK	270 ms	4 Mb/s	1 ms
FM	270 ms	6.25 MHz	1.25 ms

CHAPTER 4

Fine Search Mode

The fine search mode is initiated once the coarse search mode is complete. The objective in this case is to reduce the initial timing error due to inaccuracies in the coarse search mode by transmitting short trains of sync bursts such as those shown in Fig. 3-2. After a one-way trip time, the train of sync bursts reaches the satellite where sync window modulation occurs, as illustrated in Fig. 3-3. Finally, the signals are transmitted back to the earth station. By comparing the modulation with the characteristics of the sync burst, it is possible to measure a timing error and adjust the earth station time base. Further trains of sync bursts can then be transmitted at intervals of one round trip time with the adjustment performed after each train is received. Hence, the feedback control loop results.

Two fundamentally different techniques are considered. The first, developed by COMSAT Laboratories, relies on fixed increment adjustments and is described in Appendix B. The second, examined here in detail, provides variable increment adjustments by employing a timing adjustment gate and a voltage-controlled-oscillator (VCO)[33]. The salient points are summarized in the final section.

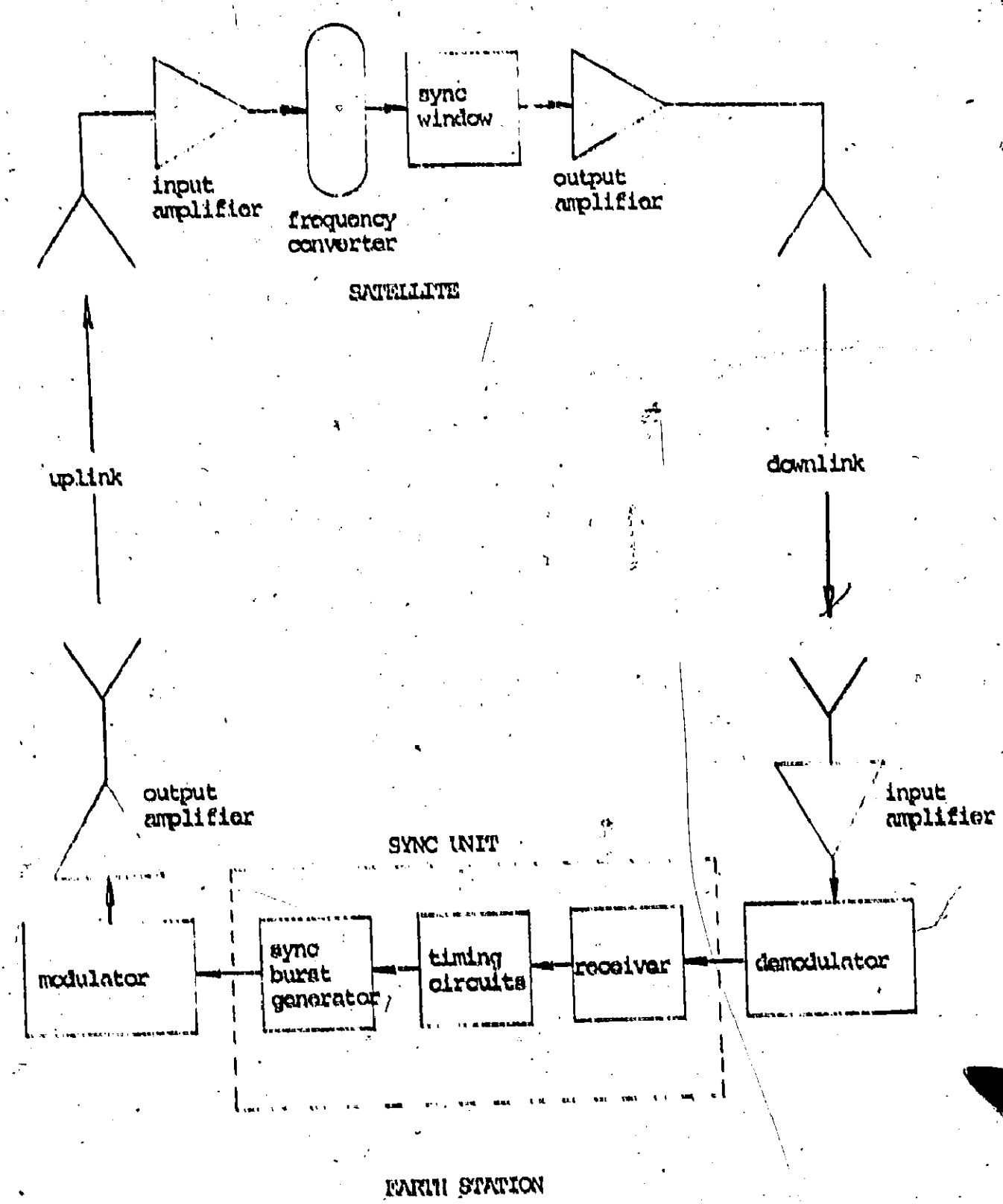

Fig. 4-1 Physical model of the synchronization loop.

4.1 VARIABLE INCREMENT SYSTEM

Consider the physical model of the synchronization loop shown in Fig. 4-1. The variables which affect the loop are the uplink space delay and attenuation, the noise of the satellite amplifiers (uplink noise), the motion of the satellite, the downlink space delay and attenuation, and the noise of the earth station amplifiers (downlink noise).

It is assumed that the loop has just started operating in the fine search mode and that the coarse search mode has provided the timing information required by the sync unit so that sync bursts can be transmitted at the proper times to be at least partially passed by the sync window. The two types of sync burst considered here, the PSK sync burst and the FSK sync burst, shown in Fig. 4-2A and 4-2B are particularly useful because of their simplicity and narrow bandwidths [20]. The reference is the transition between the two parts of the sync burst and is used by the earth station to determine the relative position between the sync burst and the sync window modulation, as shown in Fig. 4-2C. Exact synchronization occurs when the sync burst is centered in the sync window.

The timing of the sync bursts is controlled by the timing circuits in the sync unit. The timing circuits employ a VCO driving a counter and a decoder which generates pulses with an interpulse spacing equal to the sync window spacing and forms the earth station time base. Initially, a short train of pulses derived from the coarse search mode is used to trigger the sync burst generator which produces either PSK or FSK sync

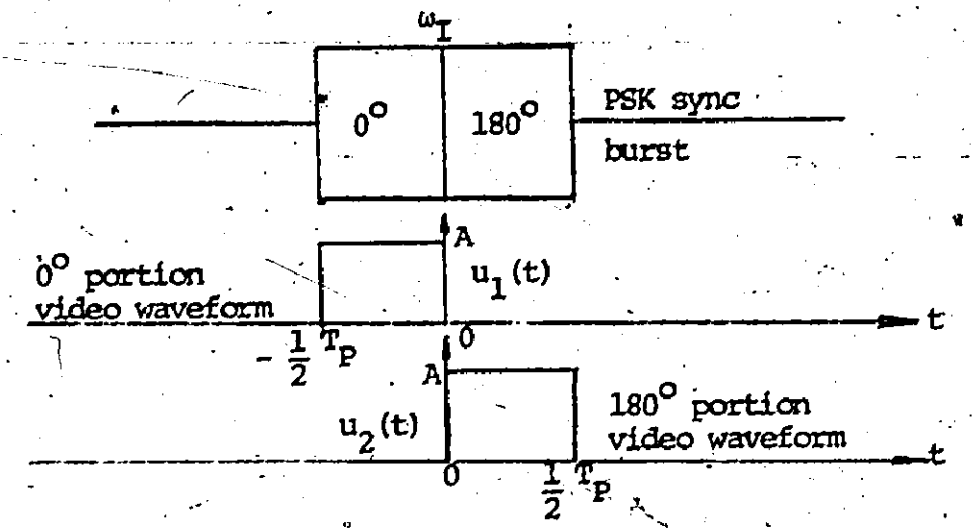

(A) PSK sync burst and video waveforms

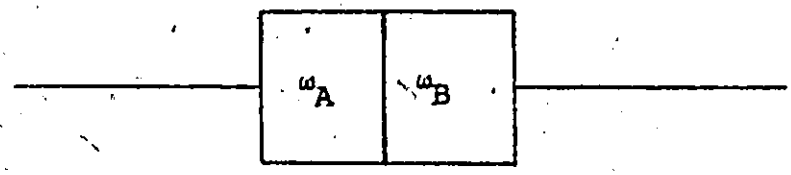

(B) PSK sync burst

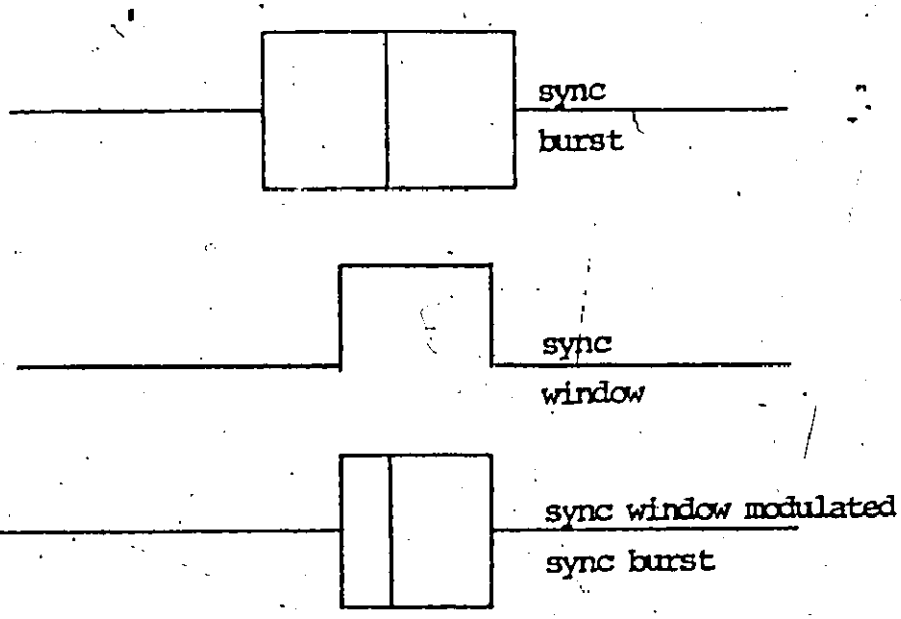

(C) Sync window modulation

Fig. 4-2 Sync bursts and sync window modulation.

bursts. The sync bursts are mixed to the uplink frequency in the modulator, amplified and transmitted toward the satellite. After a one-way trip time, the train reaches the satellite where the signals are amplified in the input amplifier, converted to the downlink frequency, modulated by the sync window, amplified by the output amplifier, and transmitted back to the spot beam zone of transmission. After another one-way trip delay, the signals reach the earth station and are amplified in the input amplifier, demodulated and processed in the receiver. By comparing the sync window modulation and the built-in timing reference of the sync burst, it is possible to measure a timing error and, with the timing circuits, to shift the earth station time base to reduce this error. Further trains of sync bursts can then be transmitted at intervals of one round trip time with the adjustment performed after each train is received thus continually reducing the error. Once the fine search mode is completed, the tracking mode described in Chapter 5 commences.

4.2 SYNCHRONIZATION LOOP ANALYSIS

The equations which describe the operation of the synchronization process are now derived in detail considering the use of the PSK sync burst. Following this, the equations using the FSK sync burst are briefly described since their derivation is similar to the case using PSK sync bursts. Indeed, in the final equations it is seen that the signal term in each case is the same but the noise terms differ.

4.2.1 PSK Sync Burst Implementation

Consider the synchronization loop model, illustrated in Fig. 4-3, where the space delays, space losses and antenna gains are shown as lumped elements. The PSK sync burst can be represented by the video signals $u_1(t)$ and $u_2(t)$ and the intermediate frequency (IF) ω_I, as shown in Fig. 4-2A. For one sync burst, the signal is given by (assuming the narrowband representation [34])

$$s_1(t) = \mathrm{Re}\{[u_1(t) - u_2(t)]e^{j\omega_I t}\} \tag{4-1}$$

where

$$u_1(t) = A \qquad -\frac{1}{2}T_p \leq t \leq 0$$
$$= 0 \qquad \text{otherwise}$$
$$u_2(t) = A \qquad 0 \leq t \leq \frac{1}{2}T_p$$
$$= 0 \qquad \text{otherwise}$$
$$T_p = \text{sync burst duration.}$$

The paths from the earth station modulator input to the sync window input and the output from the sync window to the earth station receiver are both essentially transparent. Thus, the relationships can easily be derived as follows.

The sync burst signal is mixed in the modulator with a local oscillator at frequency ω_1 to the uplink frequency band yielding

$$s_2(t) = \mathrm{Re}\{[u_1(t) - u_2(t)]e^{j(\omega_1 + \omega_I)t}\} \tag{4-2}$$

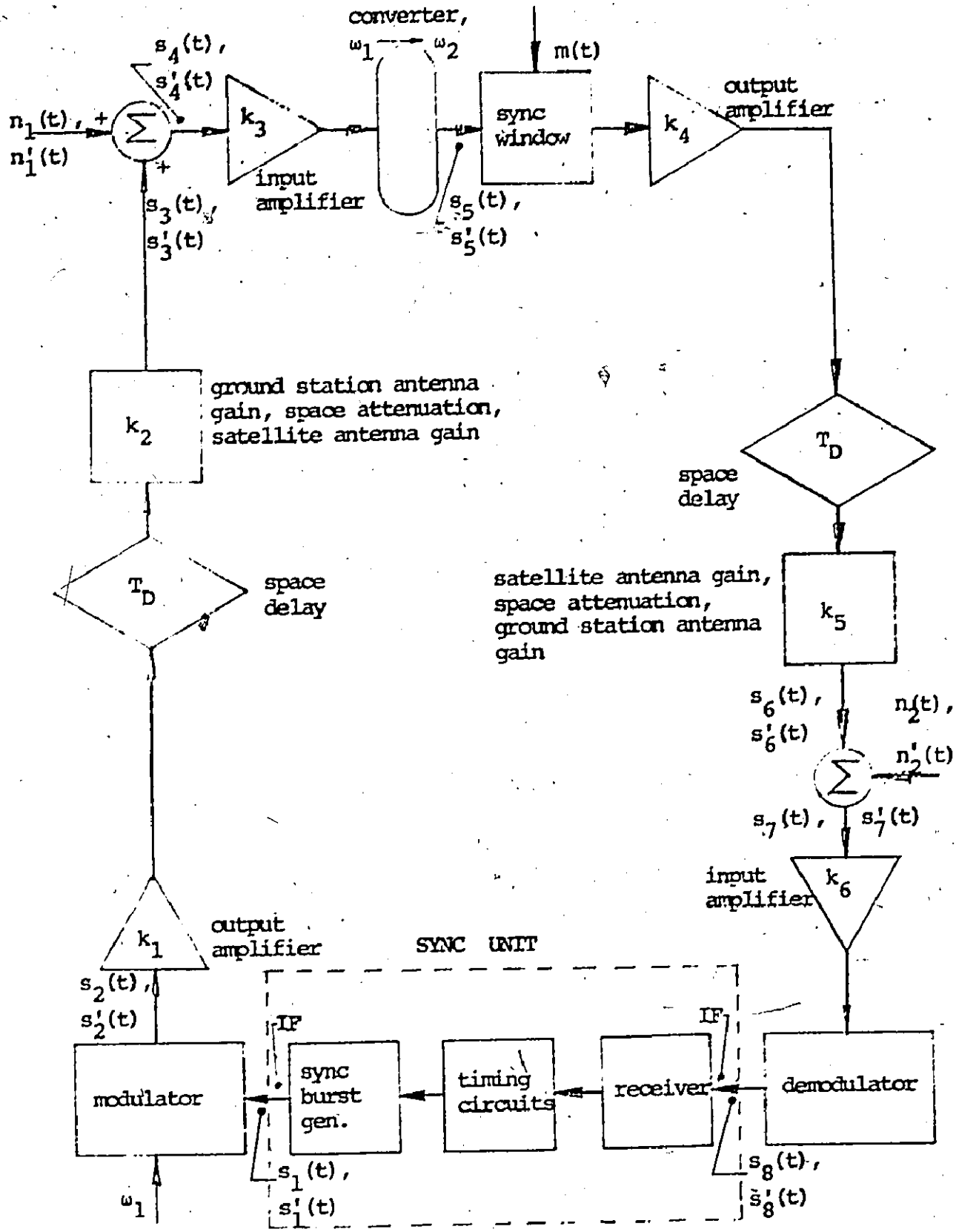

Fig. 4-3 Synchronization loop model.

Next, the signal is amplified by k_1 in the power output amplifier and transmitted. The uplink is assumed to produce only a space attenuation and a space delay T_D. The earth station antenna gain, satellite antenna gain and the space attenuation can all be lumped into an uplink gain constant k_2. Hence, the signal at the input to the first satellite amplifier is

$$s_3(t) = k_1 k_2 \, s_2(t - T_D) \tag{4-3}$$

At the satellite transponder, the signal $s_3(t)$ is perturbed by the additive uplink noise $n_1(t)$ referred to the input of the first amplifier. Thus, assuming narrowband noise [34], we may write

$$s_4(t) = s_3(t) + n_1(t) \tag{4-4}$$

where

$$n_1(t) = \mathrm{Re}\{z_1(t) \, e^{j(\omega_1 + \omega_I)t}\}$$

$$z_1(t) = x_1(t) + j \, y_1(t)$$

$x_1(t)$, $y_1(t)$ = components of the complex signal, $z_1(t)$.

The narrowband representation for the noise is valid since the signal is filtered in a narrowband filter in the earth station sync unit.

The signal is amplified by k_3 in the satellite input amplifier and converted to the downlink frequency using a transfer oscillator,

where ω_2 is the new local oscillator frequency, to give

$$s_5(t) = k_3\{k_1k_2\, \mathrm{Re}\{[u_1(t-T_D) - u_2(t-T_D)]e^{j(\omega_2+\omega_I)(t-T_D)}\} + \mathrm{Re}\{z_1 e^{j(\omega_2+\omega_I)t}\}\} \quad (4\text{-}5)$$

Next, the signal is amplitude modulated by the sync window signal, m(t). The sync window is assumed for mathematical reasons to produce perfect rectangular amplitude modulation of the signal as shown in Fig. 4-2C. This sync window modulated signal is amplified in the output amplifier by k_4 and transmitted. Again, the downlink is assumed to produce only a space attenuation and a space delay T_D. The satellite antenna gain, earth station antenna gain and the space attenuation are all lumped into the downlink gain constant k_5. Thus, the signal at the input to the first earth station amplifier is

$$s_6(t) = k_4k_5\, s_5(t - T_D) \cdot m(t - T_D) \quad (4\text{-}6)$$

The signal, $s_6(t)$, is perturbed by the additive downlink noise, $n_2(t)$, referred to the input of the first amplifier to yield

$$s_7(t) = s_6(t) + n_2(t) \quad (4\text{-}7)$$

where

$$n_2(t) = \mathrm{Re}\{z_2(t)\, e^{j(\omega_2+\omega_I)t}\}$$

$$z_2(t) = x_2(t) + j\, y_2(t)$$

$x_2(t)$, $y_2(t)$ = components of the complex signal, $z_2(t)$.

Again, the narrowband representation of noise is valid due to narrowband filtering in the sync unit.

Finally, the signal is amplified by k_6 in the earth station input amplifier and converted to the IF, ω_I, in the demodulator to yield $s_8(t)$.

Now it is necessary to examine the receiver portion of the sync unit in more detail to determine whether some optimum configuration is possible. Three features which can be provided to improve performance, shown in Fig. 4-4, are first the receiver input gate, second the coherent detector, and third the video integrator. The input gate, $q(t)$, is a train of L video gating pulses having a repetition interval equal to the frame length and a pulse width, T_Q, greater than the sync window. The gates are generated in the timing circuits based on the reception of previous signals by the coherent detector. The information would always be available starting with the reception of signals from the coarse search mode. Thus, the gates would be adjusted to pass all of the sync window modulated signal and, consequently, all of the sync window modulated uplink noise, but only the gate width, T_Q, of the downlink noise. Hence, the signal at the output of the input gate is given by

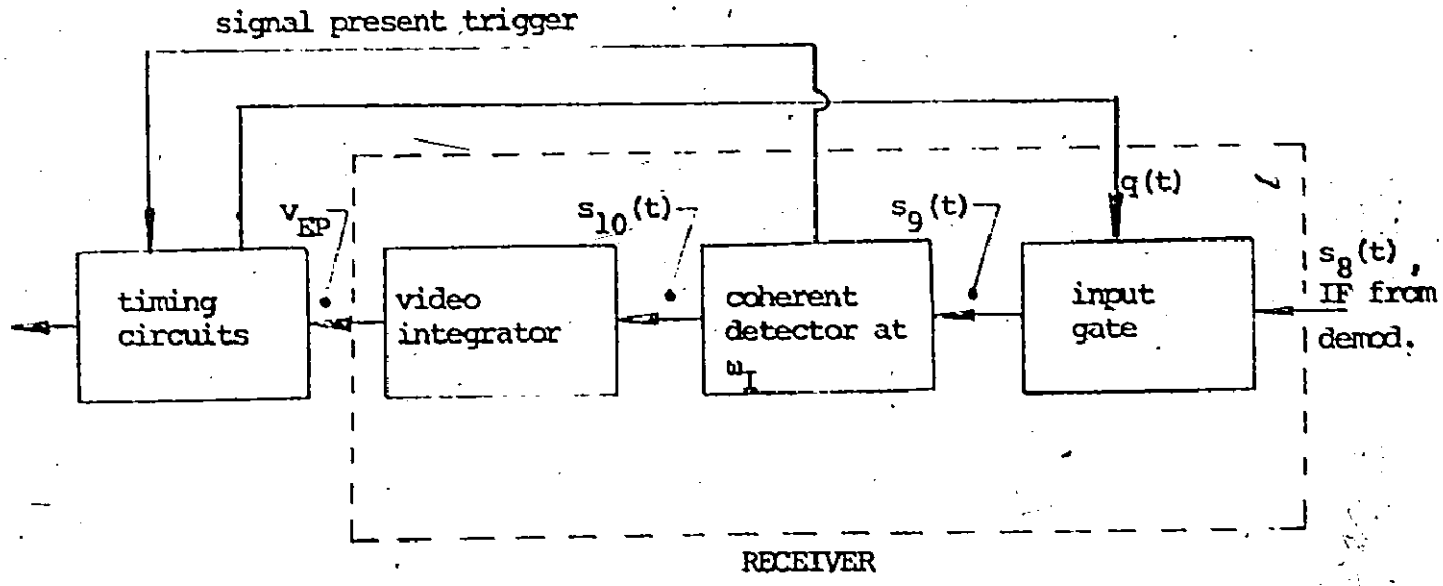

Fig. 4-4 Optimum receiver configuration for PSK sync bursts.

$$s_9(t) = s_8(t) \cdot q(t) \qquad (4\text{-}8)$$

The coherent detector, shown in Fig. 4-4, provides the best performance of all amplitude detectors [35]. It is recognized that in present-day satellites in operation, this coherent detection from frame to frame may not be possible due to instability in the satellite transfer oscillator. However, oscillators are now available in the required frequency band with stability of 3×10^{-8} per 24 hour period which is adquate for coherent detection

Thus, assuming coherent detection, the resulting signal is

$$s_{10}(t) = c_1 v_1(t) + c_2 x_1(t-T_D)\, m(t-T_D) + k_6 x_2(t)\, q(t) \qquad (4\text{-}9)$$

where

$$v_1(t) = \text{signal term}$$
$$= [u_1(t - 2T_D) - u_2(t - 2T_D)]\, m(t - T_D)$$

$$c_1 = k_1k_2k_3k_4k_5k_6$$

$$c_2 = k_3k_4k_5k_6$$

Finally, a video integrator is provided because of the inherent improvement in signal-to-noise ratio [36]. It is assumed that a certain number of sync bursts were originally transmitted. Since the sync window modulates the same timing information onto each sync burst, the

estimate of the timing error can be improved by integrating over, say, L pulses. Thus, the PSK sync burst integrated error voltage, v_{EP}, is given by

$$v_{EP} = \frac{1}{T_I} \int_{L \text{ pulses}} s_{10}(t)\, dt = v_S + v_N \qquad (4\text{-}10)$$

where

v_S = integrated signal voltage

$$= \frac{c_1 L}{T_I} \int_{1 \text{ pulse}} v_1(t)\, dt$$

v_N = PSK sync burst integrated noise voltage

$$= \frac{1}{T_I} \int_{L \text{ pulses}} [c_2\, x_1(t-T_D)\, m(t-T_D) + k_6\, x_2(t)\, q(t)]\, dt$$

T_I = integrator time constant.

After the last pulse of the train has been integrated, the error voltage is fed to the timing circuits, as described in Section 4.3.

4.2.2 PSK Sync Burst Implementation

Referring to the synchronization model, illustrated in Fig. 4-3, it is possible to derive the signal equations describing the loop behaviour for the case where the PSK sync burst is employed. For one sync

burst, as shown in Fig. 4-2B, the signal is given by (again assuming the narrowband representation [34]),

$$s_1'(t) = \mathrm{Re}\{u_1(t)\, e^{j\omega_A t} + u_2(t)\, e^{j\omega_B t}\} \tag{4-11}$$

where $u_1(t)$ and $u_2(t)$ are defined as in (4-1) and ω_A and ω_B are two different intermediate frequencies.

Following the steps in the PSK sync burst derivation, $s_2'(t)$ and $s_3'(t)$ can be calculated and, at the input to the satellite amplifier, the signal is combined with narrowband uplink noise $n_1'(t)$ to yield

$$s_4'(t) = s_3'(t) + n_1'(t) \tag{4-12}$$

where

$$n_1'(t) = \mathrm{Re}\{z_1'(t)\, e^{j(\omega_1+\omega_A)t} + z_1''(t)\, e^{j(\omega_1+\omega_B)t}\}$$

$$z_1'(t) = x_1'(t) + j\, y_1'(t)$$

$$z_1''(t) = x_1''(t) + j\, y_1''(t)$$

$x_1'(t)$, $y_1'(t)$

and $x_1''(t)$, $y_1''(t)$ = components of the respective complex signals $z_1'(t)$ and $z_1''(t)$.

The expressions for $s_5'(t)$ and $s_6'(t)$ can be derived in a similar fashion to $s_5(t)$ and $s_6(t)$, respectively. Hence, combining $s_6'(t)$ with narrowband downlink noise $n_2'(t)$ gives

$$s_7'(t) = s_6'(t) + n_2'(t) \tag{4-13}$$

where

$$n_2'(t) = \mathrm{Re}\{z_2'(t)\, e^{j(\omega_2+\omega_A)t} + z_2''(t)\, e^{j(\omega_2+\omega_B)t}\}$$

$$z_2'(t) = x_2'(t) + j\, y_2'(t)$$

$$z_2''(t) = x_2''(t) + j\, y_2''(t)$$

$$x_2'(t),\ y_2'(t)$$

and $x_2''(t)$, $y_2''(t)$ = components of their respective complex signals $z_2'(t)$ and $z_2''(t)$.

The receiver configuration for the FSK sync burst still employs the input gate but now it is possible to use either coherent detectors or envelope detectors to obtain the video portions of the two frequency FSK signal. The coherent detectors, as shown in Fig. 4-5, provide the highest signal-to-noise ratio and will be assumed here. (It is noteworthy that for high signal-to-noise ratio, which appears to be an excellent assumption, the performance using linear envelope detectors is essentially the same as for the coherent detectors). The video integrator can also be employed, as in the PSK sync burst case, to improve the signal-to-noise ratio. Hence, the output at the input gate is

$$s_9'(t) = s_8'(t) \cdot q(t) \tag{4-14}$$

The output of the coherent detector is

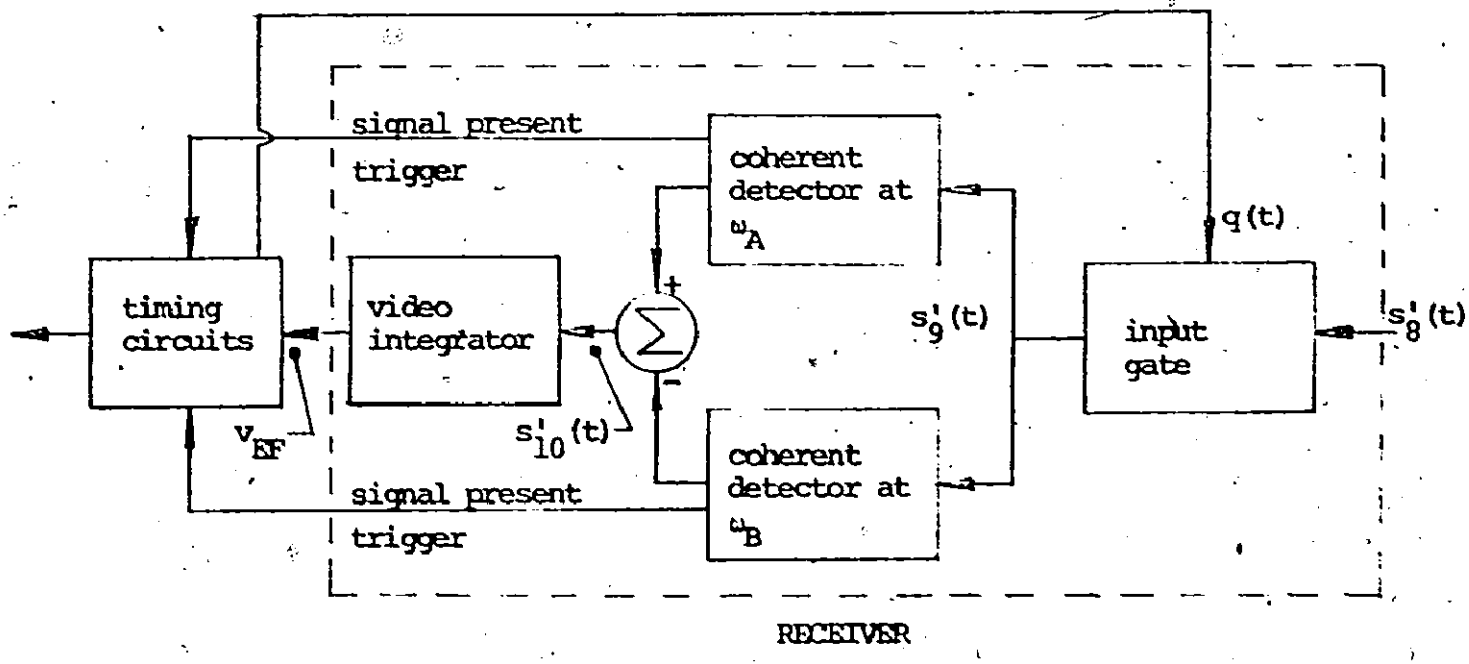

Fig. 4-5 Optimum receiver configuration for FSK sync bursts.

$$s'_{10}(t) = c_1 v'_1(t) + c_2[x'_1(t-T_D) - x''_1(t-T_D)]m(t-T_D) + k_6[x'_2(t) - x''_2(t)]q(t) \quad \text{------ (4-15)}$$

where

$$v'_1 = [u_1(t - 2T_D) - u_2(t - 2T_D)] \cdot m(t - T_D)$$

$$= v_1(t) \quad \text{(as in (4-9))}$$

It is seen that the signal portion of (4-15), $c_1 v'_1(t)$, for the FSK sync burst is the same as the signal portion of (4-9), $c_1 v_1(t)$, for the PSK sync burst. Equation (4-15), however, has two more noise terms than (4-9) due to the characteristics of the FSK sync burst.

Finally, the output of the integrator is the FSK sync burst integrated error voltage, given by

$$v_{EF} = \int_{L \text{ pulses}} s'_{10}(t)\, dt = v'_S + v'_N \quad (4\text{-}16)$$

where

$$v'_S = v_S \quad \text{(as in (4-10))}$$

v'_N = FSK sync burst integrated noise voltage

$$= \frac{1}{T_I} \int_{L \text{ pulses}} \{c_2[x'_1(t-T_D) - x''_1(t-T_D)]\, m(t-T_D) + k_6[x'_2(t) - x''_2(t)]\, q(t)\}\, dt$$

On completion of the integration, the error voltage is applied to the timing circuits as described next.

4.3 FINE SEARCH TIMING ADJUSTMENTS

The error voltage at the output of the video integrator using either the PSK sync burst (v_{EP}) or the FSK sync burst (v_{EF}), and referred to here as simply v_E, is applied to the control terminal of the VCO through the timing adjustment gate, shown in Fig. 4-6, for the gate duration T_G. The VCO changes frequency for this duration by an amount proportional to the error voltage v_E. Hence, the counter reaches full-count earlier than normal if the frequency of the VCO increases or later than normal if the frequency of the VCO decreases. After the gate is over, the VCO returns to its normal stable frequency but the timing of the pulse train has been shifted by the gated error voltage. The mode control logic provides the sync unit with parameters such as the number of pulses to be transmitted, the number to be received, L, the input gate q(t), and the length of the pulse T_G, to the timing adjustment gate.

Consider the operation of the VCO and the counter. The inter-pulse spacing of pulses produced by the counter and the decoder is given by

$$T = \frac{K_C}{f} \qquad (4\text{-}17)$$

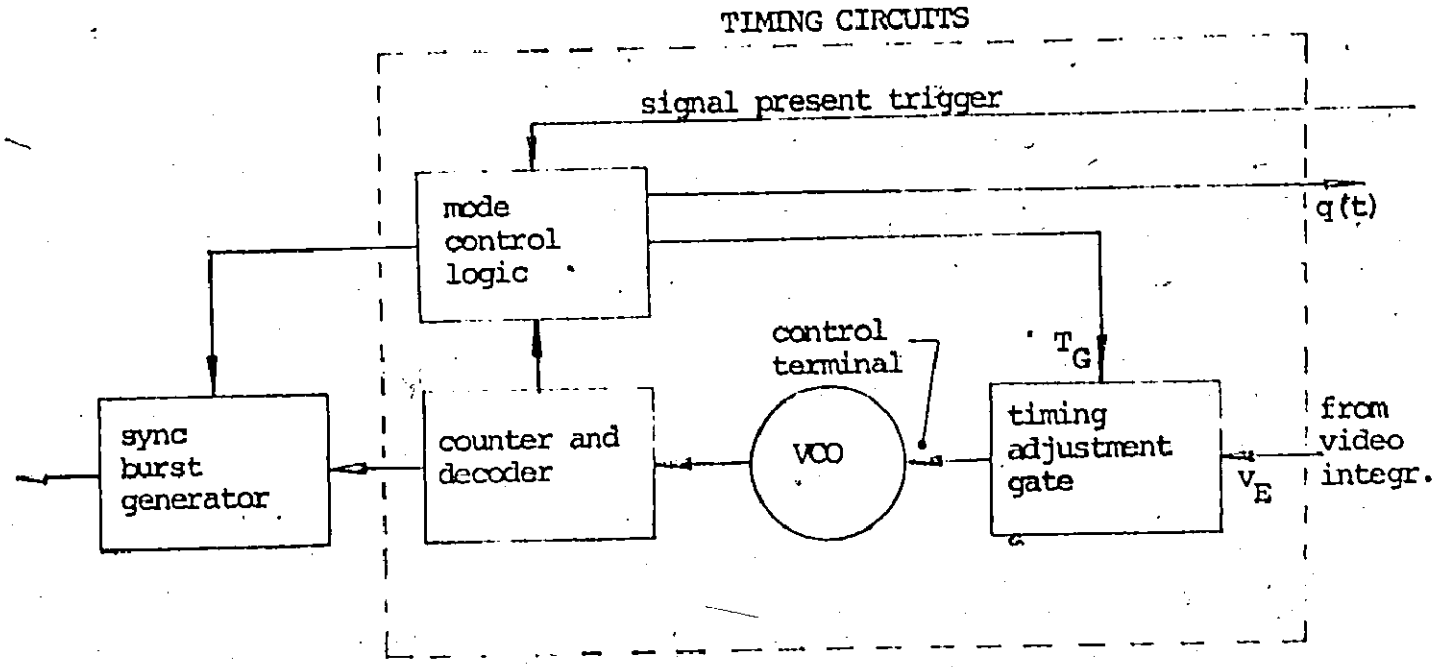

Fig. 4-6 Detailed block diagram of the timing circuits.

where

K_C = constant of the counter and decoder

f = frequency of the VCO

The frequency of the VCO is assumed to be related linearly to the voltage on the control terminal by

$$f = f_0 + S\, v_E \tag{4-18}$$

where

f_0 = center frequency of the VCO with $v_E = 0$

S = sensitivity of the VCO in Hz/volt.

From equations (4-17) and (4-18)

$$T = \frac{K_C}{f_0 + S\, v_E} = \frac{K_C}{f_0}\left(1 - \frac{S\, v_E}{f_0}\right) \tag{4-19}$$

$$= T_0\left(1 - \frac{S\, v_E}{f_0}\right)$$

where

T_0 = interpulse spacing of pulses from the counter with $v_E = 0$.

Thus, the timing shift over an interval T_0 is $-\frac{T_0\, S\, v_E}{f_0}$ and for a gate length of T_G, the total shift is

$$t_S = -\frac{S\, T_G\, v_E}{f_0} \tag{4-20}$$

It is now necessary to examine in more detail the value of the error voltage v_E and its variation as the timing error varies.

4.4 ERROR DETECTION CHARACTERISTICS OF THE SYNC UNIT

It is seen in (4-10) and (4-16) that the integrated signal voltage v_S, containing the signal modulated by the sync window, is the same for both the PSK sync burst and the FSK sync burst. By integrating in (4-10) and (4-16), the time dependence disappears and the signal portion of the error voltage v_S is a function of only the timing error between the sync burst and the sync window.

Assume that the first pulse of a transmitted train of sync bursts has just arrived back at the earth station and is being processed in the sync unit. The timing error t_E, illustrated in Fig. 4-7, is the time difference between the center of the sync window and the built-in timing reference contained in the sync burst and is defined at the satellite. The value of t_E was determined when the sync burst was modulated by the sync window at time $t = T_D$. The value of v_S can be related to t_E using (4-9) and (4-10) by

$$\frac{v_S}{c_1'} = \int_{1\ \text{pulse}} [u_1(t - 2T_D) - u_2(t - 2T_D)]\ m(t - T_D)\ dt \qquad \text{-----(4-21)}$$

$$= \int_{2T_D - t_E - \frac{1}{2}T_W}^{2T_D - t_E + \frac{1}{2}T_W} [u_1(t - 2T_D) - u_2(t - 2T_D)]\ dt$$

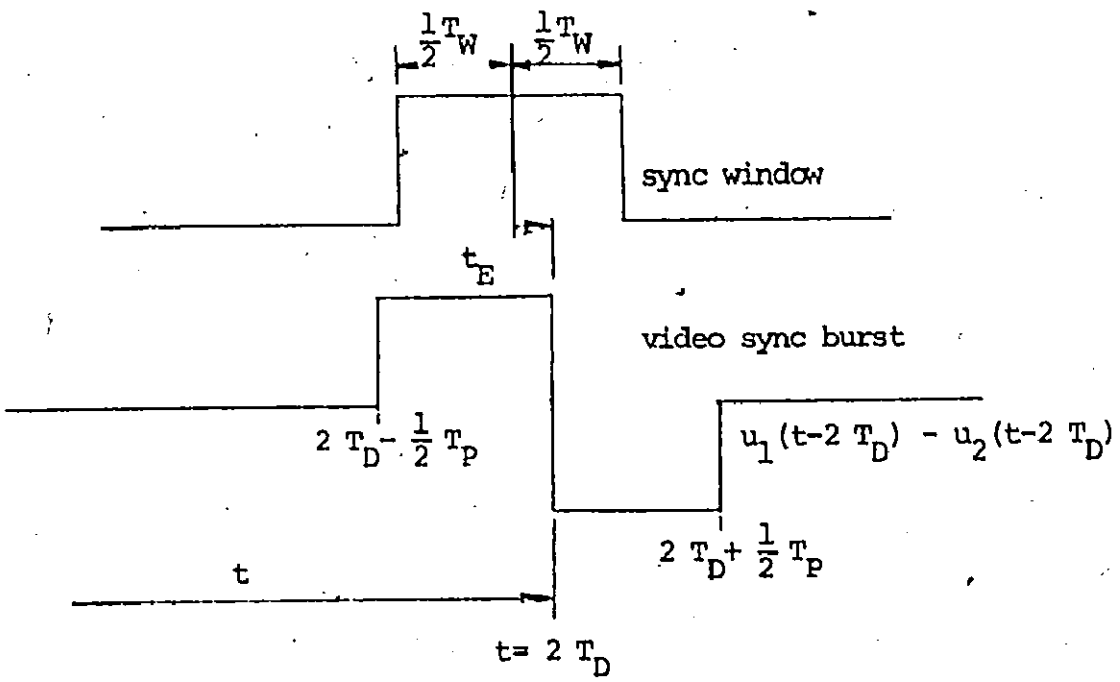

Fig. 4-7 Sync burst timing error. Note that the timing error is defined at the satellite.

since

$$m(t - T_D) = 1 \qquad 2T_D - t_E - \frac{1}{2}T_W \leq t \leq 2T_D - t_E + \frac{1}{2}T_W$$

$$= 0 \qquad \text{otherwise.}$$

and where

$$c_1' = \frac{c_1 L}{T_I}$$

It important to note that by using the integration technique, any video waveform with odd symmetry may provide a suitable PSK sync burst. Similarily, any video waveform with even symmetry may provide a suitable PSK sync burst. Appendix A lists several different simple video waveforms.

The value of v_S as a function of t_E can be calculated for three separate ranges of T_P as follows:

Error Detection Characteristic I; $T_W < T_P \leq 2T_W$ (See Fig. 4-8A)

$$\frac{v_S}{c_1'} = \begin{cases} 2A\, t_E & ; \quad -\frac{1}{2}(T_P - T_W) \leq t_E \leq \frac{1}{2}(T_P - T_W) \\ A[t_E + \frac{1}{2}(T_P - T_W)] & ; \quad \frac{1}{2}(T_P - T_W) \leq t_E \leq \frac{1}{2}T_W \\ A[\frac{1}{2}(T_P + T_W) - t_E] & ; \quad \frac{1}{2}T_W \leq t_E \leq \frac{1}{2}(T_P + T_W) \\ -A[\frac{1}{2}(T_P - T_W) - t_E] & ; \quad -\frac{1}{2}T_W \leq t_E \leq -\frac{1}{2}(T_P - T_W) \\ -A[\frac{1}{2}(T_P + T_W) + t_E] & ; \quad -\frac{1}{2}(T_P + T_W) \leq t_E \leq -\frac{1}{2}T_W \\ 0 & \text{otherwise.} \end{cases} \qquad (4\text{-}22)$$

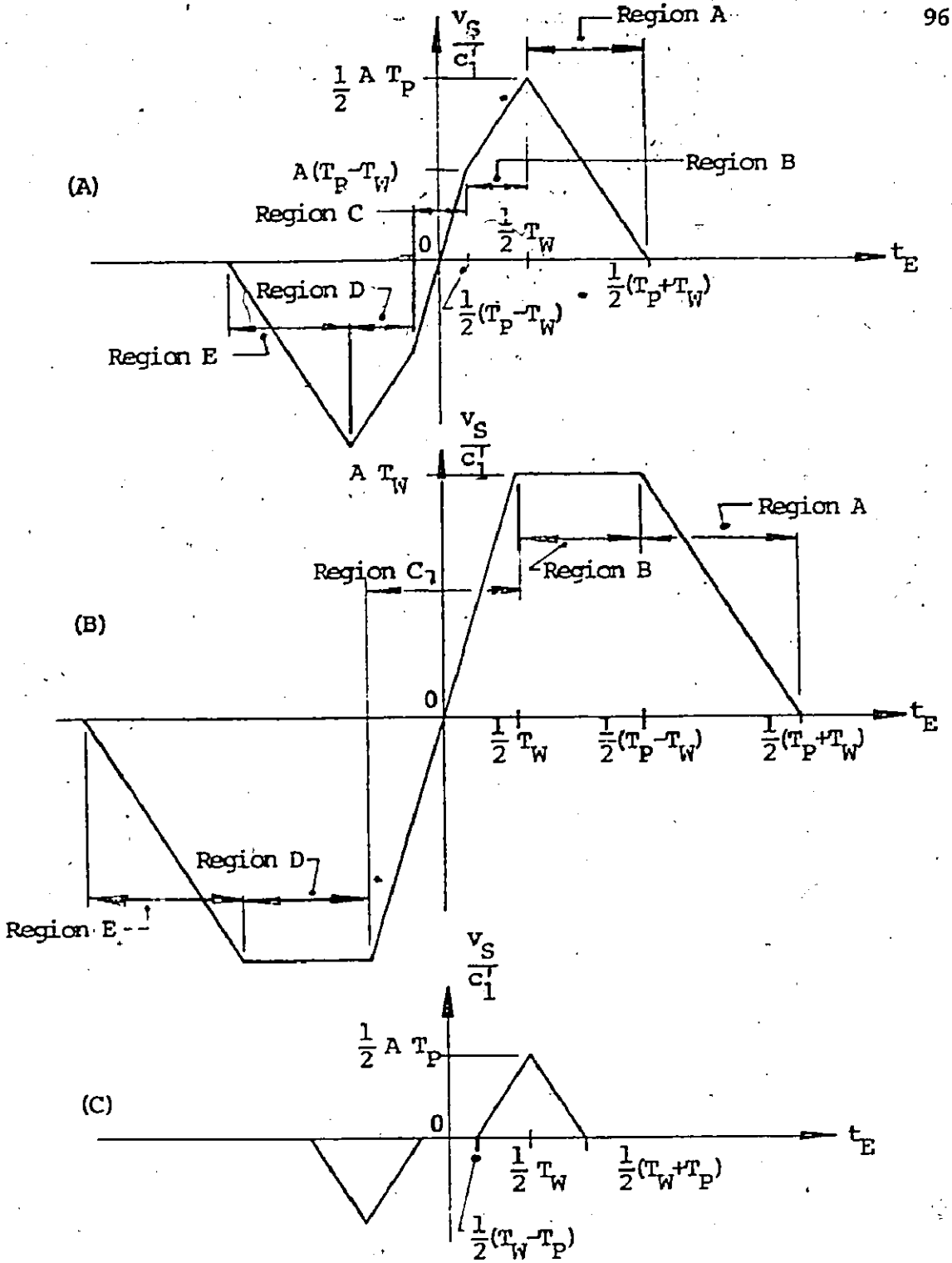

Fig. 4-8 (A) Error Detection Characteristic I,
(B) Error Detection Characteristic II,
(C) Error Detection Characteristic III.

Error Detection Characteristic II; $2T_W < T_P$ (See Fig. 4-8B)

$$\frac{v_S}{c_1'} = \begin{cases} 2A\, t_E & ; \quad -\frac{1}{2}T_W \le t_E \le \frac{1}{2}T_W \\ A\, T_W & ; \quad \frac{1}{2}T_W \le t_E \le \frac{1}{2}(T_P - T_W) \\ A[\frac{1}{2}(T_P + T_W) - t_E] & ; \quad \frac{1}{2}(T_P - T_W) \le t_E \le \frac{1}{2}(T_P + T_W) \\ -A\, T_W & ; \quad -\frac{1}{2}(T_P - T_W) \le t_E \le -\frac{1}{2}T_W \\ -A[t_E + \frac{1}{2}(T_P + T_W] & ; \quad -\frac{1}{2}(T_P + T_W) \le t_E \le -\frac{1}{2}(T_P - T_W) \\ 0 & \text{otherwise.} \end{cases} \tag{4-23}$$

Error Detection Characteristic III; $T_P \le T_W$ (See Fig. 4-8C)

$$\frac{v_S}{c_1'} = \begin{cases} 0 & ; \quad -\frac{1}{2}(T_W - T_P) \le t_E \le \frac{1}{2}(T_W - T_P) \\ A[t_E - \frac{1}{2}(T_W - T_P)] & ; \quad \frac{1}{2}(T_W - T_P) \le t_E \le \frac{1}{2}T_W \\ A[\frac{1}{2}(T_P + T_W) - t_E] & ; \quad \frac{1}{2}T_W \le t_E \le \frac{1}{2}(T_P + T_W) \\ A[t_E + \frac{1}{2}(T_W - T_P)] & ; \quad -\frac{1}{2}T_W \le t_E \le -\frac{1}{2}(T_W - T_P) \\ -A[t_E + \frac{1}{2}(T_P + T_W)] & ; \quad -\frac{1}{2}(T_P + T_W) \le t_E \le -\frac{1}{2}T_W \\ 0 & \text{otherwise.} \end{cases} \tag{4-24}$$

These curves have the S-shape property which is similar to that of the delay lock loop [44], [45]. Both Error Detection Characteristic I and II give useful curves whereas Error Detection Characteristic III has a null region in the center which gives no timing information inside this region and, consequently, will not be considered further.

From Fig. 4-8A and 4-8B, it is seen that for $|t_E| < \frac{1}{2}(T_P+T_W)$, the value of v_S is positive for positive values of timing error and negative for negative values of timing error. At the origin. the timing error is zero and the value of v_S is also zero. The timing shift given by (4-20) is opposite in sign to that of the timing error and, consequently, the application of this timing shift in the timing circuits always tends to reduce the timing error. This reduction in timing error is investigated next.

4.5 ANALYSIS OF ERROR DETECTION CHARACTERISTIC I USING PSK SYNC BURSTS

4.5.1 Error Detection Characteristic I

The error detection characteristic can be divided into five regions, as shown in Fig. 4-8A. Whenever the initial value of the timing error, referred to hence as the initial timing error, falls outside Region C, the sync unit must provide timing shifts to reduce the error until it does fall in this center region. Each timing shift requires transmission of a train of sync bursts around the synchronization loop which is referred to here as an iteration.

It is possible to analyse each region separately by considering the reduction of the timing error as more iterations occur. The number of iterations required to pass from a point in one region to a point in

a new region is determined and, thus, the initial timing error in the new region can be calculated. It is then possible to calculate the total number of iterations required to reach the center region and, since each iteration requires approximately one round trip time, the time to reach Region C can be estimated. Finally, the effects of up-link and downlink noise and satellite motion place a restriction in a root mean square sense on the reduction of the timing error toward the origin.

The initial timing error in each region is given the subscript of that region. In Regions B, C and D the initial timing error can arise either as a result of the first iteration or as a result of a later iteration where the magnitude of the timing error has been decreased from another region. For example, the timing error might pass from Region A to Region B or Region D to Region C. In Regions A and E, the initial timing error can result only from the first iteration. Analysis is not provided for Regions D and E since due to the odd symmetry of the error detection characteristic, the timing error is described by the analysis for Regions B and A, respectively. Thus, if the initial timing error falls in either Region D or E, the behaviour can be examined by simply changing the sign to convert to the other corresponding regions.

4.5.2 Effects of Satellite Motion

The effects of satellite motion on synchronization can be determined by assuming that the radial component of satellite velocity relative to the earth station varies slowly [37] and produces path

length time delay changes between iterations which are small compared to the sync window duration. The change in path delay, typically of the order of 18 ns [16], is given by

$$t_M(r) = \frac{\bar{v}_X(r)}{c} (2\,T_D + T_{GP}) \qquad (4\text{-}25)$$

$t_M(r)$ = change in path delay from the r^{th} to the $(r+1)^{th}$ iteration.

$\bar{v}_X(r)$ = average radial velocity between the r^{th} and the $(r+1)^{th}$ iterations.

c = velocity of light.

$2\,T_D$ = round trip time.

T_{GP} = time required for the ground station to process L sync bursts.

$= L.T_0$

T_0 = interpulse spacing of sync bursts.

For constant velocity satellite motion, the value of $t_M(r)$ is taken to be the initial value $t_M(1)$.

4.5.3 Detailed Analysis for Region A; $\frac{1}{2}T_W < t_E < \frac{1}{2}(T_P + T_W)$

(a) Timing Error Equation

In Region A, the equation for Error Detection Characteristic I is given from (4-22) by

$$v_S = c_1' A[\tfrac{1}{2}(T_P + T_W) - t_E] \qquad (4\text{-}26)$$

where t_E is the timing error variable.

Assume $t_{EA}(0)$ to be the initial timing error in Region A. Then, after the first iteration, the error voltage is given by (4-10) and the first timing shift from (4-20) is

$$t_{SA}(1) = -\frac{S\,T_G}{f_0} v_E(0) \qquad (4\text{-}27)$$

$$= -\frac{S\,T_G}{f_0} [c_1 A[\tfrac{1}{2}(T_P+T_W) - t_{EA}(0)] + v_N(1)]$$

where $v_N(1)$ = PSK sync burst integrated noise voltage from (4-10).

After the first timing shift, the timing error becomes

$$t_E(1) = t_{EA}(0) + t_{SA}(1) + t_M(1) \qquad (4\text{-}28)$$

$$= t_{EA}(0)\ (1 + \tfrac{1}{2}m) - \tfrac{1}{4}m(T_P+T_W) + t_M(1) - b\,v_N(1)$$

where

m = dimensionless loop constant

$$= \frac{2\,L\,A\,c_1\,S\,T_G}{T_I\,f_0}$$

$$b = \frac{S\,T_G}{f_0}$$

It is shown in Section 4.5.6 that the value of m, the dimensionless loop constant, is restricted by $0 < m < 2$.

After the r_A^{th} iteration and the r_A^{th} timing shift, the timing error is

$$t_E(r_A) = t_E(r_A-1)\,(1+\tfrac{1}{2}m) - \tfrac{1}{4}m(T_P+T_W) + t_M(r_A) - b\,v_N(r_A) \qquad (4\text{-}29)$$

To solve for $t_E(r_A)$ in terms of $t_{EA}(0)$, we may calculate the z-transform [38] of $t_E(r_A)$ to obtain

$$T_E(z) = \frac{t_{EA}(0) + \frac{1}{4}m(T_P+T_W)}{1 - (1+\frac{1}{2}m)\,z^{-1}} - \frac{\frac{1}{4}m(T_P+T_W)\,z(1)}{1 - (1+\frac{1}{2}m)\,z^{-1}} + \frac{T_M(z)}{1 - (1+\frac{1}{2}m)\,z^{-1}} - \frac{V_N(z)}{1 - (1+\frac{1}{2}m)\,z^{-1}} \qquad (4\text{-}30)$$

where

$T_E(z)$ = z-transform of $t_E(r_A)$.

$T_M(z)$ = z-transform of $t_M(r_A)$.

$V_N(z)$ = z-transform of $v_N(r_A)$.

Taking the inverse z-transform of (4-30) yields the timing error after r_A iterations

$$t_E(r_A) = t_{EA}(0)\,(1+\tfrac{1}{2}m)^{r_A} - \tfrac{1}{2}(T_P+T_W)\,[(1+\tfrac{1}{2}m)^{r_A}-1] + \sum_{s=1}^{r_A} t_M(s)\,(1+\tfrac{1}{2}m)^{r_A-s} - b\sum_{p=1}^{r_A} v_N(p)\,(1+\tfrac{1}{2}m)^{r_A-p} \qquad (4\text{-}31)$$

This relationship is the timing error equation. By calculating the mean and the root mean square, it is possible to determine the convergence characteristics of the synchronization loop as shown below.

(b) Average Timing Error

It is useful to calculate the expectation of $t_E(r_A)$ assuming that the values of $t_M(s)$ are all identically equal to $t_M(1)$ which implies constant velocity satellite motion. This gives an indication of how, on the average, the loop converges to smaller timing errors as more iterations are performed. Hence, the average timing error after r_A iterations, given by taking the expectation of (4-31), is

$$t_E(r_A)_{ave} = E\{t_E(r_A)\} = t_{EA}(0)\left(1+\tfrac{1}{2}m\right)^{r_A} - \tfrac{1}{2}(T_P+T_W)\left[\left(1+\tfrac{1}{2}m\right)^{r_A} - 1\right] + 2\,\frac{t_M}{m}(1)\left[\left(1+\tfrac{1}{2}m\right)^{r_A} - 1\right] \qquad (4\text{-}32)$$

where $E\{v_N(p)\} = 0$ for all p since $v_N(p)$ are all Gaussian Markov processes [39] having zero mean.

(c) Convergence with Satellite Motion

To reduce the average timing error in Region A as more iterations are performed, it is necessary for $t_E(r_A)_{ave} < t_E(r_A-1)_{ave}$. If the value of $t_M(1)$ is positive, it is possible for the timing shifts to be less than the satellite motion. Thus, to achieve this convergence, the minimum value of m can be determined and is given by solving

$$t_{EA}(0)\left(1+\tfrac{1}{2}m\right)^{r_A} - \tfrac{1}{2}(T_P+T_W)\left[\left(1+\tfrac{1}{2}m\right)^{r_A} - 1\right] + \frac{2\,t_M(1)}{m}\left[\left(1+\tfrac{1}{2}m\right)^{r_A} - 1\right]\Bigg|_{m=m_{min}}$$

$$< t_{EA}(0)\left(1+\tfrac{1}{2}m\right)^{r_A-1} - \tfrac{1}{2}(T_P+T_W)\left[\left(1+\tfrac{1}{2}m\right)^{r_A-1} - 1\right] + \frac{2\,t_M(1)}{m}\left[\left(1+\tfrac{1}{2}m\right)^{r_A-1} - 1\right]\Bigg|_{m=m_{min}} \qquad (4\text{-}33)$$

Thus, if $t_M(1)$ is positive, the minimum value of m is given by

$$m_{min} > \frac{2\, t_M(1)}{\frac{1}{2}(T_P+T_W) - t_{EA}(0)} \qquad (4\text{-}34)$$

(d) Transition to Region B

To determine the average number of iterations required to pass from any value of $t_{EA}(0)$ in Region A to the nearest point in Region B, it is necessary to calculate the largest integer, $r_{A_{max}}$, such that $t_E(r_{A_{max}}) > \frac{1}{2} T_W$, where $\frac{1}{2} T_W$ is the boundary between Region A and Region B. Thus,

$$t_{EA}(0)\,(1+\tfrac{1}{2}m)^{r_{A_{max}}} - \tfrac{1}{2}(T_P+T_W)\,[(1+\tfrac{1}{2}m)^{r_{A_{max}}} - 1] + \frac{2\, t_M(1)}{m}\,[(1+\tfrac{1}{2}m)^{r_{A_{max}}} - 1] > \tfrac{1}{2}T_W \qquad (4\text{-}35)$$

or $r_{A_{max}}$ is the largest integer satisfying the relation

$$r_{A_{max}} < \frac{\ln\left\{\dfrac{T_P - 4\,\frac{t_M(1)}{m}}{T_P + T_W - 2\, t_{EA}(0) - 4\,\frac{t_M(1)}{m}}\right\}}{\ln(1 + \frac{1}{2}m)} \qquad (4\text{-}36)$$

To reach Region B from Region A, the number of iterations required is then $r_{A_{max}} + 1$. Values of $r_{A_{max}} + 1$ are plotted in Fig. 4-9 as a function of the ratio $t_{EA}(0)/T_W$ for $T_P/T_W = 1.25$, $t_M(1) = 0$, and

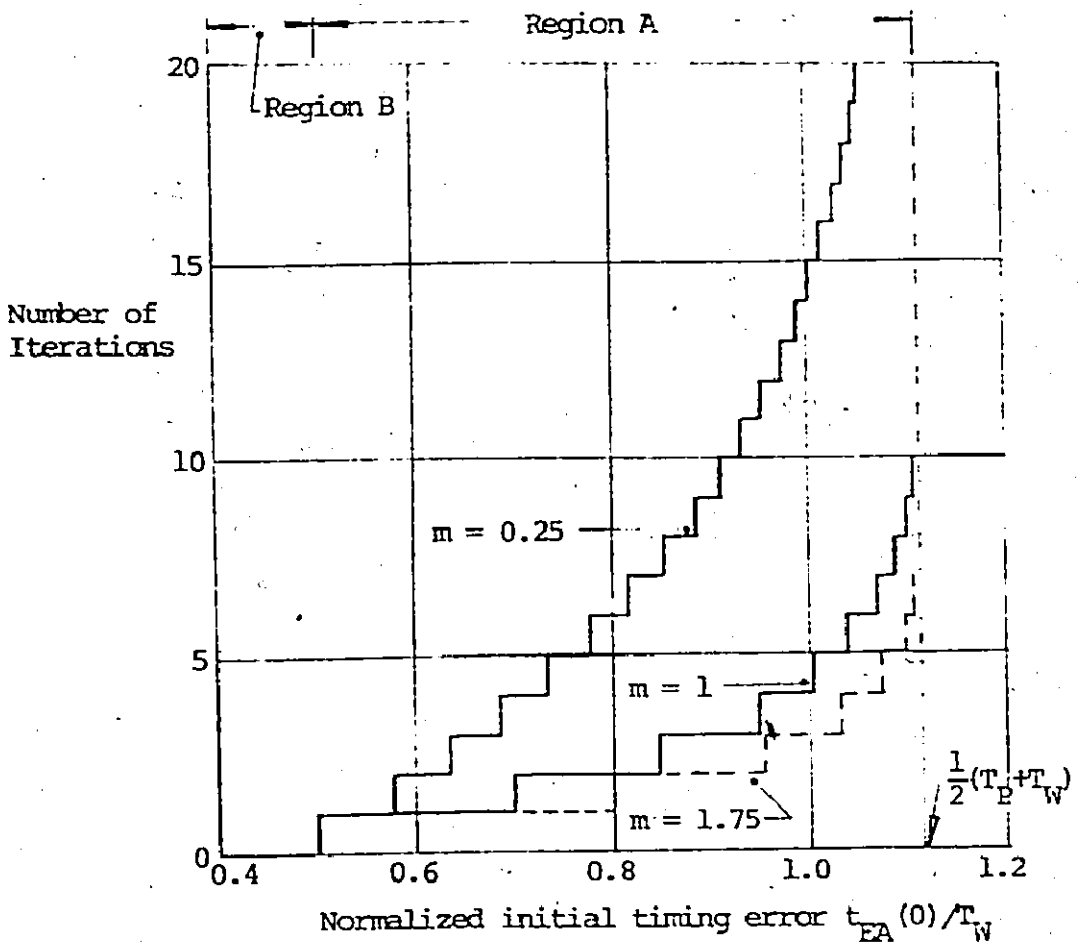

Fig. 4-9 Number of iterations required to reach Region B from Region A for a given ratio of $T_P/T_W = 1.25$.

several values of the dimensionless loop constant m. Since each iteration requires one round trip time of 270 ms, it is seen that for the values plotted it would take from 270 ms to 5.4 s to reduce the timing error from Region A to Region B. As the value of the initial timing error approaches the limit of $\frac{1}{2}(T_P+T_W)$, the number of iterations increases greatly depending on the value of m. Near this boundary, it is possible for satellite motion or noise to cause timing shifts which would increase the timing error so as to fall outside the capture range of the sync unit.

After $r_{A_{max}}+1$ iterations, the timing error enters Region B and the initial timing error in that region is given by

$$t_{EB}(0) = t_{EA}(0)\,(1+\tfrac{1}{2}m)^{r_{A_{max}}+1} - \tfrac{1}{2}(T_P+T_W)\,[(1+\tfrac{1}{2}m)^{r_{A_{max}}+1}-1]$$

$$\frac{2t_M(1)}{m}[(1+\tfrac{1}{2}m)^{r_{A_{max}}+1}-1] \qquad (4\text{-}37)$$

(e) RMS Timing Error

The timing error due to noise can be determined by considering the square root of the expectation of the mean square timing error. Define the rms timing error for the PSK sync burst after r_A iterations to be

$$t_E(r_A)_{rms} = [E\{t_E(r_A)\}^2]^{1/2}$$

$$= [E\{t_{EA}(0)\,(1+\tfrac{1}{2}m)^{r_A} - \tfrac{1}{2}(T_P+T_W)\,[(1+\tfrac{1}{2}m)^{r_A}-1] + \frac{2t_M(1)}{m}[(1+\tfrac{1}{2}m)^{r_A}-1]$$

$$- b\sum_{p=1}^{r_A} v_N(p)\,(1+\tfrac{1}{2}m)^{r_A-p}\}^2]^{1/2} \qquad (4\text{-}38)$$

$$= [t_E^2(r_A)_{ave} + E\{b \sum_{p=1}^{r_A} v_N(p) (1+\tfrac{1}{2}m)^{r_A-p}\}^2]^{1/2}$$

since $E\{t_E(r_A)_{ave} \cdot v_N(p)\} = 0$ for all p [39].

If $v_N(x)$ and $v_N(y)$ are orthogonal increments, that is $x \neq y$, then

$$E\{v_N(x) \cdot v_N(y)\} = 0 \qquad (4\text{-}39)$$

Thus,

$$E\{b \sum_{p=1}^{r_A} v_N(p) (1+\tfrac{1}{2}m)^{r_A-p}\}^2 = E\{b^2 E \sum_{p=1}^{r_A} v_N^2(p) (1+\tfrac{1}{2}m)^{2(r_A-p)}\} \qquad (4\text{-}40)$$

The expectation of $v_N^2(p)$ can be found from (4-10) to be [39]

$$E\{v_N^2(p)\} = \frac{\frac{1}{2} c_2^2 F_S N_0 L T_W}{T_I^2} + \frac{\frac{1}{2} k_6^2 F_G N_0 L T_Q}{T_I^2} \qquad (4\text{-}41)$$

where

F_S = noise figure of the satellite receiver.

F_G = noise figure of the ground station receiver.

N_0 = single-sided noise spectral density.

Thus, the rms timing error using PSK sync bursts is given by

$$t_E(r_A)_{rms} = [t_E^2(r_A)_{ave} + \frac{1}{2}\frac{b^2 N_0 L}{T_I^2}[c_2^2 F_S T_W + k_6^2 F_G T_Q] \sum_{p=1}^{r_A} (1+\tfrac{1}{2}m)^{2(r_A-p)}]^{1/2} \quad \text{---- (4-42)}$$

But, $\sum_{p=1}^{r_A} (1+\frac{1}{2}m)^{2(r_A-p)} = \frac{(1+\frac{1}{2}m)^{2r_A}-1}{m+\frac{1}{4}m^2}$. Hence, it is now possible to substitute $b = \frac{m T_I}{2 L c_1 A}$ and define the signal-to-noise ratio by $SNR = \frac{2E}{N_0}$ [40], which is the maximum for a matched filter where E is the signal energy. Then, the uplink signal-to-noise ratio, $SNR_U = \frac{2(A k_1 k_2)^2 T_W}{F_S N_0}$, and the downlink signal-to-noise ratio, $SNR_D = \frac{2(A k_1 k_2 k_3 k_4 k_5)^2 T_W}{F_G N_0}$.

Thus, the rms timing error is given by

$$t_E(r_A)_{rms} = [t_E^2(r_A)_{ave} + \frac{1}{4L}(\frac{T_W^2}{SNR_U} + \frac{T_W T_Q}{SNR_D}) \frac{m}{1+\frac{1}{4}m}[(1+\tfrac{1}{2}m)^{2r_A}-1]]^{1/2} \quad \text{---- (4-43)}$$

The timing error due to noise in (4-43) is a product of two factors, the first which is defined by (4-44) and the second, $f_A(r_A,m)$, which is a function of r_A and m as defined by (4-45). Values of t_N are plotted in Fig. 4-10, normalized to the sync window duration for the case $SNR_U = SNR_D = SNR$ and several values of L and T_Q.

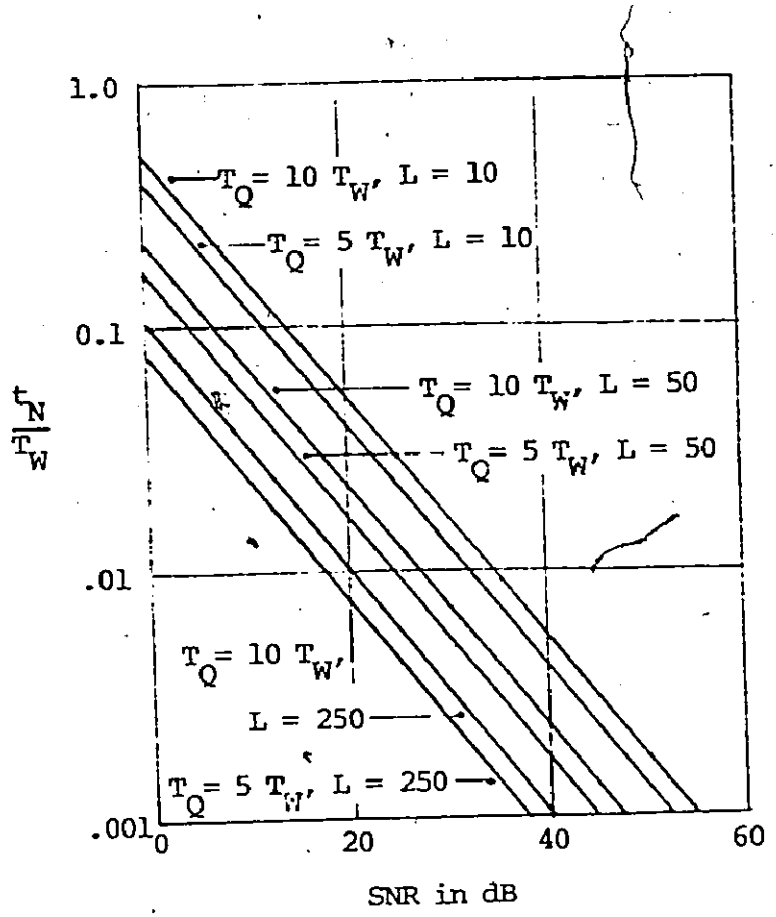

Fig. 4-10 Timing error due to noise.

$$t_N = \sqrt{\frac{1}{4L}\left(\frac{T_W^2}{SNR_U} + \frac{T_W T_Q}{SNR_D}\right)} \qquad (4\text{-}44)$$

$$f_A(r_A, m) = \left\{\frac{m}{1+\frac{1}{4}m}\left[\left(1+\frac{1}{2}m\right)^{2r_A} - 1\right]\right\}^{1/2} \qquad (4\text{-}45)$$

The expression $f_A(r_A,m)$ is now examined in more detail.

(f) Bound for $f_A(r_A,m)$

The value of $f_A(r_A,m)$ appears to become large as r_A increases. However, this factor can be bounded by noting that r_A has a maximum value, on the average, given by $r_{A_{max}} + 1$ where $r_{A_{max}}$ is defined by (4-36). Thus, after $r_{A_{max}} + 1$ iterations, the timing error enters Region B where a new expression for the error detection curve applies. The value of $f_A(r_A,m)$ is then bounded by

$$f_A(r_A,m) \leq \text{supremum}\,\{f_A(r_A,m)\} \qquad (4\text{-}46)$$

$$= \left\{\frac{m}{1+\frac{1}{4}m}\left[\left(1-\frac{1}{2}m\right)^2\left\{\frac{\ln\left\{\frac{T_P-\frac{4}{m}t_M(1)}{T_P+T_W-2t_{EA}(0)-\frac{4}{m}t_M(1)}+1\right\}}{\ln\left(1+\frac{1}{2}m\right)}\right\} - 1\right]\right\}^{1/2}$$

$$= \left\{\frac{m}{1+\frac{1}{4}m}\left[\left(1+\frac{1}{2}m\right)^2\left(\frac{T_P-\frac{4}{m}t_M(1)}{T_P+T_W-2t_{EA}(0)-\frac{4}{m}t_M(1)}\right)^2 - 1\right]\right\}^{1/2}$$

Curves are plotted in Fig. 4-11 showing the value of supremum $\{f_A(r_A,m)\}$ for $T_P/T_W = 1.25$ and several values of m as a function of the ratio $t_{EA}(0)/T_W$ assuming $t_M(1) = 0$ (stationary satellite).

(g) Capture Range

The capture range of the sync unit can be estimated by noting that after the first iteration and timing shift, the value of the rms timing error, $t_E(1)_{rms}$, must be less than $t_{EA}(0)$ to achieve a reduction in the timing error. The capture range, t_{capt}, is the boundary where $t_E(1)_{rms} = t_{EA}(0)$ in (4-43) and is reduced as the additive noise entering the system increases. Thus, assuming (4-34) is satisfied

$$t_{capt}^2 = m^2 t_N^2 + t_E^2(1)_{rms} \Big|_{t_{EA}(0) = t_{capt}} \tag{4-47}$$

or

$$t_{capt} = [\tfrac{1}{2}(T_P + T_W) - \tfrac{2}{m} t_M(1)] \left[\frac{1 + \frac{1}{2}m}{2 + \frac{1}{2}m} + f_N(t_N)\right]$$

where

$$f_N(t_N) = \frac{1}{2 + \frac{1}{2}m} \sqrt{1 - \frac{4m(1 + \frac{1}{4}m)t_N^2}{[\frac{1}{2}(T_P + T_W) - \frac{2}{m} t_M(1)]^2}}$$

The largest value for the capture range, $\frac{1}{2}(T_P+T_W) - \frac{2}{m} t_M(1)$, occurs with negative values of satellite motion and infinite uplink signal-to-noise ratio, that is, $t_N = 0$. Positive values of satellite motion not only linearly decrease the capture range, as is seen in the

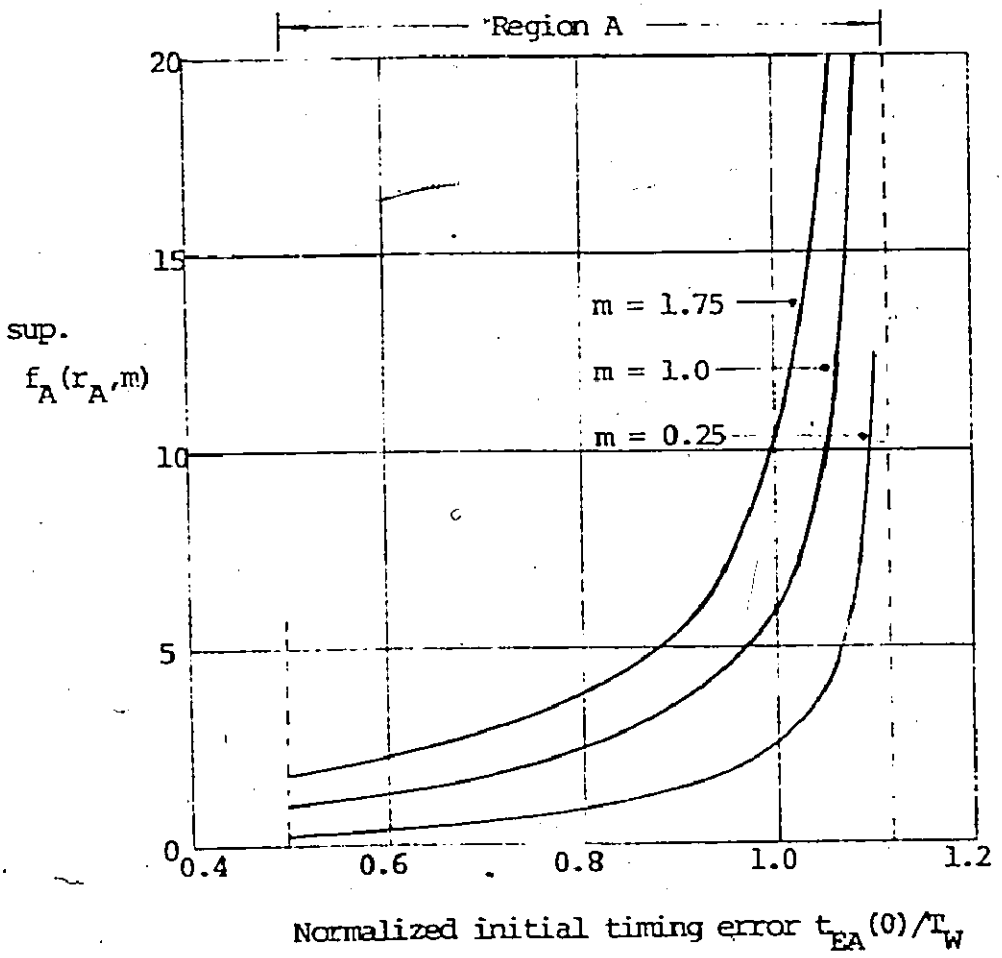

Fig. 4-11 Graphs of supremum $\{f_A(r_A,m)\}$ as a function of $t_{EA}(0)/T_W$ for a ratio of $T_P/T_W = 1.25$ and various m.

first term on the right in (4-47), but also enhance the effect of the noise. The factor $f_N(t_N)$ reduces the capture range with increasing noise and positive values of $t_M(1)$. In Fig. 4-12, the value of $f_N(t_N)$ is plotted as a function of $2\,t_N/(T_P+T_W)$ for various values of m assuming $t_M(1) = 0$.

(h) Maximum Allowable Noise Level

An estimate of the limit to the amount of noise which can be tolerated, if synchronization is to be achieved, can be calculated. This limit occurs when $f_N(t_N) = 0$, as illustrated in Fig. 4-12 for $t_M(1) = 0$, and is caused by the value of $t_E(1)_{rms}$ being greater than or equal to $t_{EA}(0)$ due to noise. This limit is given by

$$t_{NA_{max}} = \frac{\frac{1}{2}(T_P + T_W) - \frac{2}{m}\,t_M(1)}{\sqrt{4m(1 + \frac{1}{4}\,m)}} \qquad (4\text{-}48)$$

Values for $t_{NA_{max}}$ lie in the range from 0.3 to 1 μs for values of m from 0.25 to 1.75, $T_W = 1$ μs and $T_W < T_P < 2\,T_W$. Referring to Fig. 4-10, it is seen that these values of the timing error due to noise occur for values of signal-to-noise ratio near zero dB for the curves plotted. Hence, in all practical cases, capture is possible when the initial timing error falls in Region A.

4.5.4 ANALYSIS FOR REGION B; $\frac{1}{2}(T_P - T_W) \leq t_E \leq \frac{1}{2}\,T_W$

Much of the detailed analysis for Region B is similar to that in Region A. Hence, where similarities exist, only the results are

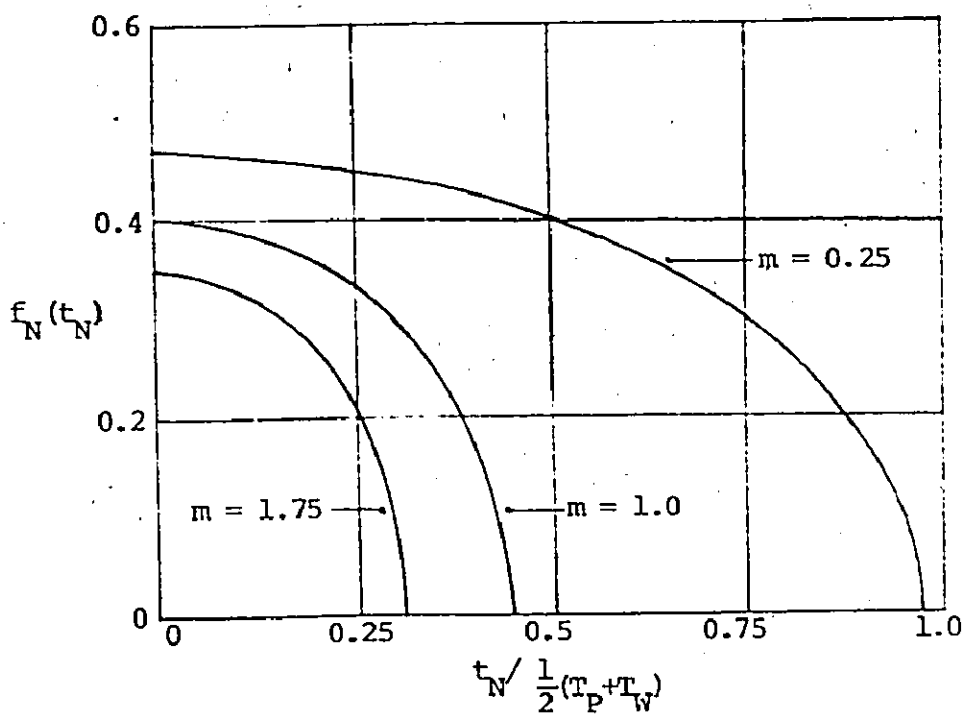

Fig. 4-12 Graph of $f_N(t_N)$ as a function of $2\ t_N/(T_P + T_W)$ for various values of m.

presented. Details are provided when necessary.

(a) Timing Error Equation

The timing error after r_B iterations in Region B is given by

$$t_E(r_B) = t_{EB}(0)\,(1-\tfrac{1}{2}m)^{r_B} - \tfrac{1}{2}(T_P-T_W)\,[1-(1-\tfrac{1}{2}m)^{r_B}] + \sum_{s=1}^{r_B} t_M(s)\,(1-\tfrac{1}{2}m)^{r_B-s}$$

$$- b \sum_{p=1}^{r_B} v_N(p)\,(1-\tfrac{1}{2}m)^{r_B-p} \qquad (4\text{-}49)$$

where $t_{EB}(0)$ is the initial timing error in Region B.

(b) Average Timing Error

The average timing error is given by

$$t_E(r_B)_{ave} = t_{EB}(0)\,(1-\tfrac{1}{2}m)^{r_B} - \tfrac{1}{2}(T_P-T_W)\,[1-(1-\tfrac{1}{2}m)^{r_B}] + \frac{2}{m}\,t_M(1)\,[1-(1-\tfrac{1}{2}m)^{r_B}$$

——— (4-50)

(c) Convergence with Satellite Motion

When the value of $t_M(1)$ is positive, the minimum value of m required to achieve convergence is Region B is given by

$$m_{min} > \frac{2\,t_M(1)}{\tfrac{1}{2}(T_P - T_W) - t_{EA}(0)} \qquad (4\text{-}51)$$

(d) Transition to Region C

The number of iterations to reach Region C from any initial value of $t_{EB}(0)$ is $r_{B_{max}} + 1$ where $r_{B_{max}}$ is the largest integer satisfying the relation

$$r_{B_{max}} < \frac{\ln\left\{\dfrac{t_{EB}(0) + \frac{1}{2}(T_P - T_W) - \frac{2}{m}\,t_M(1)}{T_P - T_W - \frac{2}{m}\,t_M(1)}\right\}}{\ln\left(\dfrac{1}{1 - \frac{1}{2}\,m}\right)} \qquad (4\text{-}52)$$

The graph of $r_{B_{max}} + 1$ is plotted in Fig. 4-13 for the ratio $T_P/T_W = 1.25$ and several values of m. Even for a small value, say $m = 0.25$, the number of iterations required to reach Region C from any point in Region B is eight or less.

(e) RMS Timing Error

The rms timing error is given by

$$t_E(r_B)_{rms} = [t_E^2(r_B)_{ave} + t_N^2\, f_B^2(r_B, m)]^{1/2} \qquad (4\text{-}53)$$

where t_N and $t_E(r_B)_{ave}$ are defined by (4-44) and (4-50), respectively, and

$$f_B(r_B, m) = \left[\frac{m}{1 - \frac{1}{4}\,m}\left[1 - (1 - \tfrac{1}{2}\,m)^{2r_B}\right]\right]^{1/2}$$

(f) Maximum Allowable Noise Level

The analysis of Region A shows that capture can be achieved if the initial timing error is less than the value given by the capture range. In Region B, the timing error due to noise cannot exceed a certain limit if the timing error is to reach Region C. This limit occurs when $t_E(1)_{rms} = t_{EB}(0) = \frac{1}{2}(T_P - T_W)$, the lower boundary of

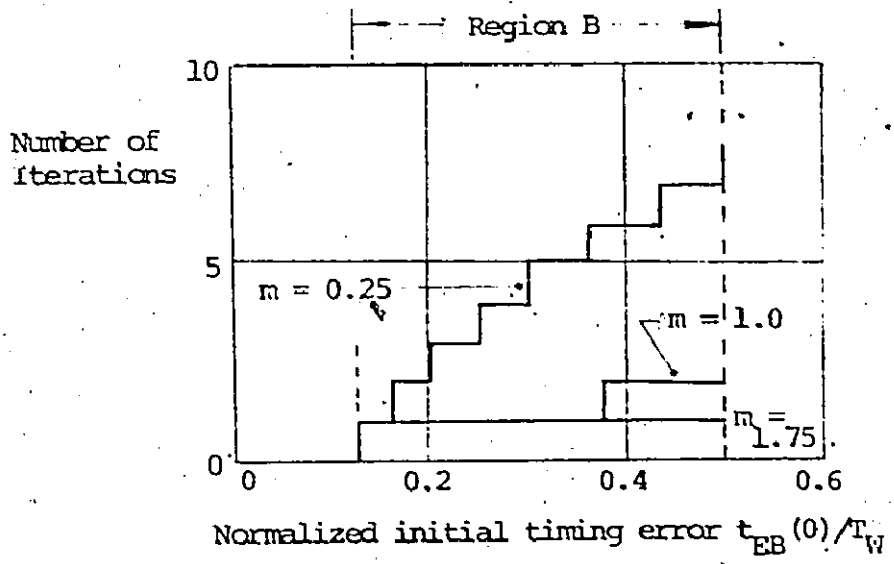

Fig. 4-13 Number of iterations required to reach Region C from Region B for a given ratio of $T_p/T_W = 1.25$.

Region B. With one more iteration, the timing error must fall in Region C, assuming (4-51) is satisfied. Thus, using (4-50) and (4-53), the maximum timing error due to noise, $t_{NB_{max}}$, is given by

$$[\tfrac{1}{2}(T_P-T_W)]^2 = \{\tfrac{1}{2}(T_P-T_W)(1-\tfrac{1}{2^m}) - \tfrac{m}{4}(T_P-T_W)+ t_M(1)\}^2 + m^2\, t^2_{NB_{max}} \quad (4\text{-}54)$$

or

$$t_{NB_{max}} = \tfrac{1}{m}\{[\tfrac{1}{2}(T_P-T_W)]^2 - [\tfrac{1}{2}(T_P-T_W)(1-m) + t_M(1)]^2\}^{1/2}$$

A typical value for $t_{NB_{max}}$ is of the order of 100 ns which, from Fig. 4-10, corresponds to values of signal-to-noise ratio of the order of 10 dB.

4.5.5 CONVERGENCE TO REGION C FROM REGION A

The total number of iterations required to reach Region C from any point in Region A can now be calculated. The number of iterations from Region B to Region C is given from (4-52) by $r_{B_{max}} + 1$, as illustrated in Fig. 4-13, but it is necessary to match the equation for Region A to the equation for Region B taking the boundary at $t_E = \frac{1}{2} T_W$ into account.

From (4-36), it is shown that $r_{A_{max}} + 1$ iterations are required to reduce the timing error from any given initial timing error $t_{EA}(0)$ in Region A to an initial timing error of $t_{EB}(0)$ in region B. The value of $t_{EB}(0)$ can be determined by first calculating the value of $r_{B_{max}}$ in (4-52) with $\frac{1}{2} T_W$ substituted for $t_{EB}(0)$. Thus, the number of iterations required to reduce the timing error from an initial timing error of $\frac{1}{2} T_W$

to Region C is then given by the largest integer, $r_{B_{tot}}$, satisfying the relation

$$r_{B_{tot}} < r_{B_{max}}\Big|_{t_{EB}(0) = \frac{1}{2}T_W} + 1 \qquad (4\text{-}55)$$

Next, it is seen from Fig. 4-13, that the required value of $t_{EB}(0)$ is simply the timing error at the edge of the first step to the left of the boundary at $\frac{1}{2}T_W$. Hence, substitute $r_{B_{tot}}$ for the value of r_B in (4-50) and $\frac{1}{2}(T_P - T_W)$ for $t_E(r_B)_{ave}$. This yields the required value of $t_{EB}(0)$ given by

$$t_{EB}(0) = \frac{(T_P - T_W)\left[1 - \frac{1}{2}(1 - \frac{1}{2}m)^{r_{B_{tot}}}\right]}{(1 - \frac{1}{2}m)^{r_{B_{tot}}}} - \frac{2t_M(1)}{m}\,\frac{\left[1 - (1 - \frac{1}{2}m)^{r_{B_{tot}}}\right]}{(1 - \frac{1}{2}m)^{r_{B_{tot}}}} \qquad (4\text{-}56)$$

Substituting this value of $t_{EB}(0)$ in (4-37) and solving for $r_{A_{max}} + 1$ results in the number of iterations required to reduce the timing error from any value $t_{EA}(0)$ in Region A, to the edge of the first step to the left of $\frac{1}{2}T_W$ in Region B. Thus,

$$r_{A_{max}} + 1 = \frac{\ln\left\{\dfrac{t_{EB}(0) - \frac{1}{2}(T_P + T_W) + \frac{2}{m}t_M(1)}{t_{EA}(0) - \frac{1}{2}(T_P + T_W) + \frac{2}{m}t_M(1)}\right\}}{\ln(1 + \frac{1}{2}m)} \qquad (4\text{-}57)$$

where $t_{EB}(0)$ is given by (4-56).

The total number of iterations, r_{AC}, is then given by

$$r_{AC} = r_{B_{tot}} + r_{A_{max}} + 1 \qquad (4\text{-}58)$$

The graph of r_{AC} is plotted in Fig. 4-14 for $T_P/T_W = 1.25$ and several values of m.

The value of the rms timing error can be determined by calculating the expectation of the square of the timing error. Thus, using (4-31), (4-32), (4-50), (4-55), (4-57) and (4-58) yields

$$t_E(r_{AC})_{rms} = [E\{[t_E(r_{A_{max}}+1)_{ave} - b \sum_{p=1}^{r_{A_{max}}+1} v_N(p)(1+\tfrac{1}{2}m)^{r_{A_{max}}+1-p}](1-\tfrac{1}{2}m)^{r_{B_{tot}}}$$

$$- \tfrac{1}{2}(T_P-T_W)[1-(1-\tfrac{1}{2}m)^{r_{B_{tot}}}] + \tfrac{2}{m}t_M(1)\,[1-(1-\tfrac{1}{2}m)^{r_{B_{tot}}}]\}^2$$

$$+ t_N^2 f_B^2(r_{B_{tot}}, m)]^{1/2} \qquad (4\text{-}59)$$

After simplification, the rms timing error becomes

$$t_E(r_{AC})_{rms} = [\{t_{EA}(r_{A_{max}}+1)_{ave}\,(1-\tfrac{1}{2}m)^{r_{B_{tot}}} - \tfrac{1}{2}(T_P-T_W)[(1-(1-\tfrac{1}{2}m)^{r_{B_{tot}}}]$$

$$+ \tfrac{2}{m}t_M(1)[1-(1-\tfrac{1}{2}m)^{r_{B_{tot}}}]\}^2 + t_N^2\{f_A^2(r_{A_{max}}+1,m)(1-\tfrac{1}{2}m)^{2r_{B_{tot}}}$$

$$+ f_B^2(r_{B_{tot}}, m)\}]^{1/2} \qquad (4\text{-}60)$$

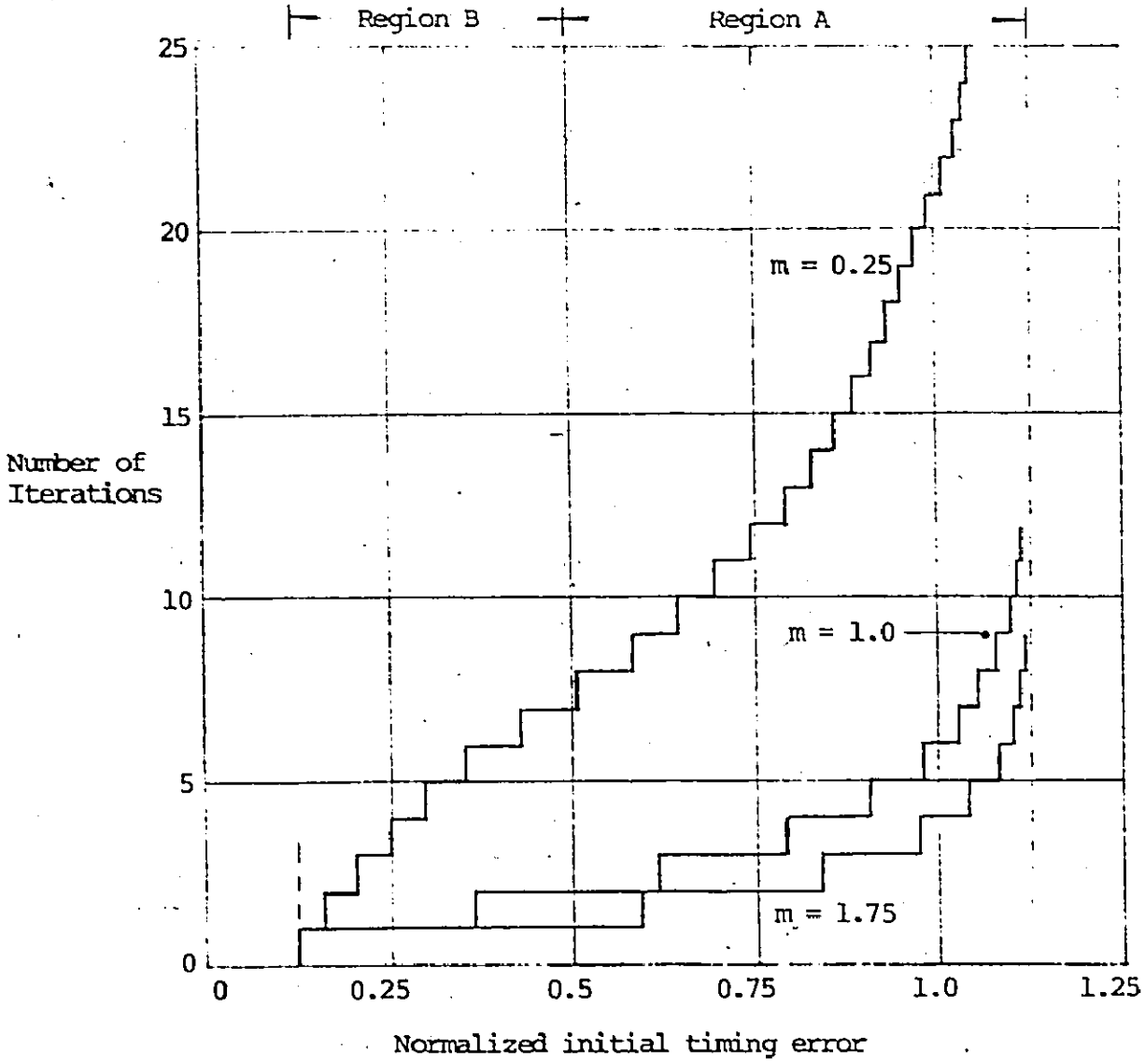

Fig. 4-14 Graph of r_{AC} for the ratio $T_P/T_W = 1.25$ and several values of m.

Note that the timing error due to noise from iterations in Region A is reduced by a multipying factor of $(1 - \frac{1}{2})^{2r_{B_{tot}}}$ which is always less than unity.

4.5.6 CONVERGENCE TO THE ORIGIN - REGION C; $-\frac{1}{2}(T_P - T_W) \leq t_E \leq (T_P - T_W)$

(a) Timing Error Equation

When the timing error reaches Region C, the system must provide convergence towards the origin as more iterations are performed. Only the salient points of the analysis are presented since the procedure is similar to that of Region A.

The z-transform of the timing error is given by

$$T_E(z) = \frac{t_{EC}(0)}{1 - (1 - m)z^{-1}} + \frac{T_M(z)}{1 - (1 - m)z^{-1}} - \frac{b\, V_N(z)}{1 - (1 - m)z^{-1}} \qquad \text{---- (4-61)}$$

where

$T_E(z)$ = z-transform of $t_E(r_C)$

$T_M(z)$ = z-transform of $t_M(r_C)$

$V_N(z)$ = z-transform of $v_N(r_C)$

$t_{EC}(0)$ = initial timing error in Region C.

For stability, the poles in (4-61) must lie outside the unit circle in the z^{-1} plane. Hence, a condition that m must satisfy is

$$0 < m < 2 \qquad (4\text{-}62)$$

The inverse z-transform of (4-61), giving the timing error

equation is

$$t_E(r_C) = t_{EC}(0)\,(1-m)^{r_C} + \sum_{s=1}^{r_C} t_M(s)\,(1-m)^{r_C-s} - b \sum_{p=1}^{r_C} v_N(p)\,(1-m)^{r_C-p} \qquad (4\text{-}63)$$

(b) Average Timing Error

The average timing error is calculated assuming that the values of $t_M(s)$ are all identically equal to $t_M(1)$ which implies a constant velocity satellite motion. This shows how, on the average, the loop converges to the origin of the error detection characteristic as more iterations are performed. Hence,

$$E\{t_E(r_C)\} = t_E(r_C)_{ave} = t_{EC}(0)\,(1-m)^{r_C} + \frac{t_M(1)}{m}\,[1-(1-m)^{r_C}] \qquad (4\text{-}64)$$

where $E\{v_N(p)\} = 0$ for all p since $v_N(p)$ are all Gaussian Markov processes having zero mean [39].

There are three regions which occur for the timing error $t_{EC}(0)\ (1-m)^{r_C}$, as shown in Fig. 4-15. The first, for $0 < m < 1$, is the overdamped case where $t_{EC}(0)\ (1-m)^{r_C}$ always has the same sign as $t_{EC}(0)$. The second case, for $m = 1$, is the critically damped case in which convergence occurs in one iteration. The third region, for $1 < m < 2$ is the underdamped case in which the value of $t_{EC}(0)\ (1-m)^{r_C}$ alternates in sign with consecutive values of r_C.

Similarly, there are three regions of convergence for $t_M(1)\ [1-\ (1-m)^{r_C}]/m$, as shown in Fig. 4-16, but in this case, the steady state error is $t_M(1)/m$. The overdamped case occurs when

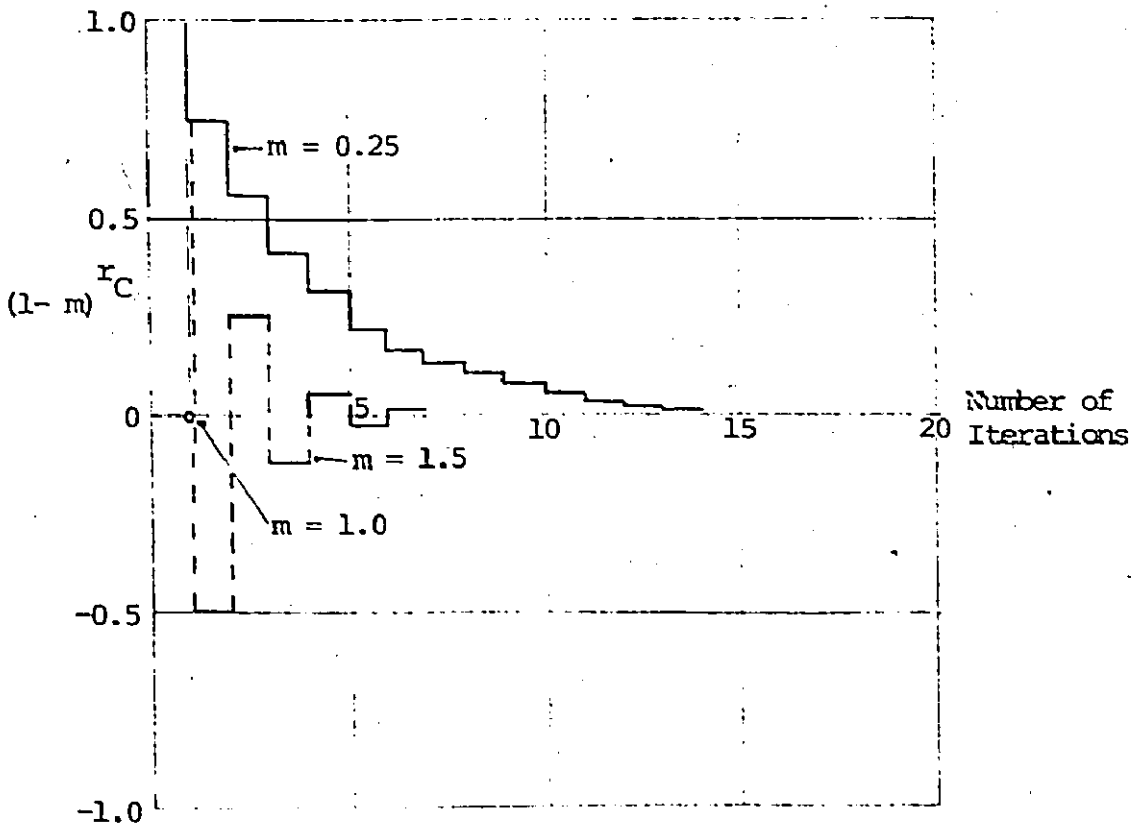

Fig. 4-15 Graph of $(1 - m)^{r_C}$ for selected values of m.

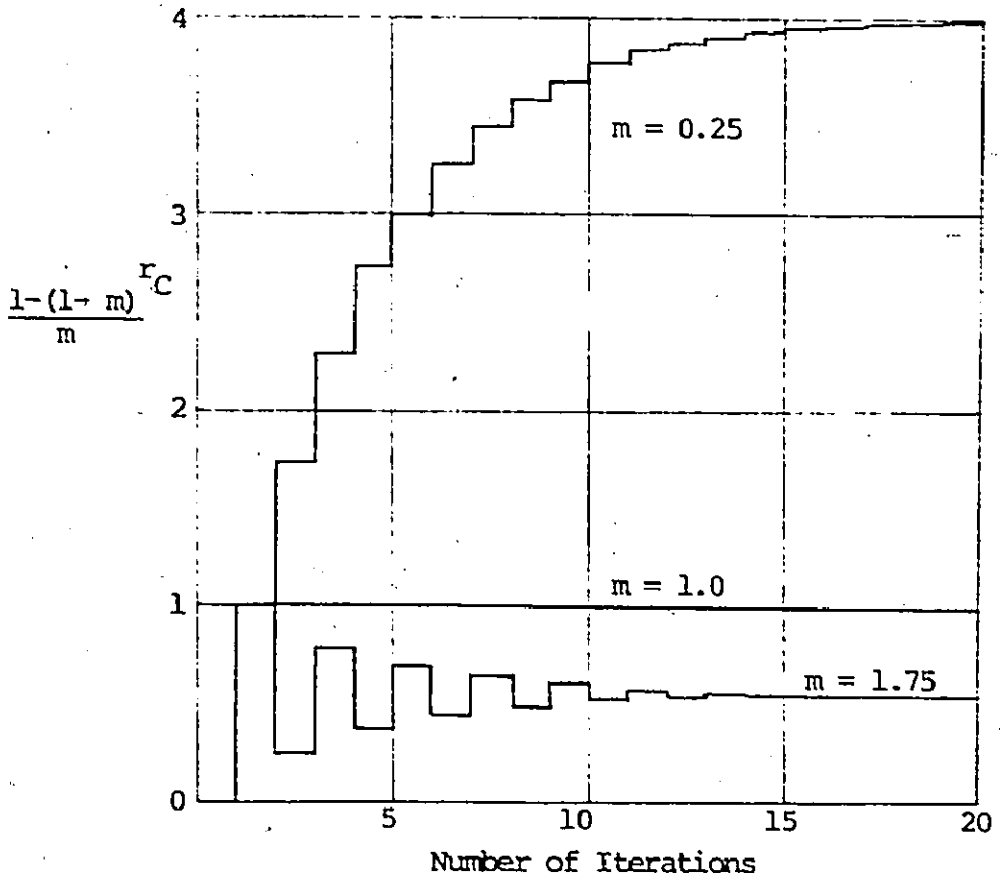

Fig. 4-16 Graph of $[1 - (1 - m)^{r_C}]/m$ for selected values of m.

$0 < m < 1$ while critical damping occurs for $m = 1$ and underdamping results when $1 < m < 2$.

(c) RMS Timing Error

The rms timing error is given by

$$t_E(r_C)_{rms} = \left[t_E^2(r_C)_{ave} + t_N^2 \cdot \frac{m}{2-m}\left[1 - (1-m)^{2r_C}\right]\right]^{1/2} \quad \text{---- (4-65)}$$

where t_N is defined by (4-44) and $t_E(r_C)_{ave}$ is defined by (4-64).

The noise term contains the factor $\frac{m}{2-m}\left[1 - (1-m)^{2r_C}\right]$ which is plotted in Fig. 4-17 for selected values of m. From the graphs of Fig. 4-15, 4-16 and 4-17 it is seen that a desirable range for m lies between approximately 0.25 and 1.75 which gives a 7:1 dynamic range. Thus, the exact value of m is not critical. This implies that synchronization can be achieved even without careful sync burst level control. Assuming this particular range of values, the loop arrives at a steady state condition after about 15 iterations. Hence, since an iteration occurs in time $2T_D + T_{GP}$ which is about 0.3 seconds, this part of the fine search mode is completed in approximately 4.5 seconds.

As the number of iterations becomes large, the magnitude of $(1-m)^{r_C}$ and $(1-m)^{2r_C}$ become negligible for $0 < m < 2$. Hence, in the steady state case the timing error is given by

$$t_E(\infty)_{rms} = \left[\left(\frac{t_M(1)}{m}\right)^2 + t_N^2 \frac{m}{2-m}\right]^{1/2} \quad (4-66)$$

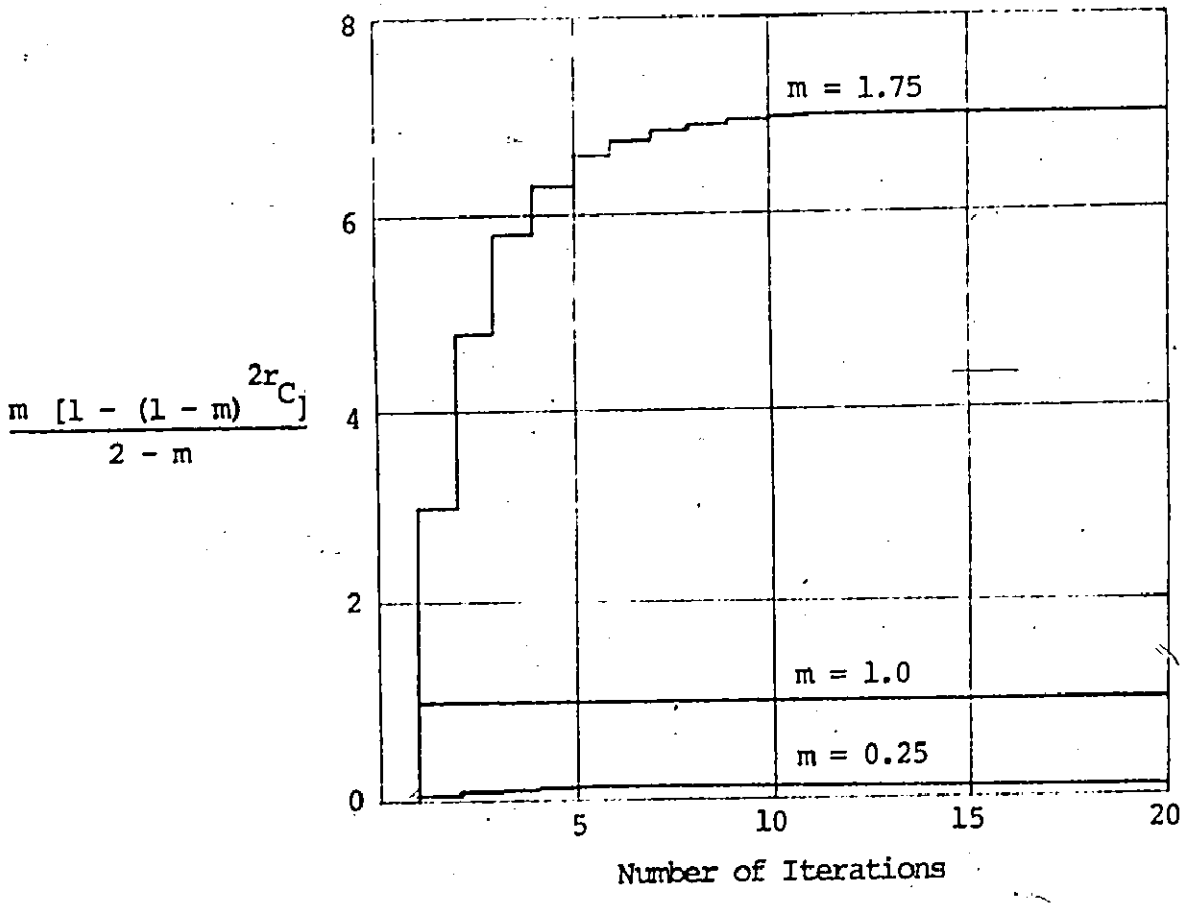

Fig. 4-17 Graph of $\frac{m}{2 - m}[1 - (1 - m)^{2r_C}]$ for selected values of m.

The value of the rms timing error is thus seen to be at least $t_M(1)/m$ due to satellite motion alone. This error is quite significant (for example, it is equal to 50 ns for $t_M(1)$ = 10 ns and m = 0.2) compared to values of the timing error due to noise as plotted in Fig. 4-10. Using a value of m near the maximum of 2 reduces the error due to satellite motion but greatly increases the contribution due to noise. However, in Chapter 5, it is shown that the timing error due to constant velocity satellite motion can be eliminated by employing a tracking network.

4.6 ANALYSIS FOR ERROR DETECTION CHARACTERISTIC I USING FSK SYNC BURSTS

Analysis of the system using FSK sync bursts shows that the resulting equations which describe the timing error are the same as for the PSK sync burst implementation wherever the effects of the uplink and downlink noise do not enter the equations. When noise effects are present in the equations, it is seen that the timing error is increased when FSK sync bursts are used rather than PSK sync bursts. The details of the analysis are essentially the same as presented in Section 4.5 and consequently, only the results are presented here.

4.6.1 Results for Region A; $\frac{1}{2} T_W < t_E < \frac{1}{2}(T_P + T_W)$

(a) Timing Error Equation

The timing error equation, derived using the same technique as Section 4.5.3(a), is given by

$$t_E(r_A) = t_{EA}(0)\,(1+\tfrac{1}{2}m)^{r_A} - \tfrac{1}{2}(T_P+T_W)\,[(1+\tfrac{1}{2}m)^{r_A}-1] + \sum_{s=1}^{r_A} t_M(s)\,(1+\tfrac{1}{2}m)^{r_A-s}$$

$$- b \sum_{p=1}^{r_A} v'_N(p)\,(1+\tfrac{1}{2}m)^{r_A-p} \qquad (4\text{-}67)$$

where $v'_N(p)$ = RSK sync burst integrated noise voltage from (4-16).

(b) Average Timing Error - see (4-32).

(c) Convergence with Satellite Motion - see (4-34).

(d) Transition to Region B - see (4-36), (4-37) and Fig. 4-9.

(e) RMS Timing Error

The rms timing error is given by

$$t_E(r_A)_{rms} = [t_E^2(r_A)_{ave} + 2\,t_N^2 f_A^2(r_A, m)]^{1/2} \qquad (4\text{-}68)$$

where $t_E(r_A)_{ave}$, t_N and $f_A(r_A, m)$ are given by (4-32), (4-44) and (4-45).

Note that the contribution due to noise is doubled from that of the PSK sync burst implementation.

(f) Capture Range

The capture range is given by

$$t'_{capt} = [\tfrac{1}{2}(T_P+T_W) - \tfrac{2}{m}\, t_M(1)]\,[\frac{1+\frac{1}{2}m}{2+\frac{1}{2}m} + f'_N(t_N)] \qquad (4\text{-}69)$$

where

$$f'_N(t_N) = \frac{1}{2+\frac{1}{2}m}\sqrt{\frac{1 - 8m(1+\frac{1}{4}m)t_N^2}{[\frac{1}{2}(T_P+T_W) - \frac{2}{m}\, t_M(1)]^2}}$$

Clearly the capture range for the FSK sync burst implementation is less than for PSK sync burst implementation since $f'_N(t_N) < f_N(t_N)$ (from (4-47)).

(g) Maximum Allowable Noise Level

An estimate of the amount of noise which can be tolerated is given by

$$t'_{NA_{max}} = \frac{\frac{1}{2}(T_P + T_W) - \frac{2}{m}\, t_M(1)}{\sqrt{8m(1+\frac{1}{4}m)}} \qquad (4\text{-}70)$$

For typical parameter values, the signal-to-noise ratio requirement from Fig. 4-10 is near zero dB.

4.6.2 Results for Region B; $\frac{1}{2}(T_P - T_W) < t_E < \frac{1}{2}T_W$

The analysis in this Region is similar to that of Section 4.5.4 and only the results which differ are presented here.

(a) Timing Error Equation

The timing error equation is given by

$$t_E(r_B) = t_{EB}(0)\,(1-\tfrac{1}{2}m)^{r_B} - \tfrac{1}{2}(T_P-T_W)\,[1-(1-\tfrac{1}{2}m)^{r_B}] + \sum_{s=1}^{r_B} t_M(s)\,(1-\tfrac{1}{2})^{r_B-s}$$

$$- b \sum_{p=1}^{r_B} v'_N(p)\,(1-\tfrac{1}{2}m)^{r_B-p} \qquad (4\text{-}71)$$

(b) Average Timing Error - see (4-50).

(c) Congergence with Satellite Motion - see (4-51).

(d) Transition to Region C - see (4-52) and Fig. 4-13.

(e) RMS Timing Error

The rms timing error due to noise is given by

$$t_E(r_B)_{rms} = [t_E^2(r_B)_{ave} + 2\,t_N^2\,f_B^2(r_B, m)]^{1/2} \qquad (4\text{-}72)$$

where $t_E(r_B)_{ave}$, t_N and $f_B(r_B, m)$ are given by (4-50), (4-44) and (4-53), respectively.

Note that the contribution due to noise is doubled as compared to the PSK sync burst implementation.

(f) Maximum Allowable Noise Level

The maximum allowable noise which can be tolerated is given by

$$t'_{NB_{max}} = \frac{1}{2m}\,\{[\tfrac{1}{2}(T_P - T_W)]^2 - [\tfrac{1}{2}(T_P - T_W)(1 - m) + t_M(1)]^2\}^{1/2} \qquad (4\text{-}73)$$

4.6.3 Convergence to Region C from Region A

The analysis for the number of iterations to reach Region C from Region A is the same as for the PSK sync burst case and the equations for $r_{B_{tot}}$, $t_{EB}(0)$, $r_{A_{max}}$, and r_{AC} are given by (4-55), (4-56), (4-57) and (4-58), respectively. Also, Fig. 4-14 and the related discussion applies here.

(a) RMS Timing Error

The rms timing error is given by

$$t_E(r_{AC})_{rms} = [\{t_{EA}(r_{A_{max}} + 1)(1 - \tfrac{1}{2}m)^{r_{B_{tot}}} - \tfrac{1}{2}(T_P - T_W)[1-(1-\tfrac{1}{2}m)^{r_{B_{tot}}}]$$

$$+ \frac{2}{m} t_M(1)[1-(1-\tfrac{1}{2}m)^{r_{B_{tot}}}]\}^2 + 2\, t_N^2\{f_A^2(r_{A_{max}}+1, m)(1-\tfrac{1}{2}m)^{2r_{B_{tot}}}$$

$$+ f_B^2(r_{B_{tot}}, m)\}]^{1/2} \qquad (4\text{-}74)$$

Again, it is seen that the contribution due to noise for the FSK sync burst implementation is twice as high as for the PSK sync burst implementation.

4.6.4 Convergence to the Origin - Region C; $-\frac{1}{2}(T_P - T_W) \leq t_E \leq \frac{1}{2}(T_P - T_W)$

(a) Timing Error Equation

The timing error after r_C iterations in Region C is given by

$$t_E(r_C) = t_{EC}(0)(1-m)^{r_C} + \sum_{s=1}^{r_C} t_M(s)(1-m)^{r_C - s} - b \sum_{p=1}^{r_C} v_N'(p)(1-m)^{r_C - p}$$

(4-75)

(b) Average Timing Error - see (4-64), Fig. 4-15 and 4-16.

(c) RMS Timing Error

The rms timing error is given by

$$t_E(r_C)_{rms} = [t_E^2(r_C)_{ave} + t_N^2 \frac{2m}{2-m}[1 - (1-m)^{2r_C}]]^{1/2} \quad (4\text{-}76)$$

where $t_E(r_C)_{ave}$ and t_N are given by (4-64) and (4-44), respectively.

This expression differs from that of (4-65) in that the term due to noise is doubled.

As the number of iterations become large. The rms timing error reduces to

$$t_E(\infty)_{rms} = [(\frac{t_M(1)}{m})^2 + t_N^2 \frac{2m}{2-m}]^{1/2} \quad (4\text{-}77)$$

4.7 ANALYSIS FOR ERROR DETECTION CHARACTERISTIC II USING PSK SYNC BURSTS

In this section, the behaviour of the timing error is examined assuming that Error Detection Characteristic II, shown in Fig. 4-8B, applied and that PSK sync bursts are used. The procedure is identical to that formulated in Section 4.5 and only the results of the analysis are presented here.

4.7.1 Results for Region A; $\frac{1}{2}(T_P - T_W) < t_E < \frac{1}{2}(T_P + T_W)$

(a) Timing Error Equation - see (4-31).

(b) Average Timing Error - see (4-32).

(c) Convergence with Satellite Motion - see (4-34).

(d) Transition to Region B

Since the lower boundary for Region A here differs from that of Error Detection Characteristic I, the value of $r_{A_{max}}$ differs and is given by

$$r_{A_{max}} < \frac{\ln\left\{\dfrac{2T_W - \frac{4}{m}t_M(1)}{T_P + T_W - 2t_{EA}(0) - \frac{4}{m}t_M(1)}\right\}}{\ln(1 + \frac{1}{2}m)} \qquad (4\text{-}78)$$

To reach Region B from Region A, the number of iterations required is then $r_{A_{max}} + 1$. Values of $r_{A_{max}} + 1$ are plotted in Fig. 4-18 as a function of the ratio $t_{EA}(0)/T_W$ for $t_M(1) = 0$ and several values of the dimensionless loop constant m. Curves for different values of the ratio T_P/T_W all have the same shape as Fig. 4-18 since $r_{A_{max}}$ in (4-78) is a function of $T_P/T_W - 2t_{EA}(0)/T_W$. A shift in T_P/T_W is reflected by a similar shift in the variable $2\,t_{EA}(0)/T_W$. Thus, the normalized range extends from $\frac{1}{2}T_P/T_W$ to $\frac{1}{2}T_P/T_W + 1$.

The value for $t_{EB}(0)$ is given by (4-37) using (4-78) for the value of $r_{A_{max}}$.

(e) RMS Timing Error - see (4-43) and (4-45) noting $\sup.f_A(r_A,m)$ given by (4-79).

(f) Bound for $f_A(r_A,m)$

As in (4-46) of Section 4.5.3, a bound for $f_A(r_A,m)$ can be calculated and given by

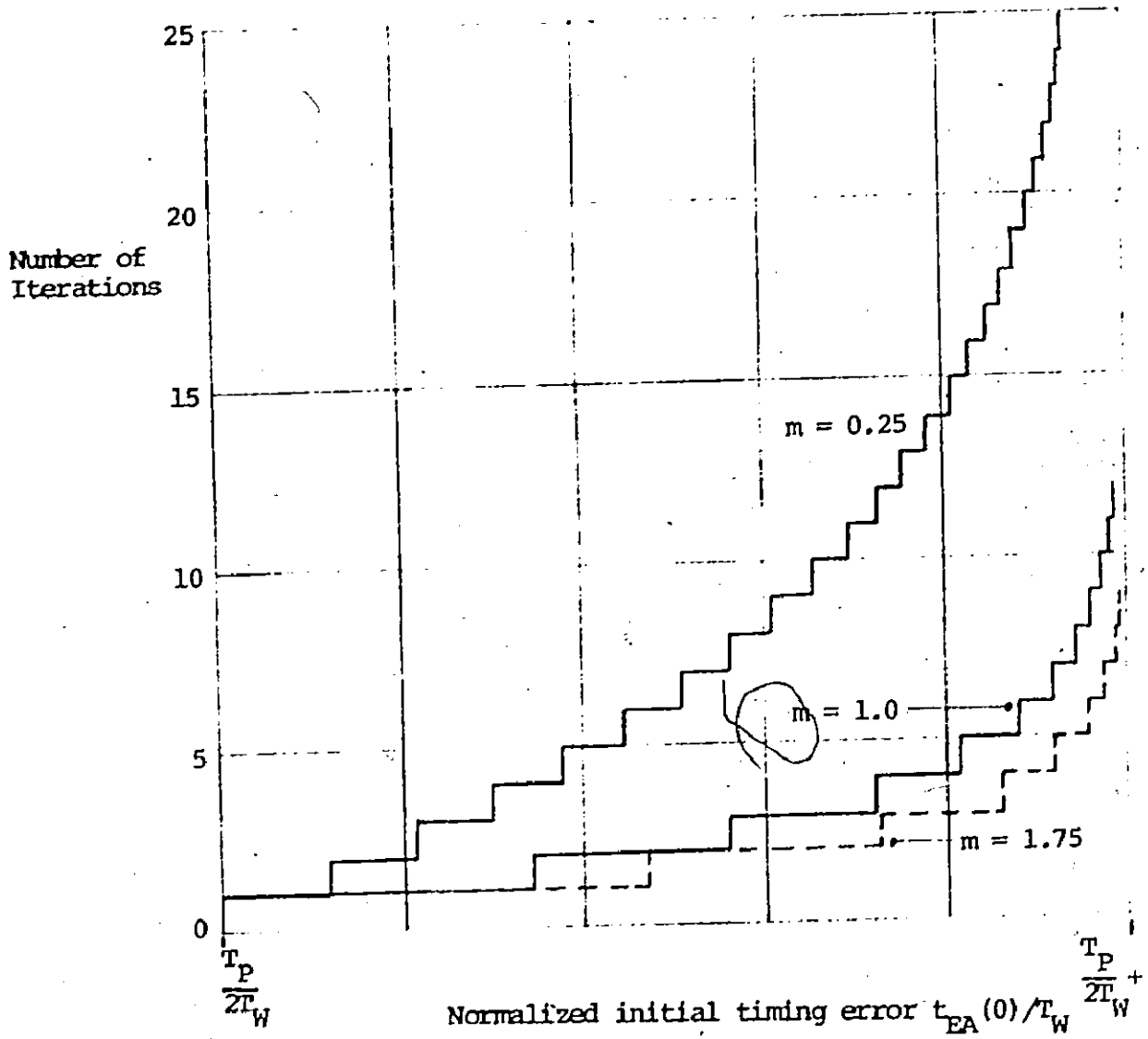

Fig. 4-18 Number of timing shifts to reach Region B from Region A for any ratio of $T_P/T_W > 2$ and specific values of m.

$$\sup. f_A(r_A,m) = \left[\frac{m}{1+\frac{1}{4}m}\left[(1+\frac{1}{2}m)^2\left(\frac{2T_W - \frac{4}{m}t_M(1)}{T_P+T_W - 2t_{EA}(0) - \frac{4}{m}t_M(1)}\right)^2 - 1\right]\right]^{1/2} \quad (4\text{-}79)$$

Curves of sup. $f_A(r_A, m)$ are similar in shape to Fig. 4-11.

(g) Capture Range - see (4-47) and Fig. 4-12.

(h) Maximum Allowable Noise Level - see (4-48).

4.7.2 Results for Region B; $\frac{1}{2}T_W \leq t_E \leq \frac{1}{2}(T_P - T_W)$

The results in Region B for Error Detection Characteristic II are quite different from those derived with Error Detection Characteristic I. This is due to the zero slope of the former as compared to the non-zero slope of the latter.

(a) Timing Error Equation

The timing error equation is given by

$$t_E(r_B) = t_{EB}(0) - \frac{1}{2}m\,r_B\,T_W + \sum_{s=1}^{r_B} t_M(s) - b\sum_{p=1}^{r_B} v_N(p) \quad (4\text{-}80)$$

(b) Average Timing Error

The average timing error is given by

$$t_E(r_B)_{ave} = t_{EB}(0) - \frac{1}{2}m\,r_B\,T_W + r_B\,t_M(1) \quad (4\text{-}81)$$

(c) Convergence with Satellite Motion

The minimum value of m for convergence with $t_M(1)$ positive is

$$m_{min} > \frac{2\,t_M(1)}{T_W} \quad (4\text{-}82)$$

(d) Transition to Region C

The number of iterations to reach Region C from an initial value of $t_{EB}(0)$ is $r_{B_{max}}$ is the largest integer such that

$$r_{B_{max}} < \frac{t_{EB}(0) - \frac{1}{2} T_W}{\frac{1}{2} m T_W - t_M(1)} \tag{4-83}$$

(e) RMS Timing Error

The rms timing error is given by

$$t_E(r_B)_{rms} = [t_E^2(r_B)_{ave} + t_N^2 m^2 r_B^2]^{1/2} \tag{4-84}$$

where $t_E(r_B)_{ave}$ and t_N are given by (4-81) and (4-44), respectively.

(f) Maximum Allowable Noise Level

$$t_{NB_{max}} = \frac{1}{m}[[\frac{1}{2} T_W]^2 - [\frac{1}{2} T_W(1 - m) + t_M(1)]^2]^{1/2} \tag{4-85}$$

4.7.3 Convergence to Region C from Region A

The analysis is similar with that presented in Section 4.5.5 and only the results are given here. The equations for $r_{A_{max}}$ and r_{AC} are given by (4-57) and (4-58) respectively.

(a) Largest Integer $r_{B_{tot}}$

$$r_{B_{tot}} < r_{B_{max}}\Big|_{t_{EB}(0) = \frac{1}{2}(T_P - T_W)} + 1 \tag{4-86}$$

(b) Value of $t_{EB}(0)$

$$t_{EB}(0) = \frac{1}{2} T_W (1 + m\, r_{B_{tot}}) - r_{B_{tot}}\, t_M(1) \qquad (4\text{-}87)$$

(c) RMS Timing Error

$$t_E(r_{AC})_{rms} = [\{t_E(r_{A_{max}}+1)_{ave} - \frac{1}{2} m\, r_{B_{tot}}\, T_W + r_{B_{tot}}\, t_M(1)\}^2 + t_N^2\{f_A^2(r_{A_{max}}+1, m) + m^2\, r_{B_{tot}}^2\}]^{1/2} \qquad (4\text{-}88)$$

4.7.4 Convergence to the Origin - Region C; $\frac{1}{2} T_W < t_E < T_W$

The results of this section are identical to those given in Section 4.5.6 since the equations for the two error detection characteristics are the same in this region.

4.8 ANALYSIS FOR ERROR DETECTION CHARACTERISTIC II USING FSK SYNC BURSTS

Analysis of the system when FSK sync bursts are used shows that many of the results are the same as for the PSK sync burst case. The similarities and differences are examined in this section.

4.8.1 Results for Region A; $\frac{1}{2}(T_P - T_W) < t_E < \frac{1}{2}(T_P + T_W)$

(a) Timing Error Equation - see (4-67).

(b) Average Timing Error - see (4-32).

(c) Convergence with Satellite Motion - see (4-34).

(d) Transition to Region B - see (4-78) and Fig. 4-18.

(e) RMS Timing Error - see (4-68).

(f) Capture Range - see (4-69).

(g) Maximum Noise Level - see (4-70).

4.8.2 Results for Region B; $\frac{1}{2} T_W \leq t_E \leq \frac{1}{2}(T_P - T_W)$

(a) Timing Error Equation

$$t_E(r_B) = t_{EB}(0) - \frac{1}{2} m r_B T_W + \sum_{s=1}^{r_B} t_M(s) - b \sum_{p=1}^{r_B} v_N'(p) \quad (4\text{-}89)$$

(b) Average Timing Error - see (4-81).

(c) Convergence with Satellite Motion - see (4-82).

(d) Transition to Region C - see (4-83).

(e) RMS Timing Error

The rms timing error is given by

$$t_E(r_B)_{rms} = [t_E(r_B)_{ave} + 2 t_N^2 m^2 r_B^2]^{1/2} \quad (4\text{-}90)$$

where $t_E(r_B)_{ave}$ and t_N are given by (4-81) and (4-44), respectively.

(f) Maximum Allowable Noise Level

The maximum permissible timing error due to noise is given by

$$t'_{NB_{max}} = \frac{1}{2m}\left[\left[\frac{1}{2}\cdot T_W\right]^2 - \left[\frac{1}{2} T_W(1 - m) + t_M(1)\right]^2\right]^{1/2} \qquad (4\text{-}91)$$

4.8.3 Convergence to Region C from Region A

The results of the analysis show that the equations for $r_{A_{max}}$, r_{AC}, $r_{B_{tot}}$ and $t_{EB}(0)$ are given by (4-57), (4-58), (4-86) and (4-87), respectively.

The rms timing error is given by

$$t_E(r_{AC})_{rms} = \left[\left(t_{EA}(r_{A_{max}} + 1) - \frac{1}{2} m\, r_{B_{tot}} T_W + r_{B_{tot}} t_M(1)\right)^2 + 2 t_N^2\left\{f_A^2(r_{A_{max}} + 1, m) + m^2 r_{B_{tot}}^2\right\}\right]^{1/2} \qquad (4\text{-}92)$$

4.8.4 Convergence to the Origin - Region C; $-\frac{1}{2} T_W \leq t_E \leq \frac{1}{2} T_W$

The results here are identical with Section 4.5.6.

4.9 SUMMARY OF THE RESULTS

Starting from a physical model, a set of three error detection characteristics has been derived which relate an error voltage measured in the sync unit to a timing error occurring at the satellite. These characteristics result by assuming the coherent detection of either PSK or FSK sync bursts.

Depending on the value of the dimensionless loop constant, m, the timing error is found to converge to zero average timing error whenever the satellite is stationary. In particular, a desirable range for m lies between 0.25 and 1.75.

The analysis of the loop behaviour is the same for PSK and FSK sync bursts whenever the effects of noise do not enter the equations. When the effect of noise is included, the PSK sync burst is found to produce a higher signal-to-noise ratio than the FSK sync burst. However, the FSK sync burst system can be implemented using envelope detectors.

Of significance is the result that the earth station will lock to the sync window even for values of signal-to-noise ratio near zero dB. To achieve accurate synchronization, a signal-to-noise ratio of the order of 30 dB is required.

CHAPTER 5

Tracking Mode

Accurate earth station synchronization to a switching satellite in motion can be achieved by providing a tracking feature in the synchronization circuits. In Chapter 4, it was shown that fine search synchronization can be obtained by the transmission of trains of sync bursts at intervals of approximately one round trip time (called iterations). After reception of each train of sync bursts back at the earth station, a timing adjustment is performed. Thus, it was shown that convergence to zero average timing error occurs whenever there is no satellite motion.

When satellite motion is assumed, a timing error results in the fine search mode which can be many times greater than the timing error due to noise. In this chapter, it is shown that for constant velocity satellite motion, a tracking network can be included in the timing circuits which reduces the average timing error to zero. Thus, in this case, the limitation in timing accuracy is due to the uplink and downlink signal-to-noise ratios.

5.1 TRACKING MODE TIMING EQUATIONS

The dynamic error caused by satellite motion can be reduced by switching in the tracking mode network, shown in Fig. 5-1, which integrates the error voltage pulse from the timing adjustment gate. With the tracking mode network switched out, this circuit is identical with the

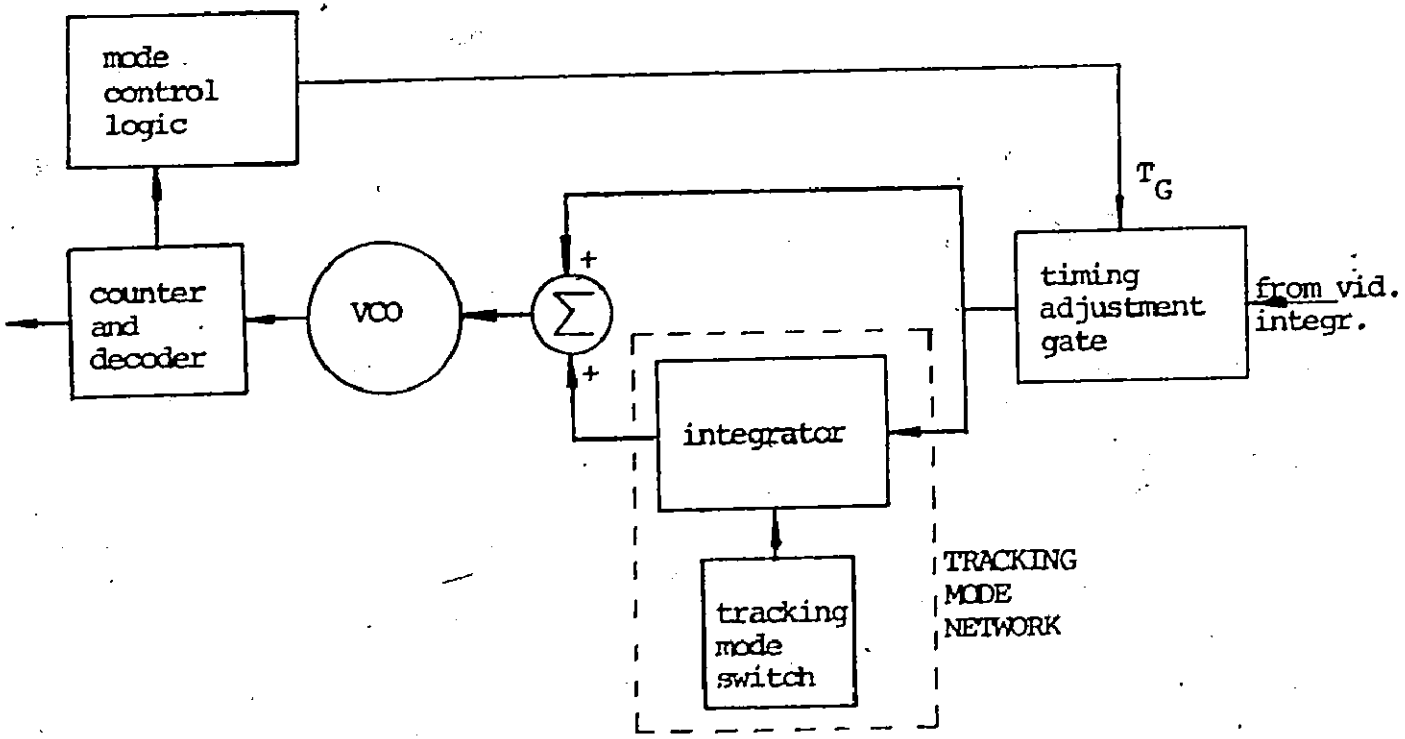

Fig. 5-1 Timing circuit configuration with the tracking mode implementation.

fine search mode system of Chapter 4. The integrator applies a very small correction voltage to the VCO at all times through the summer which causes the frequency of the VCO to be different from the center frequency whenever there is satellite motion. Thus, in effect, the tracking mode network provides a prediction of the timing shift based on previous measurements.

The relationship between the input voltage and the output voltage of the integrator is given by

$$v_O(t) = \frac{1}{T'_I} \int_{T_1}^{T_2} v_I(t)dt \qquad (5\text{-}1)$$

where

$v_O(t)$ = output voltage.

$v_I(t)$ = input voltage.

T'_I = integrator time constant.

$T_2 - T_1$ = integration interval.

The value of $v_I(t)$ is equal to the error voltage from (4-10) for the PSK sync burst implementation or (4-16) for the FSK sync burst implementation for the duration of the timing adjustment gate, T_G, and zero at other times. Hence, the output voltage can be written as a function of the number of iterations in the tracking mode, r_T, and is given by

$$v_{OT}(r_T - 1) = \frac{1}{T_I} \sum_{p=0}^{r_T-1} \int_{p(2T_D+T_{GP})}^{T_G+p(2T_D+T_{GP})} v_{ET}(t)\,dt \qquad (5\text{-}2)$$

$$= \frac{T_G}{T_I} \sum_{p=0}^{r_T-1} v_{ET}(p) \quad \text{(since } v_{ET}(t) \text{ is constant over the intervals of the integration)}$$

$v_{ET}(t)$ = error voltage in the tracking mode

$v_{ET}(p)$ = error voltage in the tracking mode after the pth iteration

$2\,T_D$ = round trip time

T_{GP} = time required for the earth station to process L sync bursts

= $L\,T_O$

T_O = interpulse spacing of sync bursts.

The subscript 'T' is used to denote that the loop is operating in the tracking mode.

The tracking mode can be initiated either by a manual switch or some automatic means on completion of the fine search mode. Whenever a timing error occurs, two types of timing shift are provided. The first is the static shift due to the error voltage being applied to the VCO for the duration of the timing adjustment gate, and second is the dynamic shift due to the integrator which is constantly fed to the VCO. Adjustments are made only when a gate trigger is applied to the timing adjust-

ment gate which is once in a round trip time.

The shift due to the gate and the tracking network can be found in a manner similar to that developed in Section 4.5.6. Assume the last error voltage at the input to the timing adjustment gate, upon completion of the fine search mode, is $v_E(r_K)$ corresponding to the timing error $t_E(r_K)$ as in (4-65). This voltage is the first error voltage applied in the tracking mode and is called $v_{ET}(0)$ corresponding to the timing error $t_{ET}(0)$. Next, the integrator is activated placing the synchronization circuits in the tracking mode. The timing adjustment gate applies the error voltage $v_{ET}(0)$ through the summer to the control terminal of the VCO. The tracking mode network integrates the voltage and adds this to the initially stored value of zero volts. The output voltage of the tracking network is also applied to the control terminal of the VCO through the summer and the period of the VCO becomes

$$T = \frac{K_C}{f} = \frac{K_C}{f_O + S(v_{ET}^1(0) + v_{OT}(0))} \qquad (5\text{-}3)$$

$$= T_O\left[1 - \frac{S\, v_{ET}(0)}{f_O}\right] - \frac{S\, T_O\, v_{OT}(0)}{f_O}$$

The first term of this expression is the same as (4-19) and the resulting timing shift is given by (4-20). The timing shift due to the second term for a duration of T_O is $-\frac{T_O\, S\, v_{OT}(0)}{f_O}$. Since this shift actually occurs over the interval $(2T_D + T_{GP})$, the time between

iterations, the total timing shift is $-\frac{(2T_D + T_{GP})\ S\ v_{OT}(0)}{f_O}$. Thus, the total timing shift for the first iteration is

$$t_{ST}(1) = -[\frac{S\ T_G\ v_{ET}(0)}{f_O} + \frac{S(2\ T_D + T_{GP})}{f_O})\ v_{OT}(0)] \qquad (5\text{-}4)$$

The timing shift over the r_T^{th} iteration is given by

$$t_{ST}(r_T) = -[\frac{S\ T_G\ v_{ET}(r_T - 1)}{f_O} + \frac{S(2\ T_D + T_{GP})}{f_O}\ v_{OT}(r_T - 1)] \qquad (5\text{-}5)$$

Solutions of (5-5) are now examined in detail for the PSK sync burst implementation and for the FSK sync burst implementation.

5.2 PSK SYNC BURST IMPLEMENTATION

5.2.1 Timing Error Equation

The method for calculating the timing error is similar to that used in Chapter 4 but the analysis now includes the additional input from the tracking network. The timing shift after the first iteration, given by substituting (5-2) into (5-4) and using (4-10) is

$$t_{ST}(1) = -[\frac{S\ T_G}{f_O} + \frac{S(2\ T_D + T_{GP})}{f_O}\frac{T_G}{T_I'}][2\ Ac_1'\ t_{ET}(0) + v_{NT}(1)]$$

$$= -[m\ t_{ET}(0) + b\ v_{NT}(1) + \beta m\ t_{ET}(0) + \beta b\ v_{NT}(1)] \qquad (5\text{-}6)$$

where $\beta = \frac{2\ T_D + T_{GP}}{T_I'}$, is the tracking mode loop constant, and m and b

are defined by (4-28). Thus, the timing error after the first iteration is

$$t_{ET}(1) = t_{ET}(0) + t_{ST}(1) + t_M(1) \qquad (5\text{-}7)$$

$$= t_{ET}(0)\ [1 - m - \beta m] - b(1 + \beta)v_{NT}(1) + t_M(1)$$

where $t_M(1)$ = timing error due to constant velocity satellite motion. Similarily, after the next iteration

$$t_{ET}(2) = t_{ET}(1)\,[1-m-\beta m] - \beta m\ t_{ET}(0) - b(1+\beta)v_{NT}(2) - \beta b\ v_{NT}(1) + t_M(1)$$

$$= t_{ET}(1)\,[2-m-\beta m] - (1-m)\,t_{ET}(0) - b(1+\beta)v_{NT}(2) + b\ v_{NT}(1) \qquad (5\text{-}8)$$

After the r_T^{th} iteration

$$t_{ET}(r_T) = t_{ET}(r_T-1)\,(1-m-\beta m) - \beta m \sum_{p=0}^{r_T-2} t_{ET}(p) - b(1+\beta)v_{NT}(r_T)$$

$$-\beta b \sum_{s=1}^{r_T-1} v_{NT}(s) + t_M(1)$$

$$= t_{ET}(r_T-1)\,[2-m-\beta m] - (1-m)\ t_{ET}(r_T-2) - b(1+\beta)\ v_{NT}(r_T)$$

$$+ b\ v_{NT}(r_T-1) \qquad \text{——(5-9)}$$

Taking the z-transform of (5-9) yields [38]

$$T_{ET}(z) = \frac{t_{ET}(0)}{1-(2-m-\beta m)\,z^{-1} + (1-m)\,z^{-2}} - \frac{[t_{ET}(0) - t_M(1)]\,z^{-1}}{1-(2-m-\beta m)\,z^{-1} + (1-m)\,z^{-2}}$$

$$+ \frac{[b\ z^{-1} - b(1+\beta)]\,V_{NT}(z)}{1-(2-m-\beta m)\,z^{-1} + (1-m)\,z^{-2}} \qquad (5\text{-}10)$$

where $T_{ET}(z)$ = z-transform of $t_{ET}(r_T)$

$V_{NT}(z)$ = z-transform of $v_{NT}(r_T)$

The stability of the system can be tested by applying the modified Schur-Cohn criterion [41] to the function in the denominators of (5-10). Three conditions must be satisfied which provide the following relationships:

(a) $\beta m > 0$ (5-11A)

(b) $m(2 + \beta) < 4$ (5-11B)

(c) $\left|1 - \frac{\beta m}{2 - m}\right| < 1$ (5-11C)

When the first two equations are satisfied, the third is automatically satisfied for this particular system.

To solve for $t_{ET}(r_T)$, calculate the inverse z-transform of (5-10). This gives

$$t_{ET}(r_T) = t_{ET}(0)\left[\frac{\gamma_1^{r_T+1} - \gamma_2^{r_T+1}}{\gamma_1 - \gamma_2}\right] - [t_{ET}(0) - t_M(1)]\left(\frac{\gamma_1^{r_T} - \gamma_2^{r_T}}{\gamma_1 - \gamma_2}\right)$$

$$+ \sum_{s=1}^{r_T} \left\{\frac{v_{NT}(s)}{\gamma_1 - \gamma_2}\left[b\left(\gamma_1^{r_T - s} - \gamma_2^{r_T - s}\right) - b(1+\beta)\left(\gamma_1^{r_T - s + 1} - \gamma_2^{r_T - s + 1}\right)\right]\right\} \quad \text{--- (5-12)}$$

where

$$\gamma_1 = \frac{2 - m - \beta m}{2} + \sqrt{\left(\frac{2 - m - \beta m}{2}\right)^2 + m - 1}$$

$$\gamma_2 = \frac{2 - m - \beta m}{2} - \sqrt{\left(\frac{2 - m - \beta m}{2}\right)^2 + m - 1}$$

and $-1 < \gamma_1 < 1$, $-1 < \gamma_2 < 1$ as a result of (5-11).

Now the average timing error and the rms timing error can be examined in detail.

5.2.2 Average Timing Error

The average timing error can be obtained by calculating the expectation of $t_{ET}(r_T)$ given by (5-12). Hence,

$$t_{ET}(r_T)_{ave} = E\{t_{ET}(r_T)\} = E\{t_{ET}(0)\}\frac{\gamma_1^{r_T+1} - \gamma_2^{r_T+1}}{\gamma_1 - \gamma_2} - E\{[t_{ET}(0) - t_M(1)]\}\frac{(\gamma_1^{r_T} - \gamma_2^{r_T})}{\gamma_1 - \gamma_2} \quad (5\text{-}13)$$

where $E\{v_{NT}(s)\} = 0$ for all s [39]. This relation results from the assumption that $v_{NT}(s)$ is a Gaussian Markov process with zero mean.

Now,

$$E\{t_{ET}(0)\} = t_{EC}(0)(1-m)^{r_K} + \frac{t_M(1)}{m}[1 - (1-m)^{r_K}] \approx \frac{t_M(1)}{m} \quad (5\text{-}14)$$

for large r_K which is the condition prior to the tracking mode. Hence,

$$t_{ET}(r_T)_{ave} = \frac{t_M(1)}{m}\left[\frac{\gamma_1^{r_T+1} - \gamma_2^{r_T+1}}{\gamma_1 - \gamma_2} + (m-1)\frac{(\gamma_1^{r_T} - \gamma_2^{r_T})}{\gamma_1 - \gamma_2}\right]$$

$$= \frac{t_M(1)}{m} F(\gamma) \quad (5\text{-}15)$$

where

$$F(\gamma) = \left[\frac{\gamma_1^{r_T+1} - \gamma_2^{r_T+1}}{\gamma_1 - \gamma_2} + (m-1)\frac{\gamma_1^{r_T} - \gamma_2^{r_T}}{\gamma_1 - \gamma_2}\right]$$

Graphs of $F(\gamma)$ are plotted as a function of r_T in Fig. 5-2 to Fig. 5-6 for selected values of β and m. It is necessary to use smaller values of β as m is increased to ensure that (5-11) is satisfied. In Fig. 5-6, it is shown that three different types of curves can result. Convergence is achieved for $\beta = 1/7$ since (5-11) is satisfied. When (5-11A) is satisfied, for $\beta = 2/7$, convergence is not achieved since (5-11B) is violated. While divergence does not occur, it is shown in the analysis for the rms timing error that the timing error due to noise increases greatly (Fig.5-11) and consequently, synchronization is not achieved. For $\beta = 3/7$, divergence occurs.

As in the fine search mode, there are three different shapes of graphs. The shapes are determined by the values of γ_1 and γ_2 given by (5-12) which consist of two functions, the first, $\frac{2-m-\beta m}{2}$ which is always real and the second, $\sqrt{\left[\frac{2-m-\beta m}{2}\right]^2 + m - 1}$ which may be real or imaginary. Table 5-1 illustrates the various combinations which can occur.

Overdamping occurs in those cases where both parts of the expression are positive or one is positive and the other is zero. Underdamping can also occur in several ways. If either part of the expression is negative, the graph will tend to converge in an oscillatory manner. Finally, there is the possibility of both parts being zero which gives critical damping. This case is quite unlikely since neither m nor β can be precisely controlled.

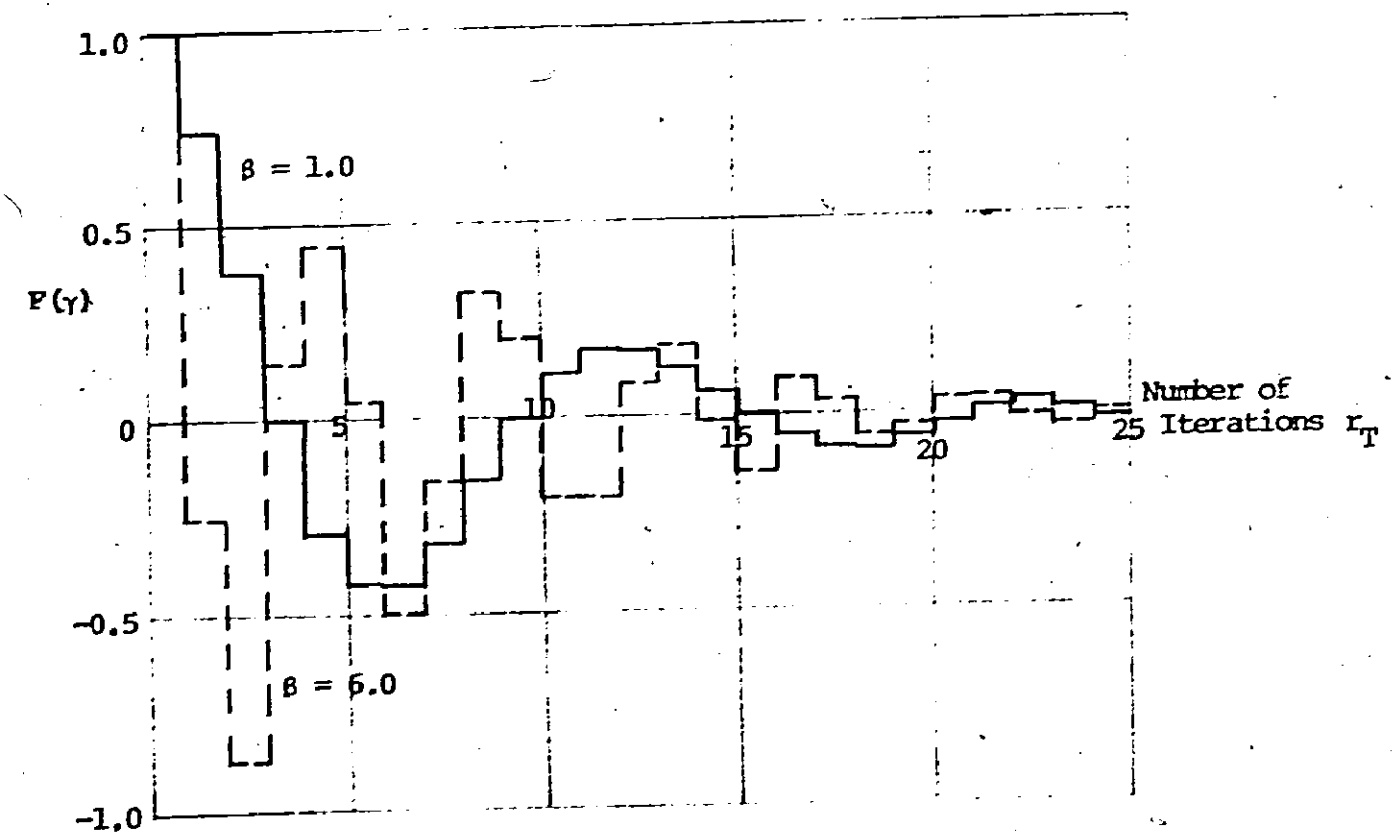

Fig. 5-2 $F(\gamma)$ as a function of r_T for m = 0.25 and selected β.

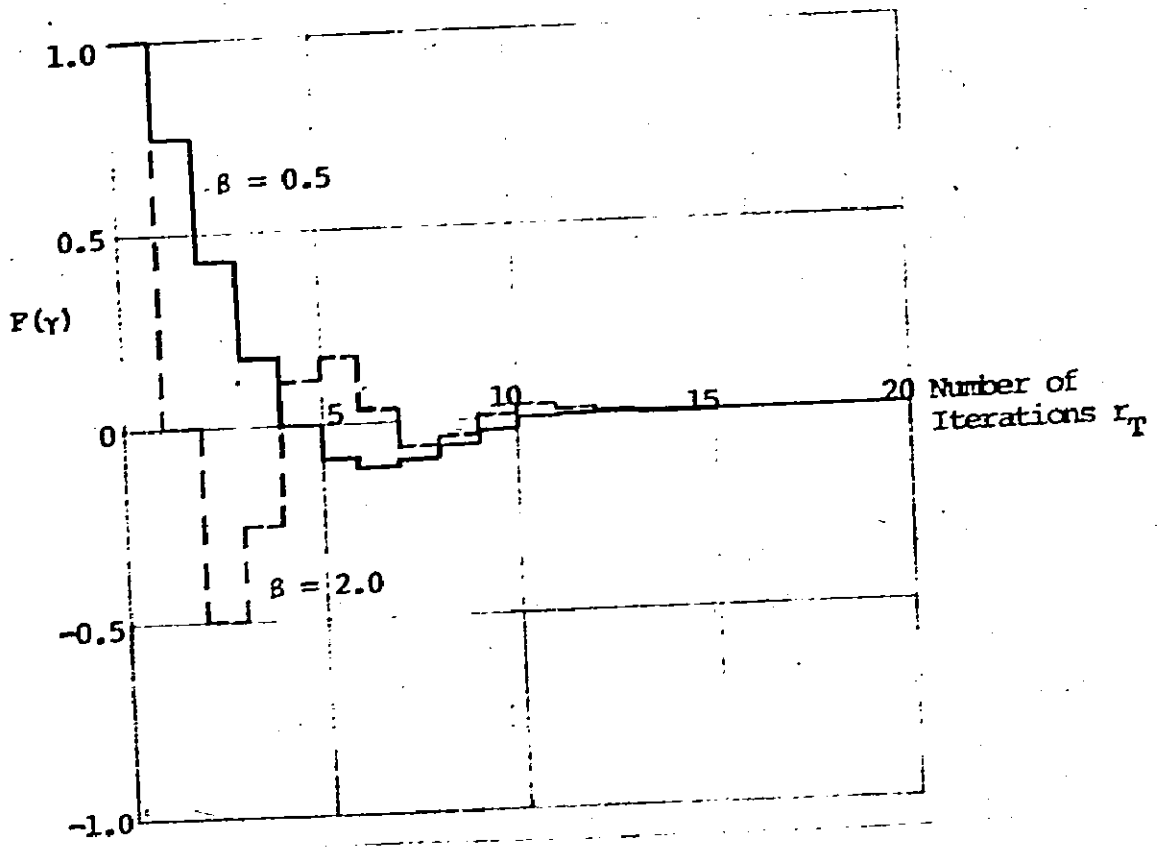

Fig. 5-3 $F(\gamma)$ as a function of r_T for m = 0.5 and selected β.

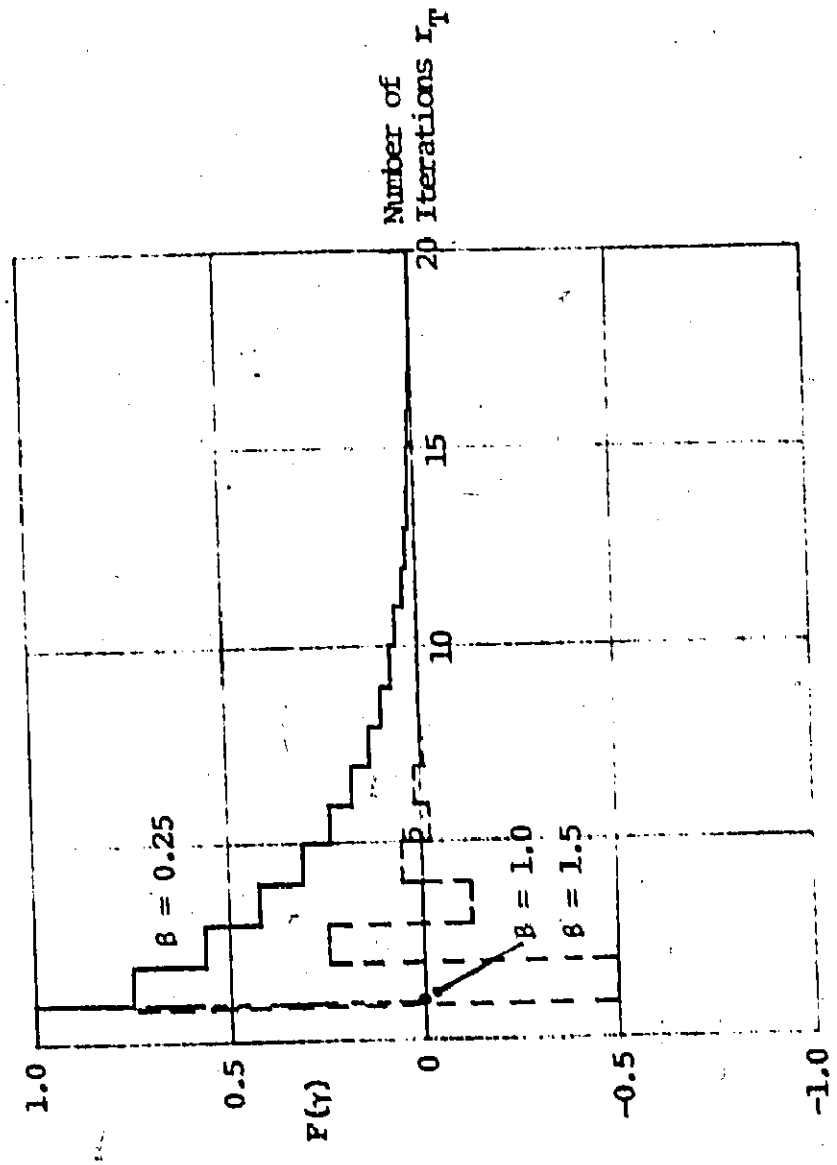

Fig. 5-4 P(γ) as a function of r_T for m = 1.0 and selected β.

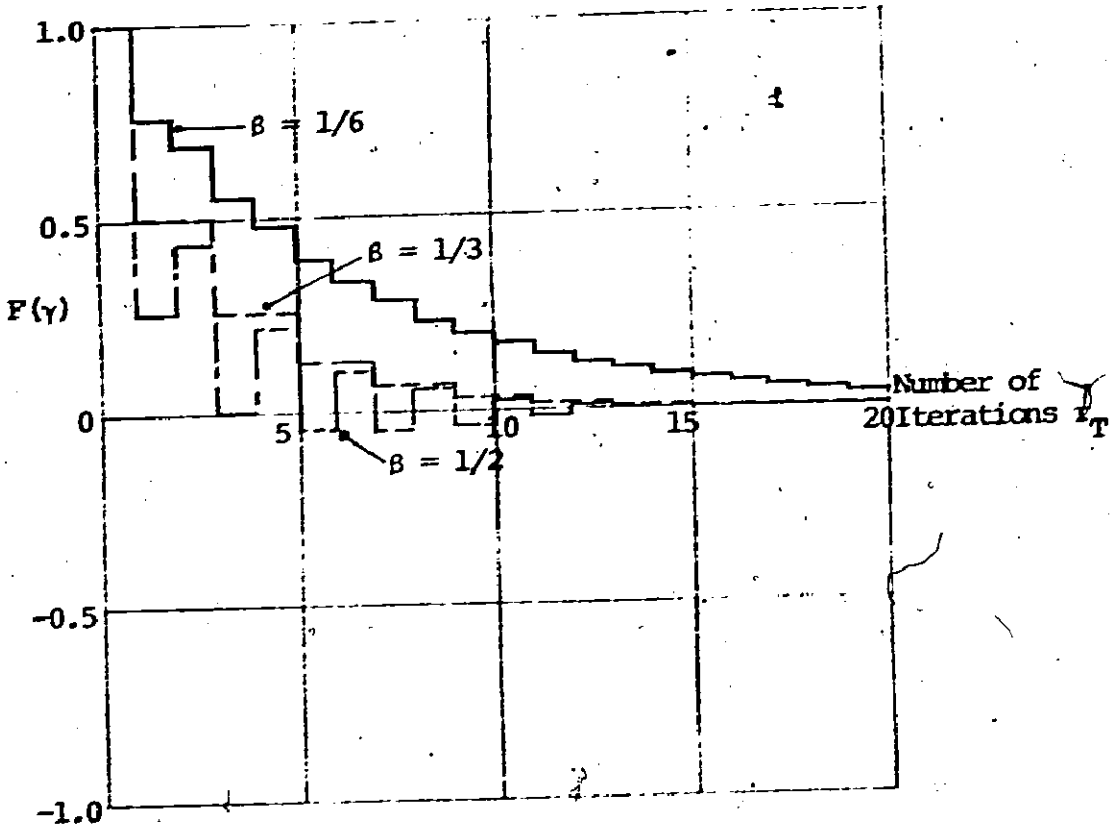

Fig. 5-5 $P(\gamma)$ as a function of r_T for m = 1.5 and selected β.

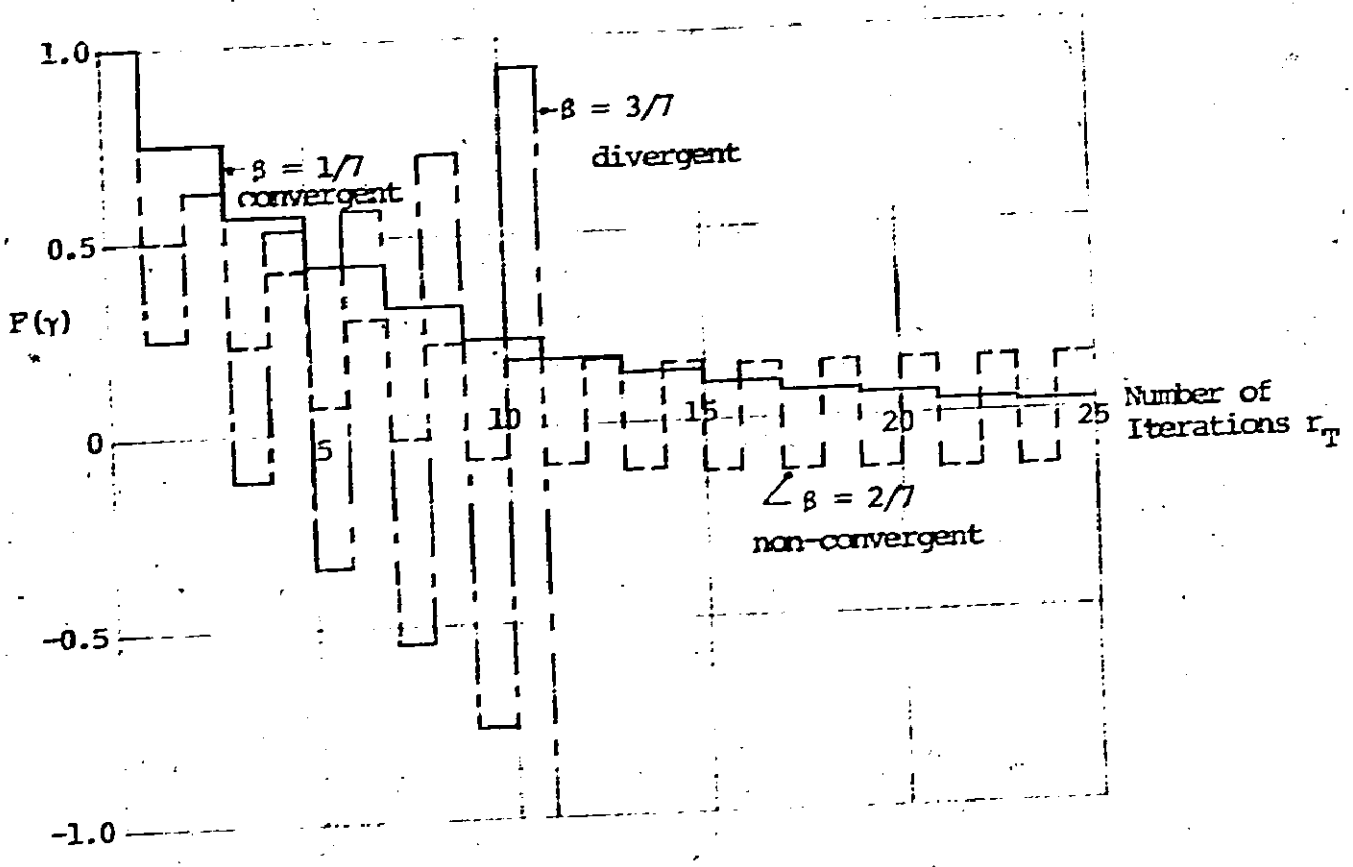

Fig. 5-6 $F(\gamma)$ as a function of r_T for m = 1.75 and selected β.

TABLE 5-1

Combinations of λ_1 and λ_2

λ_1^*	λ_2^{**}	Type of Graph	Conditions on m and β.
+	+	Overdamped	$\frac{4\beta}{(1+\beta)^2} < m < \frac{2}{1+\beta}$, $0 < \beta < 1$
0	+	Overdamped	$m = \frac{2}{1+\beta}$, $0 < \beta < 1$
+	0	Overdamped	$m = \frac{4\beta}{(1+\beta)^2}$, $0 < \beta < 1$
+	-	Underdamped	$m < \frac{4\beta}{(1+\beta)^2}$, $0 < \beta < 1$; $m < \frac{2}{1+\beta}$, $\beta > 1$
-	+	Underdamped	$m > \frac{2}{1+\beta}$, $0 < \beta < 1$; $m > \frac{4\beta}{(1+\beta)^2}$, $\beta > 1$
-	-	Underdamped	$\frac{2}{1+\beta} < m < \frac{4\beta}{(1+\beta)^2}$, $\beta > 1$
0	-	Underdamped	$m = \frac{2}{1+\beta}$, $\beta > 1$
-	0	Underdamped	$m = \frac{4\beta}{(1+\beta)^2}$ $\beta > 1$
0	0	Critically damped	$m = \beta = 1$

$$*\lambda_1 = \frac{2 - m - \beta m}{2} \qquad **\lambda_2 = \left[\frac{2 - m - \beta m}{2}\right]^2 + m - 1$$

or $\lambda_1 = \frac{1}{2}[\gamma_1 + \gamma_2]$, and $\lambda_2 = \frac{1}{4}[\gamma_1 - \gamma_2]^2$

5.2.3 RMS Timing Error

The timing error due to noise can be found as in the fine search mode by calculating the square root of the expectation of the mean square timing error using (5-12). Define the rms tracking mode timing error after r_T iterations to be

$$t_{ET}(r_T)_{rms} = [E\{t_{ET}(r_T)\}^2]^{1/2}$$

$$= [E\{t_{ET}(0)\ \frac{(\gamma_1^{r_T+1} - \gamma_2^{r_T+1})}{\gamma_1 - \gamma_2} - [t_{ET}(0) - t_M(1)]\frac{(\gamma_1^{r_T} - \gamma_2^{r_T})}{\gamma_1 - \gamma_2}\}^2$$

$$+ E\{\sum_{s=1}^{r_T} \frac{v_{NT}(s)}{\gamma_1 - \gamma_2}[b(\gamma_1^{r_T-s} - \gamma_2^{r_T-s}) - b(1+\beta)(\gamma_1^{r_T-s+1} - \gamma_2^{r_T-s+1})]\}^2]^{1/2}$$

— (5-16)

Note that $E\{t_{ET}(0).v_{NT}(s)\} = 0$ for all s and $E\{t_M(1).v_{NT}(s)\} = 0$ for all s due to the assumption that $v_{NT}(s)$ is a Gaussian Markov process with zero mean. Thus

$$t_{ET}(r_T)_{rms} = [E\{t_{ET}(0)\}^2[\frac{(\gamma_1^{r_T+1} - \gamma_2^{r_T+1}) - (\gamma_1^{r_T} - \gamma_2^{r_T})}{\gamma_1 - \gamma_2}]^2 + 2E\{t_{ET}(0)\}$$

$$[t_M(1)\frac{[(\gamma_1^{r_T+1} - \gamma_2^{r_T+1}) - (\gamma_1^{r_T} - \gamma_2^{r_T})]}{(\gamma_1 - \gamma_2)^2}\ (\gamma_1^{r_T} - \gamma_2^{r_T})] + [t_M(1)\ \frac{(\gamma_1^{r_T} - \gamma_2^{r_T})}{\gamma_1 - \gamma_2}]^2$$

$$+ E\{\sum_{s=1}^{r_T} \frac{v_{NT}(s)}{(\gamma_1 - \gamma_2)}[b(\gamma_1^{r_T-s} - \gamma_2^{r_T-s}) - b(1+\beta)(\gamma_1^{r_T-s+1} - \gamma_2^{r_T-s+1})]\}^2]^{1/2}$$

— (5-17)

From (4-66) with r_K large

$$E(t_{ET}(0))^2 = E(t_E(r_K))^2 = \left(\frac{t_M(1)}{m}\right)^2 + t_N^2 \frac{m}{2-m} \qquad (5\text{-}18)$$

From (5-14) $E(t_{ET}(0)) = \left(\frac{t_M(1)}{m}\right)^2$ for large r_K and, consequently, the first three terms in (5-17) become

$$R_P(\gamma_1, \gamma_2) = \left[\left(\frac{t_M(1)}{m}\right)^2 + t_N^2 \frac{m}{2-m}\right] \cdot \left[\frac{(\gamma_1^{r_T+1} - \gamma_2^{r_T+1}) - (\gamma_1^{r_T} - \gamma_2^{r_T})}{\gamma_1 - \gamma_2}\right]^2$$

$$+ \frac{2t_M^2(1)}{m} \frac{\gamma_1^{r_T} - \gamma_2^{r_T}}{(\gamma_1 - \gamma_2)^2} \left[(\gamma_1^{r_T+1} - \gamma_2^{r_T+1}) - (\gamma_1^{r_T} - \gamma_2^{r_T})\right] + t_M^2(1) \left(\frac{\gamma_1^{r_T} - \gamma_2^{r_T}}{\gamma_1 - \gamma_2}\right)^2 \qquad (5\text{-}19)$$

Now $E(v_{NT}(s))^2 = E(v_N(p))^2$ (evaluated in (4-41), and consequently

$$E(b\, v_{NT}(s))^2 = \frac{b^2 N_O L}{2 T_I^2} \left[c_2^2 F_S T_W + k_6^2 F_G T_Q\right] = m^2 t_N^2 \qquad (5\text{-}20)$$

where t_N is defined by (4-20).

Thus, substituting this expression into the last term of (5-17) yields

$$E(\,) = m^2 t_N^2 \cdot \sum_{s=1}^{r_T} \frac{\left[(\gamma_1^{r_T-s} - \gamma_2^{r_T-s}) - (1+s)(\gamma_1^{r_T-s+1} - \gamma_2^{r_T-s+1})\right]^2}{(\gamma_1 - \gamma_2)^2} \qquad (5\text{-}21)$$

and $(\gamma_1 - \gamma_2)^2 = m^2(1+\beta)^2 - 4\beta m$.

The summation is given by

$$F(\gamma_1,\gamma_2) = \left[\frac{1-\gamma_1^{2r_T}}{1-\gamma_1^2}\right]\frac{[1-(1+\beta)\gamma_1]^2}{(\gamma_1-\gamma_2)^2} - 2\left[\frac{1-(\gamma_1\gamma_2)^{r_T}}{1-\gamma_1\gamma_2}\right]\frac{[1-(1+\beta)\gamma_1][1-(1+\beta)\gamma_2]}{(\gamma_1-\gamma_2)^2}$$

$$+ \left[\frac{1-\gamma_2^{2r_T}}{1-\gamma_2^2}\right]\frac{[1-(1+\beta)\gamma_2]^2}{(\gamma_1-\gamma_2)^2} \qquad (5\text{-}22)$$

For the special case of $m = \beta = 1$, $\gamma_1 = \gamma_2 = 0$ and $F(\gamma_1, \gamma_2) = 4$ for all values of $r_T > 0$.

Finally, the rms error for the tracking mode using the PSK sync burst implementation is given by

$$t_{ET}(r_T)_{rms} = [\bar{R}_p(\gamma_1, \gamma_2) + t_N^2 m^2 F(\gamma_1, \gamma_2)]^{1/2} \qquad (5\text{-}23)$$

Values of $m^2F(\gamma_1, \gamma_2)$ are plotted in Fig. 5-7 through Fig. 5-11, inclusive for various values of m and β. The value $\beta = 0$ represents the case where the tracking network is not used. Thus, these curves are the same as in Fig. 4-17. In Fig. 5-7 through 5-10 it is seen that a steady state condition occurs for r_T exceeding approximately 15 iterations.

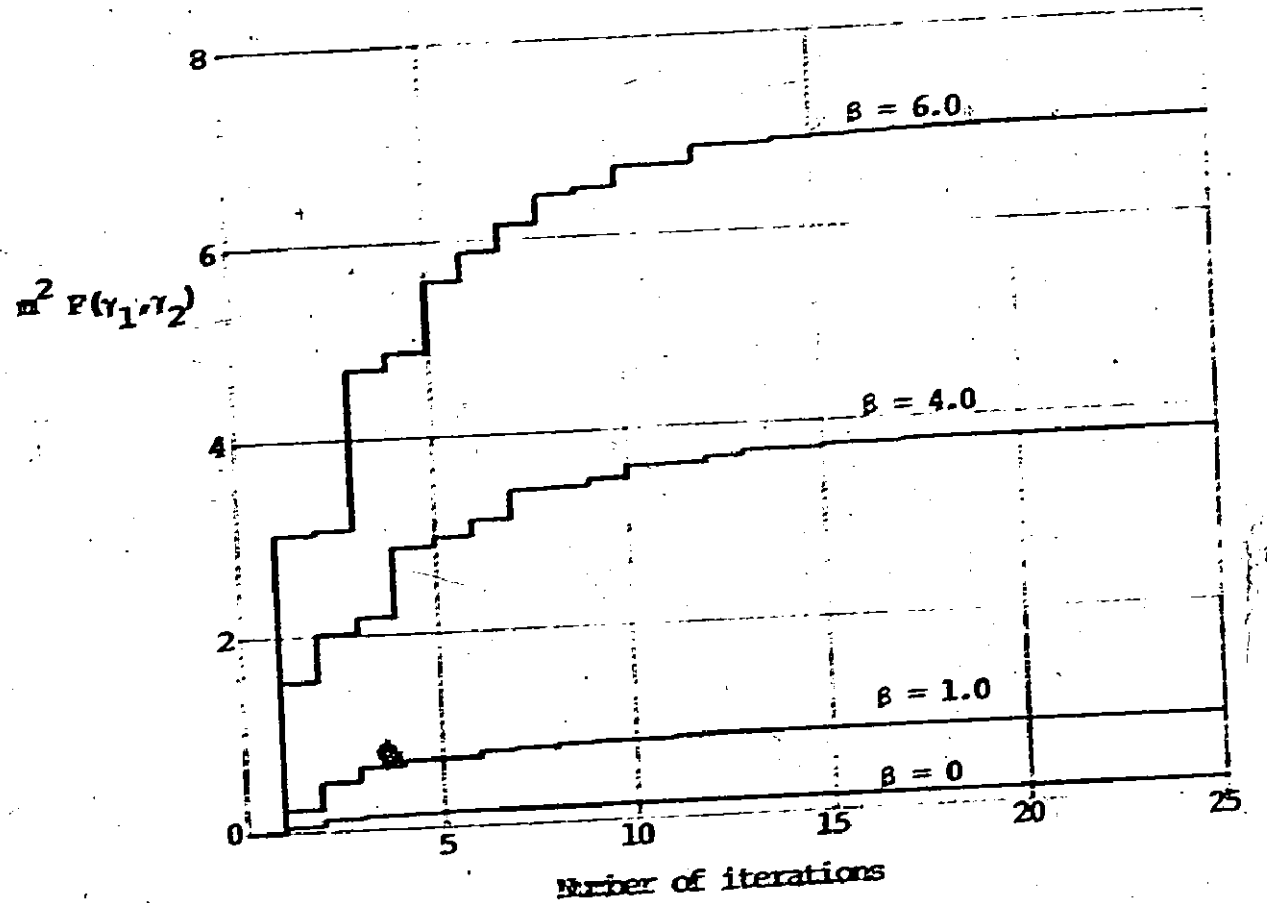

Fig. 5-7 $m^2 F(\gamma_1, \gamma_2)$ as a function of r_T for $m = 0.25$ and selected β

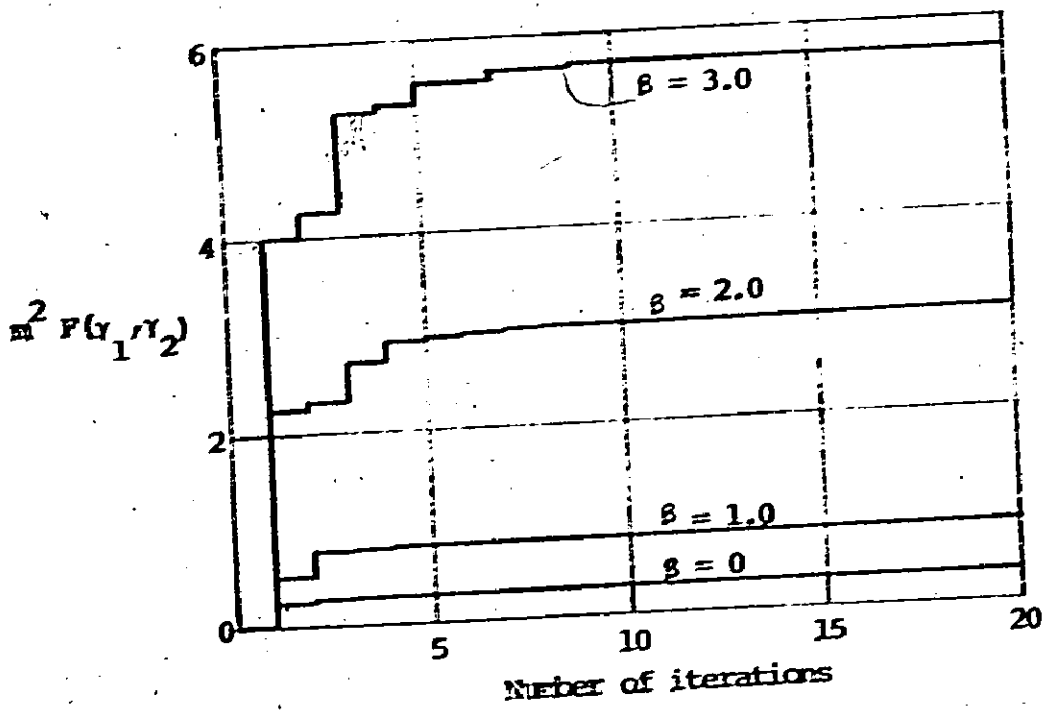

Fig. 5-8 $m^2 F(\gamma_1, \gamma_2)$ as a function of r_T for $m = 0.5$ and selected β

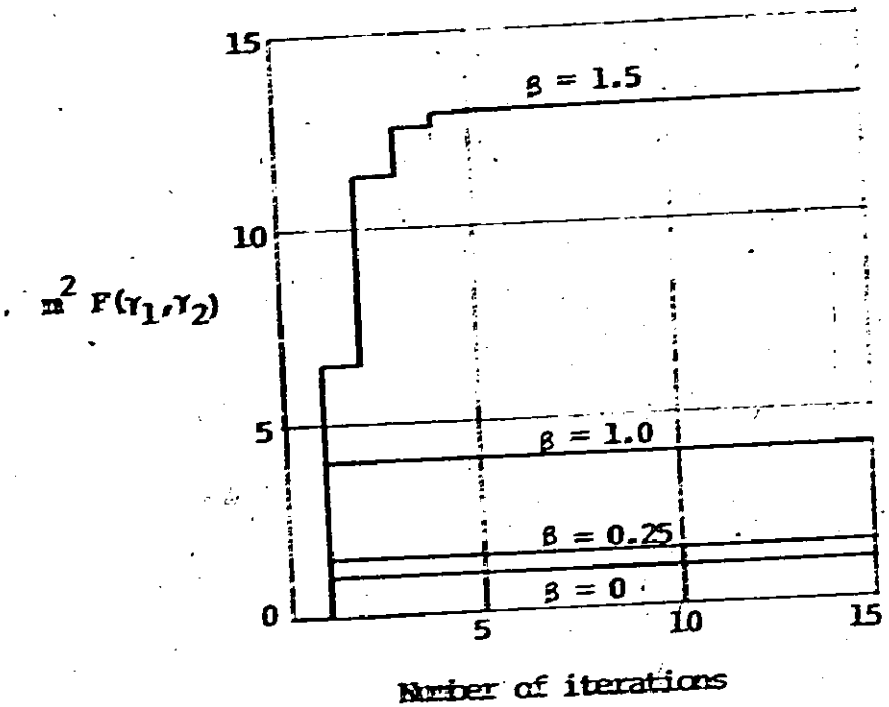

Fig. 5-9 $m^2 F(\gamma_1, \gamma_2)$ as a function of γ_T for m = 1.0 and selected β

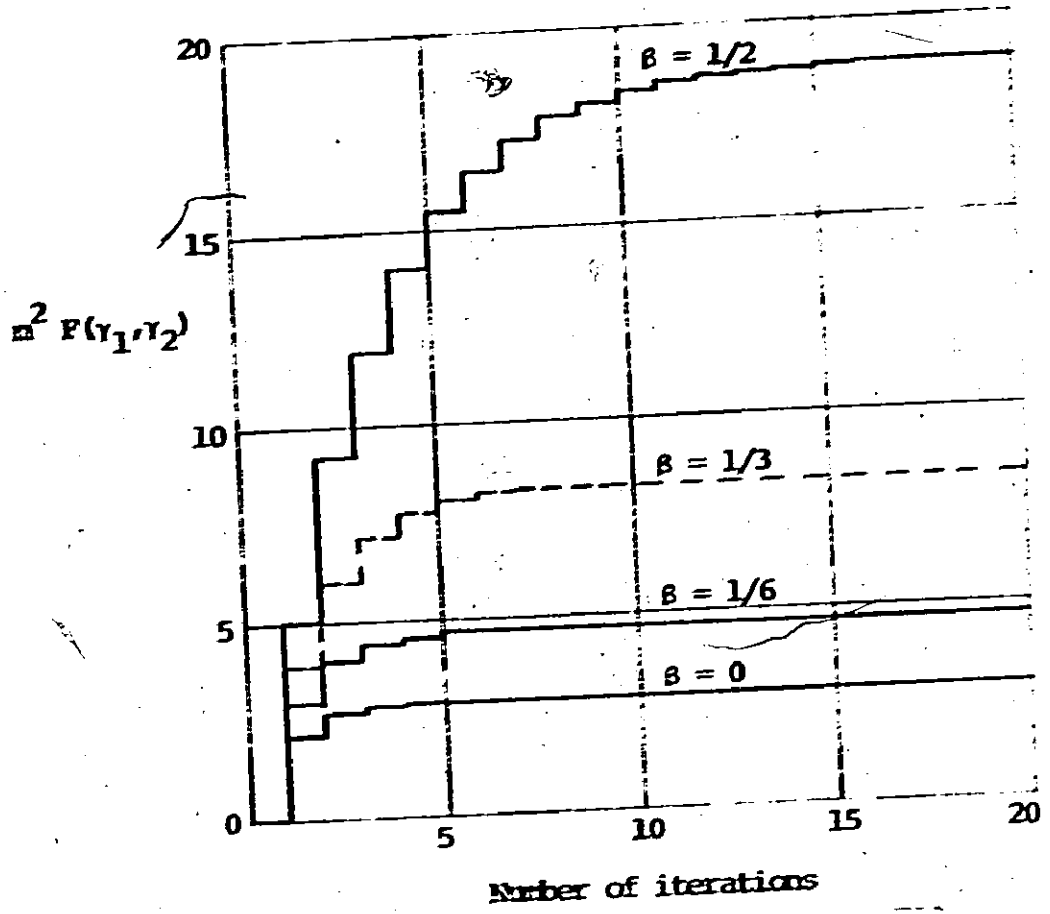

Fig. 5-10 $m^2 F(\gamma_1, \gamma_2)$ as a function of r_T for m = 1.50 and selected β

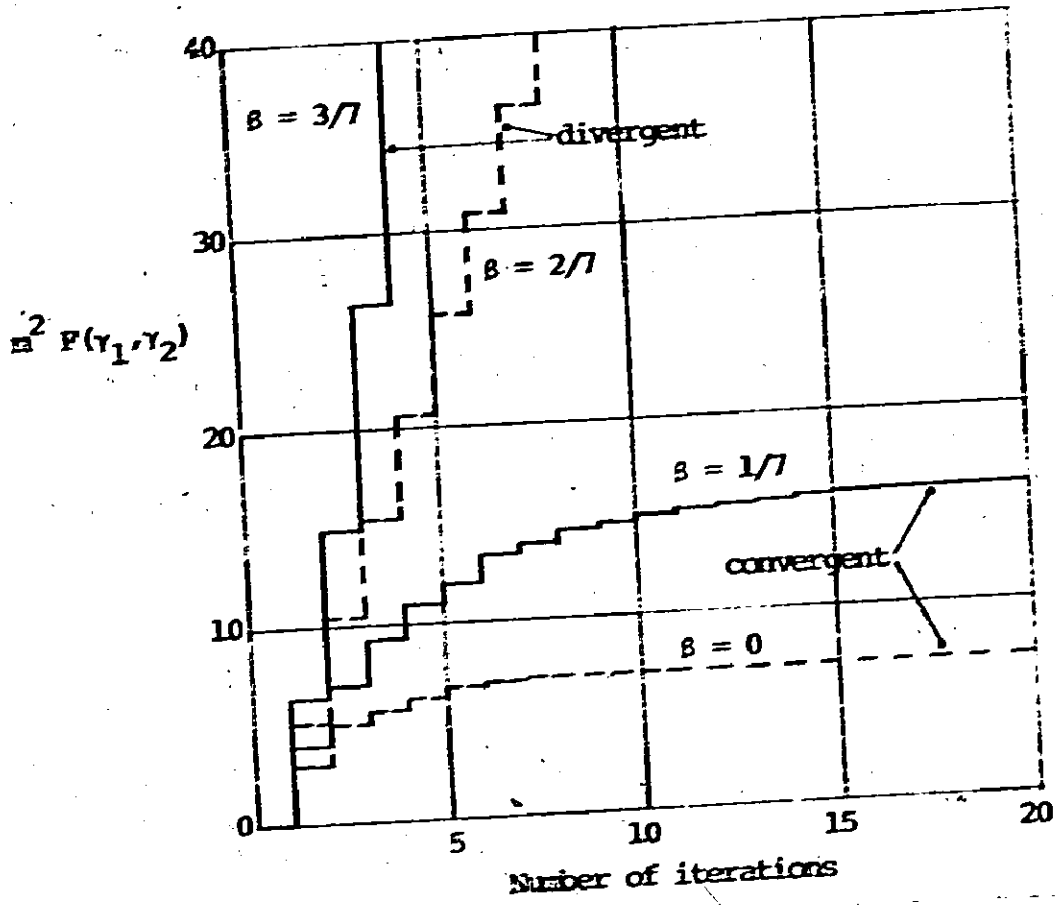

Fig. 5-11 $m^2 F(\gamma_1, \gamma_2)$ as a function of r_T for $m = 1.75$ and selected β

Thus, for these cases, the reduction of the timing error in the tracking mode is complete in 4.5 s. In Fig. 5-11, two different cases are illustrated. For the $\beta = 0$ and $\beta = 1/7$ curves, convergence occurs. However, for $\beta = 2/7$ and $\beta = 3/7$ convergence does not occur. This is a direct result of (5-11B) being violated.

These graphs show that for the first few iterations, the step sizes appear to vary considerably when $\beta > 0$. This is due to interaction between the tracking network and the fine search network. Also, the value of $m^2 F(\gamma_1, \gamma_2)$ is increased when $\beta > 0$ indicating that the reduction in the timing error due to satellite motion is achieved at the expense of greater timing error due to uplink and downlink noise.

As the number of iterations increases, the magnitude of $R_p(\gamma_1, \gamma_2)$ approaches zero since $\gamma_1^{r_T} \to 0$ and $\gamma_2^{r_T} \to 0$ as $r_T \to \infty$. Also, the value of $F(\gamma_1, \gamma_2)$ approaches a steady state value given by

$$F_S(\gamma_1, \gamma_2) = \frac{[1-(1+\beta)\gamma_1]^2}{(1-\gamma_1^2)(\gamma_1-\gamma_2)^2} - \frac{2[1-(1+\beta)\gamma_1][1-(1+\beta)\gamma_2]}{(1-\gamma_1\gamma_2)(\gamma_1-\gamma_2)^2} + \frac{[1-(1+\beta)\gamma_2]^2}{(1-\gamma_2^2)(\gamma_1-\gamma_2)^2} \quad \text{--- (5-24)}$$

Thus, in the steady state, the rms timing error is

$$t_{ET}(\infty)_{rms} = m\, t_N \sqrt{F_S(\gamma_1, \gamma_2)} \quad (5\text{-}25)$$

This result shows that the steady state timing error is independent of the initial timing error conditions and of the error due to constant velocity satellite motion.

5.3 FSK SYNC BURST IMPLEMENTATION

5.3.1 Average Timing Error

The average timing error is the same as for the PSK sync burst implementation and given by (5-15). The graphs shown in Fig. 5-2 to Fig. 5-6 inclusive, Table 5-1 and the related discussion all apply for the FSK sync burst implementation.

5.3.2 RMS Timing Error

The equation for the rms timing error can be developed by the same method used in Section 5.2.3. Thus, the rms timing error for the tracking mode using the FSK sync burst implementation is given by

$$t_{ET}(r_T)_{rms} = [R_F(\gamma_1, \gamma_2) + 2t_N^2 m^2 F(\gamma_1, \gamma_2)]^{1/2} \qquad (5\text{-}26)$$

where

$$R_F(\gamma_1, \gamma_2) = \left[\left(\frac{t_M(1)}{m}\right)^2 + 2t_N^2 \frac{m}{2-m} \right] \left[\frac{(\gamma_1^{r_T+1} - \gamma_2^{r_T+1}) - (\gamma_1^{r_T} - \gamma_2^{r_T})}{\gamma_1 - \gamma_2}\right]^2$$

$$+ \frac{2t_M^2(1)}{m} \frac{\gamma_1^{r_T} - \gamma_2^{r_T}}{(\gamma_1 - \gamma_2)^2} \left[(\gamma_1^{r_T+1} - \gamma_2^{r_T+1}) - (\gamma_1^{r_T} - \gamma_2^{r_T})\right] + t_M^2(1) \left(\frac{\gamma_1^{r_T} - \gamma_2^{r_T}}{\gamma_1 - \gamma_2}\right)^2$$

As the number of iterations increase, the magnitude of $R_F(\gamma_1, \gamma_2)$ approaches zero since $\gamma_1^{r_T} \to 0$ and $\gamma_2^{r_T} \to 0$ as $r_T \to \infty$. The value of $F(\gamma_1, \gamma_2)$ approaches the steady state value given by 5-24. Hence, in the steady state, the rms timing error is given by

$$t_{ET}(\infty)_{rms} = \sqrt{2}\, m\, t_N \sqrt{F_S(\gamma_1, \gamma_2)} \qquad (5\text{-}27)$$

As in the PSK sync burst implementation, this result shows that in the steady state, the timing error is independent of the initial timing error and of the error due to constant velocity satellite motion.

This result has a close parallel to phase lock circuits where a first order loop has a phase offset proportional to the frequency error, and a second order loop has zero phase offset as long as the frequency error remains constant [47].

CHAPTER 6

Laboratory Model and Design Measurements

The objectives in the development of the laboratory model are to produce a system which tests certain signal waveforms postulated in the theory developed in the thesis and construct a model which is equivalent to the physical model. The actual synchronization loop, shown in Fig. 3-1, consists of the sync unit which is contained in the earth station, the uplink space delay and attenuation, the satellite sync window connection and the downlink space delay and attenuation. Synchronization is separated into three distinct modes of operation: the coarse search mode, the fine search mode and the tracking mode. Coarse search synchronization is achieved by transmitting the PSK multi-frame coded search signal since this signal has the narrowest bandwidth of all coded search signals and employs only one carrier frequency. Also, the fast synchronization technique is assumed. After a one-way trip time delay, the signal is modulated at the satellite by the sync window. Pulses of the search signal arrive back at the earth station after a further one-way trip delay and are decoded to give the necessary information for transmitting PSK sync bursts at the proper times so as to pass through the sync window. Again the PSK sync bursts are employed due to the narrow bandwidth and the use of a single carrier. Thus, the fine search mode and the tracking mode can proceed using PSK sync bursts and the loop operates in a feedback control fashion.

6.1 LABORATORY MODEL

6.1.1 Loop Representation

The laboratory model must provide an accurate representation of the three modes of synchronization. Amongst the difficulties are the large uplink and downlink space delays. It is not possible to model these directly since the bandwidth of the signals is at least 2 MHz and the delay is approximately 135 ms giving a time-bandwidth product of 270,000. Hence, the delays must be produced by other techniques. To achieve this, the sync unit is separated into three parts comprising the sync signal generator, the receiver and the time base circuits. For the coarse search mode and the fine search mode, the uplink delay can be interchanged with the sync signal generator and the downlink delay can be interchanged with the receiver, as shown in Fig. 6-1. This interchange gives the same signal equations as for the physical model, but the simplification allows the use of clocked delay triggers. For the tracking mode, the technique must be modified by using a small voltage-variable delay in cascade with the uplink clocked delay trigger.

The model for the sync window includes a provision for producing satellite motion. This can be achieved either by varying the uplink and downlink video delays or by changing the interpulse spacing of the sync windows. The former method is quite difficult to implement since the delays must be synchronous with the time base circuit in order to achieve a precise relationship between the sync window modulation and the transmitted signals. However, the latter can easily be achieved since the satellite model has an independent oscillator which can be used to

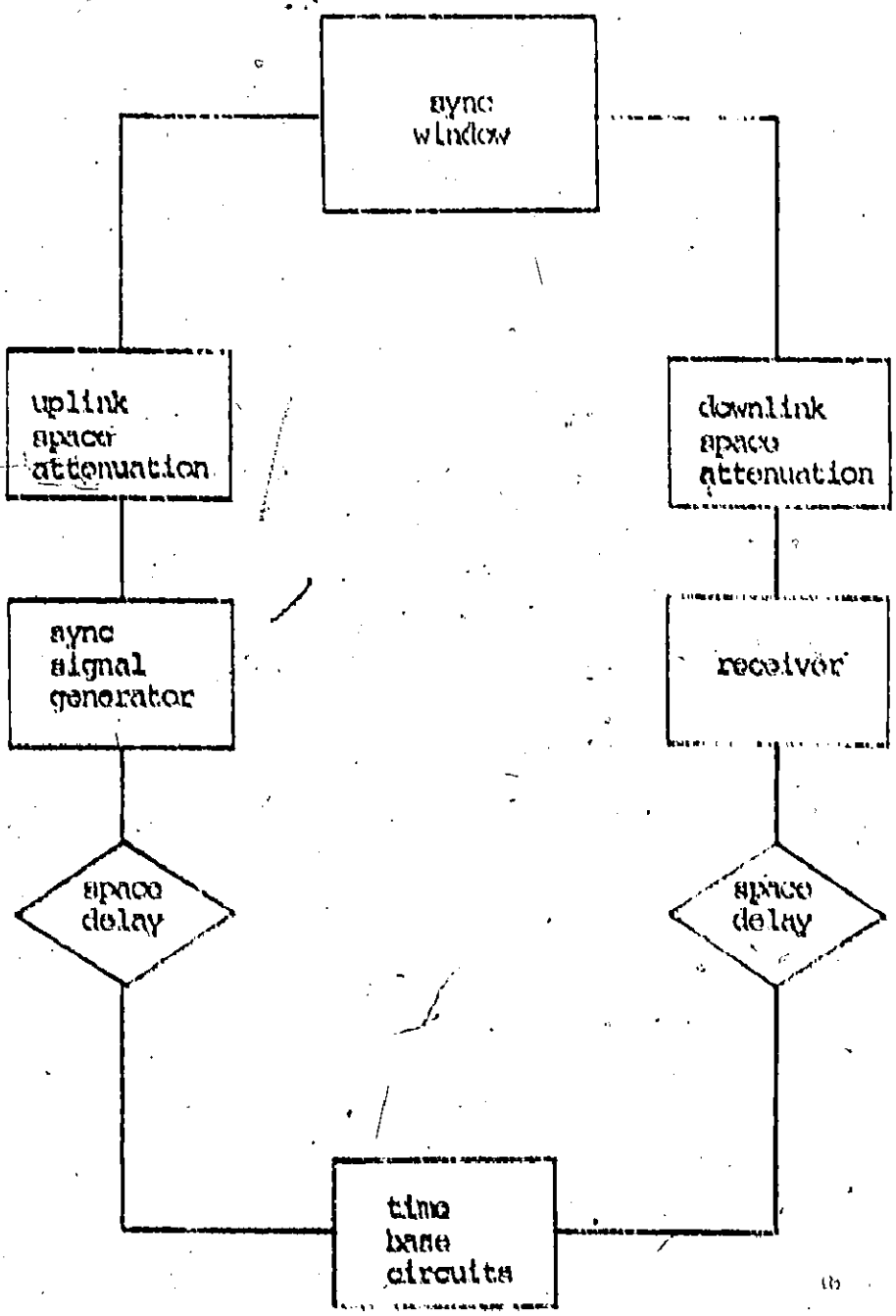

Fig. 6-1. Laboratory model of the synchronization loop

vary the interpulse spacing of the sync windows. Reducing the spacing corresponds to satellite motion towards the earth station while increasing the spacing represents satellite motion away from the earth station. Hence, this technique is incorporated into the model so that problems of synchronizing to a moving satellite can be studied.

With this representation of satellite motion, the model provides a large fixed space delay and a satellite which is moving. This is not exact since satellite motion causes changes in the space delay. However, in practice, the motion is usually of the order of 20 ns or less per round trip time which is insignificant with respect to the uplink delay of 135 ms. From the theory developed in Chapters 4 and 5, it is seen that, indeed, the space delay and the satellite motion are essentially independent.

The uplink delay represeting the path from the earth station to the satellite must be as exact as possible. The only variable will be satellite motion; hence, errors must be kept small to allow this motion to be studied. Consider the example illustrated in Fig. 6-2. The inexact space delay causes variations in the information modulated onto the sync burst. This can occur if, for example the video space delay is clocked from a source other than the earth station time base oscillator which in this case is the VCO. The error can be reduced by using a high frequency oscillator. A frequency of 200 MHz would be required for the timing error to be less than 5 ns.

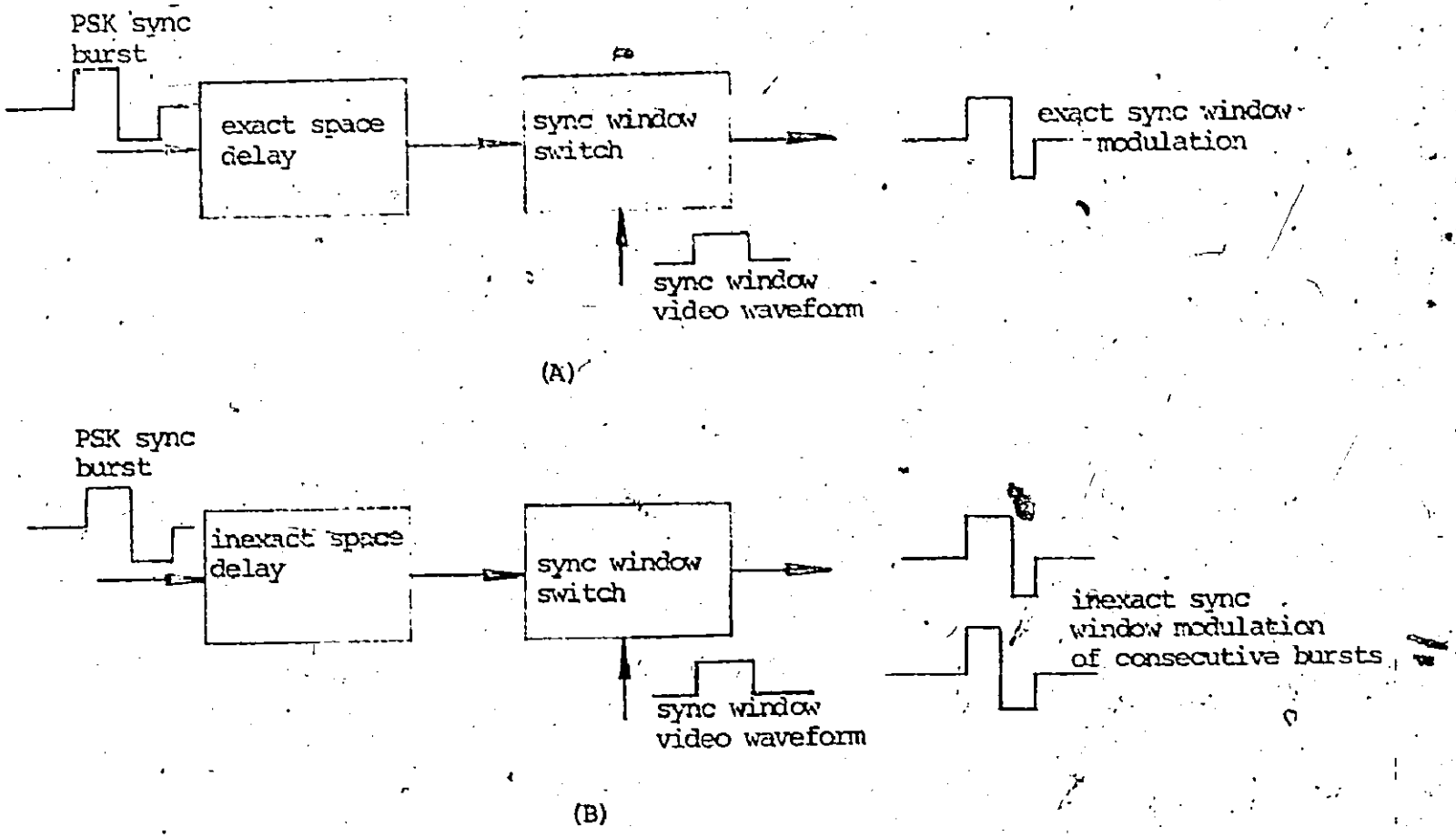

Fig. 6-2: Comparison of the effects of PSK sync bursts passing through space delay. (A) exact space delay, (B) inexact space delay.

The downlink delay does not require high precision. After the information is modulated onto the sync burst, the signal travels from the satellite to the earth station where an additional processing delay occurs. Hence, inaccuracies in the model of the downlink delay are quite insignificant as compared to the uplink delay and therefore can be represented by a triggered counter and decoder driven from a clock source.

6.1.2 Equivalent Networks

It is possible to prove that interchanging the uplink space delay and the sync signal generator produces the same signal input at the sync window as is given by the physical model. For the coarse search mode and the fine search mode, the actual uplink space delay is shown in Fig. 6-3A and the model of this delay is illustrated in Fig. 6-3B. A trigger $p(t)$ at the input to the sync burst generator produces an output signal $s_M(t)$ and the uplink space delay is T_{DU}.

Note that the space delay in the model is clocked from the timing circuits and this is possible because the control terminal of the VCO in the timing circuits is at zero volts except when timing adjustments are performed. Thus, the uplink space delay provided by the clocked video delay line is always the same and dependent only on the stability of the timing circuits and logic jitter. Consequently, it is seen that the signal equations at the output for the two models are the same.

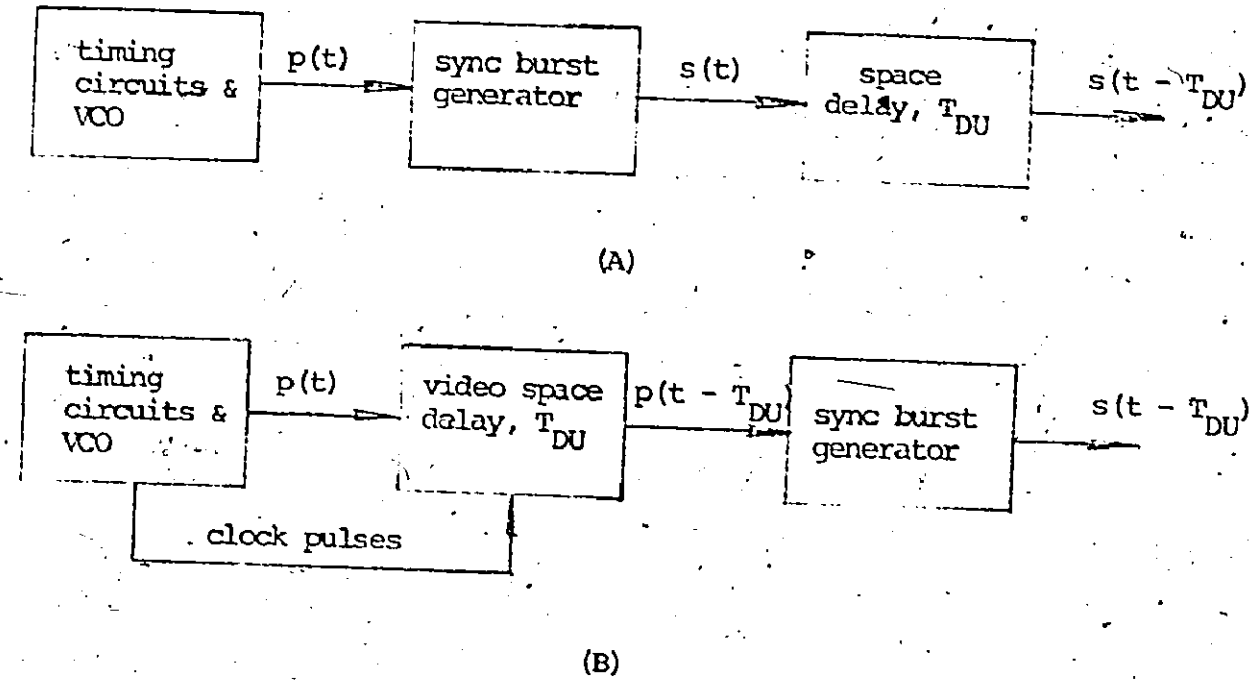

Fig. 6-3: Interchanging the uplink space delay and the sync burst generator (A) actual system, (B) laboratory model.

For the tracking mode, the uplink space delay network must be modified in the model, as shown in Fig. 6-4A, since now the VCO in the timing circuits is permitted to vary its frequency. The frequency variation is produced by a small DC voltage applied to the control terminal of the VCO to account for satellite motion. This voltage remains constant between transmissions and causes the uplink space delay in the model to change as a function of the error voltage whereas in the actual system, the space delay is independent of the error voltage. A higher VCO frequency produced by negative voltage at the control terminal reduces the space delay while a lower frequency produced by positive voltage increases the space delay. This change is directly proportional to the integrated error voltage $v_{OT}(r_T)$ and is given by:

$$T_X = \frac{S}{f_0}(T_{DU} + T_{DD} + T_{GP})\ v_{OT}(r_T) \qquad (6\text{-}1)$$

where T_{DD} = downlink space delay

T_{GP} = earth station processing time.

Taking the first derivative, $d\,T_X/d\,v_{OT}(r_T)$, gives the voltage timing characteristic slope required by the compensation network. Thus,

$$\frac{d\,T_X}{d\,V_{OT}(r_T)} = \frac{S}{f_0}\ (T_{DU} + T_{DD} + T_{GP})\ V_{OT}(r_T) \qquad (6\text{-}2)$$

In practice, this variation amounts to approximately several tens of nanoseconds maximum. Hence, a analog trigger circuit which has the opposite characteristic, as shown in Fig. 6-4B, can be used in cascade to compensate for this error. When the value of $V_{OT}(r_T)$ is zero,

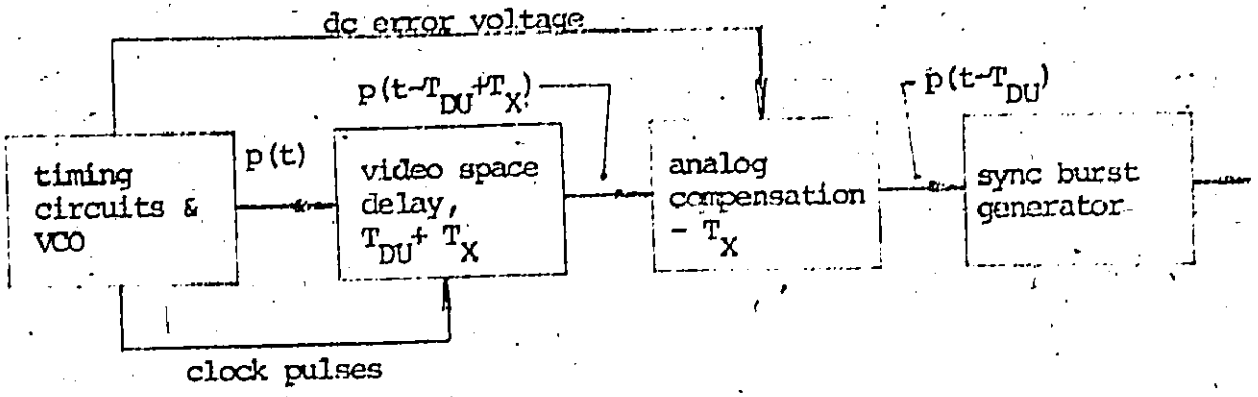

(A)

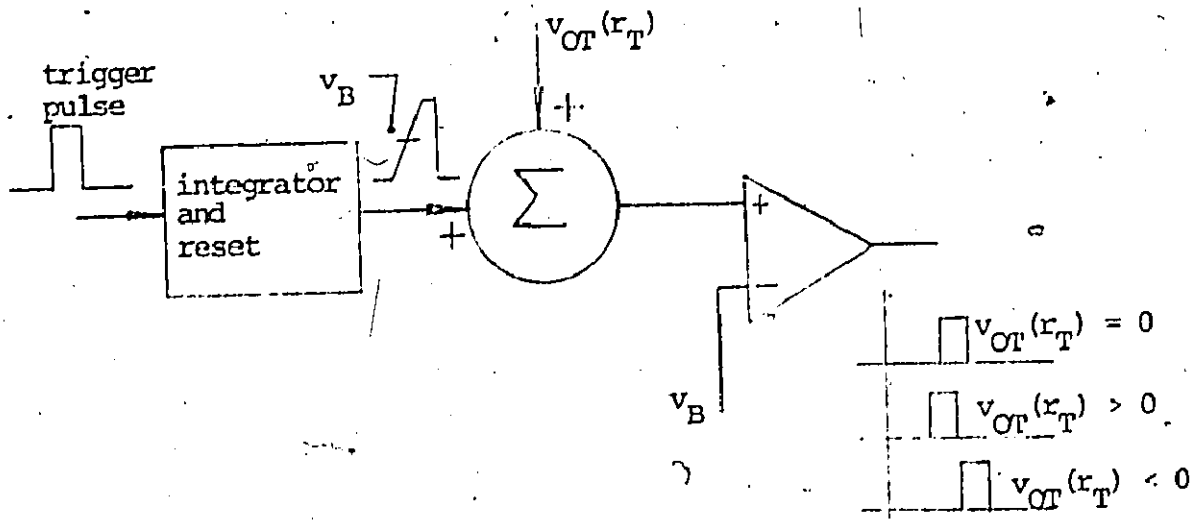

(B)

Fig. 6-4 Modified uplink space delay for the tracking mode.
(A) Block diagram, (B) simple analog compensation circuit.

the operational amplifier output is delayed by an amount T_{XD}. If $V_{OT}(r_T)$ is positive, the operational amplifier output is advanced by a small amount relative to T_{XD} and when $V_{OT}(r_T)$ is negative, the converse is true. In practice, this timing adjustment is included in the fine search video delay as well but causes no variation in the space delay since $V_{OT}(r_T)$ is always zero.

6.1.3 Comparison of the Laboratory Model with the Physical Model

The comparison of the laboratory model with the physical model is based on examining the spatial timing relationships of the processing of the signal. For the coarse search mode, fine search mode and the tracking mode the signal equations can be written for one transmission around the loop. As a result, it is shown that the two models are equivalent with the only assumption being that the uplink and downlink noise is stationary.

For the physical model, shown in Fig. 6-5 , a sync request pulse $p_1(t)$ is used to trigger the coarse search encoder into transmitting a PSK multi-frame coded search signal at time $t = 0$. The video signal, $w_1(t)$ is modulated and transmitted toward the satellite where it adds with the satellite input noise. After sync window modulation, the signal is transmitted back to the earth station where the noise from the receiver is added.

The analysis parallels that of Section 3.2.1 resulting in the signal at the output of the coherent detector in the receiver being given by

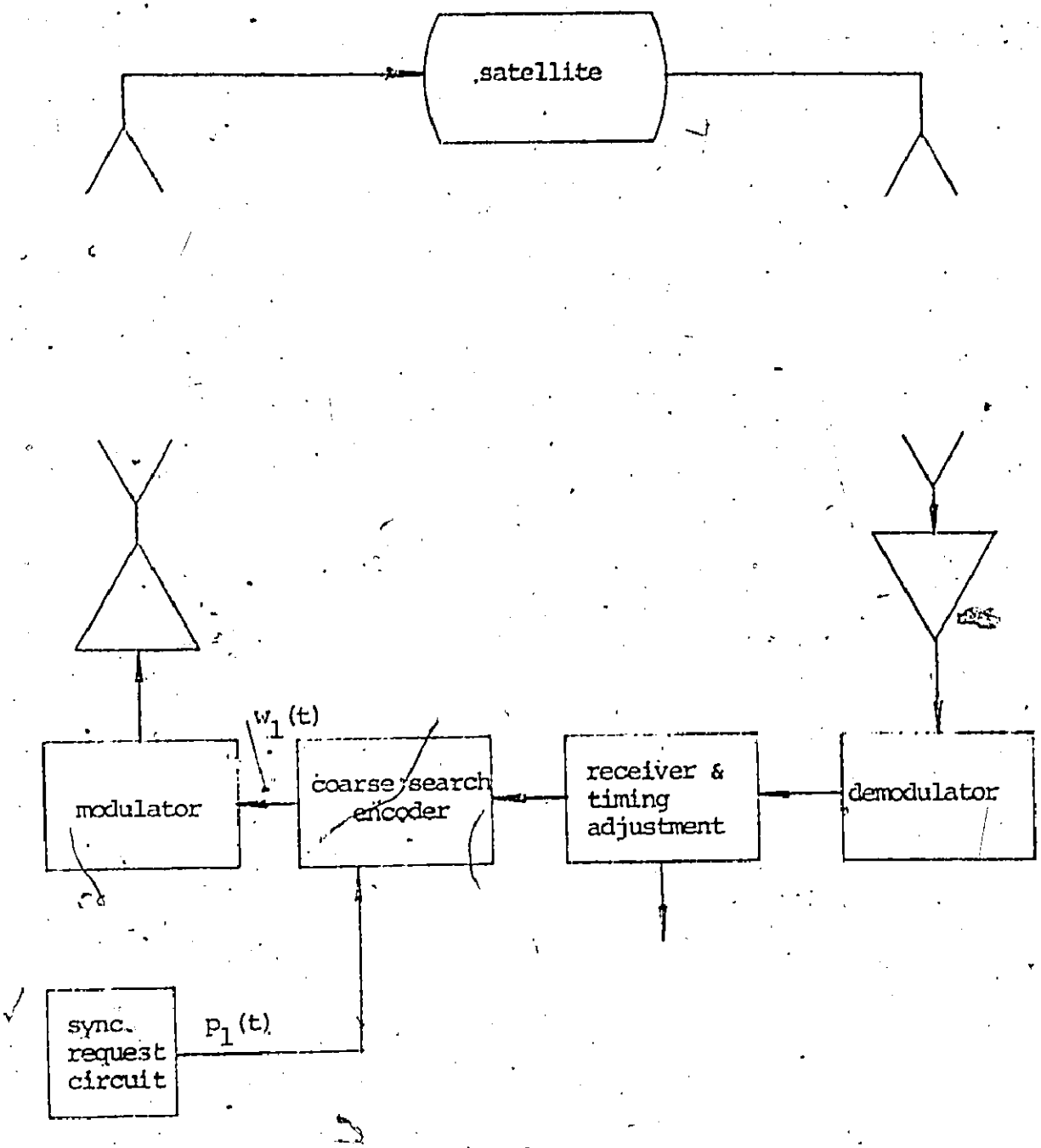

Fig. 6-5 Block diagram of the physical model.

$$
\begin{aligned}
w_2(t) &= k_{P1}\, w_1(t - T_{DU} - T_{DD})\, m(t - T_{DD}) \\
&\quad + k_{P2}\, x_1(t - T_{DD})\, m(t - T_{DD}) + k_{3P}\, x_2(t) \\
&= k_{P1}\, w(t' - T_{DU})\, m(t') + k_{P2}\, x_1(t')\, m(t') \\
&\quad + k_{3P}\, x_2(t + T_{DD})
\end{aligned}
\tag{6-3}
$$

where k_{P1}, k_{P2} and k_{P3} are constants and $t' = t - T_{DD}$

Note that the uplink and downlink space delays have been separated to show that, in fact, the sync window modulation of the signal is a function of T_{DU} but not T_{DD}.

Finally, the signal is decoded to give the estimate of the timing relationship between the earth station time base and the satellite sync window. This estimate results in a value for T_S which is applied to the timing circuits to zero the counter and occurs after a duration of $T_{DU} + T_{DD} + T_{GP}$ after the initial transmission of the PSK coded search signal.

For the laboratory model, shown in Fig. 6-6, the sync request pulse $p_1(t)$ is fed directly to the uplink clocked delay representing the uplink space delay. After a time duration of T_{DU}, the delayed pulse $p_1(t - T_{DU})$ triggers the coarse search encoder which transmits a PSK multi-frame coded search signal. The video signal $w_1(t - T_{DU})$ is modulated and passed through a level control to simulate uplink space attenuation. Next, the signal is fed to the satellite unit where uplink noise is added. The resulting signal, modulated by the sync window, is fed through a second level control to simulate downlink space attenuation

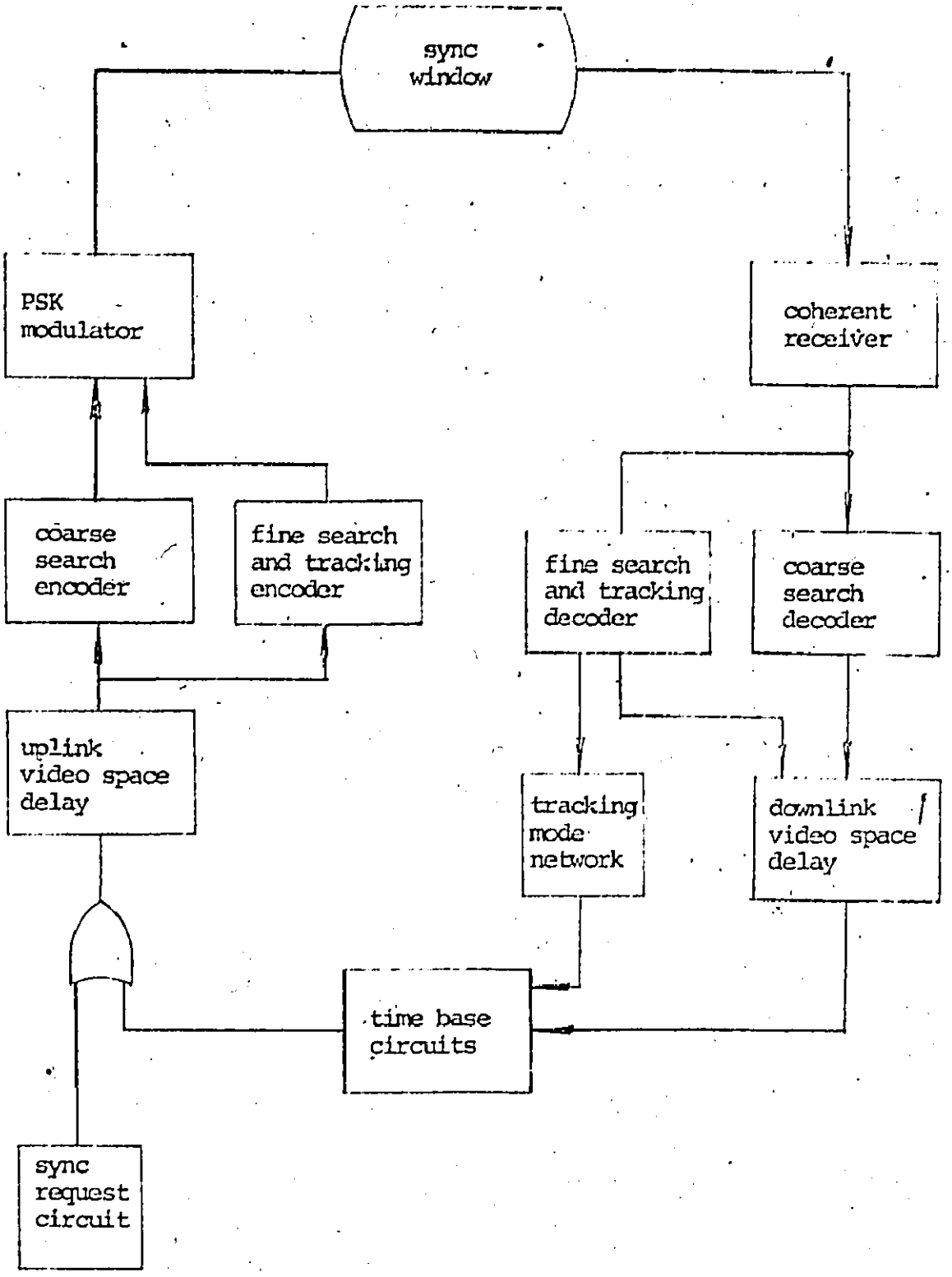

Fig. 6-6 Block diagram of the laboratory model.

to the receiver where coherent detection occurs resulting in the output signal given by

$$w_m(t) = k_{M1}\, w_1(t - T_{DU})\, m(t) + k_{M2}\, x_1(t)\, m(t) + k_{M3}\, x_2(t) \qquad (6\text{-}4)$$

where k_{M1}, k_{M2} and k_{M3} are constants.

It is seen that (6-4) is identical in form with (6-3) since the downlink noise is assumed to be stationary.

This signal is decoded after a time T_{GP} to yield the value of T_S required to zero the counter in the time base circuits but this adjustment is delayed by the downlink delay T_{DD}. Hence, a trigger given by $p_2(t - T_{DU} - T_{GP})$ is applied to the downlink delay to give an output trigger $p_3(t - T_{DU} - T_{DD} - T_{GP})$ which is used to indicate when the value of T_S should be fed to the timing circuits. Hence, as for the physical model, the timing circuits here are adjusted at time $t = T_{DU} + T_{DD} + T_{GP}$ and the correction is based on the decoded value T_S. Consequently, the two models are equivalent.

Similar results are obtained when the physical models for the fine search mode and the tracking mode are compared with the laboratory models. The only changes required in the fine search mode are the use of a PSK sync burst encoder for the transmitted signal and a special decoder for the received pulses leaving the receiver. For the tracking mode, the uplink space delay must also be modified using the circuit illustrated in Fig. 6-4. Hence, for all three modes, the spatial timing equations for the laboratory model are the same as for the physical model and, consequently, the experimental results will be representative of the actual system.

6.2 DETAILED DESIGN OF THE LABORATORY MODEL SYNC UNIT

The laboratory model synchronizer has been divided into twelve sub-units comprising the sync request circuit, earth station time base, uplink video delay, coarse search encoder, PSK modulator, satellite model, coherent receiver, coarse search decoder, downlink video delay, fine search and tracking encoder, fine search and tracking decoder, and the tracking mode network, as shown in Fig. 6-6. Each sub-unit is described in detail with circuit diagrams, and photographs of selected signal waveforms are presented. System performance results, such as decoding the PSK multi-frame coded search signal, error detection characteristics and closed loop behaviour in the fine search and tracking modes are presented in Chapter 7.

6.2.1 Sync Request Circuit

The sync request circuit is used to obtain synchronization. It is assumed that this would occur for the following reasons:

(1) Normal start-up at the beginning of the transmission day,

(2) after an outage caused by heavy rain attenuation or other atmospheric causes,

(3) after outages caused by power failures or system failures,

(4) after outages caused by other earth station failures,

(5) after outages caused by solar transits.

To generate the sync request pulse, the user simply pushes a momentary close switch connected through a discharge capacitor to the clear terminal of a flip-flop, as shown in Fig. 6-7. The flip-flop

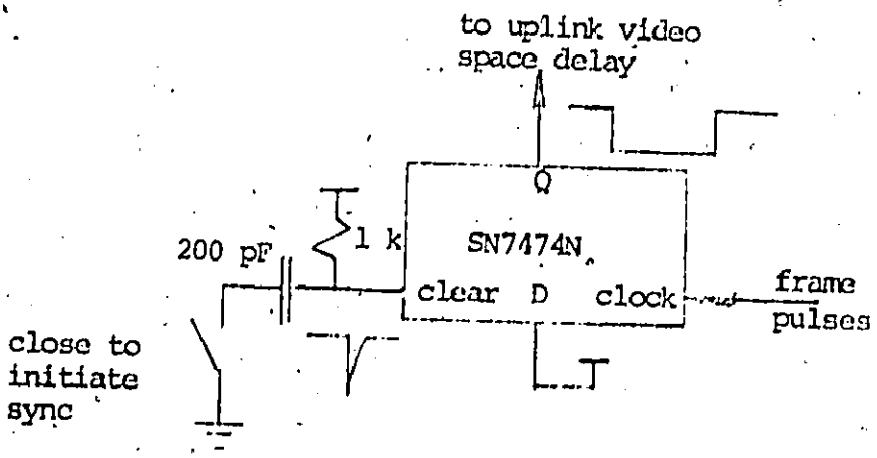

Fig. 6-7 Sync request circuit.

produces a pulse having its trailing edge synchronized by the time base circuits described next which is fed to the uplink video space delay circuit. The sync request pulse also sets flip-flops in the coarse search encoder, coarse search decoder, fine search and tracking encoder and fine search and tracking decoder in preparation for the sequence of synchronization signals.

6.2.2 Earth Station Time Base

A circuit diagram of the earth station time base is shown in Fig. 6-8. Initially, the control terminal of the VCO is at zero volts and the output signal has logic levels with a frequency of 12 MHz. The signal is divided by 6 in a counter to increase the period to 500 ns and fed to the frame counter to produce the frame pulses of the earth station time base. The frame counter comprises two four-bit counters, inverters, a multiple-input nand gate for decoding and control logic to generate 500 ns wide frame pulses having a spacing of 125 ms, as shown in Fig. 6-9.

By using the flip-flop and nand gate following the decoder, it is possible to obtain reset pulses having a duration of 250 ns which are used to zero the counter. An additional input is provided to zero the counter which is utilized by the coarse search mode.

The frame pulses are counted in another counter to provide trigger pulses at a 50 pulse per second rate. These pulses are used for high repetition rate measurements as described in Chapter 7.

The VCO has a center frequency of 12 MHz with the control terminal at zero volts. The maximum shift in frequency is ±0.03 percent of the

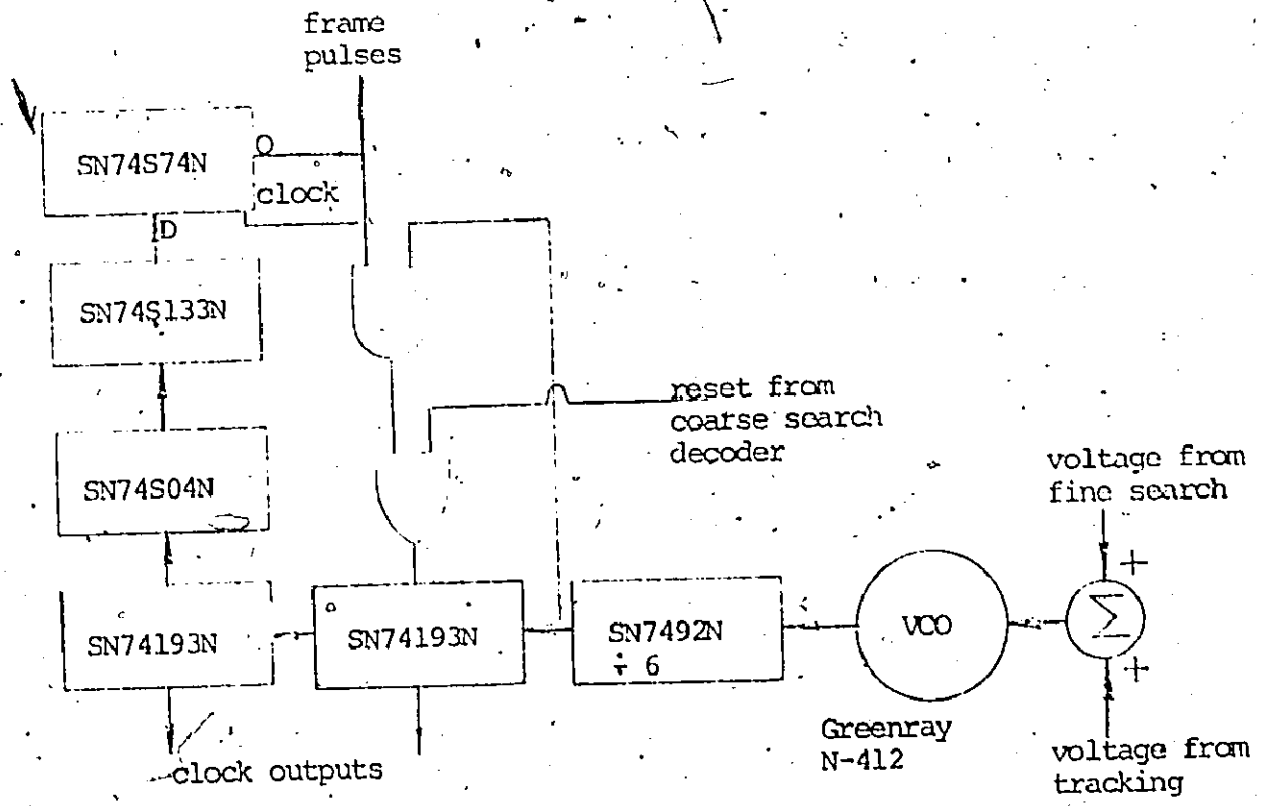

Fig. 6-8 Earth station time base.

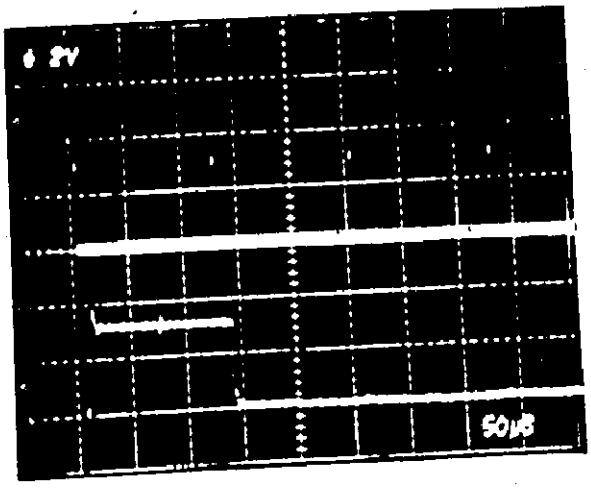

Fig. 6-9 Frame pulses with 125 µs spacing. Upper trace: train of frame pulses, lower trace: detail of one pulse (200 ns/ cm).

center frequency for a control terminal voltage of ±3 volts. Thus, the voltage-frequency relationship is given by

$$f = (12 - 0.0012\, V_E)\ \text{MHz} \qquad (6\text{-}5)$$

Comparing this relationship with (4-18), it is seen that the value for S is -1200 Hz/V.

Two outputs are provided by the time base circuits. First is the train of earth station frame pulses which has already been described. Second is the set of binary signals, shown in Fig. 6-10, which are used by the coarse search encoder to generate the PSK multi-frame coded search signals. These are taken from the eight outputs of the two-four bit binary counters. The frame length can be seen by noting the truncated clock pulse on the fifth trace.

The spacing of frame pulses can be adjusted by varying the voltage on the control terminal of the VCO. If the voltage is adjusted over a short interval, and then returned to zero, the train of frame pulses is shifted in time but the spacing of frame pulses is not affected. However, if the voltage of the control terminal is changed and not returned to zero, then the interpulse spacing of frame pulses changes. These two degrees of freedom can thus be used to match two degrees of freedom possessed by the synchronization loop; namely, the space delay and the variation in the space delay.

A digital technique for adjusting the earth station time base is described in Appendix C. It is shown that adjustments of several nanoseconds are possible without using high-speed counting methods.

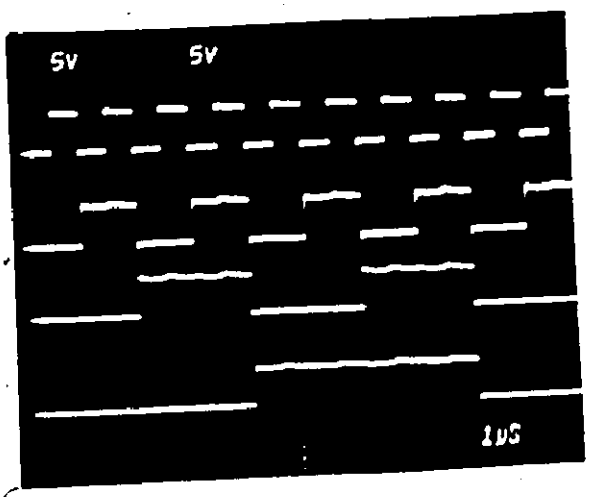

(A)

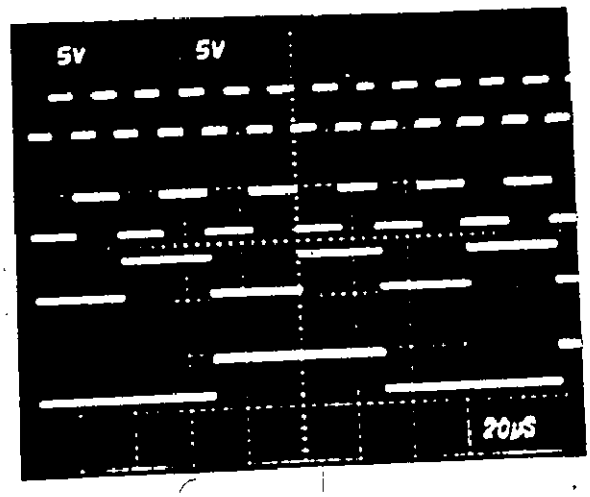

(B)

Fig. 6-10 Binary signals used for the PSK multi-frame coded search signal. (A) First four binary clock outputs, (B) last four binary clock outputs.

6.2.3 Uplink Video Space Delay

The uplink video space delay, shown in Fig. 6-11, is zeroed by reset pulses fed to the clear terminal of the counter. These reset pulses can either originate from the sync request or the fine search mode decoder. Frame pulses are fed to the count-up terminal of the first of the three four-bit binary counters in cascade. Using inverters where necessary a multiple-input nand gate is employed for decoding. When the decoded number is reached, the frame pulses are prevented from entering the first binary counter and this occurs 135 ms after application of the reset pulse which is the nominal value of the uplink space delay.

6.2.4 Coarse Search Encoder

When the sync request circuit is activated, a pulse is sent to the load input terminal of the four-bit binary counter in the coarse search encoder, shown in Fig. 6-12, causing the binary number 1101 to be loaded at the counter output. This number is decoded using a four-input nand gate to prohibit frame pulses from entering the counter. Hence, the coarse search encoder is now ready for a trigger from the uplink video delay.

The first delayed trigger from the uplink video delay feeds the coarse search encoder which generates the PSK multi-frame coded search signal described in Chapter 3 and shown in Fig. 6-13. The delayed pulse first triggers a monostable multivibrator (mono) producing a video pulse of duration 1.7 ms. This pulse is used to produce the length of carrier required for carrier lock at the receiver. The trailing edge of this

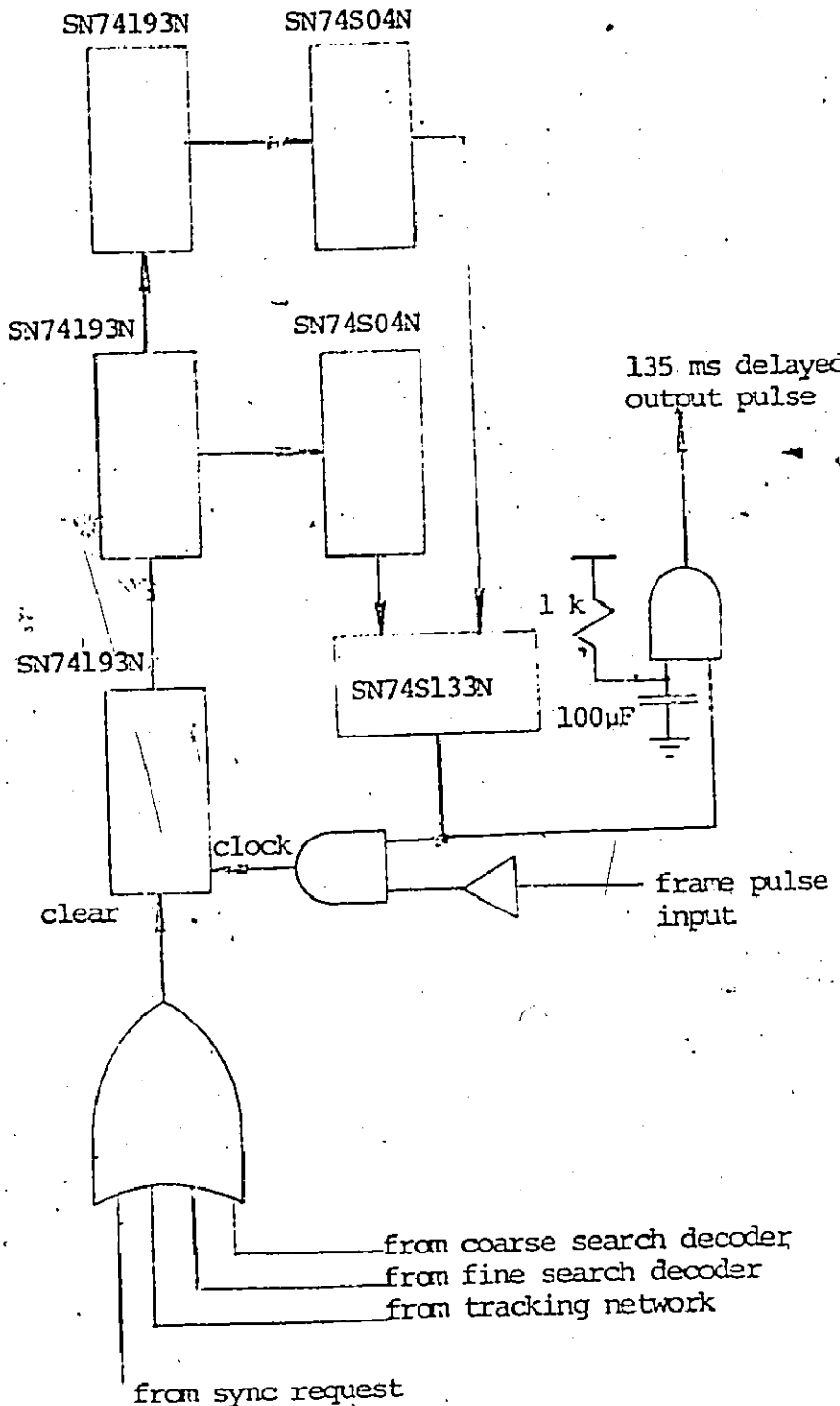

Fig. 6-11 Circuit for the uplink video space delay.

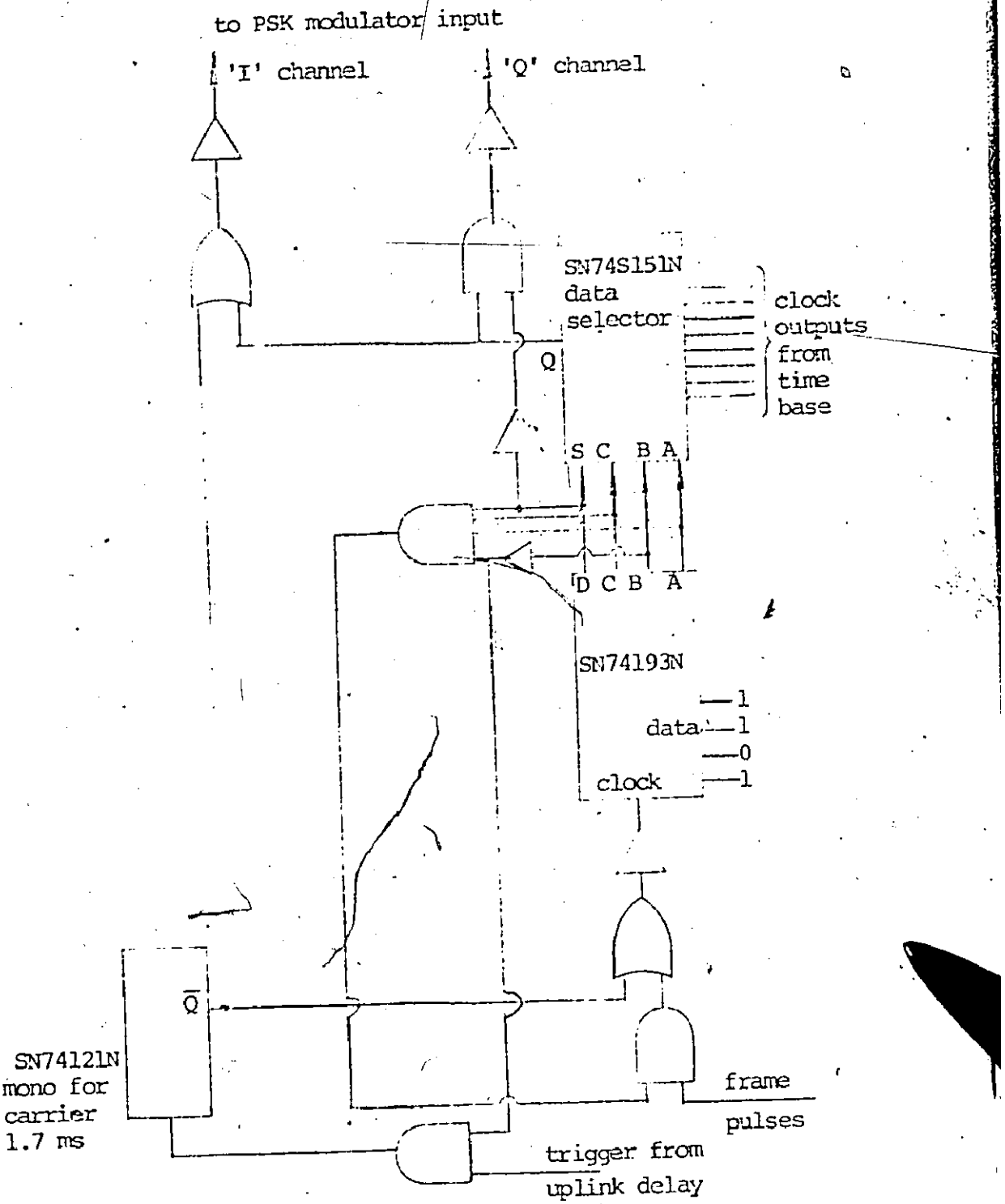

Fig. 6-12 Circuit for the coarse search encoder.

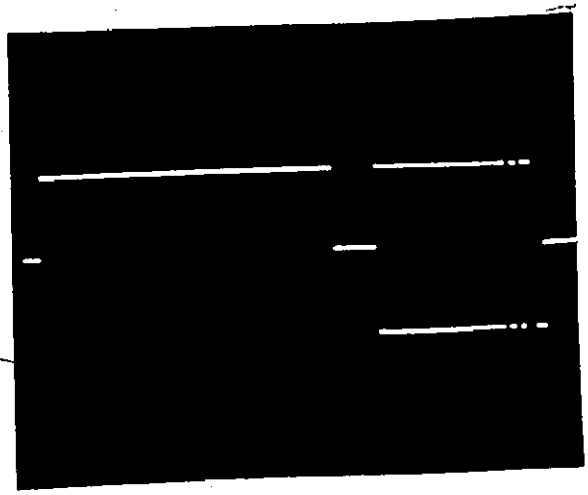

(A)

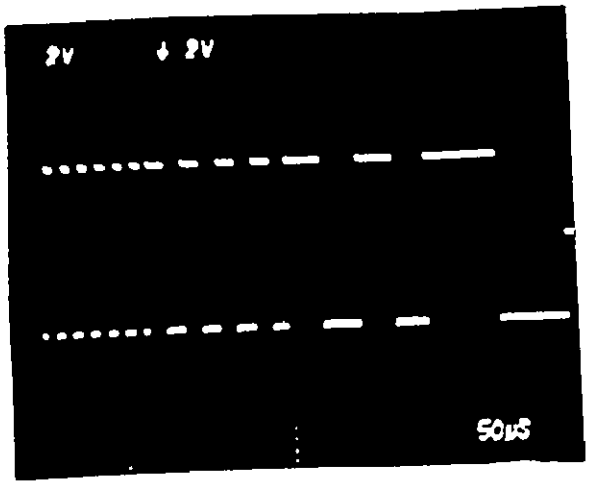

(B)

Fig. 6-13 (A) PSK multi-frame coded search signal,
(B) details of the coded sync sentence.

carrier pulse is fed to a four-bit binary counter which counts one clock pulse. This clock pulse changes the output of the counter by one digit thus causing the four-input nand to enter the high state. Once this occurs, frame pulses are gated into the counter until the number decoded by the four-input nand gate is again reached. Thence, no more frame pulses enter the counter and the number at the output remains constant.

Next, consider the operation of the eight-input data selector. Initially, the D-output from the counter, feeding the strobe input, is high which causes the output of the data selector to remain in the low state. The counter counts three clock pulses from the initial value of 1101 before reaching 0000 thus producing a null duration of approximately 375 ms when the counter reaches 0000. The strobe no longer inhibits the output and the selector starts to scan the eight inputs producing the multi-frame coded sync sentence. The eight-inputs of the data selector are provided by the timing circuits and are simply clock pulses with the bit rate being halved with each succeeding input. Hence, the selector feeds the high bit rate for one frame duration, then switches to the next input line at half the bit rate. This continues for eight frame lengths until the data selector has scanned all eight inputs. At this point, the D-output of the counter changes to the high state forcing the output of the data selector to remain in the low state thus terminating the multi-frame coded sync sentence.

The outputs of the data selector are divided into two separate bit streams. The first is combined with the output of the carrier mono to produce the waveform shown in Fig. 6-14, and the other bit stream is inverted to provide the complement. Both data streams are

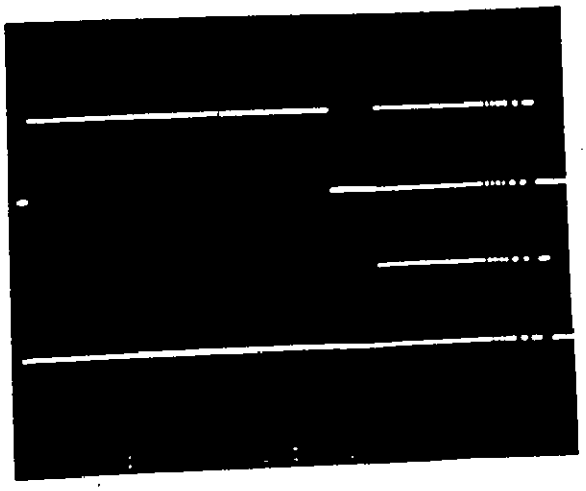

Fig. 6-14 Components of the video waveform for the PSK multi-frame coded search signal.

then fed to the PSK modulator.

6.2.5 PSK Modulator

The PSK modulator comprises two four-input gates, a standard ring modulator and an output emitter follower driver as shown in Fig. 6-15. The gates allow signals from both the coarse search encoder and the fine search encoder to be fed to the ring modulator. The ring modulator consists of four hot-carrier diodes and two ferrite toroid transformers with bifilar windings. The carrier of 30 MHz is applied to one transformer input and the modulated signal is obtained at the other transformer output. The transistor driver provides the low impedance output needed for the 50 ohm coaxial line which feeds the satellite model. The signal output is shown in Fig. 6-16.

In the model, conversion to a microwave carrier was not provided since theoretically the loop behaviour is independent of the carrier frequency. However, in future experiments this feature may be provided to study the effects of TWT amplifier non-linearities on sync window modulated synchronization signals.

6.2.6 Satellite Model

The satellite model is the most complex circuit unit of the system. In order to achieve a realistic model, it is desirable to provide for satellite motion. This can be achieved by causing the spacing of sync windows to be slightly different from the spacing of the frame pulses. If the spacing is larger than the nominal 125 μs, the satellite appears to be moving away from the earth station whereas if the spacing is less

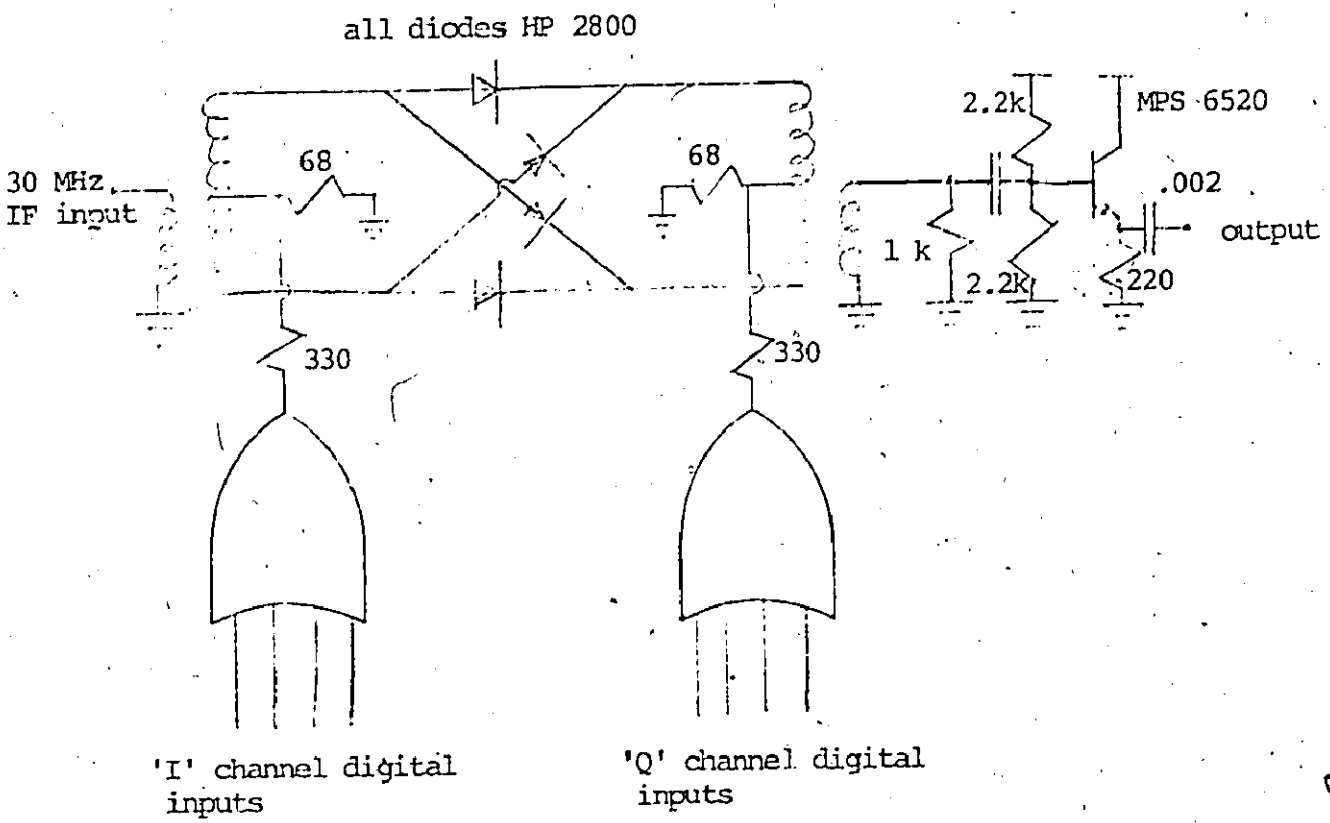

Fig. 6-15 Circuit for the PSK modulator.

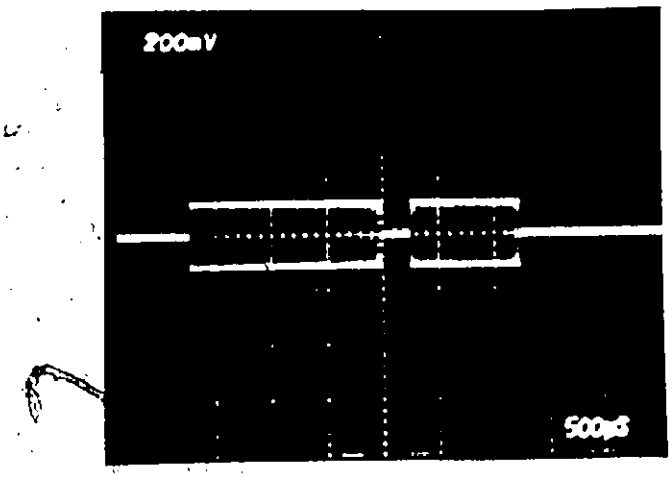

Fig. 6-16 Output signal from the PSK modulator showing the PSK multi-frame coded search signal.

than 125 μs, the satellite appears to be moving toward the earth station. Hence, it is necessary to find a technique for varying the spacing of the sync windows by very small amounts.

The system, shown in Fig. 6-17, has the capability of moving the sync window at rates as slow as 2.5 ns per 10 s interval or as fast as 2.5 ns per 1 ms interval. The main restrictions to the motion are the stability of a frequency synthesizer signal and the jitter produced by the logic packages of the network.

A 50 MHz clock signal is fed from the synthesizer through a divide by two flip-flop producing a bit rate of 25 Mb/s and this signal is fed to two counter chains which decode in the same way. The first counter network is used to provide a stable reference for measuring the motion of the satellite. The clock pulses feed a Schottky flip-flop dividing the frequency by two which in turn feeds a cascade of three four-bit binary counters. The decoding is achieved when the output carry from the last counter feeds a reset pulse through a Schottky flip-flop back to the reset of the Schottky divide by two flip-flop and the load-data inputs of the four-bit binary counters. The four-bit binary counters have hard wired logic levels connected to their data inputs. The reset pulse transfers these data levels to the counter outputs and the counters start counting up from these numbers. Thus, the spacing of reset pulses is determined simply by selecting the levels at the data inputs to produce a separation of reset pulses of 125 μs.

The second counter network has hard wired levels connected to the data inputs of the last two four-bit binary counters but the data inputs to the first binary counter are supplied by the output of another four-bit

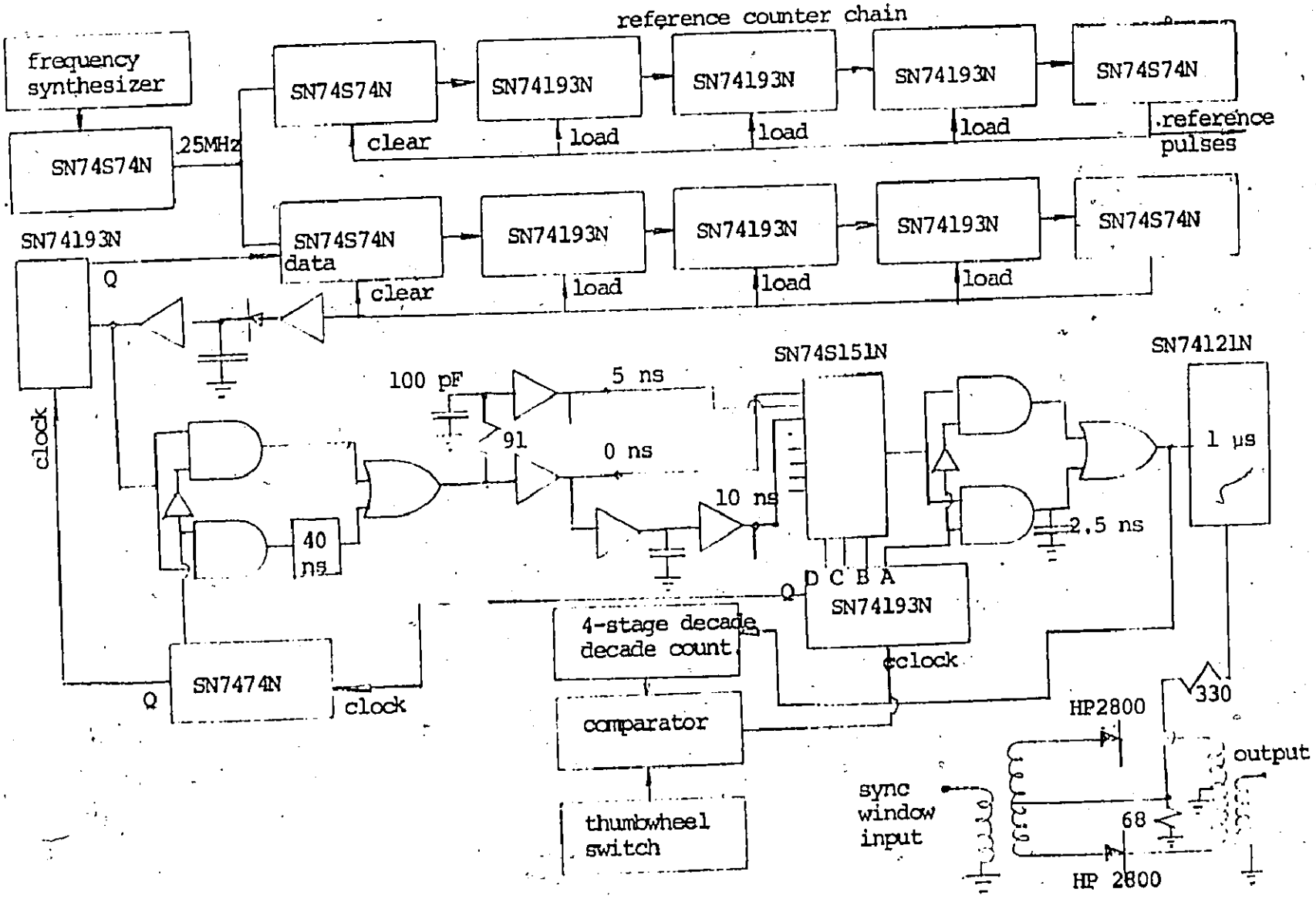

Fig. 6-17 Circuit diagram for the satellite model.

binary counter called the control counter. Whenever the duration between sync windows is to be decreased by 80 ns, a clock pulse is fed to the count-up input of the control counter decreasing the frame length by one 80 ns clock period. Conversely, when the duration between sync windows is to be increased by 80 ns, a clock pulse is fed to the count-down input of the control counter increasing the frame length by one 80 ns clock period. A pulse stretcher is used to increase the 20 ns duration of the reset pulses feeding the remaining circuits to approximately 70 ns.

The 80 ns increment time can be further divided into 40 ns increments by using the gating and delay circuit following the pulse stretcher. This network is controlled by the most significant digit from a five-bit binary counter. If the digit is low, the reset pulse passes through the undelayed path while if the digit is high, the reset pulse passes through the delayed path. The delay is provided by a cascade of inverters each loaded at its output with a capacitor. The capacitors are selected to give the overall delay of 40 ns. The delayed and undelayed pulses are shown in Fig. 6-18.

The reset pulses now are fed to a delay line having eight outputs starting with a reference of 0 ns and increasing to a maximum of 35 ns. The delay line is divided into two separate paths with the second path being delayed 5 ns with respect to the first path. In the first path each delay is provided by a driver inverter followed by a delay capacitor and finally a restoring inverter. The total delay from the input of the driver inverter to the output of the restoring inverter is 10 ns with the value of the capacitor being selected to give the desired

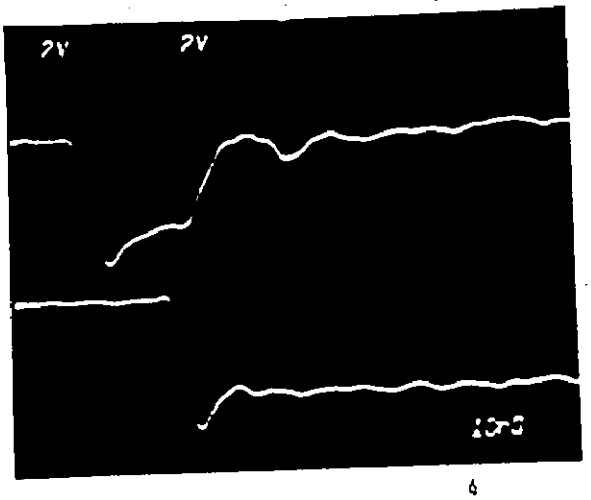

(A)

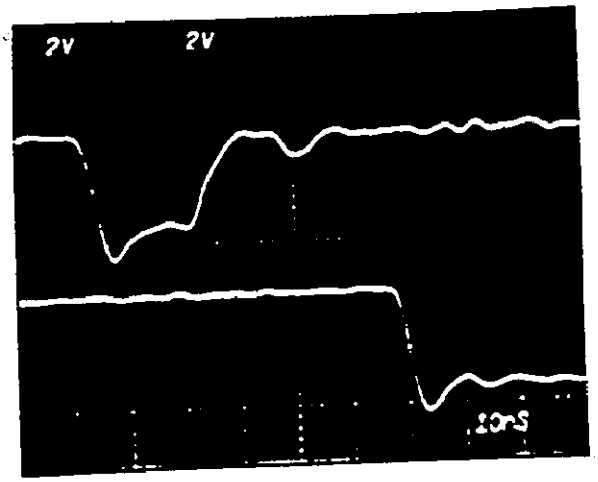

(B)

Fig. 6-18 Pulse outputs from the gating and delay circuit. (A) Zero relative delay position, (B) 40 ns relative delay position.

value. All delayed outputs are fed in sequence to the inputs of an eight-input data selector which is controlled by the next three bits of the five-bit binary counter, as shown. Thus, when these three bits are all zero, the data selector chooses the D_0 line and as the count increases the data selector output is connected to increasing values of delay. Hence, the variation in the timing of the rising edges of the pulses has been reduced to 5 ns. Figure 6-19 shows the set of delayed pulses.

The increment is finally reduced to the desired value of 2.5 ns by feeding the output of the data selector into another gating and delay circuit controlled by the least significant digit of the five-bit counter. This circuit is identical to the first except now the delay element is provided by a capacitor instead of a cascade of inverters and capacitors. Thus, the pulses can now be adjusted in increments of 2.5 ns as shown in Fig. 6-20, by simply changing the count of the five-bit binary counter.

The output pulses are fed to a mono which has a 1 μs time constant and the mono in turn drives a switch which represents the sync window. The switch comprises two hot-carrier diodes and two bifilar wound transformers. The signals from the PSK modulator are fed into one input and the sync window modulated signals are produced at the output. Sync window modulation of a 30 MHz carrier is shown in Fig. 6-21 to illustrate the performance of the sync window modulation.

The output pulses are also fed to the control and comparator circuits which determine the number of 2.5 ns increments to be applied. Four decade counters in cascade are used to achieve a variation in timing of 10^4. By comparing the outputs of the counters with a manual

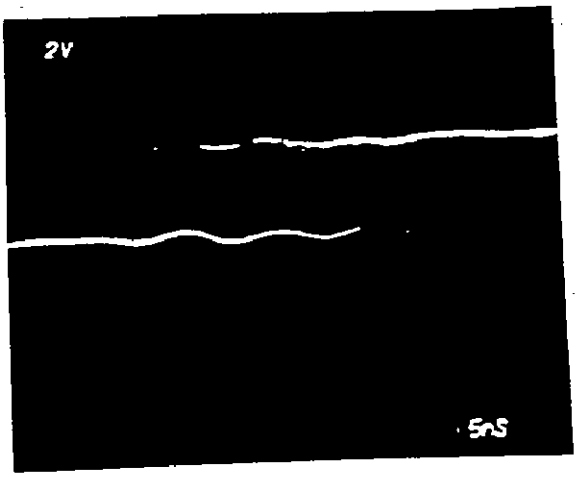

Fig. 6-19 Pulses from the data selector with 5 ns relative delay between rising edges.

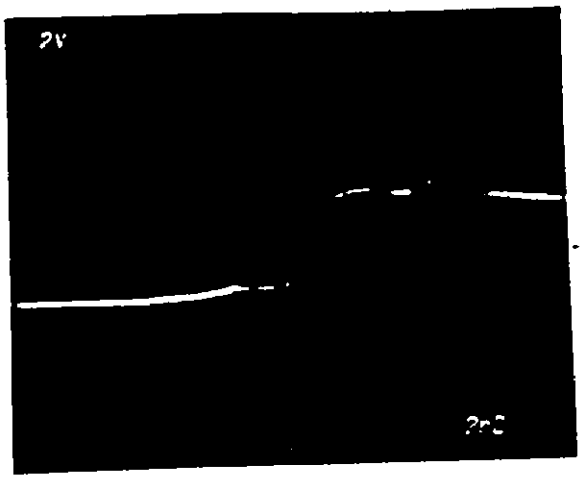

Fig. 6-20 Pulses from the gating and delay circuit with 2.5 ns relative delay between rising edges.

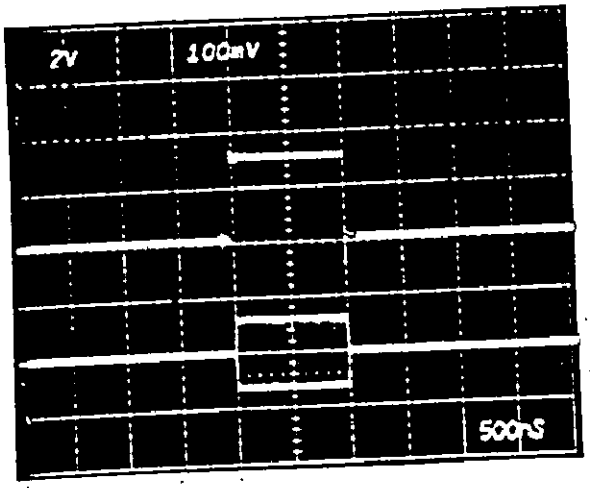

Fig. 6-21 Upper trace: Video waveform for the sync window switch. Lower trace: Sync window modulation of a 30 MHz carrier.

setting provided by a thumbwheel switch, it is possible to produce one output pulse from the comparator as often as one pulse per millisecond or as seldom as one pulse per 10 s. These output pulses are fed to the five-bit counter which then feeds the control counter.

By feeding the count-up terminals of these counters, the satellite appears to move toward the earth station while feeding the count-down terminals corresponds to motion away from the earth station. Any combination of these two movements are also possible simply by switching the connections either manually with a switch or automatically using gates.

6.2.7 Coherent Receiver

The signals produced by the sync window modulation are pulses containing information of the relationship between the earth station time base and the sync window time base. Since these signals are looped from an earth station through the satellite and back to the same earth station, it may be possible to obtain coherent detection by mixing the incoming pulse stream with the intermediate frequency (IF) used by the modulator of the earth station. The only problem which arises is in selecting the proper phase relationship.

A special coherent receiver, shown in Fig. 6-22 has been developed to process these signals. The signals are first amplified in a wideband IF amplifier having a gain of 10 dB and a center frequency of 30 MHz and then passed through a phase correcting switch, described later, to the coherent multipliers. The multipliers are also fed by a phase adjusted signal derived from the IF using a phase adjustment network.

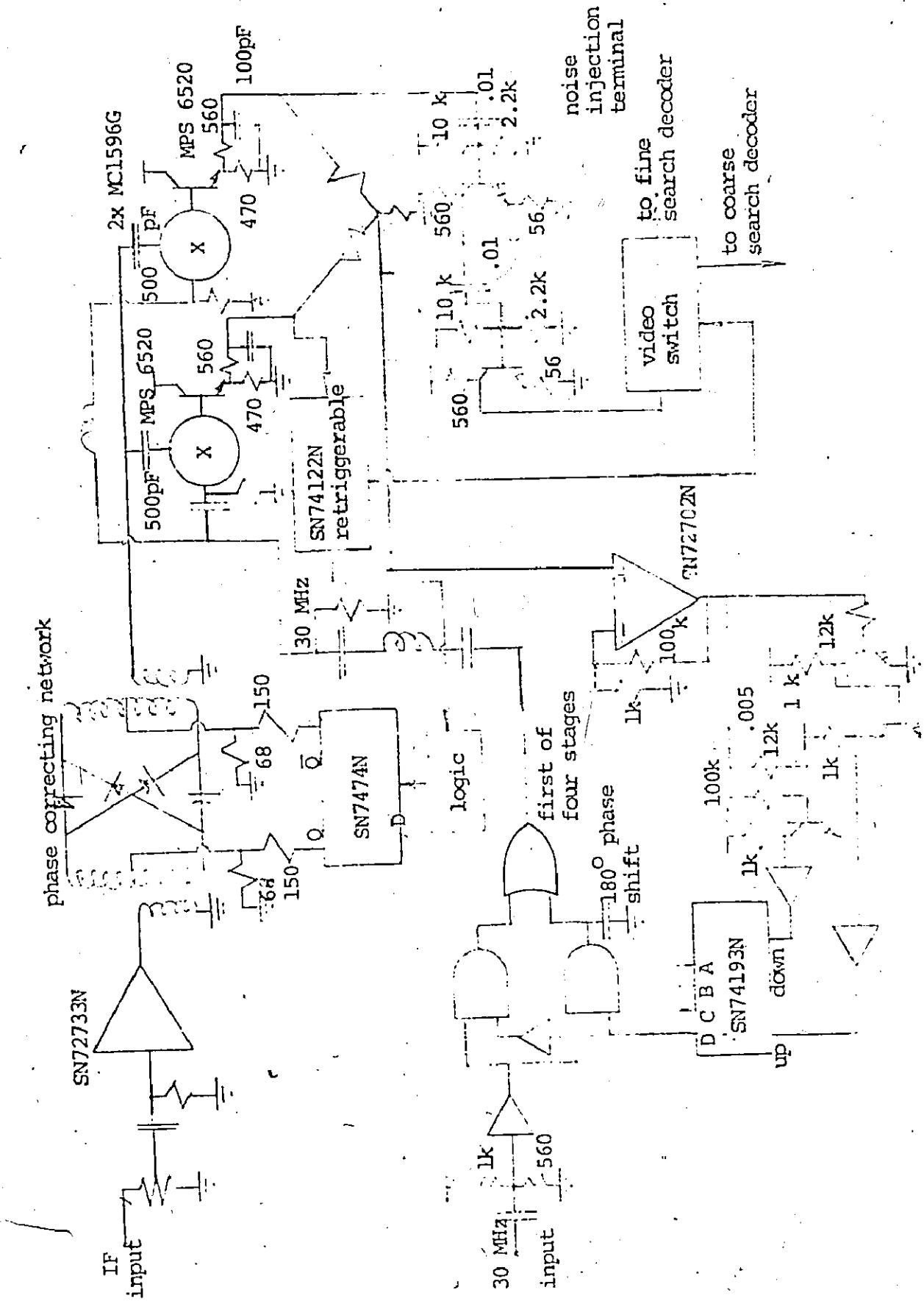

Fig. 6-22 Circuit for the phase adjusting coherent receiver.

The phase adjustment network consists of an inverter used as a driver biased to the transition voltage and a phase shift network comprising four gating and delay circuits as used in the satellite model. The input IF drive is converted to logic levels in the input driver and fed to a phase shift network, controlled by a four-bit binary counter. When the counter output is 0000, the zero phase shift path through the network is selected. As the number at the counter output increases, the phase shift is increased to a maximum of 337.5 degrees with the finest step being 22.5 degrees.

The output signal leaving the last gating and delay circuit is bandpass filtered in a circuit tuned to 30 MHz to remove harmonics and fed to the multiplier circuits through phase shift networks. The 16 phases are shown in Fig. 6-23. The network with the inductor has a phase lag of 45 degrees and the circuit with the capacitor has a phase lead of 45 degrees.

When the output pulsed signals from the multipliers are added, using emitter follower buffers and R-C filters to remove the carrier and the harmonics, the resulting video waveform can be used to adjust the phase of the phase shift network to obtain coherent detection. The combined signal pulse is first amplified in a wideband video amplifier and fed to polarity detecting transistor amplifiers. If the polarity is positive, the amplified pulse is sent to the count-up input of the four-bit binary counter and if the polarity is negative, the pulse is sent to the count-down input of the counter. In either case, the pulse causes a phase shift of 22.5 degrees in a direction which reduces the phase angle between the reference and the received pulses. When the phase of

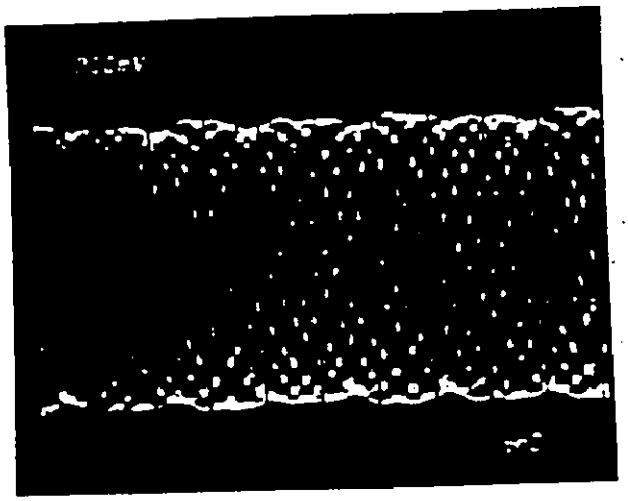

Fig. 6-23 Phase shifted signals at 30 MHz from the phase shift network.

the phase adjustment network is properly adjusted after the reception of several pulses of carrier, the two pulses from the multipliers have the same magnitude but opposite polarity and thus their sum is zero. At this point, there is no output from the video amplifier and coherent lock is achieved. In practice, there will always be a small timing error due to a phase error of up to 11.25 degrees. The loss in detection is defined by $1 - \cos^2\theta$, where θ is the phase error [22]. For $\theta = 11.25$ degrees the corresponding loss is 0.04 and, consequently, no serious degradation occurs.

The phase correcting switch is used to eliminate the phase ambiguity which exists in the coherent receiver. It is known that the received pulses of carrier are zero phase. Consequently, the detected output from one multiplier can be used to control the flip-flop feeding the phase correcting switch. The pulse is amplified in a transistor amplifier and fed to the inputs of an inverter and a nand gate. Since the DC level at the output of the transistor amplifier is approximately 3 V, the inverter does not pass positive pulses appearing at its input since 3 V is already above logic '1'. Negative pulses, however are passed and gated into the clock input of the flip-flop controlling the phase correcting network causing it to change states. The phase correcting network produces a phase shift of 180 degrees which causes the remaining pulses entering the inverter to change to positive polarity as shown in Fig. 6-24. Thus, the receiver not only coherently detects the input pulsed signals, but it also eliminates the phase ambiguity.

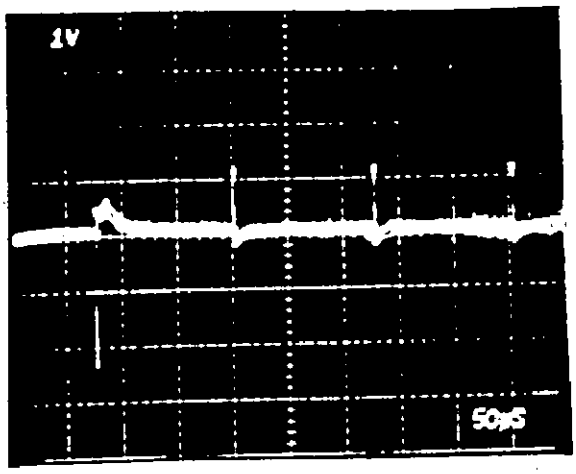

Fig. 6-24 Phase correcting the incomming pulse train. Pulses following the negative pulse are inverted showing that proper phase has been achieved.

The pulses from the transistor amplifier in the phase correction network are also fed to a nand gate which is on. The pulses then trigger a retriggerable mono which has a time constant of approximately 300 μs. Since the pulses of carrier have a spacing of 125 μs, the mono remains on for the entire reception time of the pulses of carrier even if gaps of one missing pulse occur in the reception. Upon termination of these pulses, there is a null region of approximately 375 μs which allows the mono to turn off. When this happens, the output triggers another mono which inhibits any further signals from entering either the retriggerable mono or the phase correcting network. Hence, the receiver is now ready to process these pulses of the PSK multi-frame coded search signal or the PSK sync burst signals, which are described later.

The signals are linearly amplified in two transistor amplifiers and fed into both the coarse search decoder and the fine search decoder. There are eight pulses from the coarse search mode and a certain number of pulses from the fine search mode.

6.2.8 Coarse Search Decoder

The coarse search decoder, shown in Fig. 6-25, is required to extract the timing information contained in the sync window modulated pulses of the multi-frame coded sync sentence and estimate the time at which PSK sync bursts must be transmitted in order to pass through the sync window. The pulses from the receiver are gated into the decoder by using a counting technique and a serial to parallel shift register.

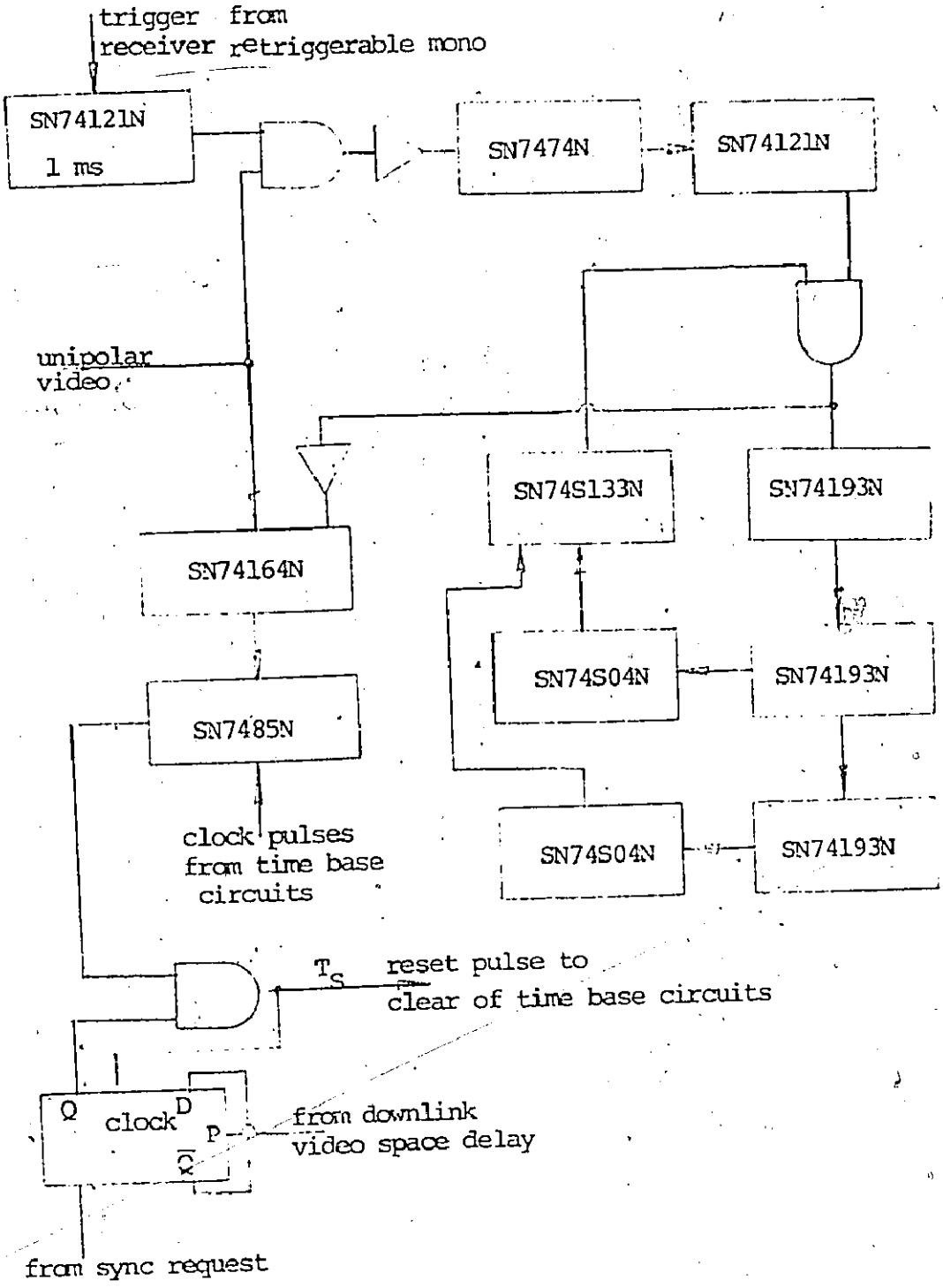

Fig. 6-25 Circuit for the coarse search decoder.

The first information pulse always contains a transition from low to high since the bit rate is twice the duration of the sync window. This transition is used to trigger a mono which clears a 12-bit counter fed from the 2 MHz output of the earth station VCO. The clock produces a set of triggers separated by 125 μs which are combined with the mono output to produce 8 falling edges separated by 125 μs. These signals are fed through an inverter to an eight-bit shift register which reads on the rising edge of the clock pulses. The data are supplied to the shift register by first amplifying in a polarity detecting amplifier. Positive pulses are converted to logic '1' while negative pulses are converted to logic '0' as shown in Fig. 6-26. Thus, the timing information has been converted to a binary number and stored in the shift register.

The output of the shift register is fed to an eight-bit comparator which is also fed by the eight clock lines from the timing circuits. When the number from the timing circuits equals the decoded number, the comparator generates a pulse which is a measure of T_S. After a pulse has been received by the downlink video space delay, this pulse representing T_S is fed to the nand gate input which clears the counter in the time base circuits and completes the coarse search mode. Thus, synchronization can proceed using PSK sync bursts.

6.2.9 Downlink Video Space Delay

The downlink video space delay, shown in Fig. 6-27, comprises one mono and three four-bit binary counters. The output from the

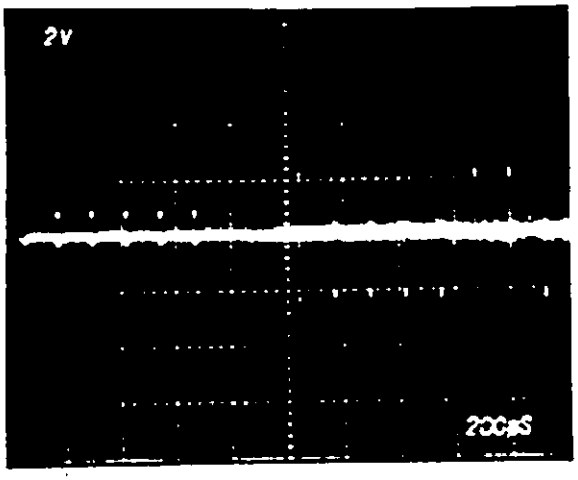

(A)

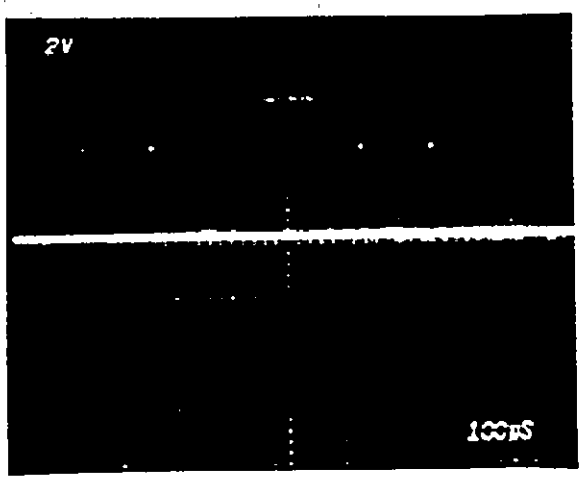

(B)

Fig. 6-26 Conversion of information to logic levels.

(A) Bipolar count of -111-1-1-1-11,

(B) Unipolar count of 01100110.

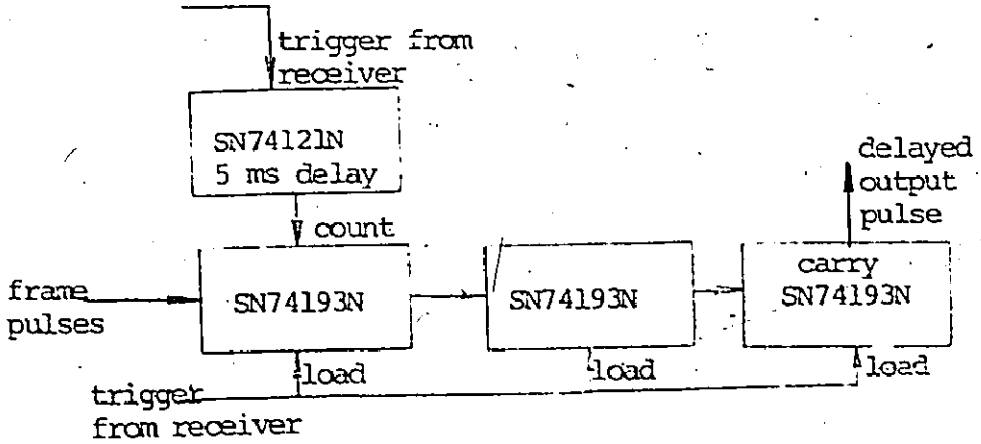

Fig. 6-27 Circuit for the downlink video delay.

retriggerable mono in the coherent receiver is used to load the number hard wired at the counter inputs. Counting does not commence until the mono has reset to account for the processing time, T_{GP}, of approximately 5 ms.

The counters are fed with frame pulses from the time base circuits. Hence, after 1080 of the frame pulses have been counted, a duration of approximately 135 ms is produced which is the nominal value of the downlink space delay and a trigger is generated to gate the pulse representing T_S to zero the counter in the time base circuits. Thus, the total delay produced by this circuit is 140 ms.

6.2.10 Fine Search and Tracking Encoder

The fine search and tracking encoder, shown in Fig. 6-28, generates the fine search signal comprising pulses of carrier followed by PSK sync bursts, as shown in Fig. 6-29, used for the fine search and tracking modes. When the sync request circuit is activated, a pulse is sent to the clear terminal of a flip-flop which prevents signals from entering the network. Upon completion of the coarse search mode, a pulse is sent to the preset of the same flip-flop preparing the encoder for the fine search and tracking modes and the uplink video space delay is triggered.

The video trigger, delayed by 135 ms in the uplink video space delay is fed to the encoder. The length of the entire fine search signal is determined by the fine search mono set for approximately 7.5 ms. The same delayed trigger also feeds another mono which determines

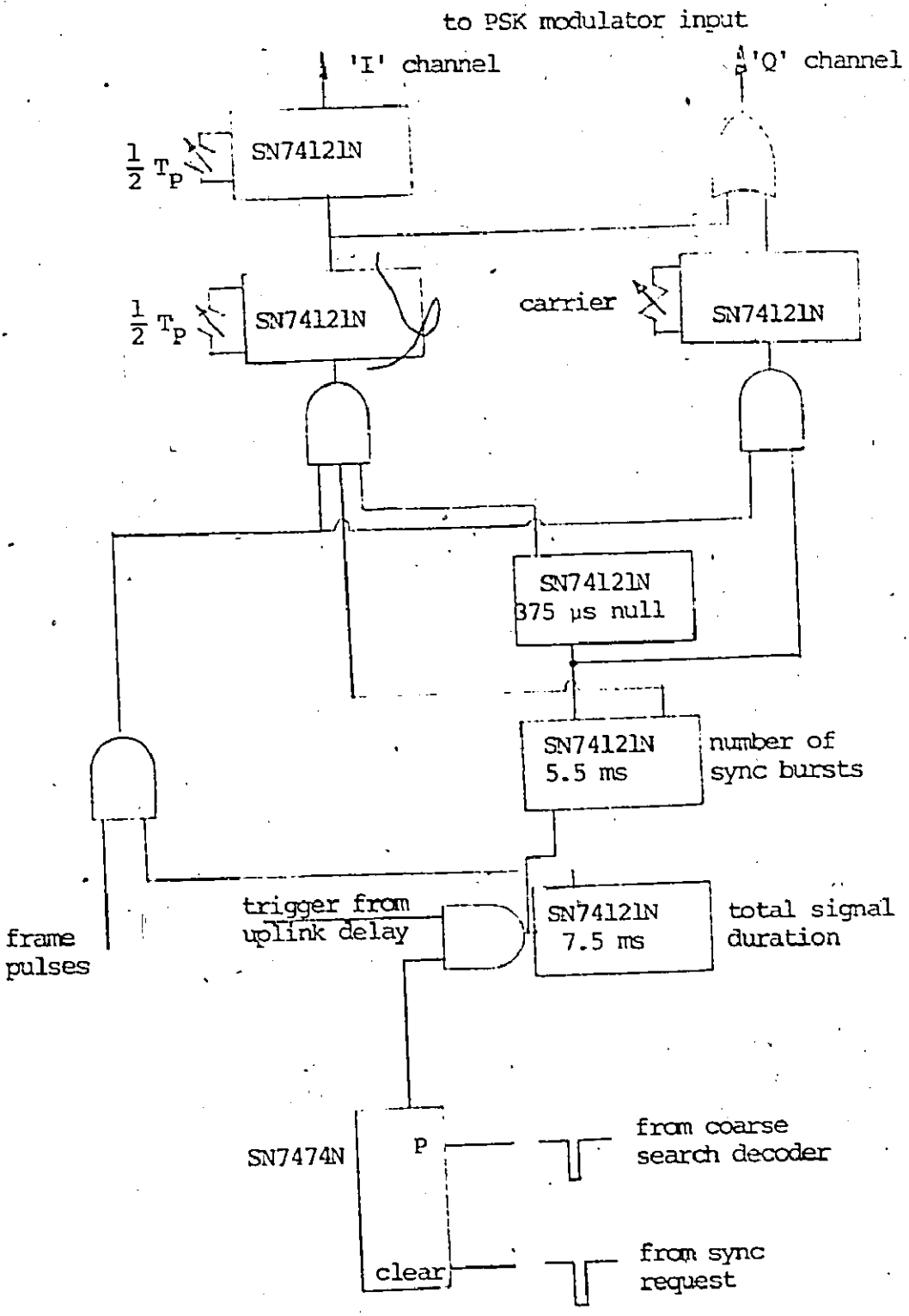

Fig. 6-28 Circuit for the fine search and tracking encoder.

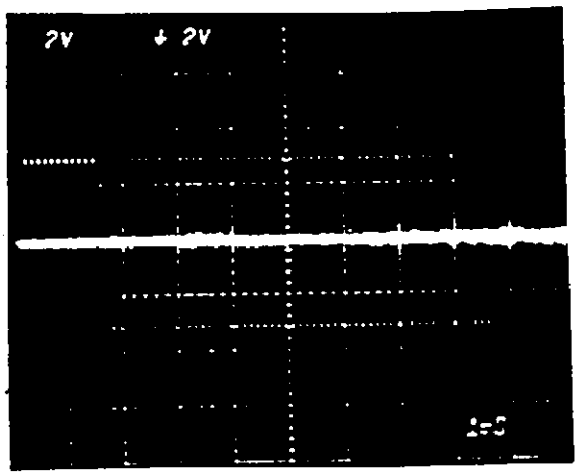

(A)

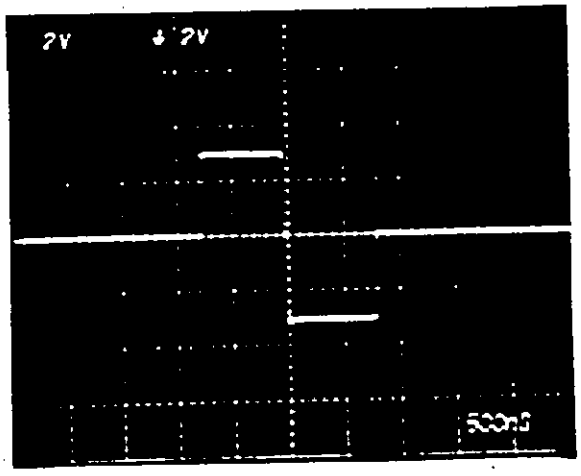

(B)

Fig. 6-29 (A) Video train of pulses of carrier and PSK sync bursts, (B) video waveform of the PSK sync burst.

the number of pulses of carrier to be transmitted.

The pulses of carrier are generated by using frame pulses to trigger a mono having a duration of approximately the sync burst length. After this train of pulses has been generated, a null region is produced by a mono of duration 375 μs. This null is used by the receiver to detect the end of the train of carrier pulses and activate gates to receive the sync bursts.

The sync burst signals are generated using two monos each having the same duration. In the model it is possible to use different lengths of signal in order to plot error detection characteristics and investigate the system performance.

Two different outputs are produced, one for the pulses of carrier and the first portion of the sync burst (0 degree phase) and the other output for the 180 degree portion of the sync burst. Both outputs are then fed to the PSK modulator video inputs and the modulated signal is transmitted toward the satellite unit.

6.2.11 Fine Search and Tracking Decoder

The processing of the fine search signal in the receiver is essentially the same as for the pulses of the coarse search signal. Thus, the signal pulses enter the fine search and tracking decoder as shown in Fig. 6-30. The received PSK sync burst signals, modulated by the sync window, are fed through an R-C filter having a 500 μs time constant to provide the narrow bandwidth and a partial integration. The sync bursts are integrated using an operational amplifier having a capacitor

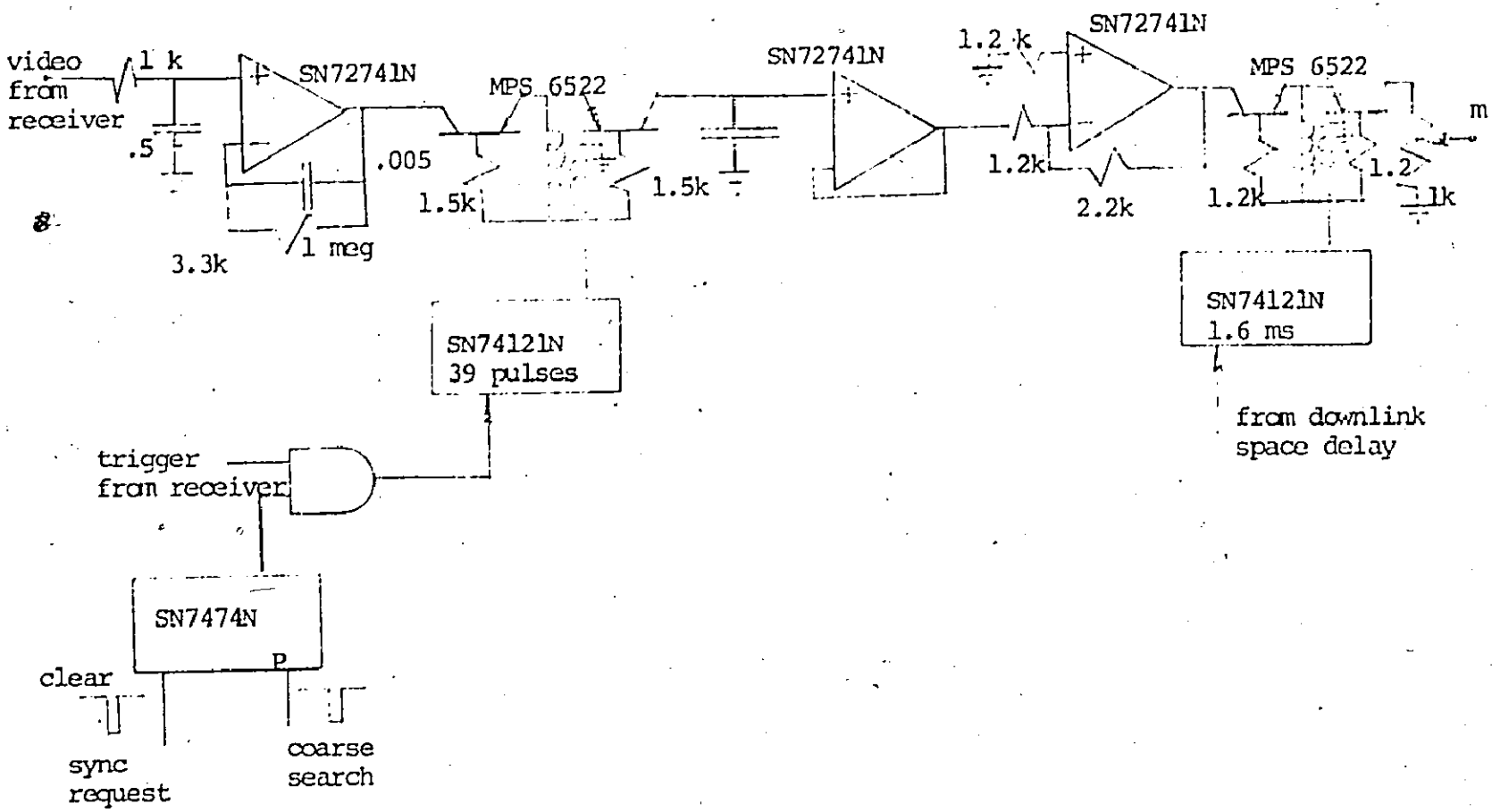

Fig. 6-30 Circuit for the fine search and tracking decoder.

in the feedback circuit producing a time constant of 5 ms. Hence, the voltage at the output of the integrator is the sum of L sync window modulated PSK sync bursts, as shown in Fig. 6-31, with L being arbitrarily chosen at 39 pulses.

To simulate the downlink space delay, this integrated voltage is switched through a bipolar transistor switch to a capacitor which feeds a high input impedance operational amplifier. When the train of sync bursts has been received by the receiver, an output pulse is sent to the downlink video space delay. After a duration of approximately 140 ms, the downlink video space delay triggers a mono of duration T_G = 1.6 ms which gates the stored error voltage through a summer to the control terminal of the VCO. This gate is called the timing adjustment gate. The other input to the summer is provided by the tracking network described in Section 6.2.12.

The value of m can thus be controlled by simply adjusting the level of the signal fed to the VCO using a potentiometer. Further trains of sync bursts can now be transmitted with the system remaining in the fine search mode until the integrated error voltage has been reduced to a small value determined by uplink and downlink noise and satellite motion. After this has been achieved, the tracking mode, described next, is employed to eliminate errors caused by constant velocity satellite motion. This timing error can be observed at the control terminal of the VCO in the form of an error voltage and compared to the actual timing error of the sync bursts relative to the sync window. In Fig. 6-32, three possible values of integrated error voltage are shown and compared to the sync window modulated sync burst.

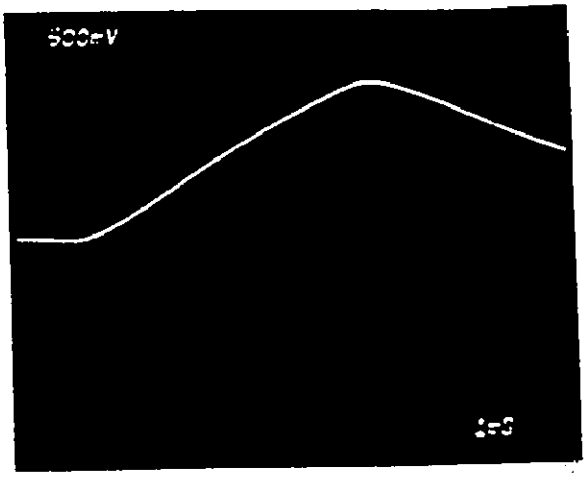

(A)

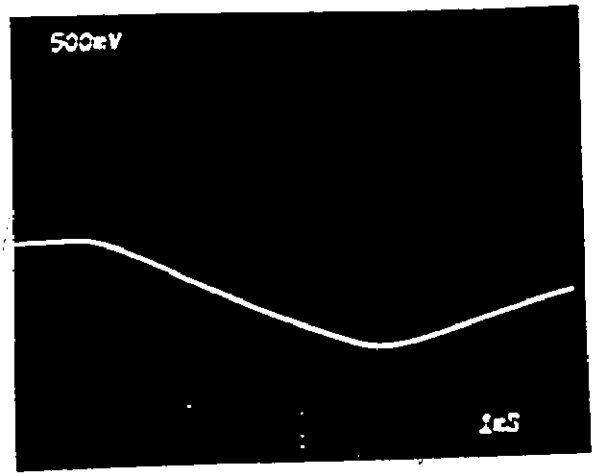

(B)

Fig. 6-31 Integration of 39 video sync burst pulses. (A) Positive timing error, (B) negative timing error.

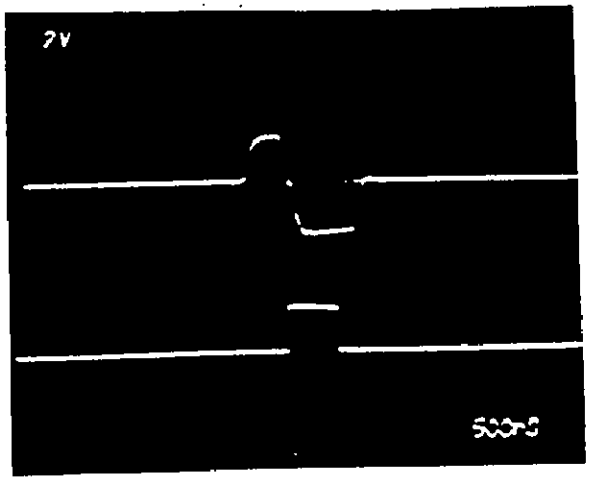

(A)

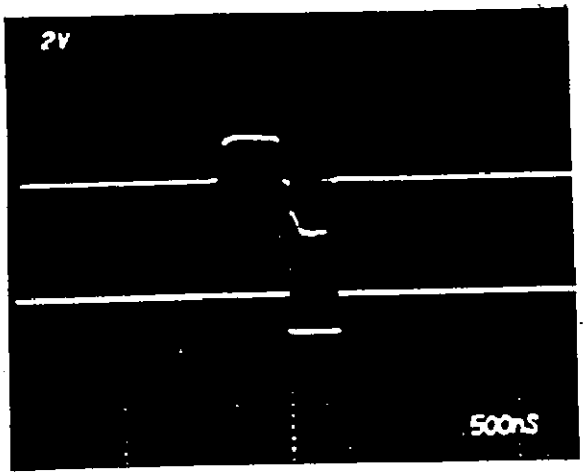

(B)

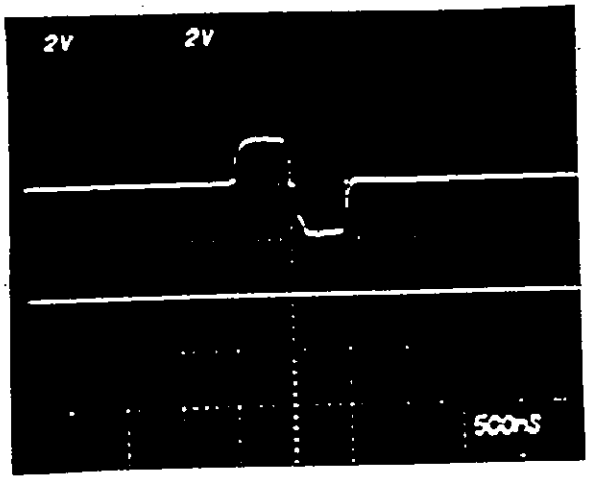

(C)

Fig. 6-32 Error voltage pulse at the control terminal of the VCO. (A) Positive timing error, (B) negative timing error, (C) zero timing error.

6.2.12 Tracking Mode Network

The tracking mode network, shown in Fig. 6-33, can be manually switched into the system once the fine search mode is complete. The error voltage pulses at the timing adjustment gate output are integrated and applied through the summer to the control terminal of the VCO producing a small dc offset. Thus, the VCO does not return to its center frequency after the timing error voltage has been applied. This change of frequency causes the frame pulses to have a slightly different spacing than for the fine search mode which compensates for the apparent change in the duration of sync windows caused by satellite motion. Finally, the value of β is controlled simply by adjusting the output level from the integrator using a potentiometer.

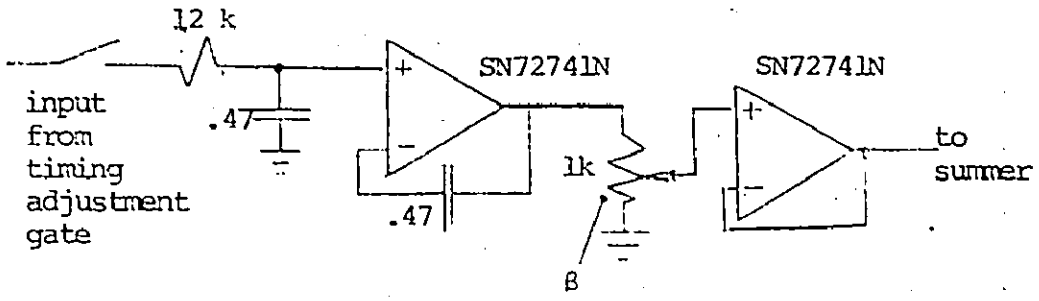

Fig. 6-33 Circuit for the tracking network.

CHAPTER 7

Experimental Results

In this chapter, the signal waveforms for the three different modes of synchronization are experimentally determined. Two types of experiment have been performed. The first type includes high repetition rate measurements where the encoder for either coarse search signals or fine search signals is repeatedly triggered with the 50 pulse per second (pps) source described in Section 6.2.2 and the uplink and downlink video delays are omitted. The second type of experiment includes the video delays in the normal mode of operation where the coarse search is initiated by activating the sync request circuit and the loop automatically achieves fine search synchronization. The tracking mode is then manually switched into operation.

7.1 COARSE SEARCH SYNCHRONIZATION

7.1.1 High Repetition Rate Signals

Using the 50 pps source to trigger the coarse search encoder, the PSK multi-frame search signal is generated and fed to the satellite model where the signal is modulated by the sync window as shown in Fig. 7-1. The output signal is fed to the coarse search decoder where the value of T_S is estimated. The output of the decoder is shown in Fig. 7-2. The upper trace shows the train of sync windows and the lower trace is the output from the 8-bit comparator. As the information is fed to the input of the 8-bit shift register, the output of the

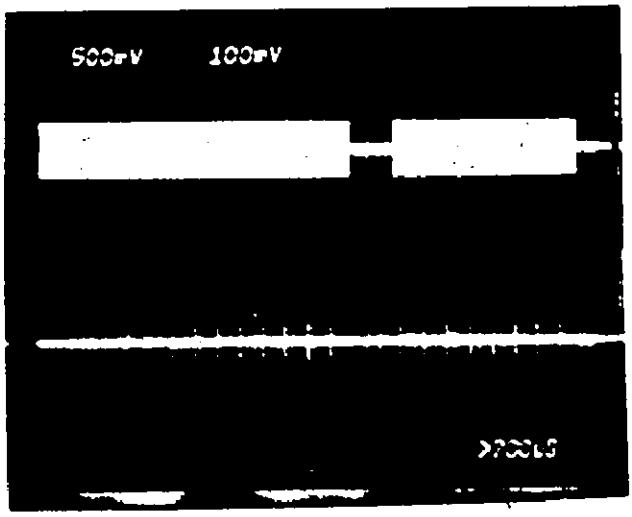

Fig. 7-1 Upper trace: PSK multi-frame coded search signal. Lower trace: Sync window modulated coded search signal.

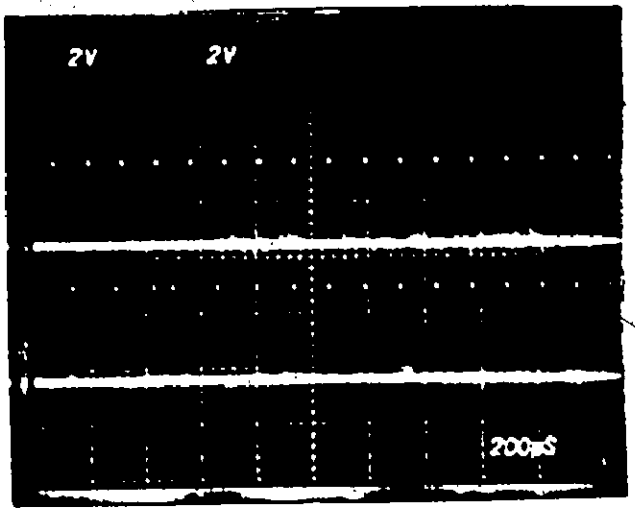

Fig. 7-2 Upper trace: Sync window train. Lower trace: Output pulses from the comparator of the coded search signal decoder. After the seventh sync window, the output pulses occur at the same time as the sync window.

comparator changes until all the pulses of the PSK multi-frame coded search signal have been received. Thence, the output pulses should appear at the same time as the sync window pulses. The exposures were taken over a duration of approximately 1 s which corresponds to 50 decoded pulses. Fig. 7-3 shows two different photographs illustrating the predicted position of the sync window. These were selected at random for two different values of T_S; however, similar results were observed for all values of T_S. Clearly, the predicted position is within $\pm\frac{1}{2}(T_P + T_W)$ of the center of the sync window, which is a necessary requirement for capture using PSK or FSK sync bursts, assuming $T_W = 1$ μs and $T_P > 1$ μs.

7.1.2 Normal Operation

The normal operation of the coarse search mode was tested by activating the sync request circuit and observing whether, on the basis of the measurement of T_S, PSK sync bursts passed through the sync window, thus achieving synchronization. The experiment was performed with no satellite motion but with different values of T_S, so that no two measurements were taken with the same relative timing between the sync unit time base and the sync window.

It was found that in 50 attempts, synchronization was achieved in 46 cases. No noise was introduced and the value of T_P was arbitrarily set at 2 μs. Assuming this result, the probability of failing to achieve synchronization with r repeated transmissions of the PSK multi-frame coded search signal is $(0.08)^r$ which is about 5.1×10^{-4} for $r = 3$.

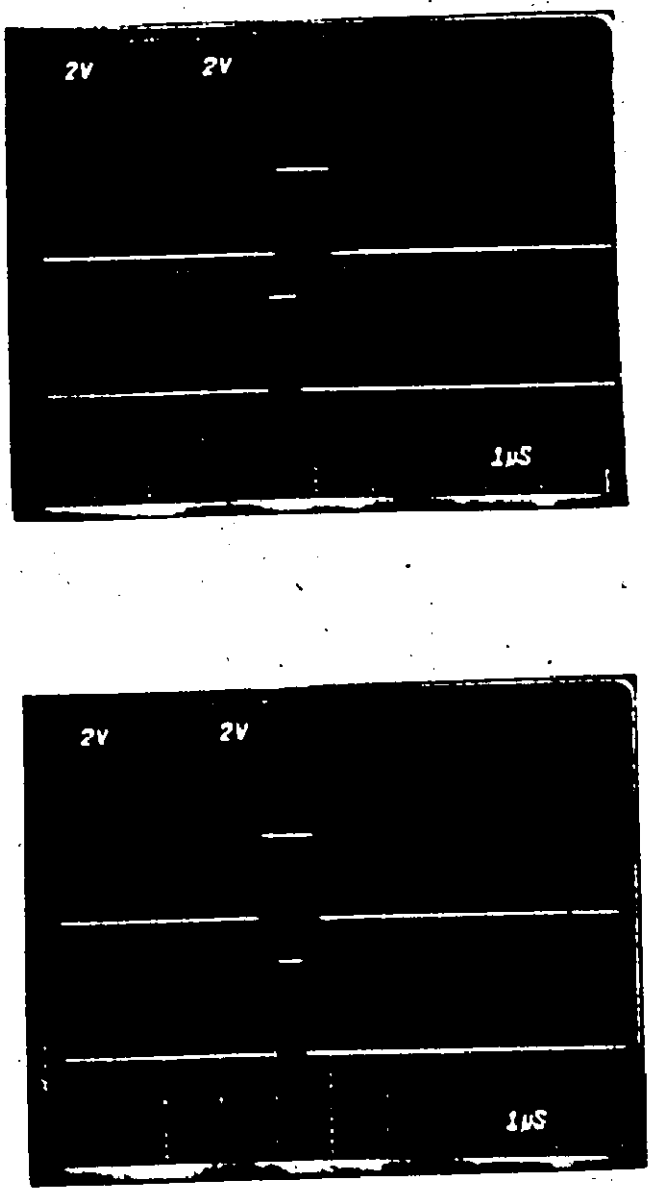

Fig. 7-3 Upper traces: Sync window position. Lower traces: Predicted position of the sync window.

7.2 FINE SEARCH SYNCHRONIZATION

7.2.1 Error Detection Characteristics

The error detection characteristics can be obtained experimentally by slowly scanning through the satellite sync window using the PSK sync burst signal triggered by the 50 pps source. The connecting link from the timing adjustment gate to the control terminal of the VCO is open circuited to prevent timing adjustments from being performed by the time base circuits. The output voltage from the integrator yields the value of v_S, as illustrated in Fig. 4-8, and the three error detection characteristics can be compared with those obtained by experiment.

Figures 7-4 through 7-7 show the error detection characteristics for several different values of T_P with T_W held fixed at 1 μs. The photographs in Fig. 7-4 illustrate Error Detection Characteristic I for the value of T_P = 1.25 μs. Figure 7-5 shows the curve at the upper bound where T_P = 2 μs. The photographs in Fig. 7-6 illustrate Error Detection Characteristic II for T_P = 2.25 μs. Error Detection Characteristic III is shown in Fig. 7-7 for T_P = 0.75 μs. The curves obtained by experiment appear to show excellent agreement with the predictions. In particular, the relationships between the slopes of the segments for each curve are very close to the theoretical values obtained from equations (4-22), (4-23) and (4-24). As well, the center segments of Error Detection Characteristics I and II are smooth and continuous at the mid-point indicating that an accurate measure of the timing error is possible.

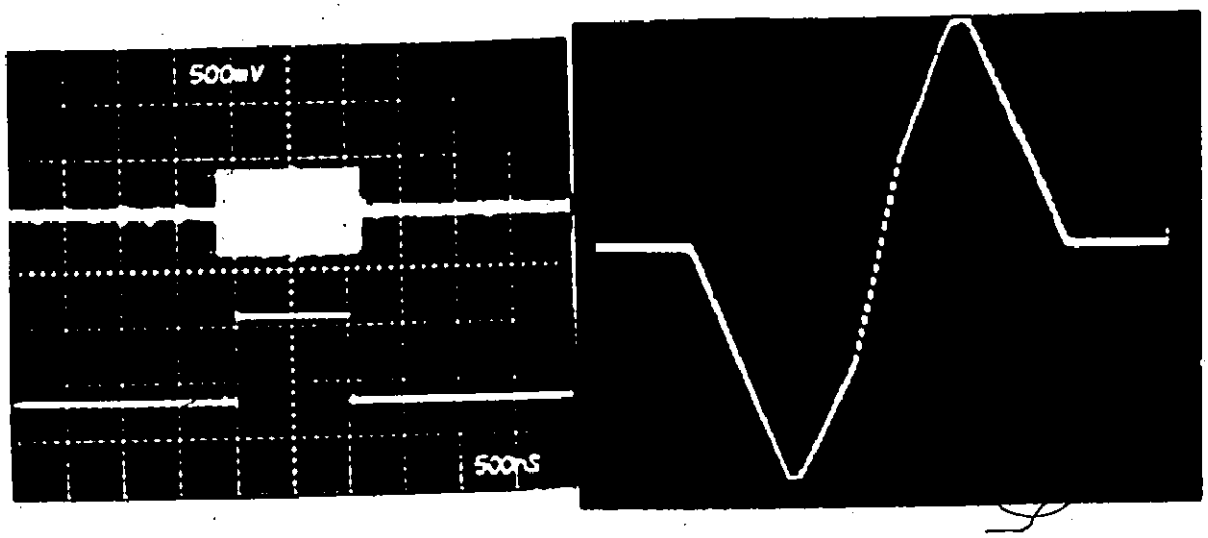

Fig. 7-4 Left: PSK sync burst-upper trace, sync window-lower trace. Right: Error Detection Characteristic I for T_p = 1.25 μs.

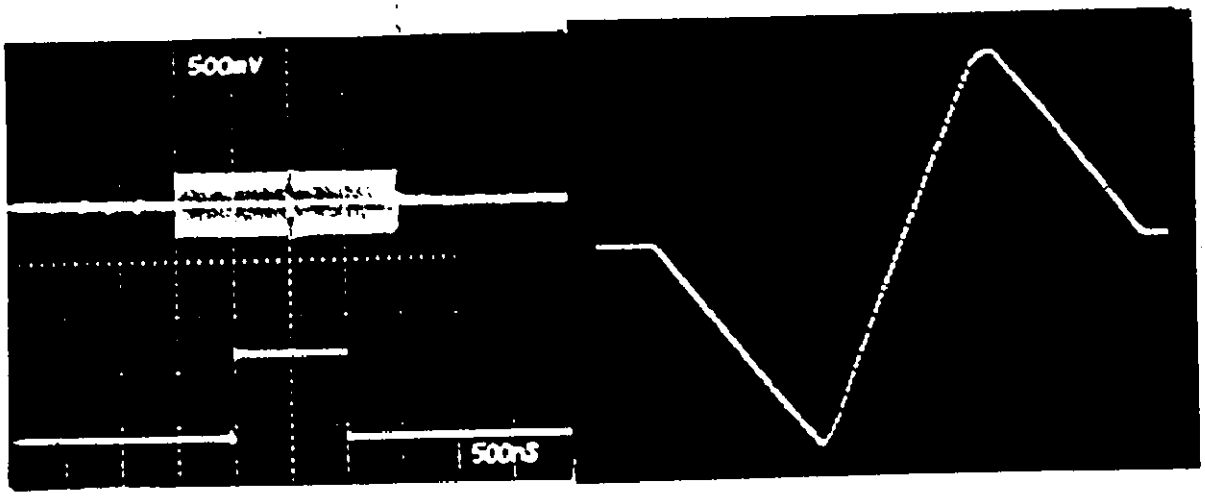

Fig. 7-5 Left: PSK sync burst-upper trace, sync window-lower trace. Right: Error Detection Characteristic I for T_p = 2 μs.

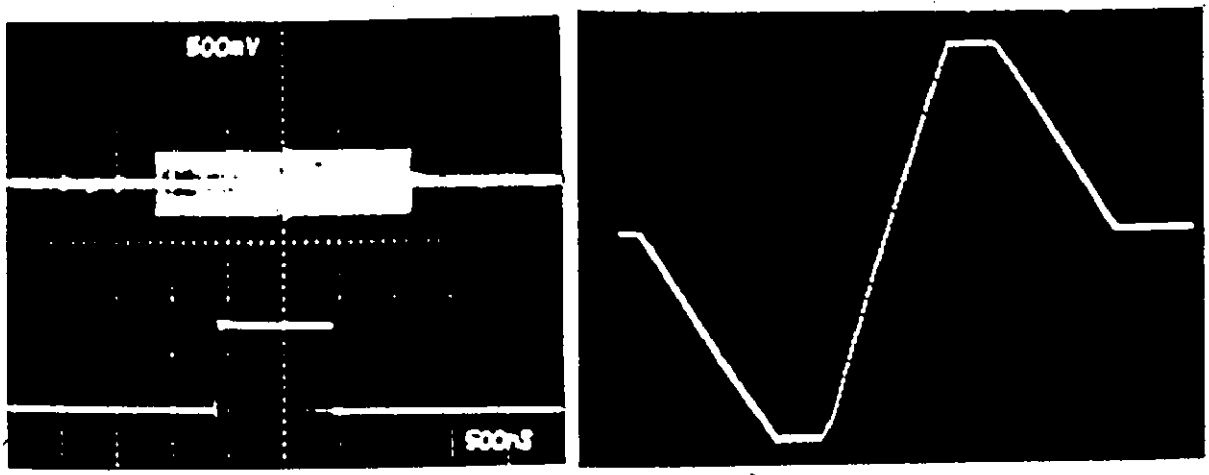

Fig. 7-6 Left: PSK sync burst-upper trace, sync window-lower trace. Right: Error Detection Characteristic II for T_p = 2.25 μs.

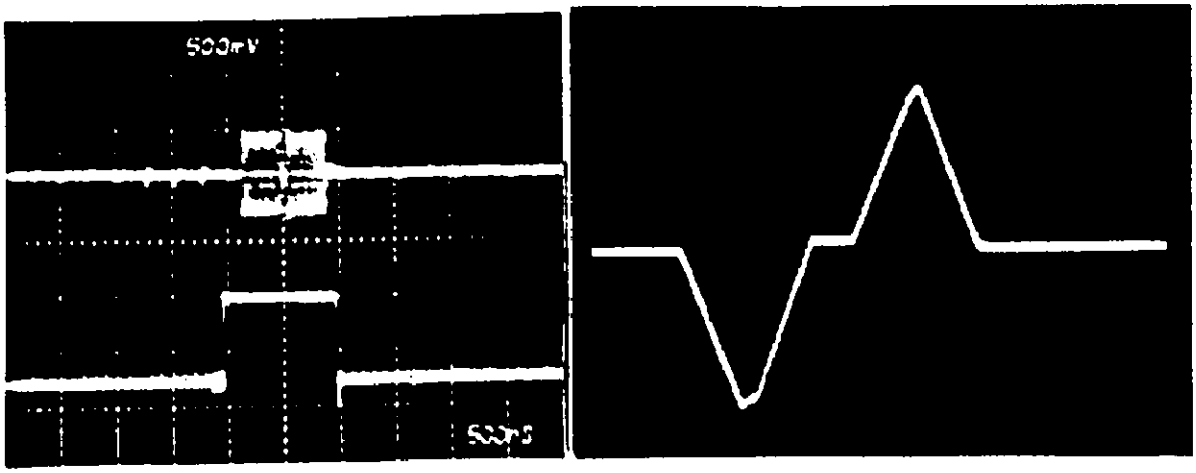

Fig. 7-7 Left: PSK sync burst-upper trace, sync window lower trace. Right: Error Detection Characteristic III for T_p = 0.75 μs.

If the 0 degree phase portion of the PSK sync burst is not equal in duration to the 180 degree portion, the error detection characteristics are altered as shown in Fig. 7-8 and 7-9. Although the odd symmetry of the curves in Fig. 7-4 through 7-7 no longer exists, the curves still exhibit the property that zero integrated error voltage occurs whenever zero timing error is achieved. Clearly, the conditions portrayed by Figs. 7-8 and 7-9 should be avoided in practice.

7.2.2 Behaviour of the Timing Error

The first requirement prior to performing closed loop experiments in the fine search mode is to estimate the value of the dimensionless loop constant m. This value can be determined experimentally once the error detection characteristics are obtained by comparing the measured slope of the center segment of Error Detection Characteristic I or II with the calculated value.

First, it is noted by definition from (4-28) that

$$m = \frac{2L\,A\,c_1}{T_I}\,\frac{S\,T_G}{f_0} \tag{7-1}$$

From the first of either of equations (4-22) or (4-23), it is noted that the slope of the center segment is

$$\frac{v_S}{t_E} = \frac{2L\,A\,c_1}{T_I} \tag{7-2}$$

For the error detection characteristic of Fig. 7-6, the peak-to-peak voltage of the center segment was found to be approximately 4 V and the width of this segment is known from theory to be $T_W = 1\ \mu s$ yielding a slope of 4 V/μs. The value of T_G is 1.6 ms and the ratio of S/f_0 for

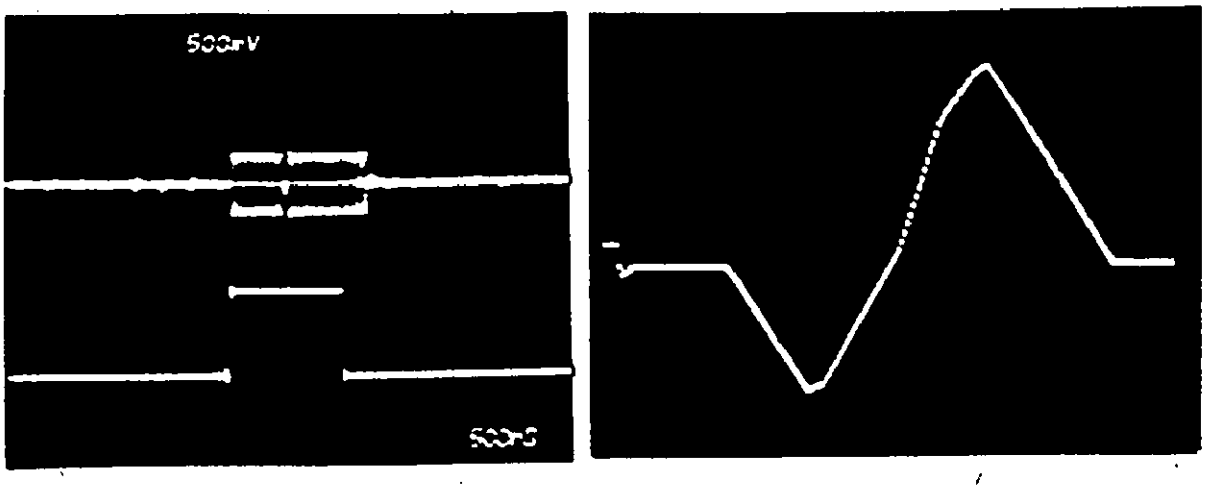

Fig. 7-8 Left: PSK sync burst-upper trace, sync window-lower trace. Right: Error detection characteristic for unequal durations of 0° phase and 180° phase. T_p = 1.25 μs.

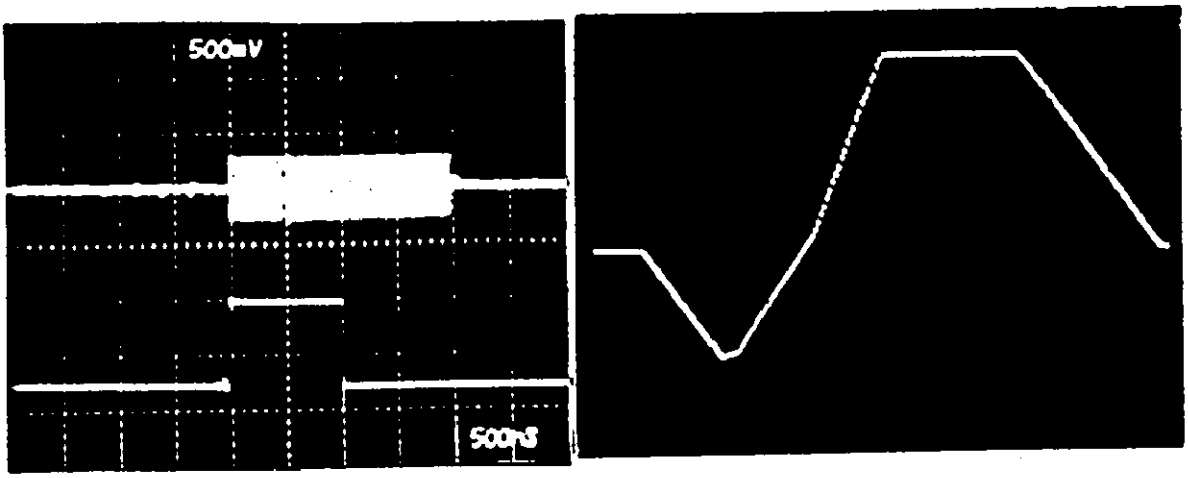

Fig. 7-9 Left: PSK sync burst-upper trace, sync window-lower trace. Right: Error detection characteristic for unequal durations of 0° phase and 180° phase. T_p = 2 μs.

the VCO employed is 10^{-4} per volt. Hence, the open loop value of m is approximately 0.64.

From the theory developed in Chapter 4, the range of m which is of interest, is given by (4-62) as $0 < m < 2$. Thus, a buffer amplifier providing a gain of approximately 2 was incorporated as shown in Fig. 6-31. Using a potentiometer at the output of the buffer amplifier, it is possible to adjust the value of m over the required range.

The behaviour of the synchronization loop was investigated using the 50 pps source to trigger the fine search and tracking encoder. The main reasons for choosing the high repetition rate were that controlled experiments could easily be performed and that each result could be verified by repetition.

Initially, the value of m was experimentally evaluated by closing the loop using a toggle switch. By observing the signal at the satellite sync window, it was possible to adjust the timing relationship between the sync window and the sync burst to any prescribed value of timing error. With this known initial value, the toggle switch was closed and the integrated error voltage in the fine search and tracking decoder was displayed on a storage oscilloscope. From equations (4-22) and (4-23), it is seen that theoretically, the timing error is linearly related to the integrated error voltage for all regions of the Error Detection Characteristic I and Regions A, C and E for Error Detection Characteristic II. Since the experimentally measured curves also exhibit this linear relationship, values for the timing error are obtained by measuring the integrated error voltage. Thus, curves showing the reduction in the timing error for the different regions of the error detection characteristics with various values of m were obtained.

For the center segment of Error Detection Characteristics I and II, convergence to zero average timing error should be obtained in one iteration for m = 1. Indeed, when the potentiometer was adjusted for unity net gain from the buffer amplifier input to the VCO control terminal, convergence was obtained as shown in Fig. 7-10. It appears that the experimental value obtained is approximately 0.9 which is reasonably close to the open loop value of 0.64.

Following the theory developed in Chapter 4, the experimental results are presented for Region A, B and C. In every case, the results were found to be repeatable.

(a) Region A, Error Detection Characteristic I

The timing error was adjusted until the edge of the sync burst signal overlapped one edge of the sync window which corresponds to a timing error of almost $\frac{1}{2}(T_p + T_w)$. Then, the toggle switch was closed and the resulting integrated error voltage for Region A was recorded. Three values of m were selected, namely 0.25, 1.0 and 1.75 and these were determined on the basis of the results obtained in Region C described below.

The resulting photographs, shown in Fig. 7-11, can be compared to Fig. 4-9. It is seen that the measured curves are in agreement with those predicted by theory.

(b) Region B, Error Detection Characteristic I

With the value of m set to 0.25 (as obtained in Region C), the timing error was adjusted to $\frac{1}{2} T_w = 0.5$ μs which is the edge of Region B. Then, the toggle switch was closed and the waveform shown in Fig. 7-12 was recorded. The transition to Region C can clearly be seen by the increase in the step size to the left of center as the timing error is

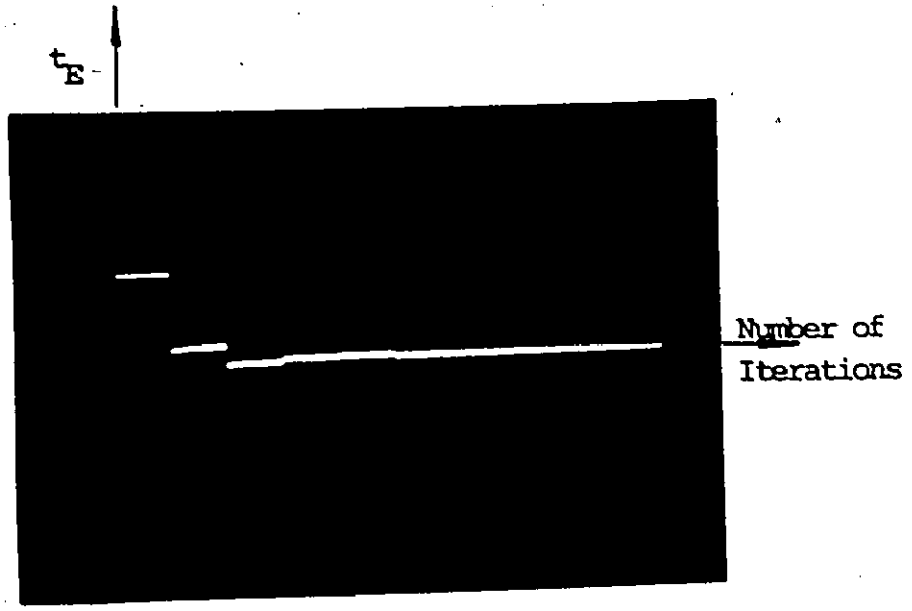

Fig. 7-10 Experimentally determined value of m = 0.9 as compared to theoretical value of 0.64.

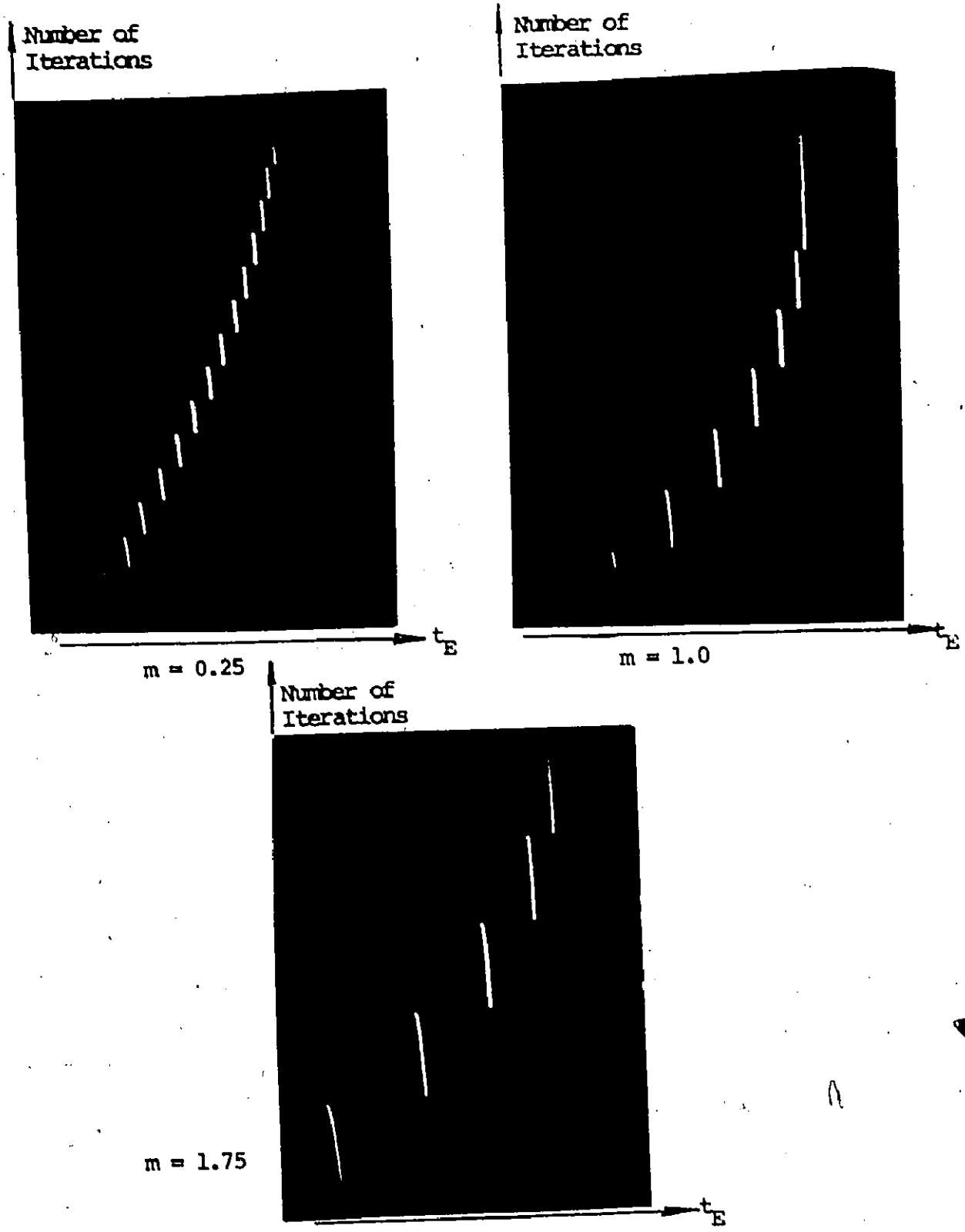

Fig. 7-11 Reduction of the timing error in Region A for $T_p = 1.25\ \mu s$ and several values of m.

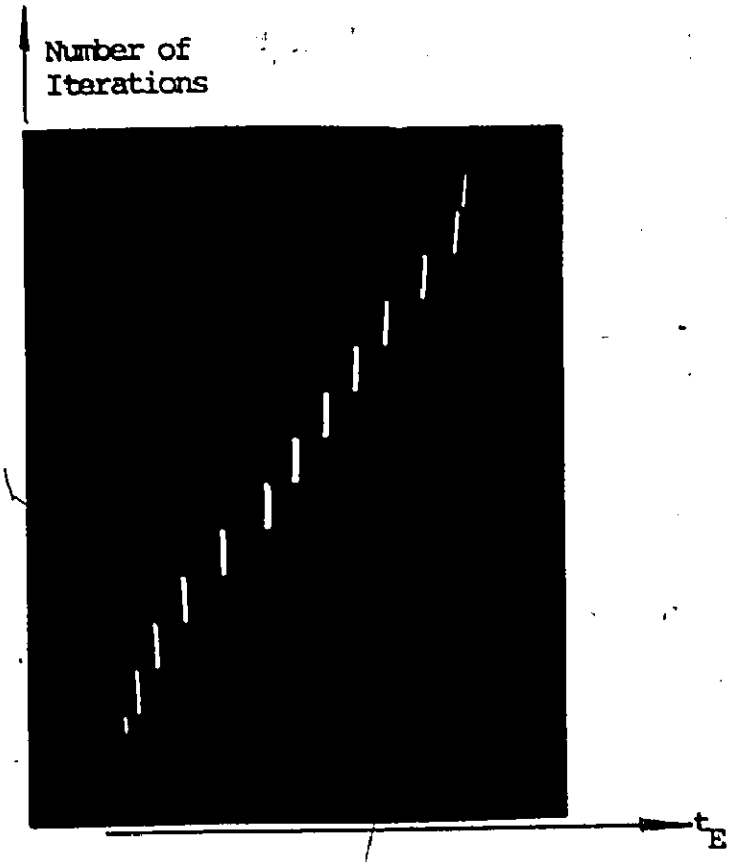

Fig. 7-12 Reduction of the timing error in Region B for $T_p = 1.25$ μs and $m = 0.25$.

reduced. Except for the first shift at the top, the curve agrees with the prediction of Fig. 4-13.

(c) Region C, Error Detection Characteristic I

(i) Convergence to Zero Timing Error

In Region C, the timing error adjustment is not critical prior to closure of the toggle switch since only the initial value of the integrated error voltage is affected. The value of m can easily be measured in this region by noting that the amplitude of each step should theoretically be $|1 - m|$ times the amplitude of the previous step. Hence, calibration to any value of m can easily be achieved by adjusting the potentiometer and observing the resulting waveform. The average timing error was measured for four values of m.

Comparing the photographs in Fig. 7-13 with the theoretical curves of Fig. 4-15, we see that the experimental behaviour is almost identical with the theoretical predictions. The value of m in each case was obtained by adjusting the potentiometer to obtain the correct amplitude relationship between the first two steps. The remaining steps appear to occur in the predicted positions

(ii) Effects of Satellite Motion

The effects of satellite motion on the average timing error were measured by employing the satellite motion feature of the satellite unit. With the time base circuits locked to the sync window, a toggle switch was used to switch from zero satellite motion to a timing variation of one 2.4 ns step every 2 ms. For the time duration of 20 ms, which is the interval between iterations provided by the 50 pps trigger,

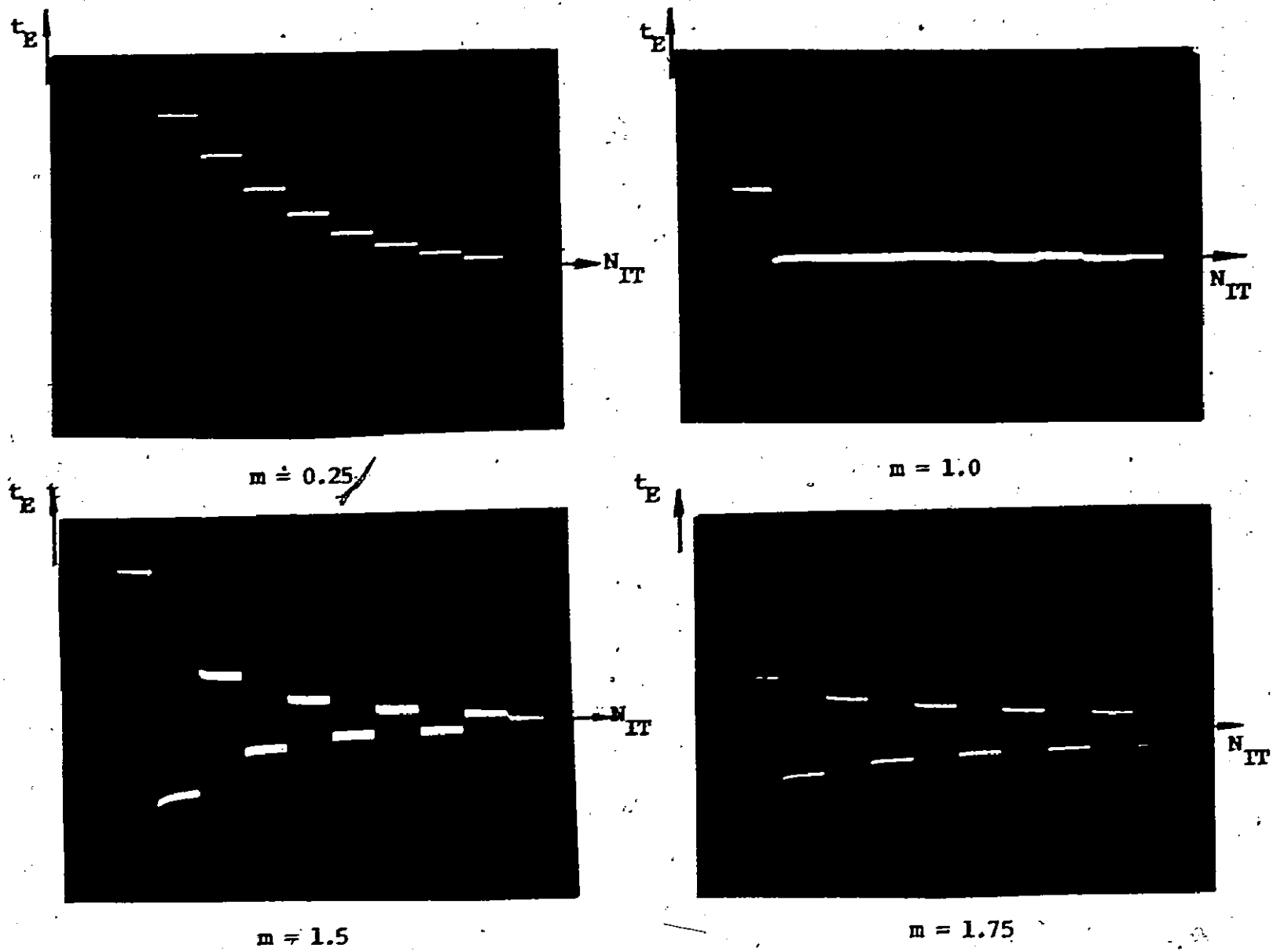

Fig. 7-13 Convergence to zero timing error in Region C for T_p = 1.25 μs. N_{IT} equals the number of iterations.

the satellite motion is thus 25 ns. This variation is comparable with the 18 ns value per round trip time which is the assumed maximum for an actual system [15].

Photographs for three different values of m obtained by experiment are shown in Fig. 7-14 and these can be compared with the theoretical curves illustrated in Fig. 4-16. Essentially, the two sets of curves agree within experimental error.

(iii) Effects of Noise

The timing error due to noise was estimated by injecting noise into the base of a transistor amplifier in the output circuitry of the coherent receiver, as shown in Fig. 6-23. The noise was provided by a 5 MHz wide video noise source generator which was gated once per frame simultaneously with the reception of a sync burst for the duration of the sync window. This is equivalent to an infinite uplink signal-to-noise ratio and the maximum downlink signal-to-noise ratio which would be obtained for an input gate duration T_Q equal to the sync window duration T_W. Thus, the results presented here are a measure of the minimum timing error due to noise.

From equation (4-66), it is seen that the timing error due to noise, t_N, is equal to the rms timing error for zero satellite motion and $m = 1$.

The noise voltage was increased until the waveform shown in Fig. 7-15 was obtained. The spread in the waveform was assumed to represent a signal-to-noise ratio of approximately 3 dB and the timing error due to noise was estimated to be approximately 70 ns by observing

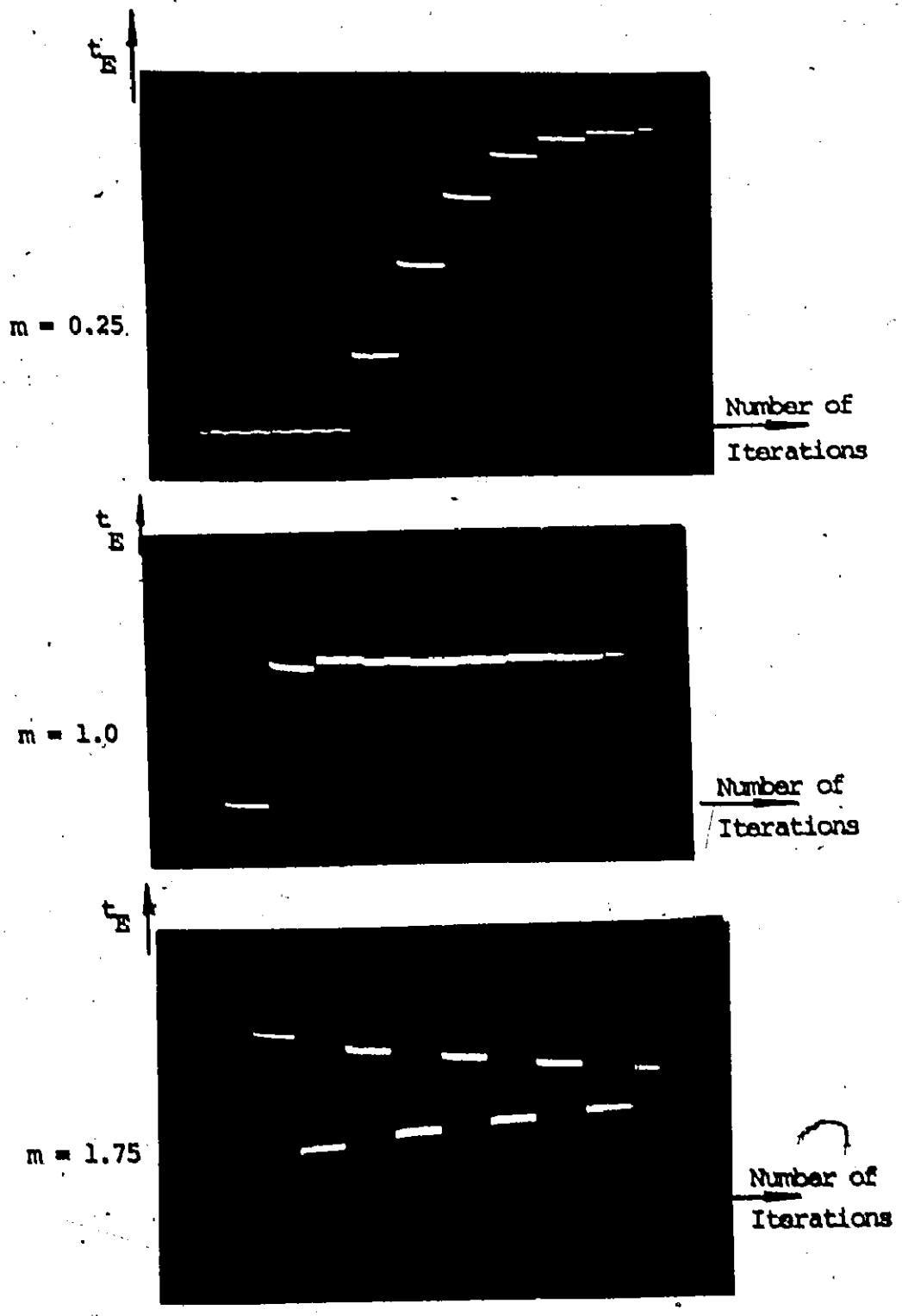

Fig. 7-14 Average timing error with satellite motion.

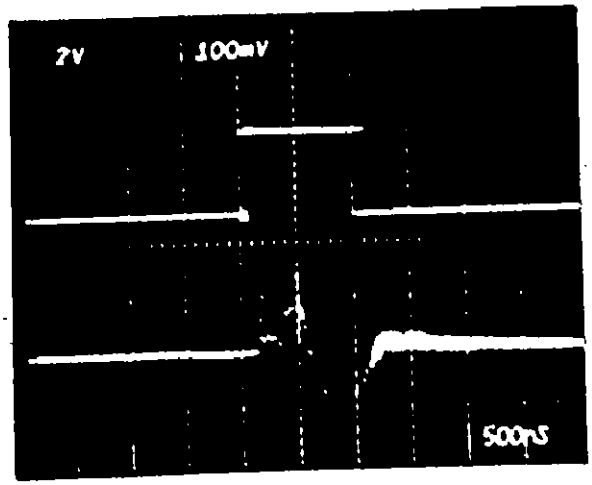

Fig. 7-15 Upper trace: Sync window, lower trace: PSK sync burst with noise added to produce a signal-to-noise ratio of approximately 3 dB.

the variation in timing of the reference transition in the sync burst. Next, using a 10 dB resistive divider to reduce the noise, the waveforms shown in Fig. 7-16 were obtained.

Finally, the resistive divider was adjusted for 20 dB attenuation and the measurements repeated. Results of the three measurements are shown in Fig. 7-17 and compared with the theoretical curve provided by equation (4-44).

The graph of Fig. 4-17 shows that the timing error due to noise is affected by the selection of m. In the steady state case, the timing error was found to increase from approximately 15 ns to 70 ns as m was increased from 0.25 to 1. The ratio of these two values of timing error is 4.6 as compared to a theoretical ratio of 7.

(d) Region A, Error Detection Characteristic II

Essentially the same experiment as described in (a) was repeated but the value of T_p was adjusted to 2.25 μs. The three photographs for different values of m are shown in Fig. 7-18. It is observed that as m increases, the step sizes also increase as shown by the theoretical curves in Fig. 4-18. Again, the measurements are in good agreement with the predictions.

7.3 TRACKING SYNCHRONIZATION

After the fine search mode is complete, the tracking network is manually switched into operation. Errors due to satellite motion are reduced by using the integrator shown in Fig. 6-34.

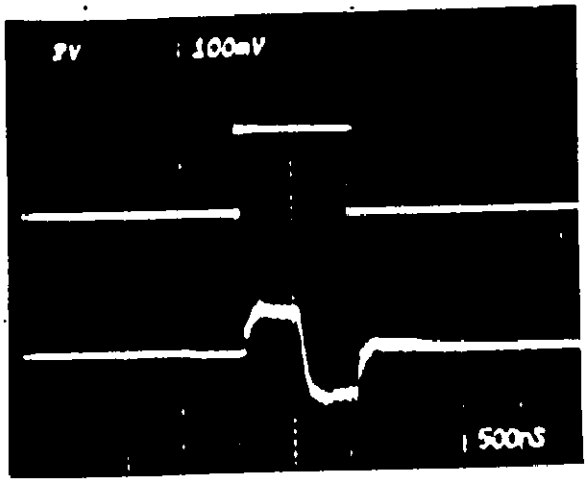

(A)

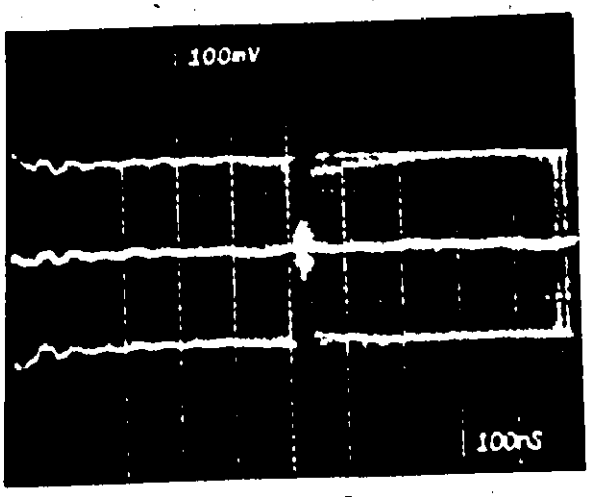

(B)

Fig. 7-16 (A) Upper trace: Sync window, lower trace: PSK sync burst with 13 dB signal-to-noise ratio.
(B) Variation in the timing of the reference transition in the sync burst with 13 dB SNR.

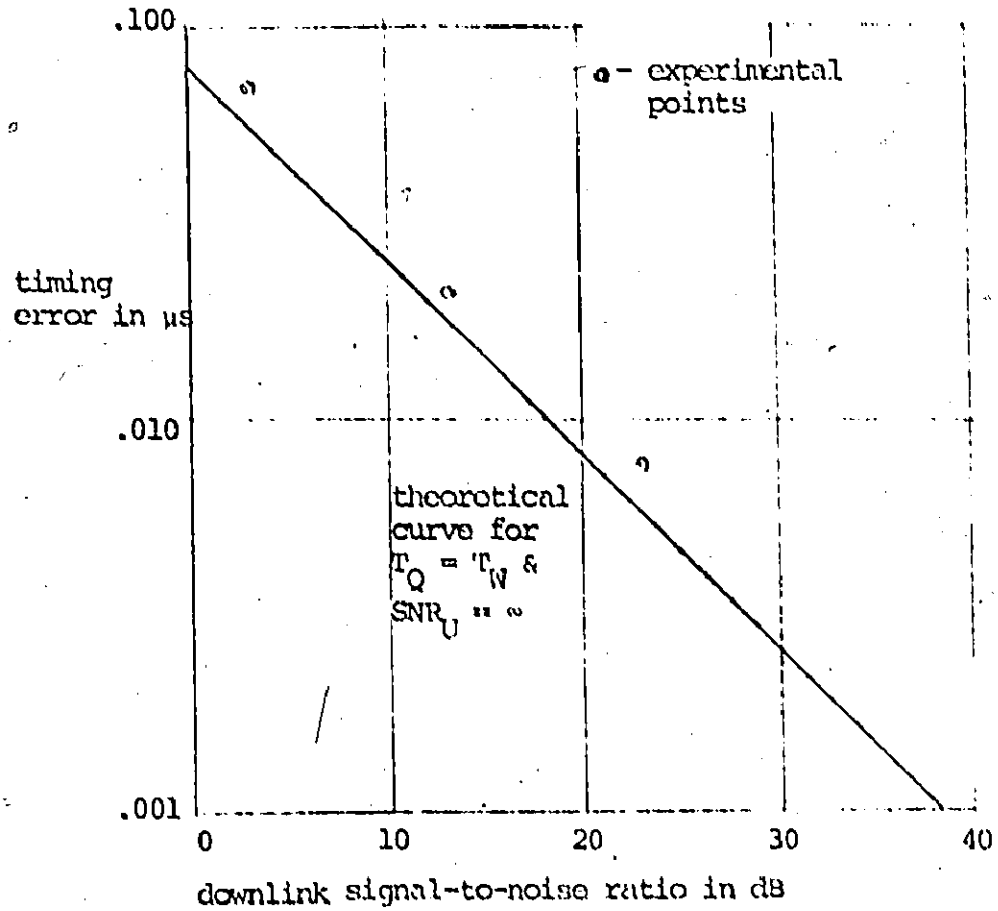

Fig. 7-17 Effects of noise on the timing error.

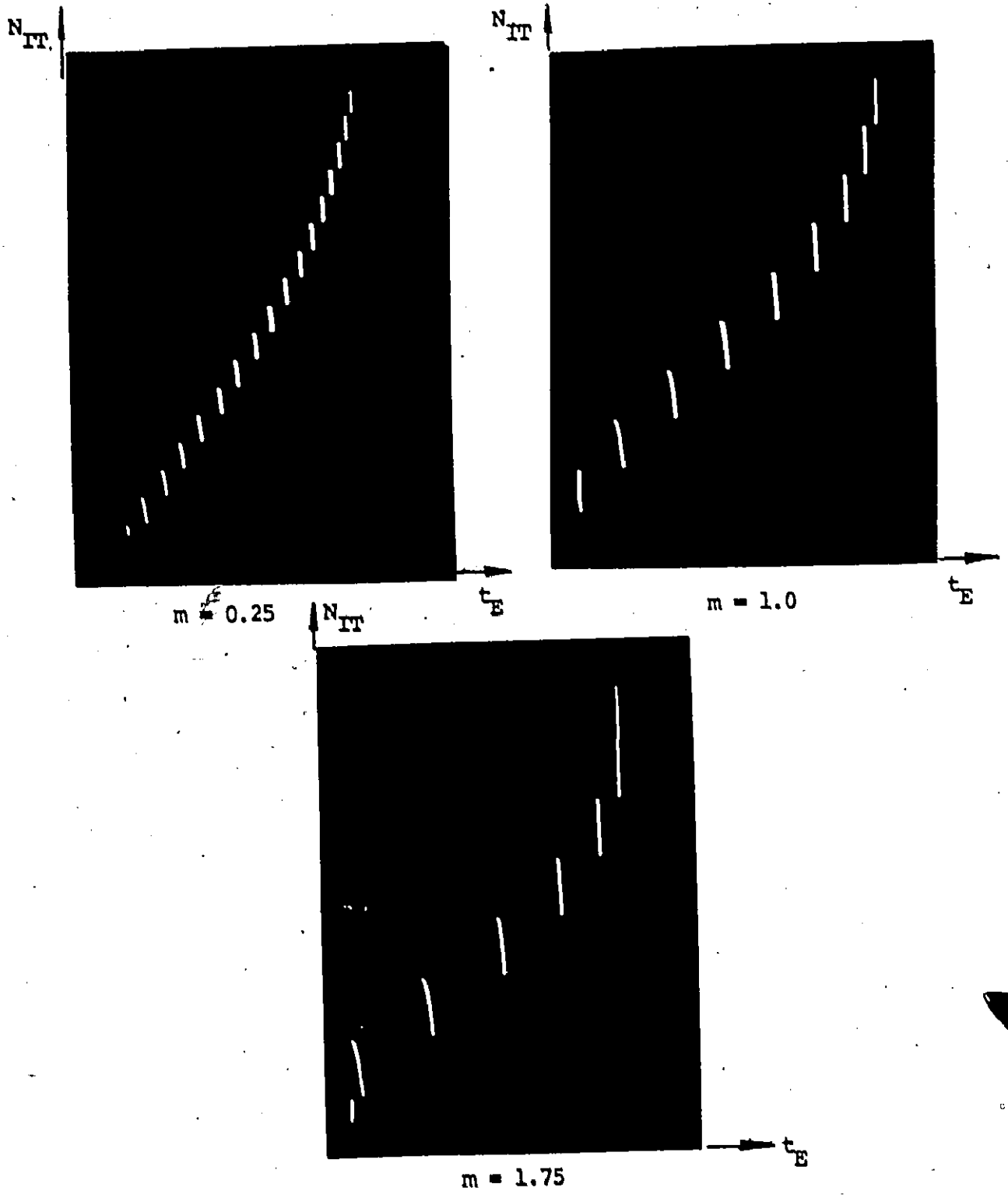

Fig. 7-18 Reduction of the timing error in Region A for $T_p = 2.25$ and several values of m. N_{IT} equals the number of iterations.

Experimentally, the loop behaviour was evaluated by first obtaining lock in Region C with T_p approximately equal to twice the sync window duration. This ensured the linear relationship of the center segment which is assumed in the theory of Chapter 5. Next, satellite motion of approximately 70 ns per round trip time was introduced using the adjustment provided by the satellite model and the integrated error voltage was observed. Finally, a toggle switch was closed to activate the tracking network and the resulting timing error was recorded using a storage oscilloscope.

The value of β was adjusted by using a potentiometer and measurements for several different values of m (adjusted experimentally using the technique described for Region C) were recorded. Fig. 7-19 illustrates the resulting waveform for $m = 0.25$ and $\beta = 1$ which is underdamped as predicted by the results of Table 5-1 since $\lambda_1 > 0$ and $\lambda_2 < 0$. The experimental result is in close agreement with the theoretical curve in Fig. 5-2. The integrated error voltage was reduced from 1.4 V to 40 mV which corresponds to a reduction in timing error by a factor of about 35.

Figures 7-20, 7-21 and 7-22 illustrate the three conditions of overdamping, critical damping and underdamping and the factors by which the timing errors were reduced are 12, 35 and 30, respectively. These curves compare favourably with those predicted by theory as illustrated in Fig. 5-4.

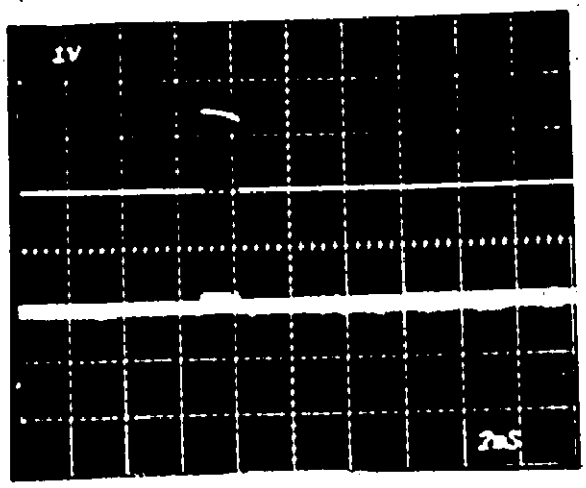

Vertical scale: 1 V/cm

Vertical scale: 200 mV/cm

(A)

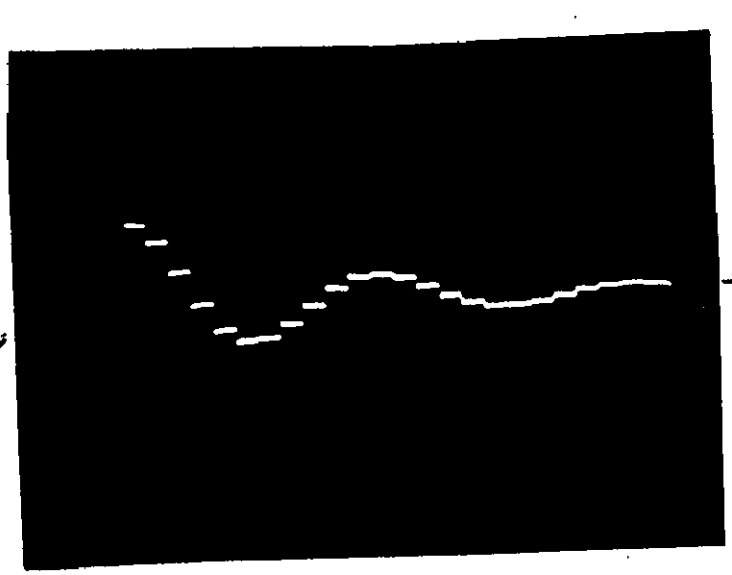

(B)

Fig. 7-19 (A) Upper trace: Error voltage prior to switching in tracking network, lower trace: Error voltage after switching in tracking network for $m = 0.25$, $\beta = 1.0$. (B) Convergence to zero timing error when satellite motion occurs

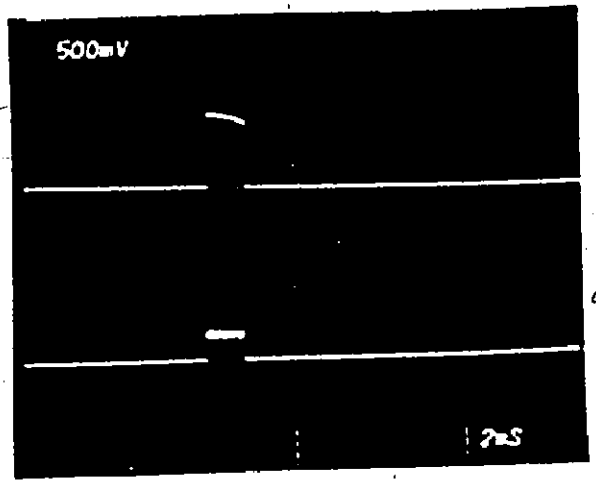

(A)

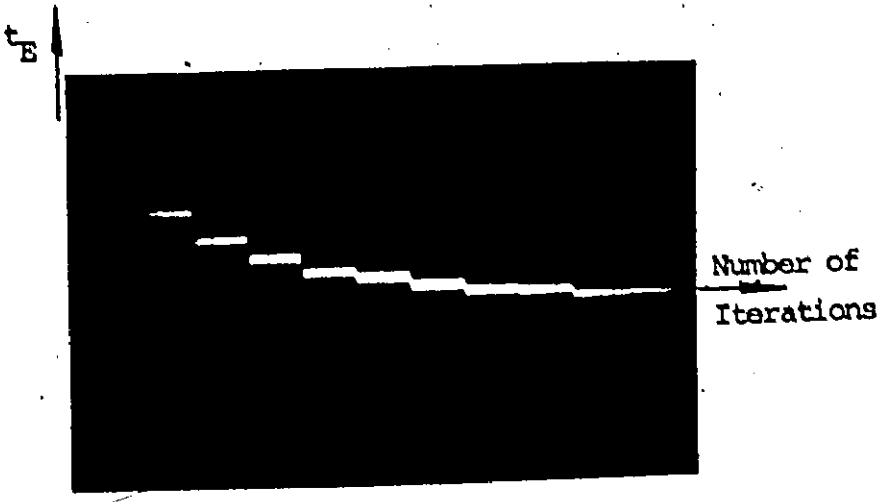

(B)

Fig. 7-20 (A) Upper trace: Error voltage prior to switching in tracking network, lower trace: Error voltage after switching tracking network for m = 1.0 and β = 0.25. (B) Convergence to zero timing error when satellite motion occurs.

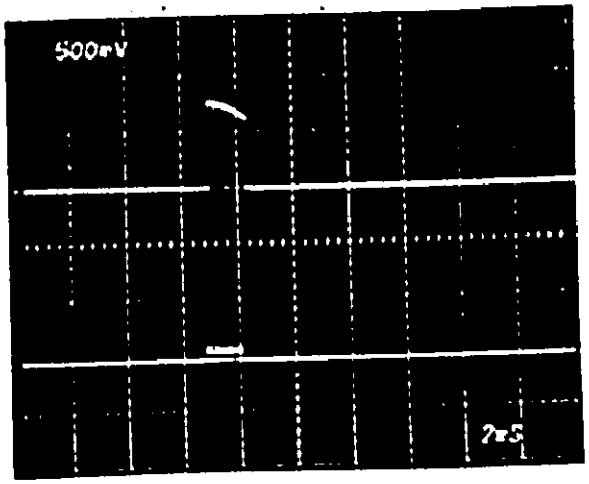

(A)

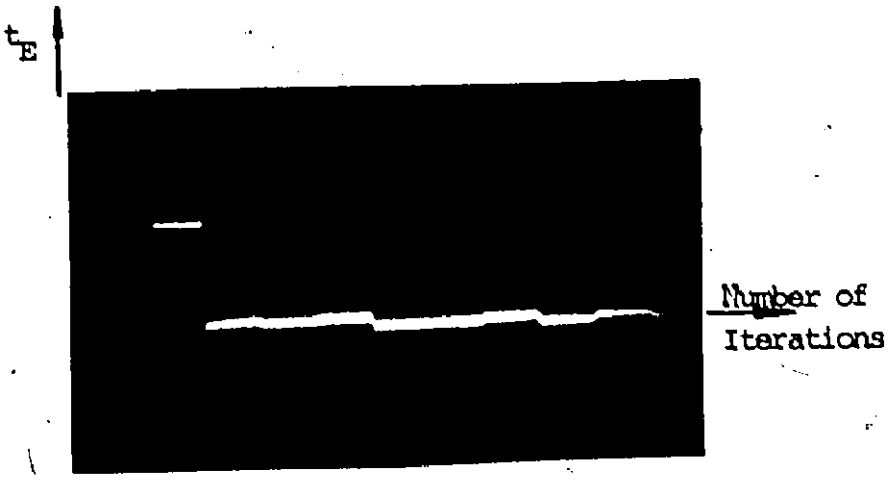

(B)

Fig. 7-21 (A) Upper trace: Error voltage prior to switching in tracking network, lower trace: Error voltage after switching in tracking network for m =1 , β =1. (B) Convergence to zero timing error when satellite motion occurs.

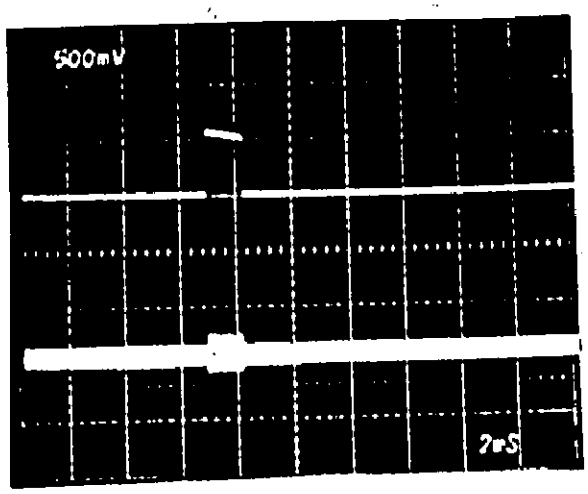

500 mV/cm

100 mV/cm

(A)

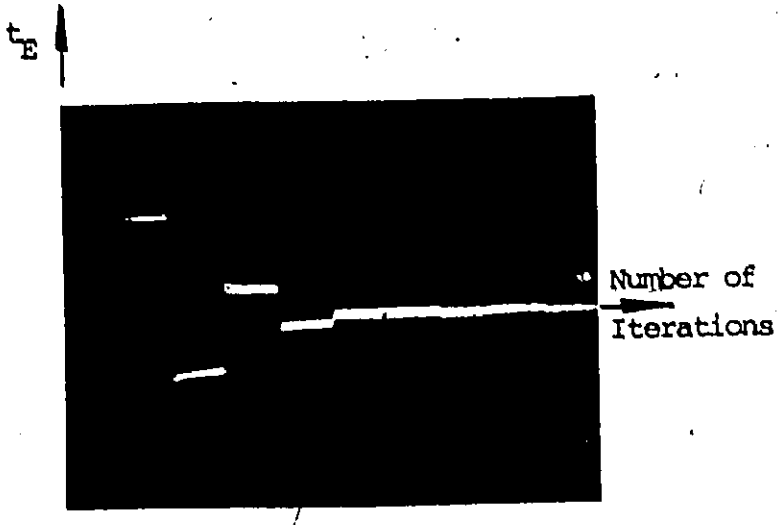

(B)

Fig. 7-22 (A) Upper trace: Error voltage prior to switching in tracking network, lower trace: Error voltage after switching in tracking network for $m = 1.0$, $\beta = 1.5$. (B) Convergence to zero timing error when satellite motion occurs.

Finally, Fig. 7-23 shows the resulting waveform when the values selected for m and β are too large. The integrated error voltage is seen to oscillate when the tracking network is switched in and the resulting waveform does not converge to zero timing error, as was shown by the curve in Fig. 5-6 for $m = 1.75$ and $\beta = \frac{2}{7}$.

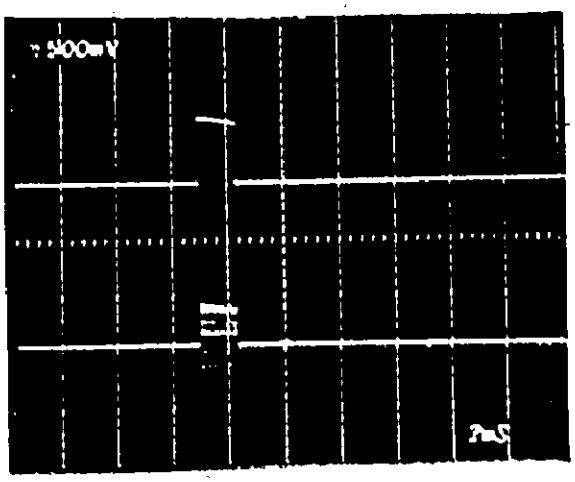

(A)

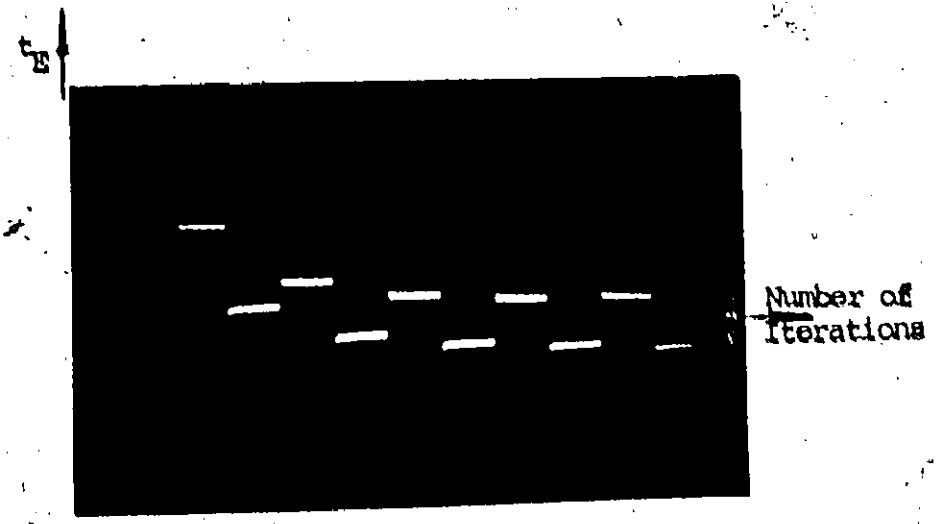

(B)

Fig. 7-23 (A) Upper trace: Error voltage prior to switching in tracking network, lower trace: Error voltage after switching in tracking network for m= 1.75, β = 2/7. Note the oscillation.

(B) Convergence to zero timing error does not occur.

CHAPTER 8

Conclusions

8.1 CONTRIBUTIONS OF THE THESIS

The major contributions of the thesis may be summarized as follows:

(1). An SDMA/SS-TDMA system is described which employs three control stations for providing synchronization for all earth stations operating in the system.

(2) To achieve synchronization in the coarse search mode of operation, a new technique has been developed using coded search signals.

(3) Three new implementations of the sync burst have been described using amplitude shift keying (ASK), phase shift keying (PSK) and frequency shift keying (coded - FSK).

(4) The behaviour of the synchronization loop during the fine search mode of operation has been analysed in detail. The analysis takes into account the uplink space delay and attenuation, uplink noise, satellite motion, downlink space delay and attenuation and downlink noise. Coherent detection from frame to frame is assumed.

(5) It is shown that by incorporating a tracking network in the form of an integrator into the loop, the timing error due to constant velocity satellite motion is eliminated.

(6) A laboratory model which closely approximates the physical model of the synchronization loop has been designed and constructed.

(7) A special coherent receiver for demodulating bursts of PSK signals has been developed using a phase adjusting network.

(8) Results of experiments using the laboratory model have been demonstrated to agree closely with theoretical predictions concerning the course search, fine search and tracking modes of operation.

8.2 SUGGESTIONS FOR FUTURE WORK

(1) As indicated earlier, the analysis of the loop operating in the fine search or tracking modes assumes coherent detection from frame to frame. It would be desirable to extend this work to include the effect of non-coherent detection.

(2) The study has assumed perfectly rectangular sync window modulation. This should be extended to include the effects of finite rise and fall times of the sync window.

(3) The performance of the loop should be examined for non-rectangular amplitude modulation of the sync bursts.

(4) The non-linear effects of the satellite output TWT amplifier on the performance of the synchronization loop should be examined.

APPENDIX A

Spectral Shapes of Sync Bursts

The spectral shape of the six different sync bursts shown in Fig. 3-2 is examined in this appendix and in particular, it is shown that amplitude modulation of PSK and FSK sync bursts can be used to modify the spectral shape of the transmitted signal.

A-1 ASK SYNC BURST

The simplest of all sync bursts is the ASK sync burst which is simply a short pulse of carrier. The spectral shape of the transmitted signal can be determined by calculating the Fourier transform of the pulsed video signal. The spectrum, which is the squared magnitude of the Fourier transform, is given by

$$S_A(f) = \frac{E\, T_p \sin^2 (\pi f T_p)}{(\pi f T_p)^2} \qquad (A\text{-}1)$$

where E = energy contained in the sync burst

T_p = sync burst duration

The spectrum is well known and the side lobes of this signal decrease quite slowly.

A-2 PSK SYNC BURST

Amplitude shaping of the PSK sync burst is possible provided that the odd symmetry of the video waveform is maintained to ensure the

reference transition in the center. This shaping can be used to control the spectrum and hence the bandwidth requirement of the transmitted signal. Table A-1 provides a comparison of several different simple video waveforms shown in Fig. A-1 which satisfy the requirements. In each case, the duration of the sync burst is assumed to be T_p and the energy contained in the sync burst is E. The sine wave modulation reduces the side lobe structure considerably compared to the square wave modulation since the level varies as $1/f^4$ for large values of fT_p.

A-3 PSK SYNC BURST

Each pulse of the PSK sync burst may be amplitude shaped provided that the even symmetry of the video waveform is maintained. Again, as with the PSK sync burst, the shaping can be used to control the bandwidth requirement of the transmitted signal. Table A-2 provides a comparison of several different simple video waveforms shown in Fig. A-3. In each case, the duration of the sync burst is assumed to be T_p and the energy contained in each portion of the sync burst is E/2. The total requirement for the PSK sync burst is two passbands each having the capacity as listed in Table A-2. The cosine wave and triangle wave provide a sizable reduction in the side lobe level as compared to the square wave due to the $1/f^4$ variation for large values of fT_p.

A-4 CODED SYNC BURSTS

The coded-ASK and the coded-PSK sync burst have essentially the same bandwidth requirement which is determined by the metric portion and the coded-FSK sync burst has about twice their bandwidth requirement.

TABLE A-1

Spectral Shapes of Simple PSK Sync Bursts

Type	Time Function	Spectrum
Square wave	$\sqrt{\frac{E}{T_p}}$; $0 \le t \le \frac{T_p}{2}$ $-\sqrt{\frac{E}{T_p}}$; $-\frac{T_p}{2} \le t \le 0$	$\frac{ET_p \sin^4(\frac{1}{2}\pi f T_p)}{(\frac{1}{2}\pi f T_p)^2}$
Sine wave	$-\sqrt{\frac{2E}{T_p}} \sin\frac{2\pi t}{T_p}$; $-\frac{1}{2}T_p \le t \le \frac{1}{2}T_p$	$\frac{2ET_p \cdot \sin^2(\pi f T_p)}{\pi^2[(fT_p)^2 - 1]^2}$
Linear slope wave	$\sqrt{\frac{E}{T_p - \frac{2}{3}T_x}}$; $\frac{T_p - T_x}{2} < \lvert t\rvert < \frac{T_p}{2}$ $-2\sqrt{\frac{E}{T_p - \frac{2}{3}T_x}}\frac{t}{T_x}$; $\lvert t\rvert$	$\frac{\cdot 4T_p}{1-\frac{2}{3}\frac{T_x}{T_p}}\left[\frac{(\sin\pi fT_p - \cdot}{(\pi f)^2 T_x T_p}\right.$ $\left.\frac{\pi f T_x \cos\pi fT_x) + (\cos\pi fT_p -}{\pi f T_p}\right.$ $\left.\cos\pi fT_x)\right]^2$

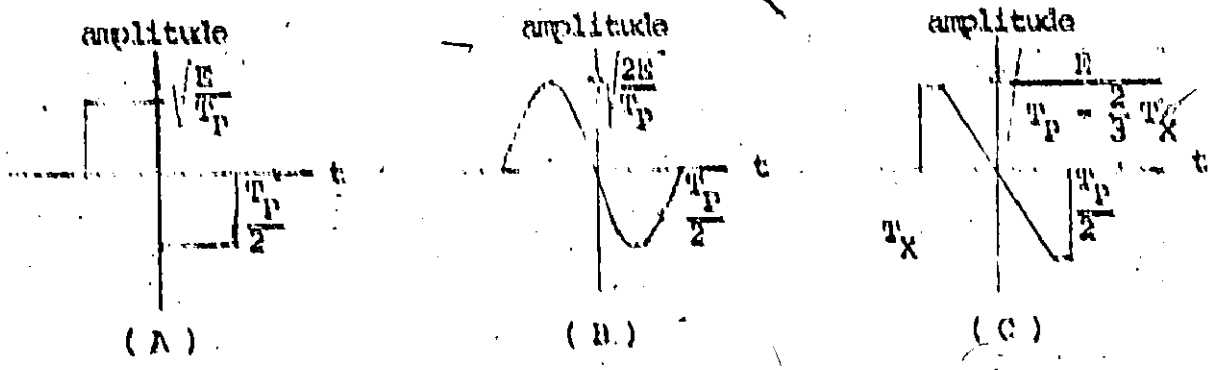

Fig. A-1 Several different PSK sync burst video waveforms.

(A) Square wave, (B) sine wave, (C) linear slope.

TABLE A-2
Spectral Shapes of Simple FSK Sync Bursts

Type	Time Function	Spectrum
Square wave	$\sqrt{\frac{E}{T_p}}$; $\frac{T_p}{4} \leq t \leq \frac{T_p}{4}$	$\frac{ET_p \sin^2(\frac{1}{2}\pi f T_p)}{(\pi f T_p)^2}$
Cosine wave	$\sqrt{\frac{2E}{T_p}} \cos\frac{2\pi t}{T_p}$; $-\frac{T_p}{4} \leq t \leq \frac{T_p}{4}$	$\frac{2ET_p \cos^2(\frac{1}{2}\pi f T_p)}{\pi^2[(fT_p)^2-1]^2}$
Triangle wave	$\sqrt{\frac{3E}{T_p}}(1-\frac{4t}{T_p})$; $0 \leq t \leq \frac{T_p}{4}$ $\sqrt{\frac{3E}{T_p}}(1+\frac{4t}{T_p})$; $-\frac{T_p}{4} \leq t \leq 0$	$\frac{3ET_p \sin^4 \frac{1}{4}\pi f T_p}{16(\frac{1}{4}\pi f T_p)^4}$

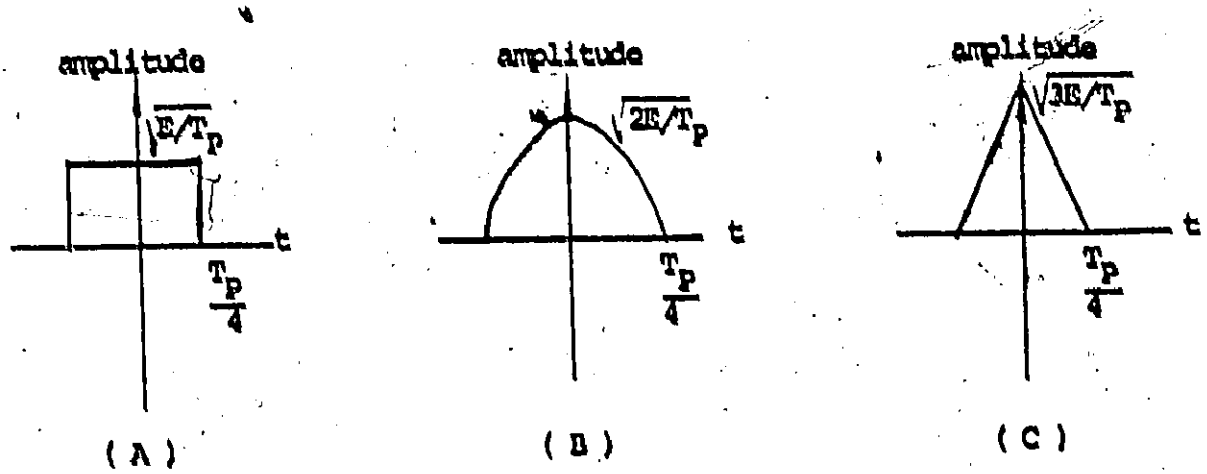

(A) (B) (C)

Fig. A-2 Several different FSK sync burst video waveforms.

(A) Square wave, (B) cosine wave, (C) triangle wave.

The metric consists of a number of bits which are used to detect the edge of the sync window modulation. Synchronization is achieved when a certain number of the metric bits are clipped off by the sync window. Unfortunately, the resolution is increased by reducing the duration of the bits which increases the bandwidth. The spectral shape can be estimated by calculating the Fourier transform of one bit of duration T_b. Hence, the spectrum is approximately

$$S_C = \frac{E_M T_M \sin^2(\pi f T_b)}{(\pi f T_b)^2}$$

where E_M = energy contained in the metric

T_M = duration of the metric.

This expression is essentially the same as for the ASK sync burst except the spectrum is broadened by the ratio T_b/T_p. A typical value for T_b is 30 ns and consequently the coded-ASK and coded-PSK sync bursts require approximately 33 times the bandwidth of the ASK sync burst and the coded-FSK sync burst requires twice this amount, assuming T_p = 1 μs.

APPENDIX B

Fixed Increment System

Rapuano and Shimasaki [16] have described two different fixed increment systems for adjusting the earth station time base. The first method utilizes the coded-ASK, coded-PSK and coded-FSK types of sync burst (referred to as coded sync bursts) to detect the number of bits of the matrix portion, shown in Fig. 3-2, which have been clipped off by the sync window modulation. The second method employs either PSK or FSK sync bursts and a count-up or count-down timing adjustment. The ASK sync burst can also be employed by using one end of the sync burst as a reference, as shown in Fig. 3-3. However, it is not possible to determine which end of the sync burst has passed through the sync window after the first sync window modulated train of sync bursts has been received at the earth station.

B-1 CODED SYNC BURST METHOD

Coded sync bursts can be used in the fine search mode to reduce the initial timing error by employing the system illustrated in Fig. B-1. Essentially, the system achieves synchronization by transmitting a short train of one type of coded sync bursts which are generated in the sync burst generator. After reaching the satellite, the sync bursts are modulated by the sync window and transmitted back to the same spot beam zone.

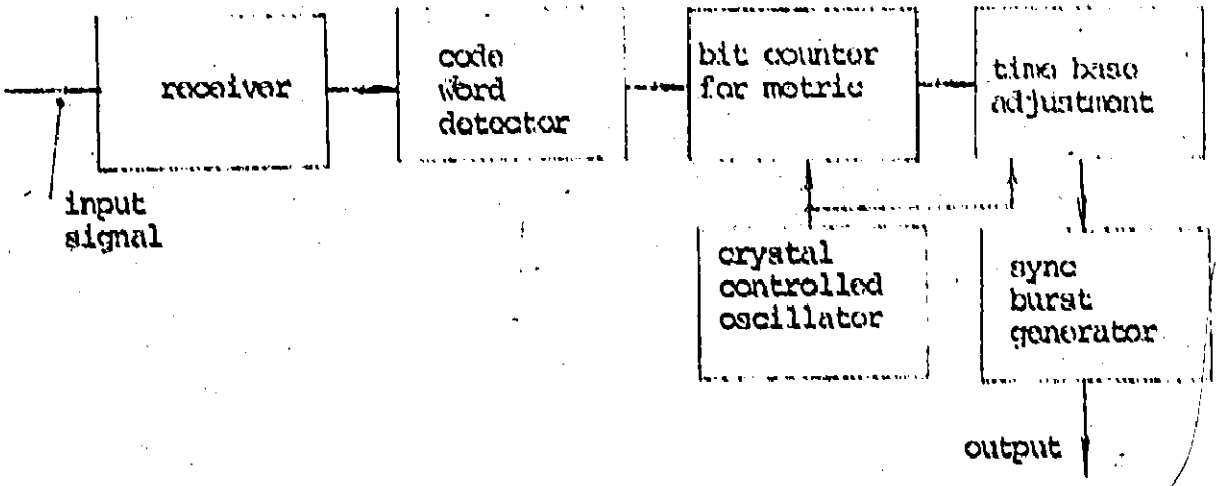

Fig. B-1 Coded sync burst timing control circuit.

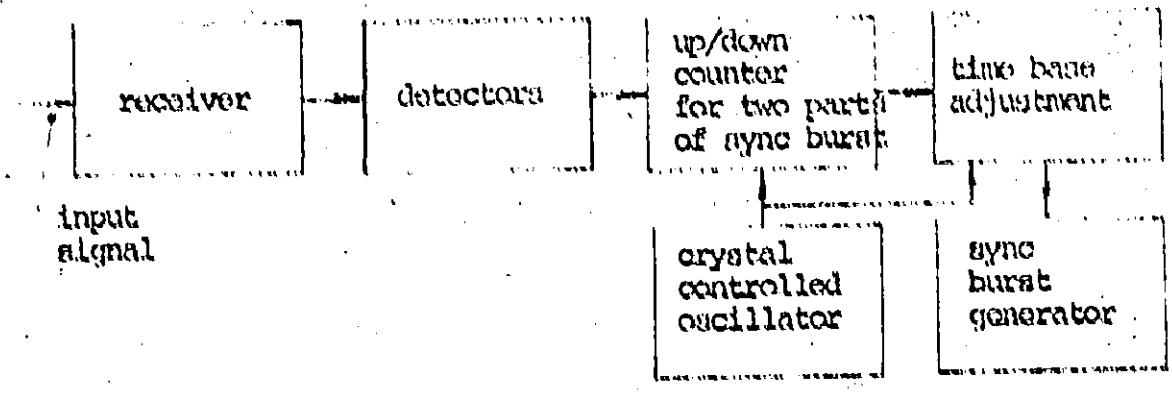

Fig. B-2 PSK/FSK sync burst timing control circuit.

When the coded sync bursts are received at the earth station, the number of bits of the metric not clipped off by the sync window modulation, N_M, are counted and compared with a reference number, N_R. If N_M is greater than N_R, the time base of the earth station is advanced, by a clock pulse equal to the bit duration; conversely, if N_M is less than N_R, the time base of the earth station is retarded by a clock pulse equal to the bit duration. When $N_M = N_R$, synchronization is achieved.

The resolution of this method is limited to the duration of one bit which is of the order of 30 ns. Also the pull-in range is only about ± 150 ns due to problems in detecting the code word of the sync burst [16].

B-2 PSK/FSK SYNC BURST METHOD

This digital control comprises a highly stable fixed frequency oscillator, synchronous dividers and logic circuits, as shown in Fig. B-2. Essentially, the system operates as follows. A short train of either PSK or FSK sync bursts, generated by the sync burst generator, are transmitted to the satellite. After sync window modulation the signals are returned to the earth station. The modulated sync bursts are fed through a limiting amplifier in the receiver and the two parts of the sync burst are detected. Each detected waveform passes through a threshold circuit and the resulting outputs along with a clock of frequency f_o are applied to a counting network to give two trains of clock pulses. The pulses of each train are counted and the difference is a measure of the timing error. Thus, the

timing adjustment circuit shifts the time base and triggers the sync burst generator producing another train of sync bursts. When the difference in the count is zero, synchronization is achieved.

The resolution of this system is simply the period of the clock pulse and is given by $\Delta t = 1/f_c$. For a clock frequency of 32 MHz, the basic resolution is 30 ns. This value can be reduced by increasing the clock frequency but to achieve a resolution of, say, half the timing error due to noise estimated to be 7 ns [16], a clock frequency of approximately 280 MHz would be required.

APPENDIX C

An Accurate Digital Time Base Control

The accuracy of the timing adjustment mechanism using an analog timing control can be compared with that achieved using a digital timing control. It is shown here that the increment size for the digital control can be reduced to less than half the estimated timing error due to noise without high speed clock circuits by using a phasing technique which relies on the high stability of a crystal-controlled clock. It is also shown that a tracking mode feature is then possible which reduces the earth station timing error due to satellite motion. Hence, the main limitation to the timing accuracy is due to the uplink and downlink noise which has been estimated to be of the order of 7 ns [5].

The analog control, shown in Fig. 3-7 uses a voltage-controlled-oscillator (VCO) to adjust the earth station time base. It is possible for errors to arise in the mechanism due to several factors which place a limitation on the accuracy of the earth station time base. The first is the short term stability of the VCO which may have a frequency variation averaged over 1 s of typically $\Delta f_s/f_0 = 10^{-9}$, where f_0 is the centre frequency of the VCO. Assuming a round trip time of 0.3 s, the resulting timing error at the earth station would be approximately 1 ns or less. Another source of error which can occur is due to variations in the voltage at the control terminal of the VCO. It is probable that a small offset voltage will be present on the control terminal of the VCO at all times. Assuming a linear characteristic for the output

frequency as a function of the control voltage, v_c, the frequency f, is given by

$$f = f_0 + S\, v_c \qquad (1)$$

where S = sensitivity of VCO in Hz/volt.

Thus, the variation $\Delta f_v/f_0$ for a small offset voltage of Δv_c is given by

$$\frac{\Delta f_v}{f_0} = \frac{S\Delta v_c}{f_0} \qquad (2)$$

The value of S is typically 10^{-5} of f_0 per volt and it may be assumed that the offset, Δv_c, can be reduced to 1 mv with careful design. Thus, the resulting value of $\Delta f_v/f_0$ is 10^{-8} resulting in timing error of the order of 3 ns in one round trip time of 0.3 s.

The total timing error due to the combined effects of short term stability and offset voltage is approximately half the timing error due to noise.

The basic resolution of the two digital methods described in Appendix B is approximately 30 ns, a value which is four times the timing error due to noise. Timing errors due to short term stability of the crystal-controlled oscillator are negligible, however the basic resolution of the digital control can be reduced to less than half the timing error due to noise with a clock frequency of only 20 to 30 MHz by using the system shown in Fig. C-1. In normal operation, pulses from the crystal-controlled oscillator are counted in the frame counter and when a predetermined number N_1 is reached, a frame pulse from the decoder is produced which resets the frame counter output to the number at its data input. The time between frame pulses from the

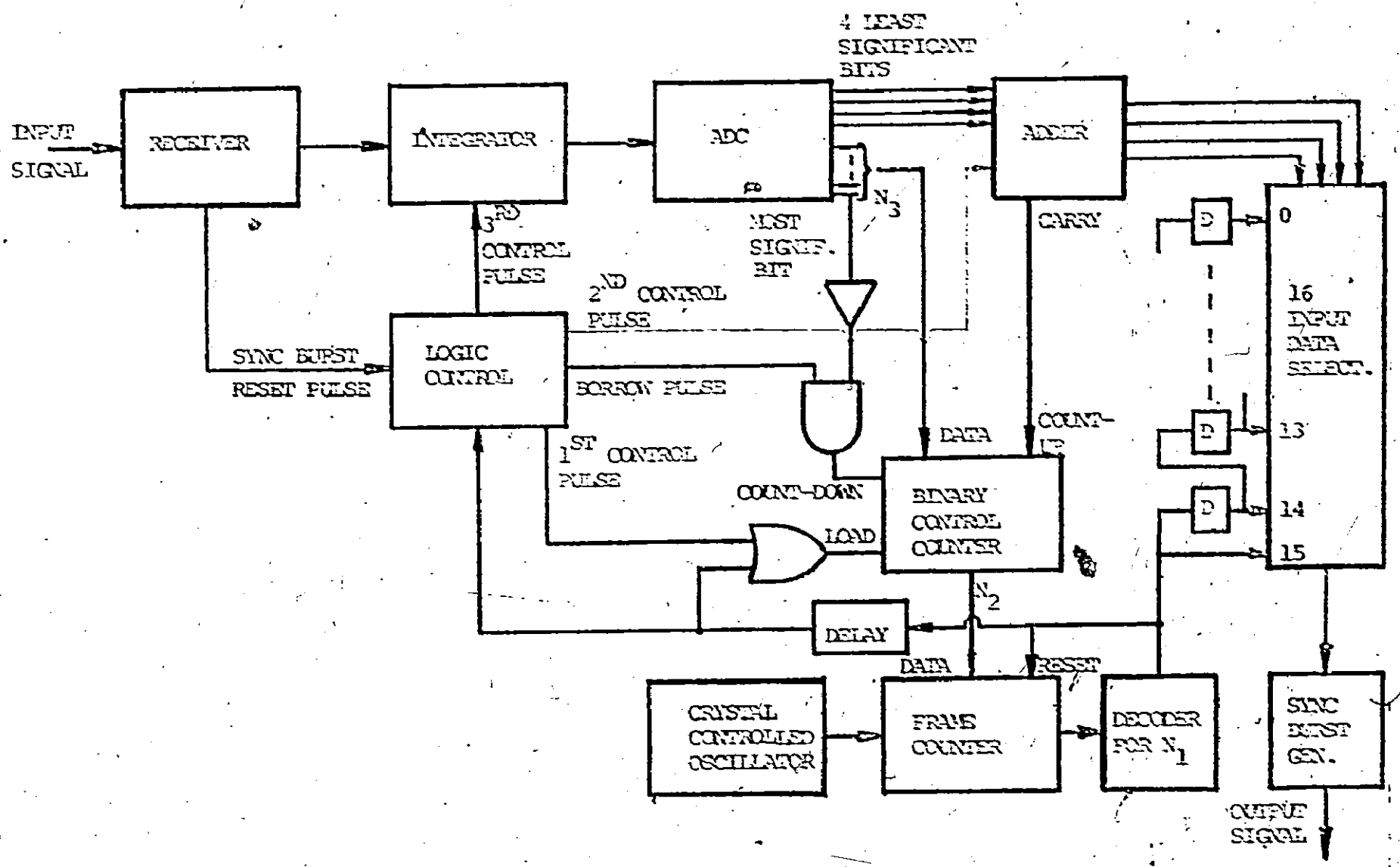

Fig. C-1 Accurate time base control circuit.

decoder is the frame length. The frame pulses proceed through the data selector and trigger the sync burst generator. The frame pulses also pass through a delay (of duration small compared to the frame length) to the binary control counter resetting its output to the number at its data input, N_2. Thus, the frame counter counts from N_2 up to N_1. The N_3 least significant bits at the data input to the frame counter are simply the N_3 most significant bits from the analog-to-digital converter (ADC), buffered through the binary control counter, and the remaining bits at the data input are hardwired to zero. The ADC is assumed to have an offset binary output, consisting of $(N_3 + 4)$ bits. When the input voltage to the ADC is zero, the most significant bit at its output is a '1' with the remainder of the bits being '0'.

After a sync burst is received, it is integrated as in the case of the analog control circuit and digitized in the ADC. The logic control, having been reset by the reception of the sync burst, generates three control pulses spaced with different delays (but all within a frame length), upon the reception of the next frame pulse. The first control pulse loads the N_3 most significant digits at the ADC output into the output of the binary control counter. Next, the second control pulse causes the four least significant digits of the ADC to be added to the output from the previous transmission. Note that due to the offset binary, negative numbers appear as 2's complement and, hence, can be added directly in the binary adder. If the output from the ADC represents a negative input, then a borrow pulse is generated upon reception of the second control pulse and sent to the count-down clock input of the binary control counter. If a carry is generated by the adder, it is fed to the count-up clock input of the binary control counter. The output from the

adder feeds the fine timing adjustment which will be described later. Finally, the third control pulse resets the integrator to zero so that the ADC output is set for normal operation.

When the next pulse from the decoder reaches the load input of the frame counter, the new value of N_2 at the data input is loaded, the system returns to normal operation, and the counter commences to count clock pulses. If the timing error, t_E defined in Fig. 4-7, is negative, the value of N_2 is less than the normal value and if the timing error is positive, the value of N_2 is greater than the normal value. Thus, a range of timing adjustments is provided in increments of the clock period.

The fine timing adjustment is provided by time delays at the inputs to a 16-input data selector. The output from the adder controls which input to the selector is connected to its output. All delays are of equal value given by the clock period divided by 16. For a clock period of 40 ns, each is 2.5 ns. Thus, combining the timing adjustments provided by incrementing the frame counter and those obtained by the data selector, a basic resolution of 2.5 ns is achieved which is less than half the timing error due to noise. Such accuracy has in fact been provided for the CTS [47].

The timing error due to constant-velocity motion of the satellite appears in the average value of the ADC output. Thus, by averaging this output, a compensating timing shift can be applied to the fine timing adjustment through the logic control which would cause a certain number of evenly spaced 2.5 ns shifts to occur over the round trip time. Hence, a tracking feature is possible.

REFERENCES

[1] PRITCHARD, W.L., and BARCELLINI, P.L.: 'Trends in technology for communications satellites', Astronautics and Aeronautics, April 1972, pp. 36-42.

[2] MORGAN, W.L.: 'Communications satellites and new technology', Microwave Systems News, April/May 1974, V. 4, N. 2, pp. 64-68.

[3] SCHMIDT, W.G.: 'An onboard switched multiple-access system for millimeter-wave satellites', Proc. INTELSAT/IEE conf. on digital sat. commun., 1969, pp. 399-407.

[4] HUANG, R.Y., and HOOTEN, P.: 'Communication satellite processing repeaters', Proc. IEEE, Feb. 1971, V. 59, N. 2, pp. 238-252.

[5] CAINER, W.B., and STAMMINGER, R.: 'Future communications satellites: Definition of three basic concepts', ICC 73, June 11-13, 1973, pp. 3-8 to 3-11.

[6] SCHMIDT, W.G., and COOPERMAN, R.S.: 'A satellite-switched sdma/tdma system for a wideband multibeam satellite', ICC 73, June 11-13, 1973, pp. 12-7, 12-12.

[7] CUCCIA, C.L.: 'Communication by satellite: a status report', Microwave Systems News, April/May 1974, pp. 27-44.

[8] SCHMIDT, W.G. and COOPERMAN, R: 'Outline for an sdma/ss-tdma system for a wideband multibeam system', COMSAT Laboratories technical memorandum, report no. CL-6-72, Feb. 7, 1972.

[9] BERMAN, A.L. and MAHLE, C.E.: 'Transponder configuration for communications satellites using frequencies above 10 GHz' IEEE Conf. on commun. (ICC 71), Montreal, Canada, June 14-16, 1971, pp. 27-17 to 27-22.

[10] PUENTE, J.G., SCHMIDT, W.G. and WERTH, A.M.: 'Multiple-access techniques for commercial satellites', Proc. IEEE, V. 59, N. 2, Feb. 1971, pp. 218-229.

[11] KINAL, G.V.: 'Multiple-beam satellite repeater tradeoffs applied to a multifunctional system', ICC'73, June 11-13, 1973, pp. 12-19 to 12-26.

[12] WARWAT, M: 'Economic considerations in a large multi-purpose domestic communications satellite system', ICC'72, June 19-21, 1972, pp. 10-6 to 10-10.

[13] ----------'One touch of venus' Newsweek, Feb. 18, 1974, pp. 78.

[14] SCHMIDT, W.G., GOODEMAN, R.S. KAISER, J. and SHIMASAKI, N: 'Multiple-access technology: Present and near future', COMSAT laboratories technical memorandum, report no. CL-19-71, April 5, 1971.

[15] SHIMASAKI, N. and PAPUNO, R.A.: 'Synchronization for a communications distribution center on board a satellite', IEEE conf. on commun. (ICC'71), Montreal, Canada, June 14-16, 1971, pp. 42-20 to 42-25.

[16] PAPUNO, R.A. and SHIMASAKI, N.: 'Synchronization of earth stations to satellite switched sequences', AIAA 4th communications satellite systems conf., Washington, D.C., April 24-26, 1972.

[17] ASAHARA, M. et. al.: 'Synchronization and acquisition in sdma satellite communication system', ICC'74, June 17-19, 1974, pp. 43E-1 to 43E-6.

[18] NOSAKA, K. and MURATANI, T.: 'New satellite transponder with regenerative repeater and higher order dpsk for tdma/sdma system', Second Int. conf. on digital satellite communication', Record of second Int. col. dig. sat. comm., Paris, France Nov. 1972, pp. 460-468.

[19] FRANKLIN, C.A. and DAVISON, E.H.: 'A high-power communications technology satellite for the 12 and 14 GHz bands', AIAA 4th communications satellite systems conf., Washington, D.C., April 24-26, 1972.

[20] DAY, J.W.B.: 'CTS communications experiments', IEEE Nat. telecomm. conf., Houston, Texas, Dec. 4-6, 1972.

[21] NUSPL, P.P.: 'Proposed Experiments in regional tdma with demand assignment', Record of second int. col. dig. sat. comm., Paris, France, Nov. 1972, pp. 18-25.

[22] NUSPL, P.P. and deBUDA, R: 'A tdma synchronization algorithm', EASTCON conf. rec., Washington, D.C., Oct. 7-9, 1974.

[23] deBUDA, R: 'Signal processing and the multiple access problem of communication satellites', Canadian General Electric Company, report no. RQ 69EE2, April 23, 1969.

[24] deBUDA, R.: 'Synchronization for time division multiple access experiments', Canadian General Electric Company, report no. RQ 72EE4, June 9, 1972.

[25] deBUDA, R.: 'Position tracking a spot beam satellite from delay data', Canadian General Electric Company, report no. RQ 73EE1, Jan. 8, 1973.

[26] BACON, W.H.: 'A multiple access problem in satellite communications', IEEE symp. digest, Canadian symp. comm., Montreal, Nov. 12-13, 1970, pp. 93-4.

[27] CARTER, C.R. and HAYKIN, S.S.: 'A comparison of the signals used for synchronizing to a switching satellite', IEEE Canadian Comm. and Power Conf., Montreal, Quebec, Nov. 7-8, 1974. Accepted for publication in the Digest.

[28] CARTER, C.R. and HAYKIN, S.S.: ' Techniques for synchronizing to switching satellite', IEEE int. electrical, electronics conf., Toronto, Ontario, Oct. 1-3, 1973, pp. 114-115.

[29] CARTER, C.R. and HAYKIN, S.S.: 'Precision synchronization to a switching satellite using psk signals', ICC'74, June 17-19, 1974, pp. 43D-1 to 43D-5.

[30] CARTER, C.R. and HAYKIN, S.S.: ' A new synchronization technique for switched tdma satellite systems', IEEE trans. on communications, V. com-22, May 1974, pp. 710-713.

[31] GANSSMANTEL, H. and EKSTROM, B.: 'Tdma synchronization for future multitransponder satellite communication', ICC'74, June 17-19, 1974, pp. 43C-1 to 43C-5.

[32] CARTER, C.R. and HAYKIN, S.S.: 'Fast synchronization of a ground station to a switching satellite', Electronics Letters, Nov. 1, 1973, V. 9, N. 22, pp. 513-514.

[33] CARTER, C.R. and HAYKIN, S.S.: 'Fine search synchronization for a switching satellite', submitted to Proceedings IEE.

[34] SCHWARTZ, M, BENNETT, W.R. and STEIN, S.: Communications systems and techniques, (McGraw-Hill, 1966), pp. 285-286.

[35] ibid pp. 179.

[36] ibid pp. 18.

[37] LUBOMI, A.G.: 'Path length variation in a synchronous satellite communications link', BSTJ, December 1968, pp. 2139-2144.

[38] GOLD, B. and RADER, C.M.: Digital processing of signals, (McGraw-Hill, 1969), pp. 30.

[39] LINDSAY, W.C.: 'Synchronization systems in communications and control, (Prentice-Hall, 1972), pp. 348.

[40] SCHWARTZ, M., BENNETT, W.R. and STEIN, S.: op.cit., pp. 67.

[41] FREEMAN, H.: Discrete-time systems, (John Wiley, 1955), pp. 172.

[42] CARTER, C.R. and HAYKIN, S.S.: 'A laboratory model for the switching satellite synchronization loop, National Telecommunications Conf., Dec. 2, 3, 4, 1974, San Diego, California. Accepted for publication in NTC Record.

[43] HARMUTH, H. F.: Transmission of information by orthogonal functions, (Springer-Verlag, 1970), pp. 19.

[44] HUFF, R. J. and REINHARD, K. L.: 'A delay-lock loop for tracking pulsed-envelope signals', IEEE trans. on aero. and elect. syst., v. aes-7, n. 3, May, 1971, pp. 478-485.

[45] SPILKER, J. J.:'Delay-lock tracking of binary signals', IEEE trans on space elect. and tele., v. set-9, March 1963, pp. 1-8.

[46] GARDNER, F. M.: Phaselock techniques, (John Wiley, 1966).

[47] CHOW, S. M. and HUCK, R. W.: 'A receiver time base locking circuit', Canadian General Electric Company, report no. RQ70EE10, Dec.31,1970.